Holography: Encoding Quantum Information In Classical Gravity

A thesis submitted to the
Graduate School of the University of Minnesota
by

Aditya Dhumuntarao

in partial fulfillment of the requirements for the
degree of Doctor of Philosophy

Professor Joseph I. Kapusta, Advisor

June 2023

Acknowledgements

With great struggle comes great success.

I met the dawn at Gilman's point on Mount Kilimanjaro with these words on my mind, a lesson I have carried throughout my time in graduate school. This dissertation, and the struggles and challenges therein, would have been insurmountable if not for constant efforts of my loving wife Emily, my supporting family, and the assistance of many scientists and friends along the way. I dedicate this thesis to those who contributed significantly to my career growth.

I would first like to acknowledge my advisor, Joe Kapusta, who laid the foundations of this thesis. After we completed a REU summer project together in 2015, I went to present our findings in San Antonio at a DNP conference later that year. During that conference, Eric Kostelich reached out and encouraged me strongly to submit an application to the NSF Graduate Research Fellowship. Fortuitously, I ran into Joe at that conference and, after a short conversation, together we drew up an ultimately successful NSF proposal supporting Part II of this thesis. I learned a great deal from Joe on how to navigate grant proposals, conduct research independently, and spearhead my own collaborations. These lessons ultimately led me to work with Aleksey Cherman on topics highlighted in Part II, and secure support from the Doctoral Dissertation Fellowship as I worked remotely from the Boston/MIT area on projects in Part III.

Externally, I have benefitted greatly from the tutelage of Niayesh Afshordi, Robert Mann, and Matthew Headrick. Niayesh took me under his wing at the Perimeter Institute in 2017 after I completed the Tripos. Under his guidance, I learned hard lessons in approaching challenging problems, the nuances of research collaboration, and the importance of framing science accurately. It was through Niayesh that I met Robert Mann, who invited me back to Perimeter in 2018 to work on topics highlighted in Part I. Robb taught me valuable lessons on surveying existing science in order to select the right question to pursue and, together, we ultimately solved an interesting open problem in black hole chemistry. Lastly, Matt Headrick was instrumental in my maturation as a scientist and my involvement in the holography community during the COVID-19 pandemic. After moving to the Boston/MIT area in 2021, Matt helped me establish several connections, provided mentorship during postdoc applications, and guided me towards a deeper understanding of gravity and its intersections with quantum information. His mentorship

is directly responsible for Part III of this dissertation.

I would be remiss if I did not note the contributions from many of my peers in my science career: Charlie Shugert and Alex Munoz have been there since my career began and have always kept me honest when discussing theoretical ideas; Soham Mukherjee and Matthew Robbins with whom, over many physics conversations at Perimeter, I was made into a decent pool player; Rafid Mahbub and Billy Munizzi who have both taught me how to set forth a research agenda, trusted in my research mission, and saw that we stuck to it despite many wandering turns; Åsmund Folkestad who has deeply impressed upon me the profound nature of holography and is one of the kindest people I am fortunate to know; and Alicia Magann who, during my time exploring career options in academia and industry, made me aware of the exciting research in quantum information science conducted by the faculty at Sandia National Laboratories.

I owe a great deal of thanks to my family and friends. There are no words which can adequately convey my gratitude towards my parents, Ramarao and Lakshmi, and my brother, Sakheth. What is there to say to my father who inspired in me a love of Star Trek and subsequent love of physics? Or my mother who painstakingly cared for my education as we moved across several continents? Or my brother without whom I would have never learned growth or appreciated the beauty in challenge. They have gone well and beyond duties expected of any parent or sibling, and I hope that I can do the same for them.

To the Dhumuntarao household, Venketa Subba Rao, Surya Kumari, Krishna Mohan, Swathi, Chai Lakshmi Prasanna, Bapiraju, Rajya Lakshmi; the Mandalaparthy household, Krishna Rao, Venketa Ramana, Veena Varalakshmi, and Ashritha; the Tatavarthy household, Sekhar, Deepti, Keerthana, Akshara; the Mantravadi household, Naresh and Sowbhagya, I appreciate all of your support and am lucky to be a part of our family.

I also want to thank the Hartsoughs. Allan, on many occasions chatting over a Minnesotan fire, has provided valuable insights and advice. Janice who has, on countless occasions, been a source of great kindness and a killer pasta.

To my invaluable friends Alexandre Mayhob, Jillian Nelson, Nick Schillaci, Ana Gabriela Smith, Chloe Meyer, Annika Faucon, Ramya Gurunathan, Nina Coyle, and Lulu Song – thank you for your words of encouragement, your insights, and for seeing me through both great and dark times over these years.

Lastly, this dissertation, the people I have become entangled with, and my upcoming postdoc at Sandia National Laboratory all emerged from the decision to start a career in physics. A decision that I would not have made if not for my partner and loving wife, Emily, who pushed me to explore my passion in 2012. Without her faith and patience, this thesis would not be possible.

Abstract

We explore the intersections between classical gravity and quantum information via holographic dualities. Such dualities provide a sophisticated mathematical dictionary which encodes information from a d-dimensional quantum theory onto a $(d+1)$-dimensional theory of gravity via equivalence of their partition functions.

In this dissertation, we bridge classical geometry and quantum information in three parts. In Part I, we elucidate the connection between geometry and thermodynamics. Using the laws of black hole thermodynamics, we prove the existence of novel liquid-gas phase transitions in the phase diagram for lower dimensional AdS black holes. We further establish a proof that thermodynamic instabilities for AdS uniform black strings are correlated with classical gravitational instabilities.

In Part II, we connect quantum statistical systems and equilibrium gravitational systems. Specifically, we study applications of holographic quantum/classical dualities and analyze putative gravitational duals to $4d$ $SU(N_c)$ Yang-Mills under various deformations. First, we demonstrate that deforming the bulk gravity dual with codimension one branes yields a scalar mass spectra concordant with lattice data at zero temperature. Next, at finite temperature, we show the presence of branes imposes an upper bound on the thermal Bekenstein-Hawking entropy. We further prove that deforming the R-charge for $4d$ $\mathcal{N}=4$ Super Yang-Mills on $S^1_\beta \times S^3_R$ avoids the deconfinement/Hagedorn phase transition at weak coupling and the Hawking/Page phase transition at strong coupling.

In Part III, we link quantum information and classical geometry holographically. Using geometric flows of extremal surfaces in asymptotically AdS spacetimes, we prove novel speed limits on the growth of entanglement entropy, equal time correlators, and spacelike Wilson loops for strongly coupled, far from equilibrium quantum systems admitting holographic duals. Our results imply new bounds on the entanglement velocity, prove the entanglement tsunami conjecture for a large class of states in $2d$, and uncover a new momentum-entanglement correspondence, proving that entanglement growth is directly related to the momentum flux crossing an extremal surface.

Contents

List of Figures

List of Tables

Part I

The Thermodynamics of Classical Geometries

Chapter 1

Introduction

Black holes evaporate.

This discovery lies at the heart of modern theoretical physics and unifies the disparate fields of gravitational, statistical mechanics, quantum field theory, quantum information, and string theory [1–9]. Over the last century, gravity has enjoyed a special status among other fundamental forces of Nature in that it is a classical field theory [10, 11]. The other forces of Nature are described by quantum field theories for which the fundamental problem is to understand their density matrix in order to systematically probe quantum phenomena. Gravity, on the other hand, has thus far has avoided a renormalizable quantum description as a quantum field theory. In the mid 1900s, Bekenstein, and later Hawking, proposed a major advance in understanding the microcanonical states of gravity by ascribing a thermal entropy to geometry [1, 2, 5]

$$S_{\rm BH} = \frac{k_{\rm B} c^3}{\hbar} \frac{A_{\mathcal{H}}}{4 G_N}, \tag{1.1}$$

where $A_{\mathcal{H}}$ is the area of the horizon and henceforth $k_{\rm B} = c = \hbar = 1$. The discovery that the Bekenstein-Hawking entropy obeys an area law leads immediately to two sharp consequences; black holes are holographic objects and spacetime is a statistical arena. The former emerges from the observation that black holes encode the information stored within their interior onto its horizon area (see Fig. 1.1). The latter consequence follows from noting that black holes are solutions to Einstein's equations and therefore gravity is not exempt from the laws of thermodynamics. However, Hawking's calculations presented a great challenge to the reconciliation of gravity and quantum field theory. After a black hole forms from collapse, quantum effects near the horizon lead a stream of Hawking radiation to escape from the black hole [5]. Over time, the black hole loses mass-energy and evaporates away thereby destroying the quantum information residing within the interior [12] (see Fig. 1.3). As black holes are classical objects without a density matrix, information was believed to be lost violating the laws of quantum mechanics.

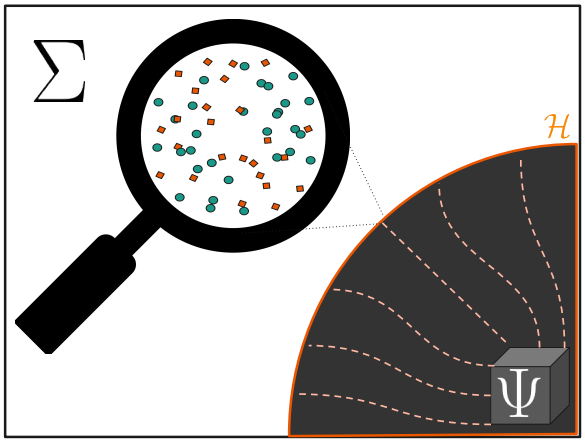

Figure 1.1: A quantum state Ψ hidden behind the horizon $\mathcal{H}$. Holographically, the black hole encodes the quantum microstates into the horizon.

Maldacena provided the last conceptual leap required to reconcile gravity and quantum mechanics in the late 1990s [13]. Maldacena discovered the gauge/gravity duality, a sophisticated mathematical tool which rests on the holographic principle. This duality encoded the density matrix of a d-dimensional boundary quantum theory into the geometry of a bulk $(d+1)$-dimensional gravitational theory. In doing so, the holographic duality rescues unitarity and provides gravity with a density matrix to store the trapped information. Equipped with a density matrix, calculations indicated that the quantum information within black hole interiors are encoded in the outgoing Hawking radiation [14, 15]. But precisely how does the quantum information become encoded holographically in classical geometry? That is the primary focus of this dissertation.

In this introductory chapter, we review in more detail the thermodynamics of classical geometries. We begin by demonstrating that observers in accelerated frames view vacuum states of quantum fields in flat spacetimes as thermal states. Via the equivalence principle, such thermal vacuum states also appear for quantum fields propagating in curved spacetimes. Near a horizon, ingoing and outgoing modes of a quantum field naturally lead an asymptotic observer to view the apparent horizon as a radiating body. We then show that when these effects are applied in the vicinity of black hole horizons, and in conjunction with the laws of black hole mechanics, one obtains a concrete prescription for a thermodynamic description of classical geometries. Once this has been established, we can use Euclidean methods to confirm this description and study finer phase structures in the thermodynamics of black holes.

For our purposes, we restrict ourselves to studying scalar fields in flat/curved backgrounds in four spacetime dimensions. When discussing the Euclidean gravitational path integral, we study vacuum black hole solutions to Einstein's equations in general dimensions. For a full treatment of quantum field theory and general relativity, we refer to the canonical texts on the subjects [16–19].

1.1 Quantum Fields in Curved Spacetimes

In order to motivate the thermodynamics of curved spacetimes, we will first consider the case of an accelerated detector moving through a quantized scalar field theory on a standard four-dimensional Minkowskian background.

We introduce a flat four dimensional Minkowski spacetime $\mathbb{R}^{3,1}$ with three spatial dimensions. We denote by x^μ the points of Minkowski spacetime with $x^0 = t$ being the time direction and $x^i = \boldsymbol{x}$ being the spatial directions. In this system, the Minkowski metric is given by

$$\mathrm{d}s^2 = -\mathrm{d}t^2 + \mathrm{d}\boldsymbol{x}\cdot\mathrm{d}\boldsymbol{x} = \eta_{\mu\nu}\mathrm{d}x^\mu \mathrm{d}x^\nu. \tag{1.2}$$

On such a background a massless scalar field, $\Psi(x) \equiv \Psi(\boldsymbol{x}, t)$, freely propagates according to the wave equation,

$$\Box\Psi(\boldsymbol{x}, t) \equiv \left(\frac{\partial^2}{\partial t^2} - \Delta_{\boldsymbol{x}}\right)\Psi(\boldsymbol{x}, t) = 0 \tag{1.3}$$

where $\Delta_{\boldsymbol{x}}$ is the spatial Laplacian of the scalar field. If we wish to quantize the theory, the scalar field is promoted to an operator $\hat{\Psi}(\boldsymbol{x}, t)$ satisfying the wave equation and admits a plane wave mode representation

$$\hat{\Psi}(\boldsymbol{x}, t) = \int \frac{\mathrm{d}^3\boldsymbol{k}}{(2\pi)^3}\frac{1}{\sqrt{2\omega}}\Big\{a^\dagger_{\boldsymbol{k}} e^{i(\omega t - \boldsymbol{k}\cdot\boldsymbol{x})} + a_{\boldsymbol{k}} e^{-i(\omega t - \boldsymbol{k}\cdot\boldsymbol{x})}\Big\}. \tag{1.4}$$

with operators satisfying the commutation algebra $[a_{\boldsymbol{k}}, a^\dagger_{\boldsymbol{k}'}] = (2\pi)^3\delta^3(\boldsymbol{k} - \boldsymbol{k}')$. These commutation relations are similar to the quantum harmonic oscillator, therefore we interpret the operators as the annihilation, $a_{\boldsymbol{k}}|0\rangle = |0\rangle$, and creation, $a^\dagger_{\boldsymbol{k}}|0\rangle = |\boldsymbol{k}\rangle$, operators of particles with momentum $\boldsymbol{k}$ respectively. The vacuum state, the state for which no particles are present, is given by $|0\rangle$.

Now, let us consider an accelerated observer on this flat background. The simplest case is of observers with constant acceleration, a, moving along the (t, x) plane in Minkowski spacetime,

$$x^2 = x^3 = 0, \quad x^1 = +\sqrt{t^2 + a^{-2}}, \quad t(\tau) = \frac{1}{a}\sinh(a\tau) \tag{1.5}$$

where τ is the proper time of the observer. Under these transformations, the wave equation and the mode decomposition for the scalar wave change accordingly in the rest frame of the observer. For our purposes, it is more instructive to understand the corresponding change in the symmetrized Wightman function which takes on the form

$$G^+_A(x', x) = -\left[\frac{4\pi}{a}\sinh\left(\frac{as(x', x)}{2}\right)\right]^{-2} \tag{1.6}$$

where $s[x(\tau'), x(\tau)] = \tau' - \tau$ is the proper distance [19]. Along any trajectory, one can choose to couple their motion to a particle detector. The detector in the rest frame of the observer would observe an absorption of quanta at the rate of

$$\Gamma \propto \int \mathrm{d}\Delta\tau\, e^{-i(E - E_g)(\tau' - \tau)} G^+(x', x), \tag{1.7}$$

where $E > E_g$ is the energy of the excited state and E_g is the ground state energy [19]. Using the Wightman function Eqn. (1.6) of a uniformly accelerating observer in a flat background one finds an absorption rate of

$$\Gamma_A \propto \frac{1}{e^{2\pi(E-E_g)/a} - 1}. \tag{1.8}$$

The appearance of the Planck factor $e^{2\pi(E-E_g)/a} - 1$ in the absorption rate indicates that an accelerated detector in equilibrium with a quantized scalar field in the vacuum state $|0\rangle$ is equivalent to an *un*accelerated detector in equilibrium with a bath of thermal radiation at a temperature

$$T = \frac{a}{2\pi}. \tag{1.9}$$

This is the Unruh effect [20] (see [21] for a more general procedure). Though the field is in its vacuum state, in the rest frame of the accelerated observer the field appears to emit a steady rate of radiation. Observe that if the observer stopped accelerating, then the absorption rate vanishes $\Gamma_A \to 0$ as our vacuum and the vacuum of the scalar field are the same. Hence, two observers, one accelerated and one inertial, will disagree on the vacuum state of an ambient quantum field.

This is not special to Minkowski spacetime. Indeed, when gravitational fields are present, inertial observers become free-falling observers via the equivalence principle. Hence, even in more general curved spacetimes with standard fields and accelerated observers, the Unruh effect is present [22, 23]. This observation lies at the heart of prescribing thermal properties to geometry. In the next section, we consider quantum fields just outside a horizon and show that an inertial observer at asymptotic infinity views the horizon radiating with a Hawking temperature.

1.2 Horizons and Hawking Radiation

Suppose instead of the flat Minkowski spacetime we considered earlier, we now are interested in a general, spherically symmetric, time-dependent geometry. Such a geometry can be expressed in Painlevé–Gulstrand coordinates [24],

$$\mathrm{d}s^2 = -(A(r,t)^2 - B(r,t)^2)\mathrm{d}t^2 - 2B(r,t)\mathrm{d}r\mathrm{d}t + \mathrm{d}r^2 + r^2(\mathrm{d}\theta^2 + \sin^2(\theta)\mathrm{d}\phi^2). \tag{1.10}$$

This geometry contains an apparent horizon $\mathcal{A}$ located at $A(r,t) = |B(r,t)|$ but the metric remains non-singular at the horizon. Now, rather than an observer who is on an accelerated trajectory, the geometry is naturally curved and any inertial observer would experience free-fall towards the apparent horizon. Hence, we only need to focus on the curved geometry and on a quantum field existing outside the apparent horizon.

One can repeat the above analysis in this context. This involves employing the eikonal approximation, assuming that the background geometry evolves slower than the natural

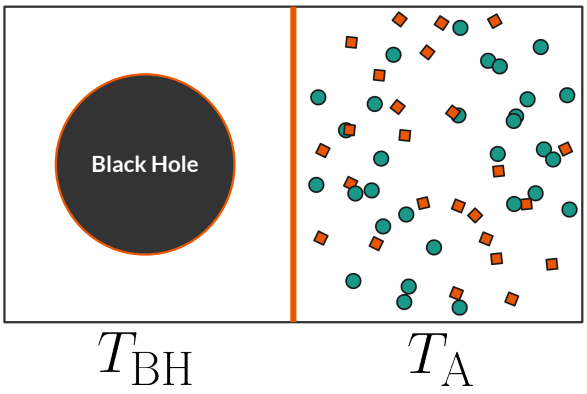

Figure 1.2: A black hole in thermal contact with a gas of particles. Classically, the black hole has no temperature. Hence, the system never reaches thermal equilibrium at finite temperature as the black hole is classically prevented from heating. Semi-classically, black holes are in equilibrium with a thermal bath radiating at a temperature $T_{\mathrm{H}} = \kappa/2\pi$.

timescale of the scalar field, and solving the wave equation near the apparent horizon and at asymptotic infinity. These calculations are quite involved, we refer the reader to [25] for details. A careful analysis shows that there is an outgoing flux of quanta at a rate

$$\Gamma(t) \propto \frac{1}{e^{2\pi\Delta E/a(t)} - 1} \tag{1.11}$$

where $\kappa(t)$ refers to the surface gravity, or acceleration, felt by an object kept at the apparent horizon and is given by

$$\kappa(t) = \frac{\mathrm{d}}{\mathrm{d}r}(A(r,t) - |B(r,t)|)\Big|_{\mathcal{A}}. \tag{1.12}$$

Hence, an outside observer at asymptotic infinity would view a stream of particles emanating from the apparent horizon. As the apparent horizon converges onto its event horizon in the infinite future and the geometry stops evolving, an asymptotic observer would view the event horizon as being in equilibrium with a thermal bath at temperature

$$T = \frac{\kappa(t_\infty)}{2\pi} = \frac{1}{2\pi}\frac{\mathrm{d}}{\mathrm{d}r}(A(r,t_\infty) - |B(r,t_\infty)|). \tag{1.13}$$

For a local observer at the apparent horizon, they see no thermal bath. Indeed, the freely falling observer should not see anything special at the event horizon according to the equivalence principle and thus the preferred vacuum state is that which the inertial observer experiences at the horizon. The vacuum of the asymptotic observer, however, registers a thermal bath purely from the geometry around the apparent horizon.

This outgoing flux is Hawking radiation [5]. Indeed, if we were to express the Schwarzchild metric of a black hole with mass M (justified below) in Painlevé–Gulstrand coordinates

$$\mathrm{d}s^2 = -\left(1 - \frac{2G_{\mathrm{N}}M}{r}\right)\mathrm{d}t^2 + 2\sqrt{\frac{2G_{\mathrm{N}}M}{r}}\mathrm{d}t\mathrm{d}r + \mathrm{d}r^2 + r^2(\mathrm{d}\theta^2 + \sin^2(\theta)\mathrm{d}\phi^2), \tag{1.14}$$

then a straightforward calculation would recover Hawking's celebrated result; black holes are in equilibrium with a thermal bath radiating with a temperature

$$T_{\rm H} = \frac{\kappa}{2\pi} = \frac{1}{8\pi G_{\rm N} M}. \tag{1.15}$$

That black holes, and other objects with apparent horizons, in conjunction with quantum fields propagating outside their horizons leads to Planckian distributions is a profound connection between geometry and thermodynamics. In the next section, we use the laws of black hole mechanics and the fact that black holes radiate analogous to black bodies to formalize this relationship.

1.3 The Laws of Black Hole Mechanics

A gravitationally collapsing body gives rise to a black hole that is classically characterized by three parameters; the mass M, charge Q, and angular momentum J. Provided the final state of gravitational collapse is a stationary state, the mass, charge, and angular momentum are conserved quantities. Other information, such as the various quantum numbers, are not expected to be preserved by classical black holes [26, 27]. Furthermore, geometric information, such as the horizon area $A_{\mathcal{H}}$, can be expressed purely in terms of these conserved quantities. Indeed, these quantities (M, Q, J, A) are not independent. Even in the simplest case of a non-rotating, uncharged black hole, throwing in a finite-sized object will change both the area and the mass of the final black hole. These observations lead us to the first law of black hole mechanics [3]:

Theorem 1 (The 1^{st} Law)**.** *For a differential change in a stationary black hole, the change of the internal mass-energy M is related to a change in the area, charge, and angular momentum by*

$$\mathrm{d}M = \frac{\kappa}{8\pi G_N}\mathrm{d}A_{\mathcal{H}} + \Phi \mathrm{d}Q + \Omega \mathrm{d}J, \tag{1.16}$$

where the surface gravity κ, the electrostatic potential Φ, and the angular velocity Ω are the corresponding chemical potentials to the area $A_{\mathcal{H}}$, charge Q, and angular momentum J respectively.

While certainly the form of the first law of black hole mechanics is reminiscent of the first law of thermodynamics, the first term proportional to $\kappa \mathrm{d}A_{\mathcal{H}}$ lacks a thermal interpretation at first glance. In order to provide this interpretation, we turn to the second and third laws of black hole mechanics:

Theorem 2 (The 2^{nd} Law)**.** *The horizon area $A_{\mathcal{H}}$ is non-decreasing*

$$\mathrm{d}A_{\mathcal{H}} \geq 0 \tag{1.17}$$

provided the weak energy condition holds.

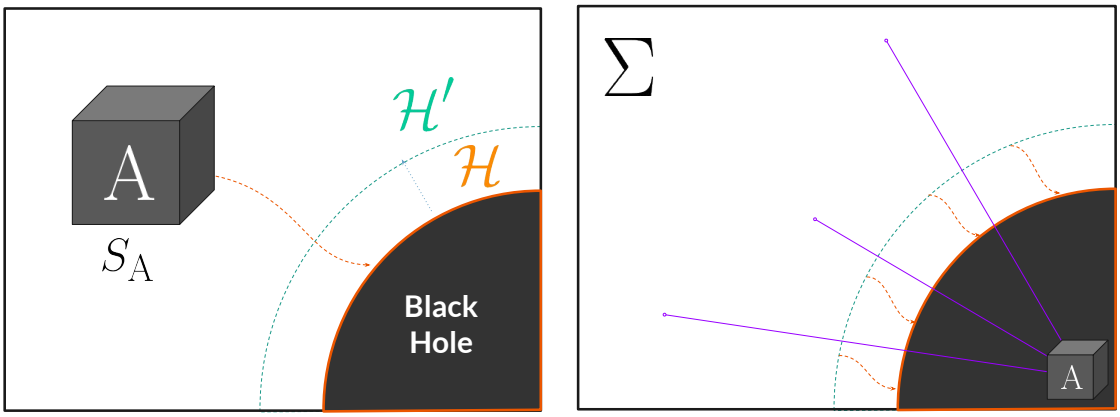

Figure 1.3: Left: A black box with entropy S_A falling into a black hole. The energy absorbed by the black hole causes the horizon to grow from $\mathcal{H} \to \mathcal{H}'$. Right: Hawking radiation emanating from a black hole. The quantum state on the interior are encoded in the outgoing Hawking radiation. The horizon shrinks are the information escapes.

Theorem 3 (The 3^{rd} Law)**.** *The surface gravity κ of the horizon cannot be reduced to zero in a finite number of steps.*

This second law is the statement of Hawking's area theorem [28]. Analogous to the second law of thermodynamics in which the entropy of an isolated system is non-decreasing, a black hole's area is also non-decreasing under a differential change. Furthermore, reducing the surface gravity to zero would require infinite energy as $\kappa = (4G_{\rm N}M)^{-1}$ is directly analogous to the infinite number of operations required to reduce the temperature of a closed system to zero. The proviso that the weak energy condition holds places a restriction on contribution from fields outside the horizon. Indeed, classical matter fields obey the weak energy condition, which stipulates that timelike observers see a non-negative energy density, or Hamiltonian density. Even in the simplest case of quantized scalar field theory, Casimir contributions need to be regulated before one has a meaningful positive definite Hamiltonian operator. As such, quantum fields generally violate this condition.

While these observations are suggestive of a connection, it is precisely in the arena where quantum fields and classical black holes coexist that geometry obtains a thermodynamic interpretation. Using Hawking's celebrated result [5] that black holes radiate at a temperature $T_{\rm H} = \frac{\kappa}{2\pi}$, one can write the first law as

$$\mathrm{d}M = T_{\rm H}\mathrm{d}\left(\frac{A_{\mathcal{H}}}{4G_{\rm N}}\right) + \Phi \mathrm{d}Q + \Omega \mathrm{d}J. \tag{1.18}$$

Observe that since quantum fields do not obey the weak energy condition, the second law of black hole mechanics is violated and the horizon area can decrease $\mathrm{d}A_{\mathcal{H}} < 0$. Since the surface gravity is always positive, an uncharged, non-rotating black hole would then lose mass $\mathrm{d}M \leq 0$ under a differential process. However, this is precisely consistent with

the phenomena of Hawking radiation. An asymptotic observer views the black hole at a temperature $T_{\rm H}$ evaporating away by an outgoing flux of Hawking radiation.

In order to maintain equilibrium, the outgoing flux of Hawking radiation would have to be balanced by an ingoing flux of energy. The simplest scenario is to consider placing the black hole in a geometry where the outgoing Hawking radiation is reflected at some potential barrier and falls back into the horizon, i.e., anti-de Sitter spacetime. In doing so, we recover a stationary system in which an evaporating classical black hole is in equilibrium with infalling Hawking radiation. Thus, the second law holds once again. This equilibrium naturally leads us to identifying an area-entropy law for a black hole

$$S_{\rm BH} = \frac{A_{\mathcal{H}}}{4G_{\rm N}}. \tag{1.19}$$

This is the Bekenstein-Hawking entropy of a black hole. Bekenstein was the first to propose that black holes, and generally objects with horizons, carry entropy proportional to their areas $S_{\rm BH} \propto A_{\mathcal{H}}/G_{\rm N}$ [1, 2]. Later, Hawking formulated a precise characterization of quantum fields in curved backgrounds and obtained a formula for the black hole temperature [4, 5]. Combining their *tour de force* calculations lead us inevitably to the realization that the laws of black hole mechanics are laws of thermodynamics applied to classical geometry.

In the next section, we demonstrate that the thermodynamics of classical geometries may be computed directly from the Euclidean gravitational path integral.

1.4 The Euclidean Gravitational Path Integral

The thermodynamics of classical geometries may be understood by studying the Euclidean path integral for gravity [8, 29, 30]. The canonical partition function for gravity at temperature $T = 1/\beta$ is given by

$$\mathcal{Z}(\beta) = \int [\mathcal{D}g][\mathcal{D}\Psi_i] e^{-\mathcal{I}[g,\Psi_i]} \tag{1.20}$$

where the integral is performed over all Riemannian metrics, and quantum fields, satisfying certain asymptotic fall-off conditions. The right-hand side also depends on β via the asymptotic periodicity which has to be satisfied by all geometries. In practice, the above partition function is difficult to evaluate in general. Instead, we may approximate the partition function using its classical saddle points as

$$\mathcal{Z}(\beta) \simeq e^{-\sum_j \mathcal{I}_j[g^*,\Psi_i^*]}. \tag{1.21}$$

The saddle point geometries $\mathcal{I}_j$ are solutions of the classical equations of motion of the action and are required to be regular. We denote $\mathcal{I}^* = \mathcal{I}_j[g^*, \Psi_i^*]$ as the normalized value of the classical action for j saddle point geometries and background matter fields. Given the

partition function, we can then calculate thermodynamic quantities using the standard definitions. In this introduction, we demonstrate how to find such saddle points, the computation of the thermodynamics, and phase transitions. This will serve as background to the two chapters in the part.

1.4.1 Gravitational Saddle Points

Here, we review the purely gravitational saddle points allowed for a $(d+2)$-dimensional, maximally symmetric, Lorentzian spacetime. Let $\mathcal{X}$ be a Lorentzian manifold and $\partial\mathcal{X}$ a codimension one boundary. We consider the theory

$$\mathcal{I} = -\frac{1}{8\pi G_{d+2}} \times [\mathcal{S}_{\mathcal{X}} + \mathcal{S}_{\partial\mathcal{X}}] \tag{1.22}$$

where the bulk and the boundary actions are respectively

$$\mathcal{S}_{\mathcal{X}} = \frac{1}{2}\int_{\mathcal{X}} \mathrm{d}^{d+2}x\sqrt{-g}[R - 2\Lambda], \tag{1.23}$$

$$\begin{aligned}\mathcal{S}_{\partial\mathcal{X}} = \int_{\partial\mathcal{X}} \mathrm{d}^{d+1}x\sqrt{-h}\Bigg[\mathcal{K} + \frac{d+1}{\ell^2} + c_1(d)\mathcal{R} \\ + c_2(d)\Big(\mathcal{R}_{ab}\mathcal{R}^{ab} - c_3(d)\mathcal{R}^2\Big) + \cdots\Bigg].\end{aligned} \tag{1.24}$$

The boundary action is comprised of the canonical Gibbons-Hawking term [29] and additional counterterms [31]. The first is necessary for a well-posed variational principle and the second is requried to regularize the bulk action. Here $\Lambda = \pm d(d+1)/2\ell^2$, $R(g)$ is the scalar curvature, and $\mathcal{K}$ and $\mathcal{R}$ are the extrinsic and scalar curvatures of the boundary metric h respectively. Note that higher curvature corrections to the boundary action appear in $d \geq 6$ and the coefficients $c_i(d)$ are sensitive to the dimension and the symmetries of the bulk spacetime. The equations of motion for the above action and the respective trace yield

$$R_{ab} - \frac{1}{2}g_{ab}R + \Lambda g_{ab} = 0 \tag{1.25}$$

$$\frac{d}{2}R - (d+2)\Lambda = 0 \tag{1.26}$$

from which the on-shell bulk action then simplifies considerably to a single volume integral

$$\mathcal{S}_{\mathcal{X}} = \frac{1}{2}\int_{\mathcal{X}} \mathrm{d}^{d+2}x\sqrt{-g}\left(\frac{4\Lambda}{d}\right) = \frac{2\Lambda}{d}\mathrm{Vol}(\mathcal{X}). \tag{1.27}$$

Hence, the bulk contribution to the gravitational path integral is a given by divergent volume factor. There are two distinct divergent contributions. The first is purely topological, e.g., if the maximally symmetric spacetime has flat or hyperbolic directions. The second, more universal contribution, is integrating the time direction from its initial data

to the infinite future. While the boundary action $\mathcal{S}_{\partial\mathcal{X}}$ regulates the spatial divergence, the temporal divergence will have to be controlled via analytic continuation as shown below.

Let us now compute the action $\mathcal{I}$ along its time independent saddle points. The $(d+2)$-dimensional, maximally symmetric, static general solutions are

$$\mathrm{d}s^2 = -f(r)\mathrm{d}t^2 + \frac{\mathrm{d}r^2}{f(r)} + \frac{r^2}{\ell^2}\mathrm{d}\Sigma_{d,k}^2 \tag{1.28}$$

$$f(r) = k - \frac{m}{r^{(d-1)}} \mp \frac{r^2}{\ell^2}. \tag{1.29}$$

The upper branch of Eqn. (1.29) corresponds to Anti-de Sitter (AdS) spacetime, a maximally symmetric, static solution with negative cosmological constant $\Lambda < 0$. Whereas, the lower branch corresponds to a de Sitter (dS) spacetime with a postive cosmological constant. In the $\ell \to \infty$ limit ($\Lambda \to 0$), both spacetimes converge onto the familiar asymptotically flat, Minkowski solution.

Furthermore, there are two relevant parameters m and k. Here, k denotes the various topologies which are consistent with the isometries of (A)dS$_{d+2}$ or Mink$_{d+2}$ spacetime. In particular,

$$\mathrm{d}\Sigma_{d,k}^2 = \begin{cases} \ell^2\mathrm{d}\Omega_d^2 & \text{for } \ k=1, \\ \sum\limits_{i=1}^{d} \mathrm{d}x_i^2 & \text{for } \ k=0, \\ \ell^2\mathrm{d}\Xi_d^2 & \text{for } \ k=-1, \end{cases} \tag{1.30}$$

where $\mathrm{d}\Omega_d^2$ and $\mathrm{d}\Xi_d^2$ are the unit metrics on S^d and H^d. Thus $k = \{+1, 0, -1\}$ represents spherical, planar, and hyperbolic topologies respectively.

To understand m, we first denote by r_+ the outer horizon which is located at the largest positive root of $f(r_+) = 0$. Then the parameter m is given by

$$m = r_+^{d-1}\left(k \mp \frac{r_+^2}{\ell^2}\right) \tag{1.31}$$

and may be dentified with the ADM mass of the spacetime

$$M_{\mathrm{ADM}} = \frac{d\,\sigma_{d,k}}{16\pi G_{d+2}} m \tag{1.32}$$

where $\sigma_{d,k}$ is the unit-volume of the codimension two base space. For physically relevant static saddle points, the ADM mass should be non-negative $M_{\mathrm{ADM}} \geq 0$ and hence $m \geq 0$. This restriction on the saddle points eliminates several candidates solutions. In particular, since $k \mp r_+^2/\ell^2 \geq 0$, solutions with hyperbolic symmetry are not allowed in Mink$_{d+2}$. Similarly, solutions without spherical symmetry in dS$_{d+2}$ are eliminated as vaiable on-shell contributions to the gravitational path integral. However, all topologies are permitted in AdS$_{d+2}$ provided $r_+^2/\ell^2 \geq -k$.

Henceforth, in much of the following dissertation, we will focus on AdS_{d+2} spacetimes. We refer to solutions with $m > 0$ as Schwarzschild-AdS_{d+2} (SAdS_{d+2}) black holes or, in the case where $\ell \to \infty$, $\mathrm{Schwarzchild}_{d+2}$ (Sch_{d+2}) black holes.

1.4.2 Euclidean AdS Gravity and Thermodynamics

Now, we turn to computing the thermodynamic properties of SAdS_{d+2} black holes. To do so, we perform an analytic continuation of time into the Euclidean section $t \to \mathrm{i}\tau$. This serves two purposes. First, it resolves the issue of the divergent time integral in $\mathrm{Vol}(\mathcal{X})$ as now the "Euclidean" time coordinate is periodic $\tau \sim \tau + \beta$ with period β. Secondly, this procedure identifies the temperature via $\beta = 1/T$. Observe, using $f(r_+) = 0$, we may expand the metric near the horizon to find

$$\mathrm{d}s^2 = f'(r_+)(r - r_+)\mathrm{d}\tau^2 + \frac{\mathrm{d}r^2}{f'(r_+)(r - r_+)} + \cdots \tag{1.33}$$

$$= R^2\mathrm{d}\phi^2 + \mathrm{d}R^2 + \cdots \tag{1.34}$$

where we have omitted the symmetric base and have transformed coordinates to

$$R^2 = \frac{4(r - r_+)}{f'(r_+)}, \qquad \phi = \frac{f'(r_+)}{2}\tau. \tag{1.35}$$

In order to aviod a conical singularity in the Euclidean section, ϕ must be periodic with period 2π, i.e., $\phi(\tau) \sim \phi(\tau + 2\pi)$. Thus, we must have $\tau \sim \tau + \frac{4\pi}{f'(r_+)}$. Hence, this Euclidean trick yields the temperature

$$\beta^{-1} = T = \frac{f'(r_+)}{4\pi} = \frac{(d-1)k}{4\pi r_+} + \frac{(d+1)r_+}{4\pi\ell^2}. \tag{1.36}$$

The remaining thermodynamic quantities are

$$\mathcal{I}^* = \beta\frac{\sigma_{d,k}}{16\pi G_{d+2}}\left[r_+^{d-1}\left(k - \frac{r_+^2}{\ell^2}\right)\right] - \mathcal{I}_k^0, \tag{1.37}$$

$$E = \frac{\partial\mathcal{I}}{\partial\beta} = \frac{d\,\sigma_{d,k}}{16\pi G_{d+2}}m - E_k^0 = M_{\mathrm{ADM}} - E_k^0, \tag{1.38}$$

$$S = \frac{A(\mathcal{H})}{4G_{d+2}} = \frac{\sigma_{d,k}r_+^d}{4G_{d+2}} \tag{1.39}$$

Hence, we see that the ADM mass of the black hole is indeed the energy of the spacetime. Here, we have evaluated the action on-shell using the metric Eqn. (1.28) and have used the Bekenstein-Hawking formula.

For $k = +1, 0$, the thermodynamics and the on-shell Euclidean action can either be calculated with the usual counterterm method [31] or through a background subtraction technique. The background subtraction identifies the locally AdS_d space, i.e., $m = 0$, as the reference ground state in which case $r_{+,k} = 0$. However, with $k = -1$, the locally AdS_d

solution contains a bifurcate Killing horizon at $r_c = \ell$ at a fixed temperature. In this case, performing either a background subtraction or utilizing the counterterm method introduces a conical singularity. These singularities are removed when one subtracts an extremal saddle leading to the corrections $\mathcal{I}_k^0$.

1.4.3 Hawking-Page Phase Transitions in AdS

The classical and thermodynamic stability of these solutions have been rigorously explored in Refs. [32–34]. The heat capacity for these solutions is

$$C = \frac{d\sigma_{d,k}}{4G_{d+2}} r_+^d \left(\frac{(d+1)r_+^2 + (d-1)k\ell^2}{(d+1)r_+^2 - (d-1)k\ell^2} \right). \tag{1.40}$$

We see that, for non-positive k, the heat capacity is always non-negative indicating planar, and hyperbolic black holes are thermodynamically stable. For $k = -1$, the heat capacity vanishes precisely when $r_{+,c} = \sqrt{(d-1)/(d+1)}\ell$. For $k = 1$, the SAdS_{d+2} black hole competes with thermal AdS_{d+2} saddle and undergoes a phase transition precisely when the free energy $\mathcal{F} = \mathcal{I}/\beta = 0$, i.e., when $r_{+,c} = \ell, T_c \equiv T(r_{+,c})$.

This completes the background on the thermodynamics of classical gravity. In the following chapters, I explain my findings on exotic liquid-gas phase transitions for gravity in lower dimensions and demonstrate that thermodynamic instabilities are related to classical instabilities for SAdS black holes with planar directions.

Chapter 2

Criticality of Lower Dimensional AdS$_d$ Black Holes

This chapter is a faithful reproduction of the published work **A. Dhumuntarao and R. Mann, Phys. Rev. D 104, 064006 (2021)** with minor edits [35].

Abstract

In lower dimensions, charged AdS black holes in an extended phase space, where the cosmological constant is interpreted as the thermodynamic pressure, are typically absent of liquid/gas phase transitions. We investigate the criticality of lower dimensional charged, dilatonic, asymptotically AdS (CDAdS$_d$) black holes generated from consistent truncations of RNAdS$_{d+2}$ black objects. We demonstrate that CDAdS$_d$ black holes in $d < 4$ can exhibit rich van der Waals behavior and confirm that the associated critical exponents match those expected from mean field theory.

2.1 Introduction

In recent years, black hole chemistry has substantially sharpened the connection between the thermodynamics of AdS black holes and ordinary fluid systems. For rotating, charged black holes with mass M, angular momentum J, and charge Q, it is well known that the first law of black hole mechanics

$$\mathrm{d}M = \frac{\kappa}{8\pi}\mathrm{d}A + \Omega \mathrm{d}J + \Phi \mathrm{d}Q \tag{2.1}$$

is identical to the first law of thermodynamics provided one makes the identifications and temperature $T = \kappa/2\pi$, between surface gravity κ and temperature T, and $S = A/4$ between horizon area A and entropy S [1, 2, 4, 5]. However, a notable omission in the first law of black hole thermodynamics is a pressure-volume term, which canonically lacks a gravitational interpretation in spacetimes without a cosmological constant Λ. The

fundamental idea of black hole chemistry is to extend the thermodynamic phase space by promoting the cosmological constant of AdS spacetimes to a thermodynamic variable

$$P = -\frac{\Lambda}{8\pi} \tag{2.2}$$

with a corresponding conjugate volume, V [36–40].

The motivation for this identification is twofold. First, it was observed that the Smarr relation [41] is no longer satisfied in spacetimes with a cosmological constant [37, 42]. By extending the thermodynamic phase space, the resulting pressure-volume term was found to saturate the Smarr relation. Secondly, the phase diagram of Einstein-Maxwell-AdS$_d$ theory has long been known to contain classic swallowtail and cusp behavior suggestive of a van der Waals liquid-gas phase transition for $d \geq 4$ [32, 33]. The program of black hole chemistry has completed this analogy by demonstrating that the equation of state for charged Reissner-Nördstrom AdS$_d$ (RN-AdS$_d$) black holes shares identical critical behavior at the second order transition point and universal compressibility ratio in $d = 4$ to a van der Waals fluid [43, 44]. To date, the correspondence between black hole chemistry and real world fluid systems has yielded an interesting array of thermodynamic features in $d \geq 4$, including reentrant phase transitions [44, 45], and tricritical points analogous to triple points in the phase diagram of water [46].

In contrast to the numerous explorations in $d \geq 4$, black hole chemistry in lower dimensions is not as thermodynamically rich. Indeed, the phase diagram of Einstein-Maxwell-AdS$_d$ revealed that charged black holes in $d < 4$ have ideal gas like behavior [44, 47, 48]. In $d = 3$, the charged BTZ$_3$ black hole solution was observed to be absent of critical behavior [44] and shown to violate the Smarr relation unless additional thermodynamic work terms are introduced [49]. Furthermore, in $d = 2$, the lack of an area also significantly impacts the canonical definitions of entropy, and thermodynamic volume [49]. In general, pure gravity in lower dimensions is topological and lacks the necessary degrees of freedom to support critical behavior. Hence, an outstanding challenge is to find lower dimensional black holes that support non-trivial van der Waals behavior and obey canonical Smarr scalings.

In this paper, we resolve this tension by identifying thermodynamically rich, charged, dilatonic, asymptotically AdS black hole solutions to the action

$$\mathcal{I} = -\int \left[\frac{1}{2}(\nabla\psi)^2 + \frac{\psi^2}{4}(R - 2\Lambda - \mathcal{L}) + \frac{\lambda}{4}\right]\sqrt{-g}\mathrm{d}^d x$$

in $d < 4$. In Section II, we first review criticality of charged black holes in $d \geq 4$ paying close attention to the emergent van der Waals behavior. In Section III, we consider consistent truncations of higher dimensional gravity theories admitting RNAdS$_{d+2}$ black objects and search for black hole solutions to the effective action in $d < 4$. Using lower dimensional techniques in conjunction with Euclidean methods, we explore the thermodynamics of these solutions in the extended phase space. We confirm that the Smarr

relation is satisfied in each case and that the equations of state contain local minima indicative of a van der Waals phase transition.

2.2 PV Criticality of Charged AdS$_d$ Black Holes in $d \geq 4$

To set the stage for studying black hole chemistry in lower dimensions, we review some salient features of the Reissener-Nördstrom solution to Einstein-Maxwell-AdS$_d$ theory in the extended phase space. We describe the thermodynamics in $d \geq 4$ and study the corresponding equation of state. We then conclude by remarking on the critical behavior and exponents.

2.2.1 Criticality of RN-AdS$_d$ Black Holes in $d \geq 4$

To demonstrate criticality of charged black holes, the natural starting point is to study the thermodynamics of Einstein-Maxwell-AdS$_d$ theory in $d \geq 4$. This theory has been thoroughly analyzed in diverse dimensions with the on-shell regularized Euclidean action first calculated in [32, 33]. Explorations of these black holes in an extended phase space were considered in [44, 50]. The bulk action in d-dimensions reads

$$\mathcal{I} = -\frac{1}{16\pi}\int \left[R - 2\Lambda - F^2\right] \mathrm{d}^d x\sqrt{-g} \tag{2.3}$$

with $\Lambda = -(d-2)(d-1)/2\ell^2$ being the cosmological constant. The RN-AdS$_d$ solution, in static coordinates, and the purely electric $U(1)$ gauge field are then

$$\mathrm{d}s^2 = -f(r)\mathrm{d}t^2 + \frac{\mathrm{d}r^2}{f(r)} + r^2\mathrm{d}\Omega_{d-2}^2 \tag{2.4}$$

$$F = \mathrm{d}A, \quad A = \frac{1}{c}\frac{q}{r^{d-3}}\mathrm{d}t \tag{2.5}$$

where $\mathrm{d}\Omega_n^2$ indicates the metric on the n-dimensional sphere, $c = \sqrt{2(d-3)/(d-2)}$, and the metric function has the form

$$f(r) = 1 - \frac{m}{r^{(d-3)}} + \frac{q^2}{r^{2(d-3)}} + \frac{r^2}{\ell^2}. \tag{2.6}$$

Here, the outer horizon r_+ is located at the largest positive root of $f(r_+) = 0$. The parameters m and q appearing in the metric function are related to the ADM mass and the total charge [32] of the black hole

$$M = \frac{(d-2)\,\omega_{d-2}}{16\pi}m, \tag{2.7}$$

$$Q = \sqrt{2(d-2)(d-3)}\frac{\omega_{d-2}}{8\pi}q, \tag{2.8}$$

where ω_n is the volume of the unit n-dimensional sphere,

$$\omega_n = \frac{2\pi^{\frac{n+1}{2}}}{\Gamma(\frac{n+1}{2})}. \tag{2.9}$$

The standard thermodynamic quantities are then

$$T = \frac{f'(r_+)}{4\pi} = \frac{d-3}{4\pi r_+} + \frac{(d-1)r_+}{4\pi\ell^2} - \frac{(d-3)q^2}{4\pi r_+^{2d-5}} \tag{2.10}$$

$$S = \frac{A(\mathcal{H})}{4} = \frac{\omega_{d-2}r_+^{d-2}}{4} \qquad \Phi = \frac{1}{c}\frac{q}{r_+^{d-3}}. \tag{2.11}$$

In the formalism of the extended phase space [43, 44, 50], the cosmological constant Λ is identified with the thermodynamic pressure of the system via

$$P = -\frac{\Lambda}{8\pi} = \frac{(d-2)(d-1)}{16\pi\ell^2}. \tag{2.12}$$

It is then natural to reinterpret the black hole mass as the enthalpy rather than the internal energy and consider a thermodynamic volume conjugate to the pressure

$$V = \left.\frac{\partial M}{\partial P}\right|_{S,Q} = \frac{\omega_{d-2}r_+^{d-1}}{d-1}. \tag{2.13}$$

In $d > 4$, these quantities satisfy the Smarr formula as well as the (extended phase-space) $1st$ law of black hole thermodynamics

$$M = \frac{d-2}{d-3}TS + \Phi\, Q - \frac{2}{d-3}VP \tag{2.14}$$

$$\mathrm{d}M = T\,\mathrm{d}S + \Phi\,\mathrm{d}Q + V\,\mathrm{d}P. \tag{2.15}$$

The identification of a pressure term invites a reintrepretation of the black hole temperature, Eqn. (2.10), as an equation of state [44]

$$P = \frac{(d-2)T}{4r_+} - \frac{(d-3)(d-2)}{16\pi r_+^2} + \frac{(d-3)(d-2)q^2}{16\pi r_+^{2(d-2)}} \tag{2.16}$$

where we have used Eqn. (2.12). To make contact with the van der Waals equation of state, one must identify the specific volume of the corresponding fluid [43]. In the context of black hole chemistry, the specific volume v is defined by the total volume of the black hole via [44, 50]

$$V = \frac{\omega_{d-2}}{d-1}\left(\frac{d-2}{4}\right)^{d-1} v^{d-1}. \tag{2.17}$$

Hence, by employing the definitions of P, T, and v, one finds an equation of state for charged black holes

$$P = \frac{T}{v} - \frac{(d-3)}{(d-2)\pi v^2} + \frac{(d-3)q^2}{4\pi v^{2(d-2)}\kappa^{2d-5}} \tag{2.18}$$

where $\kappa = (d-2)/4$ [44]. The liquid/gas phase transition experienced by van der Waals fluids is now mapped onto a small-large black hole phase transition in the system for temperatures $T < T_c$ for all $d \geq 4$. The critical points in the equation of state occur at stationary points of inflection in the $P - v$ diagram given by

$$\frac{\partial P}{\partial v} = 0, \qquad \frac{\partial^2 P}{\partial v^2} = 0. \tag{2.19}$$

The critical triple (P_c, T_c, v_c) have the values

$$\begin{aligned} T_c &= \frac{(d-1)^2}{\pi \kappa v_c (2d-1)}, \qquad P_c = \frac{(d-1)^2}{16\pi\kappa^2 v_c^2}, \\ v_c &= \frac{1}{\kappa}\Big[q^2 d(2d-1)\Big]^{\frac{1}{2(d-1)}}. \end{aligned} \tag{2.20}$$

Analogous to the construction of the universal ratio found for van der Waals fluids, the above triple yields

$$\frac{P_c v_c}{T_c} = \frac{2d-5}{4d-8}. \tag{2.21}$$

For RN-AdS$_4$, i.e., when $d = 4$, one recovers the canonical result of the van der Waals compressibility ratio $P_c v_c / T_c = 3/8$.

2.2.2 Critical Exponents

Given that the equation of state not only reproduces van der Waals behavior but also the universal compressibility ratio, it is natural to consider the critical exponents calculated in the vicinity of the critical point. To compute critical exponents, we define

$$p = \frac{P}{P_c}, \qquad \nu = \frac{v}{v_c} \qquad \tau = \frac{T}{T_c} \tag{2.22}$$

which translates the equation of state into a 'law of corresponding states' analogous to the same function appearing in van der Waals theory, we have [44]

$$p = \frac{4(d-2)}{(2d-5)}\frac{\tau}{\nu} - \frac{(d-2)}{(d-3)\nu^2} + \frac{\nu^{-2(d-2)}}{(d-3)(2d-5)}. \tag{2.23}$$

Note that the only functional dependence on the dimension appears in the last term. As we will demonstrate shortly, the critical exponents are independent of the dimension in $d \geq 4$. This is analogous to the situation in mean field theory where the critical exponents are again independent of the dimension above the upper critical dimension. In this context, this suggests that any equation of state which admits a 'law of corresponding states' of the above form will have critical exponents consistent with mean field theory.

To observe this, we may consider an expansion of this equation near the critical point

$$\tau = 1 + t, \qquad \nu = (1+\omega)^{1/z} \tag{2.24}$$

where $z = d - 1 > 0$. It may be shown that the pressure admits the following expansion

$$p = 1 + A_d t - B_d t\omega - C_d \omega^3 + \mathcal{O}(t\omega^2, \omega^4). \tag{2.25}$$

where the coefficients satisfy $A_d, B_d, C_d > 0$ and depend on the dimension in the following way

$$A_d = \frac{4d-8}{2d-5}, \quad B_d = \frac{4d-8}{(2d-5)(d-3)}, \quad C_d = \frac{2d-4}{3(d-1)^3}. \tag{2.26}$$

Differentiating the series at a fixed $t < 0$, we obtain the following differential of the pressure

$$\frac{\mathrm{d}p}{\mathrm{d}\omega} = -(B_d t + 3C_d \omega^2). \tag{2.27}$$

Then employing Maxwell's equal area law, see [43], the following system of equations emerge for the 'volume' of small and large black holes, ω_s and ω_l respectively,

$$\begin{aligned} p &= 1 + A_d t - B_d t\omega_l - C_d \omega_l^3 = 1 + A_d t - B_d t\omega_s - C_d \omega_s^3 \\ 0 &= -\int_{\omega_l}^{\omega_s} \omega(B_d t + 3C_d \omega^2)\mathrm{d}\omega \end{aligned} \tag{2.28}$$

The unique solution relates the two volumes via

$$\omega_s = -\omega_l = \sqrt{\frac{B_d|t|}{C_d}}. \tag{2.29}$$

Given these definitions, we are now in a position to define the critical exponents α, β, γ, and δ. The exponent α describes the behavior of the specific heat at constant volume via

$$C_v = T\frac{\partial S}{\partial T}\bigg|_v \propto |t|^{-\alpha}. \tag{2.30}$$

Using the volume, Eqn. (2.13), in conjunction with the entropy $S \equiv S(T, V)$, Eqn. (2.11), we have

$$S(T, V) = \omega_{d-2}^{\frac{1}{d-1}}[(d-1)V]^{\frac{(d-2)}{(d-1)}} \tag{2.31}$$

which sets $\alpha = 0$ as the entropy is independent of the temperature in the canonical ensemble. Next, β describes the behavior of the order parameter η, which is the difference of the volume of the gas v_g phase and the volume of the liquid phase v_l, on a given isotherm

$$\eta = V_c(\omega_l - \omega_s) \propto |t|^{\beta} \implies \beta = \frac{1}{2}. \tag{2.32}$$

Using Eqn. (2.29), we have $\eta = 2V_c\omega_l \propto \sqrt{|t|}$ thereby setting $\beta = (1/2)$. Next, the exponent γ determines the behavior of the isothermal compressibility defined by

$$\kappa_T = -\frac{1}{V}\frac{\partial V}{\partial p}\bigg|_T \propto |t|^{-\gamma} \tag{2.33}$$

which yields $\gamma = 1$ after a direct computation using Eqn. (2.27). Lastly, δ governs the behavior of the critical isotherm via

$$|p-1| \propto |v-v_c|^{\delta}. \tag{2.34}$$

The 'shape of the critical isotherm' is then straightforward to obtain by evaluating the series, Eqn. (2.25), at $t = 0$ yielding $\delta = 3$. Collecting our results, we see that RN-AdS$_d$ black holes have the critical exponents

$$\alpha = 0, \quad \beta = \frac{1}{2}, \quad \gamma = 1, \quad \delta = 3 \tag{2.35}$$

matching precisely with a mean field theory analysis of a van der Waals fluid. This behavior may also be extended to include rotations [44].

2.3 PV Criticality in Lower Dimensions

PV criticality is sensitive to the horizon topology. To make this observation sharp, consider the equation of state for RN-AdS$_d$ black holes with maximally symmetric horizons in $d \geq 4$

$$P = \frac{T}{v} - \frac{(d-3)\hat{k}}{(d-2)\pi v^2} + \frac{(d-3)q^2}{4\pi v^{2(d-2)}\kappa^{2d-5}}. \tag{2.36}$$

For non-spherically symmetric horizons ($\hat{k} \neq 1$), the equation of state no longer contains a local minimum [43] in which case these black hole solutions do not satisfy the condition Eqn. (2.19) thereby precluding critical behavior.

In lower dimensions, Einstein-Maxwell-AdS$_d$ gravity has insufficient spherical symmetry to support PV criticality. In $d = 3$, for example, the theory admits the charged BTZ black hole solution [47, 48] with a planar horizon topology, $\hat{k} = 0$, which may be compactified onto an S^1 by coordinate transformations. Indeed, studies of the charged BTZ equation of state [44], and its rotating generalization [49], confirms the lack of critical behavior is tied to the horizon topology rather than the logrithmic behavior of electromagnetism. In $d = 2$, Einstein-Maxwell-AdS$_d$ gravity is purely topological as the Einstein-Hilbert term in the action, Eqn. (2.3), is related to the Euler characteristic of the spacetime and the metric is conformally flat without a black hole present. Therefore the theory is not as thermodynamically rich, and it becomes necessary to study dilaton gravity models to source black holes in $d = 2$. A general class of dilaton-gravity actions coupled to additional scalar fields Φ_M fall within the category [51, 52]

$$\mathcal{I} = -\int \Big[H(\psi)(\nabla\psi)^2 + D(\psi)R + V(g,\psi,\Phi_M)\Big]\sqrt{-g}\mathrm{d}^2x. \tag{2.37}$$

Presently, the dilaton-gravity model with $H(\psi) = (1/2)$, $D(\psi) = \psi$, and $V(\psi, \Phi_M) = -2\Lambda$ is the only known example to us to be studied in the context of black hole

chemistry [49]. Although this model was observed to admit asymptotically AdS$_d$ black holes with constant charge, the pressure equation of state was nonetheless absent of critical behavior due to the point-like structure of the horizon.

Clearly, gravity in lower dimensions requires, at a minimum, additional degrees of freedom equal to those provided by an S^2 to support non-trivial van der Waals behavior. One natural way that lower dimensional gravity can inherit such degrees of freedom is through consistent truncations of higher dimensional gravity theories. Consider the simplest theory of Einstein-AdS$_{d+2}$ gravity coupled to a matter Lagrangian

$$\mathcal{I} = -\frac{1}{16\pi}\int \left[\tilde{R} - 2\Lambda - \mathcal{L}\right]\sqrt{-\tilde{g}}\mathrm{d}^{d+2}x \tag{2.38}$$

where $\Lambda = -d(d+1)/2\ell^2$, $\tilde{g}_{MN}$ is the metric, and $\tilde{R}$ is the Ricci scalar. We assume the above action admits spacetimes that fiber into $\mathcal{M}_d \times S^2$ according to the ansatz

$$\mathrm{d}s^2_{d+2} = \tilde{g}_{MN}\mathrm{d}x^M\mathrm{d}x^N = g_{ab}\mathrm{d}x^a\mathrm{d}x^b + \psi^2(x^a)\mathrm{d}\Omega_2^2 \tag{2.39}$$

with matter fields taking values on $\mathcal{M}_d$. Integrating out the spherical directions, the truncated theory is (App. A.1)

$$\mathcal{I} = -\int\left[\frac{1}{2}(\nabla\psi)^2 + \frac{\psi^2}{4}(R - 2\Lambda - \mathcal{L}) + \frac{\lambda}{2}\right]\sqrt{-g}\mathrm{d}^dx. \tag{2.40}$$

The spherical directions now descend into lower dimensions via dilaton-gravity couplings. Here, $\lambda = R_{S^2}/2$, where the R_{S^2} is the scalar curvature of the round unit two-sphere and henceforth, we set $\lambda = 1$. Clearly, this action is a special case of Eqn. (2.37) extended to d-dimensions. The quadratic mass term $\sim \psi^2(R - 2\Lambda - \mathcal{L})$ preserves the transverse spherical degrees of freedom allowing for metric and gauge fields to have a leading order fall off as $\mathcal{O}(1/r^{d-1})$ akin to RN-AdS$_{d+2}$ black holes.

In what follows, we will concentrate on the action Eqn. (2.40) in $d = 2, 3$ and search for charged, dilatonic, asymptotically AdS$_d$ (CDAdS$_d$) solutions to the equations of motion,

$$0 = \Box\psi - \frac{\psi}{2}(R - 2\Lambda - \mathcal{L}), \tag{2.41}$$

$$0 = \frac{\psi^2}{4}G_{ab} - T_{ab} \tag{2.42}$$

where $G_{ab} = R_{ab} - (R/2)g_{ab}$ is the Einstein tensor and the stress-energy tensor is

$$\begin{aligned} T_{ab} = &-\frac{1}{2}\left(\nabla_a\psi\nabla_b\psi - \frac{1}{2}g_{ab}[(\nabla\psi)^2 - \Lambda\psi^2]\right) \\ &+ \frac{1}{4}\left[\nabla_a\nabla_b\psi^2 - g_{ab}\Box\psi^2\right] + \frac{\psi^2}{2}T^{\mathcal{L}}_{ab} + \frac{1}{4}g_{ab}. \end{aligned} \tag{2.43}$$

We compute the thermodynamics using a combination of lower dimensional techniques and the on-shell Euclidean action. Using the extended phase space, we demonstrate that CDAdS$_d$ black holes admit PV criticality and have critical exponents which match those expected from mean field theory.

2.3.1 Van der Walls Behavior in $d = 2$

Here, we consider an Einstein-Maxwell-Dilaton-AdS action with $\mathcal{L} = F^2$ in $d = 2$. The uplift of this theory to $4d$ corresponds to Eqn. (2.3) for which the RN-AdS$_4$ black hole, Eqn. (2.4), is a solution. We search for the consistently truncated black hole solution in $d = 2$ and concentrate on static, purely electric, and radial solutions to the field equations (2.41)-(2.43) with the ansatz

$$\mathrm{d}s^2 = g_{ab}\mathrm{d}x^a\mathrm{d}x^b = -f(r)\mathrm{d}t^2 + f(r)^{-1}\mathrm{d}r^2, \tag{2.44}$$

$$A \equiv A(r)\mathrm{d}t \qquad \psi \equiv \psi(r). \tag{2.45}$$

For the Maxwell Lagrangian, the stress-energy contribution and equation of motion are

$$T^{\mathcal{L}}_{ab} = F_{ac}F_b{}^c - \frac{1}{4}g_{ab}F^2, \qquad \nabla_a(\psi^2 F^{ab}) = 0. \tag{2.46}$$

Given this ansatz, the general solution reads

$$f(r) = 1 - \frac{\Lambda r^2}{3} - \frac{\mu}{r} + \frac{\rho^2}{r^2}, \tag{2.47}$$

$$F = \mathrm{d}A, \quad A = -\frac{\rho}{r}\mathrm{d}t, \quad \psi(r) = r. \tag{2.48}$$

Inserting $\Lambda = -3/\ell^2$, the horizon is given by the largest, real, positive root of

$$f(r_+) = 1 + \frac{r_+^2}{\ell^2} - \frac{\mu}{r_+} + \frac{\rho^2}{r_+^2} = 0. \tag{2.49}$$

which imposes $\mu > 0$.

In lower dimensions, computing the thermodynamics requires some care. We follow the procedure outlined in [51, 52] to determine the mass and charge in terms of μ and ρ in $d = 2$. The chemical potential may be computed using standard holographic arguments [32]. The entropy is more subtle, as the area of the horizon is reduced to a point. We use the prescription outlined by Wald which may be formally applied in any dimension $d \geq 2$ [53, 54]. We compare these quantities against an on-shell evaluation of the Euclidean action to confirm their interpretation and then study PV criticality.

For dilaton-gravity theories of the form Eqn. (2.37), it was demonstrated that in $d = 2$ the current $\mathcal{J}_a \equiv T_{ab}\xi^b$ is conserved regardless of whether the stress-energy is conserved or if ξ^a is a Killing vector [51]. Such a conserved current exists provided that $\xi^a \equiv \epsilon^{ab}\nabla_b\mathcal{F}(D, H)$ is chosen to conserve T_{ab} along its flow lines. Then, since a divergenceless current is always dual to the gradient of a scalar, the black hole mass may be computed via [51]

$$M = \int \epsilon_{ab}\mathcal{J}^a\mathrm{d}x^b = \int \epsilon_{ab}T^a{}_c\xi^c\mathrm{d}x_b. \tag{2.50}$$

For Eqn. (2.40), it is possible to show $\xi^a = (1, 0)$. Then evaluating Eqn. (2.43) along Eqn. (2.47), the mass reads

$$M = \frac{\mu}{2}. \tag{2.51}$$

Next, it has been shown [52] that for $2d$ dilaton-gravity theories that are coupled to a $U(1)$ gauge field, the total charge may be computed via

$$Q = \frac{\psi^2}{\sqrt{-g}} F_{10} = \rho \tag{2.52}$$

The corresponding chemical potential is then given by considering the electrostatic potential difference between the horizon and infinity via [32]

$$\Phi = \int_{r_+}^{\infty} \mathrm{d}r F_{10} = \frac{\rho}{r_+}. \tag{2.53}$$

Finally, it is well known that an entropy can be associated with $2d$ black holes by considering an 'area' associated with the codimension two surface to the $t-r$ disk [49]. A collapsing fluid in $2d$ contains a single point as its boundary on the half line $r > 0$; analogously the codimension two boundary of a black hole corresponds to an horizon-point, r_+, which has area unity. The Bekenstein-Hawking entropy of the horizon-point is $S_{\mathrm{BH}} = (1/4)$. However, this entropy conflicts with the one obtained from the Euclidean action.

An alternative definition of the entropy may be provided by the Wald formula [53]. In $2d$, the Wald entropy may formally be computed on the codimension two surface to the $t-r$ disk [54], i.e., the horizon. We find

$$S_{\mathrm{Wald}} = -2\pi \frac{\delta \mathcal{I}}{\delta R^{abcd}} \epsilon_{ac} \epsilon_{bd} \Big|_{r_+} = \pi r_+^2. \tag{2.54}$$

In order to confirm the interpretation of these quantities, we consider the on-shell Euclidean action in the canonical ensemble. Rotating the solution into the Euclidean section, $t \to \mathrm{i}\tau$, we find that the counterterm method yields the on-shell Euclidean action (see App.A.1)

$$\bar{\mathcal{I}} = \frac{\beta}{4} \left(r_+ - \frac{r_+^3}{\ell^2} + 3 \frac{\rho^2}{r_+} \right) \tag{2.55}$$

where β denotes the period the Euclidean section

$$\beta = \frac{4\pi}{\partial_r f} \Big|_{r=r_+} = \frac{4\pi r_+^3 \ell^2}{(r_+^2 - \rho^2)\ell^2 + 3r_+^4}. \tag{2.56}$$

The corresponding thermodynamic quantities are

$$M = \frac{\partial \bar{\mathcal{I}}}{\partial \beta} \Big|_Q = \frac{\mu}{2}, \tag{2.57}$$

$$\Phi = \frac{1}{\beta} \frac{\partial \bar{\mathcal{I}}}{\partial Q} \Big|_\beta = \frac{\rho}{r_+}, \tag{2.58}$$

$$S = \frac{\partial \bar{\mathcal{I}}}{\partial \beta} \Big|_Q - \bar{\mathcal{I}} = \pi r_+^2 \tag{2.59}$$

precisely matching Eqns (2.51)–(2.54).

This completes the identification of the standard thermodynamic parameters in $2d$. We now turn our attention to the extended phase space. Asymptotically, $f \to \frac{r^2}{\ell^2}$, and hence the spacetime is AdS_2 with the characteristic length scale ℓ. According to the definitions of the extended phase space, we interpret the pressure as

$$P = -\frac{\Lambda}{8\pi} = \frac{3}{8\pi\ell^2}. \tag{2.60}$$

Correspondingly, the conjugate volume may be computed from

$$V = \frac{\partial M}{\partial P}\Big|_{\beta,Q} = \frac{4\pi}{3} r_+^3. \tag{2.61}$$

It is then straightforward to check that the first law and the following Smarr relation hold

$$\mathrm{d}M = T\mathrm{d}S + \Phi \mathrm{d}Q + V\mathrm{d}P, \tag{2.62}$$

$$M = 2(TS - VP) + \Phi Q. \tag{2.63}$$

The Smarr scaling may be understood by considering the length dimension of mass. From Eqn. (2.47), the mass has dimension $[M] = L$ due to the quadratic dilaton-gravity couplings in the action. This mass dimension is identical to the RN-AdS_4 black hole solution and hence the $d = 2$ theory has a similar Smarr scaling.

The PV equation of state is obtained from expressing the Euclidean period, Eqn. (2.56), in terms of temperature and pressure. In this case, the fluid volume is related to the horizon via $v = 2r_+$ and hence the $d = 2$ equation of state reads

$$P(T, v) = \frac{T}{v} - \frac{1}{2\pi v^2} + \frac{2\rho^2}{\pi v^4} \tag{2.64}$$

which has the critical point

$$P_c = \frac{1}{96\pi\rho^2} \qquad T_c = \frac{1}{3\sqrt{6}\pi\rho} \qquad v_c = 2\sqrt{6}\rho. \tag{2.65}$$

The ratio $(P_c v_c/T_c) = (3/8)$ precisely coincides with the universal van der Waals ratio, analogous to the RN-AdS_4 case. Hence, we have determined a class of $2d$ charged, black hole solutions to the dilaton-gravity model, Eqn. (2.40), which supports non-trivial van der Waals behavior.

Using the definitions $p = \frac{P}{P_c}$, $\nu = \frac{v}{v_c}$, and $\tau = \frac{T}{T_c}$, we have the 'law of corresponding states'

$$p(\tau, \nu) = \frac{8}{3}\frac{\tau}{\nu} - \frac{2}{\nu^2} + \frac{1}{3\nu^4}. \tag{2.66}$$

Following the analysis given above, it is straightforward to conclude that the critical exponents are those of mean field theory;

$$\alpha = 0, \qquad \beta = \frac{1}{2}, \qquad \gamma = 1, \qquad \delta = 3. \tag{2.67}$$

2.3.2 Van der Walls Behavior in $d = 3$

We now turn our attention to $3d$ black hole solutions that result from consistent truncations of the bulk action in $5d$, Eqn. (2.38). It was shown in [55] that homogeneous uncharged, AdS_d black strings are permissible geometries that solve the field equations of the action (2.38) with $\mathcal{L} = (\nabla\Sigma)^2$. The massless scalar field modifies the cosmological constant to support the black string along flat directions. Here, we construct charged, dilatonic, AdS_3 planar black holes using $\mathcal{L} = F^2 + (\nabla\Sigma)^2$. The uplift of this solution to $d = 5$ dimensions corresponds to charged AdS_5 black strings with horizon topologies $S^2 \times \mathbb{R}^1$.

We search for planar $3d$ black hole solutions with purely electric solutions to the field equations (2.41)–(2.43) with the ansatz

$$ds_3^2 = -f(r)dt^2 + f(r)^{-1}dr^2 + h(r)^2dx^2 \tag{2.68}$$

$$A \equiv A(r)dt \qquad \psi \equiv \psi(r) \qquad \Sigma \equiv \Sigma(x) \tag{2.69}$$

In this case, the equations of motion for the gauge and scalar fields are

$$\nabla_a(\psi^2 F^{ab}) = 0, \qquad \nabla_a(\psi^2 \nabla^a \Sigma) = 0 \tag{2.70}$$

and the corresponding stress-energy contribution is

$$T^{\mathcal{L}}_{ab} = F_{ac}F_b{}^c - \frac{1}{4}g_{ab}F^2 - \nabla_a\Sigma\nabla_b\Sigma + \frac{1}{2}g_{ab}(\nabla\Sigma)^2. \tag{2.71}$$

Given this ansatz, it is straightforward to demonstrate that the equations of motion are satisfied for the solution

$$f(r) = \frac{1}{2\varphi^2} - \frac{\Lambda r^2}{6} - \frac{\mu}{r^2} + \frac{\rho^2}{r^4}, \tag{2.72}$$

$$\psi(r) = \varphi r, \qquad h(r) = r, \tag{2.73}$$

$$A = -\sqrt{\frac{3}{4}}\frac{\rho}{r^2}dt, \qquad \Sigma(x) = \frac{x}{\sqrt{2}\varphi}. \tag{2.74}$$

Here, the horizon is given by the largest positive root of

$$f(r_+) = \frac{1}{2\varphi^2} + \frac{r_+^2}{\ell^2} - \frac{\mu}{r_+^2} + \frac{\rho^2}{r_+^4} = 0 \tag{2.75}$$

where we have used $\Lambda = -6/\ell^2$. Note that for a real root, the bound $\mu > 0$ must be saturated. The free parameter is set by demanding $2\varphi^2 = 1$.

As we will demonstrate, the parameters μ and ρ are again respectively related to the black hole mass and charge. When computing the thermodynamics, the presence of a planar horizon leads to infinities. To circumvent this, we consider thermodynamic densities with respect to the planar direction.

We first compute the ADM mass using the the background subtraction procedure outlined in [30, 56]. The total charge is given by the weighted flux across the planar horizon and the chemical potential is determined by considering the electrostatic potential difference from the horizon and infinity [32]. In $3d$, the spherically symmetric horizon allows for a direct computation of both the Bekenstein-Hawking and Wald entropies. We check these quantities against the on-shell Euclidean action and identify the correct entropy before studying the PV behavior.

To determine the ADM mass, we use the background subtraction procedure outlined in [30, 56]. In $3d$, the mass function reads

$$\mathcal{M}(r) = 2\sqrt{f}\left(\sqrt{f_{\text{ref}}} - \sqrt{f}\right)\frac{\mathrm{d}}{\mathrm{d}r}\left(\frac{\psi^2}{4}\mathcal{A}\right) \tag{2.76}$$

where $\mathcal{A} = x\, r$ is the area function of planar horizon. In this case, the reference spacetime

$$\mathrm{d}s^2_{\text{ref}} = -\left(1 + \frac{r^2}{\ell^2}\right)\mathrm{d}t^2 + \frac{\mathrm{d}r^2}{\left(1 + \frac{r^2}{\ell^2}\right)} + r^2\mathrm{d}x^2 \tag{2.77}$$

is simply the asymptotically[1] AdS_3 solution obtained by $\mu = \rho = 0$. The ADM mass density, computed at the radial boundary, is

$$m = \lim_{r\to\infty}\frac{1}{x}\mathcal{M}(r) = \frac{3\mu}{8}. \tag{2.78}$$

For our purposes, it is important to compute the total charge using a weighted flux across the planar horizon. To motivate this calculation, we consider the charge of the uplifted solution. In $5d$, the electric flux across the $S^2 \times \mathbb{R}$ horizon determines the total charge of an RN-AdS_5 black string. Inserting Eqn. (2.68) into Eqn. (2.39), the total charge reads

$$Q = \frac{1}{4\pi}\int \star F = \frac{1}{4\pi}\int F_{10}(\psi^2 h)\mathrm{d}\Omega\mathrm{d}x. \tag{2.79}$$

Integrating out the spherical directions, we interpret the charge density in $3d$ as

$$q = \frac{1}{x}\int \star(\psi^2 F) = \frac{\sqrt{3}}{2}\rho. \tag{2.80}$$

The corresponding chemical potential follows the standard definition [32],

$$\Phi = \int_{r_+}^{\infty}\mathrm{d}r F_{10} = \sqrt{\frac{3}{4}}\frac{\rho}{r_+^2}. \tag{2.81}$$

In $3d$, we have the freedom to either consider the Bekenstein-Hawking entropy or the Wald entropy. Using the standard formulas, one has the entropy densities

$$s_{\text{BH}} = \frac{1}{x}\frac{\mathcal{A}}{4} = \frac{r_+}{4}, \tag{2.82}$$

$$s_{\text{Wald}} = \frac{2\pi}{x}\int\left(\frac{\delta\mathcal{I}}{\delta R^{abcd}}\epsilon^{ac}\epsilon^{bd}\right)\mathrm{d}x = \frac{\pi r_+^3}{2}. \tag{2.83}$$

[1] Provided the toroidal identification $x \sim x + 2\pi$, the space is locally AdS_3 at the expense of a discontinuity in $\Sigma(x)$.

To single out the correct thermal entropy, once again we can appeal to the on-shell Euclidean action. Using the counterterm subtraction method [31], the on-shell Euclidean action in the canonical ensemble reads

$$\bar{\mathcal{I}} = \frac{\beta x}{8\ell^2}\left(\frac{r_+^4\ell^2 - r_+^6 + 5\rho^2\ell^2}{r_+^2}\right) \tag{2.84}$$

where β denotes the period of the Euclidean section

$$\beta = \frac{4\pi}{\partial_r f}\bigg|_{r=r_+} = \frac{2\pi r_+^5\ell^2}{(r_+^4 - \rho^2)\ell^2 + 2r_+^6}. \tag{2.85}$$

In the fixed charge ensemble, the mass, chemical potential, and entropy are straightforward to compute

$$m = \frac{\partial\bar{i}}{\partial\beta}\bigg|_Q = \frac{3\mu}{8}, \tag{2.86}$$

$$\Phi = \frac{1}{\beta}\frac{\partial\bar{i}}{\partial Q}\bigg|_\beta = \sqrt{\frac{3}{4}}\frac{\rho}{r_+^2}, \tag{2.87}$$

$$s = \frac{\partial\bar{i}}{\partial\beta}\bigg|_Q - \bar{i} = \frac{\pi r_+^3}{2\pi}, \tag{2.88}$$

where we have used the action density $\bar{i} = (\bar{\mathcal{I}}/x)$. Comparing these quantities against Eqn. (2.78), Eqn. (2.81), and Eqn. (2.83) respectively confirms the interpretation of the charge and selects the Wald entropy as the correct thermodynamic entropy.

We are now in the position to study PV criticality. Clearly, the spacetime is asymptotically AdS_3 with respect to the length scale ℓ, and hence the pressure in the extended phase space formalism may be identified with

$$P = -\frac{\Lambda}{8\pi} = \frac{3}{4\pi\ell^2}. \tag{2.89}$$

In the fixed charge ensemble, this invites a reinterpretation of the ADM mass as the enthalpy $m \equiv m(P, S)$ and we can compute the thermodynamic volume

$$V = \frac{\partial m}{\partial P}\bigg|_{S,Q} = \pi^2 r_+^4. \tag{2.90}$$

One can check that the first law and Smarr relation

$$\mathrm{d}M = T\mathrm{d}S + \Phi\mathrm{d}Q + V\mathrm{d}P \tag{2.91}$$

$$M = \frac{3}{2}TS - VP + \Phi Q. \tag{2.92}$$

hold with these identifications. The corresponding equation of state may be found from inverting the periodicity, Eqn. (2.85), and using the definition of the fluid volume. In this

case, the fluid volume is related to the horizon via $v = 4r_+\ell_p/3$ resulting in the equation of state

$$P(T, v) = \frac{T}{v} - \frac{2}{3\pi v^2} + \frac{512\rho^2}{243\pi v^6} \tag{2.93}$$

where we have set $\ell_p = 1$. The critical point of the equation of state yields the triple

$$P_c = \frac{1}{4\sqrt{15}\pi\rho}, \qquad T_c = \frac{4}{5\pi(15\rho^2)^{\frac{1}{4}}}, \qquad v_c = 4\Big(5\rho^2/3\Big)^{\frac{1}{4}}. \tag{2.94}$$

and satisfies the ratio $P_c v_c/T_c = 5/12$. Note that this ratio is also shared by RN-AdS$_5$ black holes, Eqn. (2.21). This suggests that the charged AdS$_5$ black string uplift of CDAdS$_3$ black holes belongs in the same universality class as RN-AdS$_5$ black holes.

Constructing the law of corresponding states follows the same procedure as in higher dimensions. Employing the definitions $p = \frac{P}{P_c}$, $\nu = \frac{v}{v_c}$, and $\tau = \frac{T}{T_c}$, the law of corresponding states can be written as

$$p = \frac{12\tau}{5\nu} - \frac{3}{2\nu^2} + \frac{1}{10v^6} \tag{2.95}$$

which coincides precisely Eqn. (2.23) for $d = 5$. Hence, we conclude that the critical exponents are again consistent with mean field theory and this completes the identification of lower dimensional black holes demonstrating critical behavior.

2.4 Conclusions

Given the lack of lower dimensional charged black hole solutions admitting van der Waals behavior, we constructed gravity theories in $d = 2, 3$ via consistent truncations and explored the extended phase space of black hole solutions using lower dimensional techniques and Euclidean methods. We have found classic van der Waals structures in the equation of state of charged, dilatonic, asymptotically AdS black hole solutions in $d = 2, 3$ and confirmed that the critical exponents match those expected from mean field theory.

In $d = 2$, the mass and charge of the CDAdS$_2$ solution, Eqn. (2.47), were computed with lower dimensional methods outlined in [51, 52]. We found, rather than the standard definition of Bekenstein-Hawking entropy, the Wald entropy yields an expression that agrees with the entropy calculated from the on-shell Euclidean action. Furthermore, this solution has several features reminiscent of RN-AdS$_4$ black hole solutions of Einstein-Maxwell-AdS$_4$ theory, especially the similarity between the respective equations of state and the coincident van der Waals ratios. The CDAdS$_2$ solution, however, does not satisfy the canonical Smarr relation in $d = 2$ but instead saturates the formula with $d = 4$. This is due to the quadratic dilaton-gravity coupling in the action, which raises the mass dimension of the black hole to that of $4d$.

In $d = 3$, searching for black hole solutions required some care. We performed consistent truncations of theories admitting charged AdS$_5$ black strings with horizon topologies

$S^2 \times \mathbb{R}$ along the spherical directions. The dimensionally reduced theory had an additional scalar field that supported planar charged, asymptotically AdS black strings in $d = 3$. To regulate infinites arising from the planar direction, we computed the thermodynamic densities and confirmed that the mass and charge density have a standard interpretation. Again, the Wald entropy density matches the entropy density computed from the on-shell Euclidean action, confirming that the Wald entropy, rather than the Bekenstein-Hawking entropy, is the correct thermal entropy. Similar to the case in $d = 2$, the canonical Smarr relation was not satisfied with $d = 3$. Instead, the scaling properties of these black hole solutions were identical to RN-AdS$_5$ black strings. The Smarr scaling in our work contrasts an earlier analysis [49] where new work terms were required to satisfy Smarr laws for Einstein-Maxwell-AdS$_3$ theory without additional scalar fields. We confirmed that the equation of state contains critical phenomena and the van der Waals ratio is identical to that of RN-AdS$_5$ black holes. The latter observation suggests that compactification of black objects with various horizon topologies preserves the van der Waals universality class.

There are several interesting directions to pursue. We were here primarily concerned with searching for rich van der Waals behavior in lower dimensions with a dynamical scalar field. However other phase transitions may be available. Indeed by imposing a constant scalar field, the action reduces to

$$\mathcal{I}[\psi_0] = -\int \left[\frac{\psi_0^2}{4}(R - 2\Lambda - \mathcal{L}) + \frac{\lambda}{2}\right]\sqrt{-g}\mathrm{d}^d x \tag{2.96}$$

with an effective cosmological constant $\Lambda_{\text{eff}} = \frac{\psi_0^2}{4}\Lambda + \frac{-\lambda}{4}$. The action in $d = 3$ has known black hole solutions, namely the charged BTZ solution with a planar horizon. Hence the scalar behaves analogous to an order parameter that supports the CDAdS$_3$ string phase with pressure corresponding to Λ, or to the charged BTZ$_3$ string phase with pressure given by Λ_{eff}. It would be fruitful to explore an ensemble which allows for such Landau-Ginzburg phase transitions and study if the CDAdS$_3$ solution lies within the BTZ mass gap.

Similar arguments can be made for the action in $d = 2$. In this case, it is convenient to recall that the near horizon extremal geometry of an RN-AdS$_4$ black hole fibers into AdS$_2 \times S^2_{\psi_0}$, i.e, the Robinson-Bertolli spacetime. Upon compactification, this spacetime should appear as a classical solution to the above action if one treats ψ_0 as a Lagrange multiplier. Again the dynamics of the scalar provides access to different black hole phases of the theory. It would be very interesting to precisely chart out the complete phase space of solutions to the general compactified action (2.40).

Finally, another possible direction is to consider our approach in $d > 3$. Here several new features are available, such as magnetic black hole solutions, p-form electromagnetism, Gauss-Bonnet and Lovelock sectors of gravity, and novel phase transitions in addition to van der Waals.

Acknowledgments

This work was supported in part by the Natural Sciences and Engineering Research Council of Canada. AD is further supported by the National Science Foundation Graduate Research Fellowship under Grant No. 00039202. This research was supported in part by the Perimeter Institute for Theoretical Physics. Research at Perimeter Institute is supported by the Government of Canada through the Department of Innovation, Science and Economic Development Canada and by the Province of Ontario through the Ministry of Research, Innovation and Science.

Chapter 3

Gravitational Instabilities of Uniform Black Strings in AdS$_d$

This chapter is a faithful reproduction of the published work **A. Dhumuntarao and R. Mahbub, Phys. Rev. D, 105, L041501 (2022)** with minor edits [57].

Abstract

Locally AdS$_{d-1} \times \mathbb{R}$ uniform black strings (UBS) in the presence of a massless scalar field are believed to avoid the onset of the Gregory-Laflamme (GL) instability in $d \geq 4$ as no tachyonic modes exist in the spectrum of the Laplace-Beltrami operator. We present analytic and numerical evidence of GL modes in the Lichnerowicz spectrum indicating that AdS$_{d-1}$ UBSs are classically and thermodynamically unstable at the linear level in $d > 4$. In $d = 4$, we confirm that uniform BTZ$_3$ strings are indeed stable as previously suggested. We propose that linear instabilities of black strings are triggered if and only if a tachyonic mode exists in the Lichnerowicz spectrum. At the end state of the instability, AdS$_{d-1}$ UBSs of finite length may tunnel to a SAdS$_d$ black hole or converge onto a novel non-uniform AdS$_d$ black string. We conjecture that weak cosmic censorship is violated if the non-uniform solution is an exact AdS$_d$ black funnel and compute entropy estimates in $d > 4$ as evidence.

3.1 Introduction

Black objects with translationally invariant horizons suffer from classical instabilities. A famous example is the Gregory-Laflamme (GL) instability of Ricci-flat black strings in $d > 4$, with horizon topologies $S^{d-3} \times S^1$, where tachyonic modes develop in the Lichnerowicz operator spectrum ($\Delta_{\rm L}$) under generic long wavelength perturbations [58–61]. These classical instabilities persist to four spacetime dimensions and higher [62–65, 65–78] for black strings with asymptotics that are conformal to AdS$_{d-1} \times \mathbb{R}$. There

is strong numerical evidence that GL modes lead to the horizon developing a finite time pinch-off – constituting a violation of weak cosmic censorship [79]. For black strings with non-trivial matter configurations, tachyonic modes are also observed in the Laplace-Beltrami operator ($\Box$) (see [75–78]). It is generally believed that the spectra of scalar operators on black string backgrounds are correlated. Thus finding tachyonic modes in the matter sector is a necessary and sufficient condition for classical instability and indeed, several numerical and analytic situations exist where such instabilities were sourced from Spec($\Box$) only [76–78].

These linear instabilities are correlated to local thermodynamic instabilities. In its modern form, correlated stability states, for black strings with mass M and conserved charges Q_A, classical instabilities are triggered precisely when a positive eigenvalue exists in the Hessian of the microcanonical entropy $S(M, Q_A)$ [76, 77]. For unique black strings with conserved charges, correlated stability has demonstrated that tachyonic modes develop in the spectrum of scalar operators precisely when the heat capacity becomes negative [63–66, 70, 80–84], and enjoys a general proof for asymptotically flat spacetimes [85].

Recently, a new class of locally $\mathrm{AdS}_{d-1} \times \mathbb{R}$ uniform black string (AdS_{d-1} UBS) solutions in the presence of a massless scalar field has furnished two interesting questions [55, 86]. First, no such tachyonic modes were identified in Spec($\Box$) leading to the conjecture that these solutions are linearly stable in four spacetime dimensions and higher [55]. This result is clearly in tension with earlier studies which have numerically and analytically confirmed a tachyonic mode in Δ_{L} for black strings which are locally conformal to $\mathrm{AdS}_{d-1} \times \mathbb{R}$ [60–75]. As the stability analysis performed in [55, 86] primarily focused on Spec($\Box$), it is natural to ask *does a GL mode persist in Spec*(Δ_L) *in four spacetime dimensions and higher?*

Secondly, the AdS_{d-1} UBS is thermodynamically unstable when the radius of the string is sufficiently thin but remains classically stable in this regime. It is well known that non-unique black brane configurations with exotic scalar charge are counterexamples to correlated stability [69]. However, the AdS_{d-1} UBS is a unique configuration without a conserved charge associated with the massless scalar [55, 86], naturally raising the question *are these solutions a new counterexample to the stronger form of correlated stability?*

In this Letter, we present an analytic and numerical study of the classical and thermodynamic instability of locally $\mathrm{AdS}_{d-1} \times \mathbb{R}$ uniform black strings coupled to a massless scalar. In concordance with the study initiated in [55], we confirm that no GL modes exist in the Spec($\Box$). However, we find evidence of tachyonic modes in Spec(Δ_{L}) in $d > 4$ suggesting that the $\mathrm{AdS}_{d-1} \times \mathbb{R}$ UBS is classically unstable. We also find a positive eigenvalue in Hess(S) which, together with the GL modes in Δ_{L}, is sufficient to rescue correlated stability in $d > 4$. The reason the scalar operator spectra are uncorrelated may be under-

stood by performing Kaluza-Klein (KK) compactifications along the flat direction. The resulting tower of masses for the scalar fluctuations satisfy the Breitenlöhner-Freedman bound on the locally AdS_{d-1} background [87, 88]. Hence deformations from the matter sector do not grow sufficiently fast to trigger an instability, whereas the same is not true for propagating tensor modes in $\mathrm{Spec}(\Delta_{\mathrm{L}})$. To our knowledge, this is the first example where the spectra of scalar operators are uncorrelated for AdS black strings in the presence of non-trivial matter. This suggests tachyonic modes in $\mathrm{Spec}(\Box)$ are sufficient, but not necessary as previously thought, to generate classical instabilities, and supports earlier studies that linear black string instabilities are triggered only if tachyonic modes exist in $\mathrm{Spec}(\Delta_L)$.

3.2 The Model

We parameterize the AdS_{d-1} UBS solution by

$$\begin{aligned}
\mathcal{S} &= \frac{1}{16\pi G_d}\int\left[R - 2\Lambda_{\mathrm{bulk}} - \frac{1}{2}(\partial\sigma)^2\right]\sqrt{-g}\mathrm{d}^d x, \\
\mathrm{d}s^2 &= \frac{(d-2)}{(d-1)}\frac{L_d^2}{\ell_{d-1}^2}\left[\mathrm{d}z^2 - V(r)\mathrm{d}t^2 + \frac{\mathrm{d}r^2}{V(r)} + r^2\mathrm{d}s^2_{S^{d-3}}\right], \\
V(r) &= 1 - mr^{4-d} + r^2\ell_{d-1}^{-2},\ \sigma(z) = \sqrt{2(d-2)}(z/\ell_{d-1}).
\end{aligned} \tag{3.1}$$

The bulk and boundary AdS length scales are set via $\Lambda_{\mathrm{bulk}} = -\frac{(d-1)(d-2)}{2L_d^2}$ and $\Lambda_{\mathrm{bdy}} = -\frac{(d-2)(d-3)}{2\ell_{d-1}^2}$. We consider a finite string with $z \in \mathbb{I} = [-\pi L_z/2, \pi L_z/2]$ and restrict our attention to $d \geq 4$. The UBS is a solution to the equations

$$R_{ab} = \frac{2\Lambda_{\mathrm{bulk}}}{d-2}g_{ab} + \frac{1}{2}\partial_a\sigma\partial_b\sigma \qquad \Box\sigma = 0 \tag{3.2}$$

provided the massless scalar σ satisfies Neumann boundary conditions. Clearly, the scalar modifies Λ_{bulk} along the z direction and additional flat directions x_i may be appended at the expense of adding scalars σ_i with identical asymptotics. Henceforth, the volume of the space transverse to the UBS horizon is unity, $(16\pi G_d)^{-1}\int_{S^{d-3}\times\mathbb{I}}\sqrt{\gamma} = 1$[1].

3.3 Correlated Stability

On constant z hypersurfaces, the geometry describes an SAdS_{d-1} BH where the largest positive root of $V(r_+) = 0$ designates the horizon. The mass and entropy may then be

[1]This yields the normalization

$$G_d = \frac{\omega_{d-3}L_z}{8}\left(\frac{d-2}{d-1}\right)^{\frac{1}{2}(d-2)}\left(\frac{L_d}{\ell_{d-1}}\right)^{d-2} \tag{3.3}$$

which is convenient to use when computing the thermodynamics

directly computed using standard formulas on the codimension one surface

$$M = (d-3)r_+^{d-4}\left[E_{S^{d-3}} + \frac{r_+^2}{\ell_{d-1}^2}\right], \qquad S = 4\pi r_+^{d-3} \tag{3.4}$$

where $E_{S^{d-3}}$ is the energy of the sphere which vanishes in $d = 4$ and is unity otherwise. As noted in [55], there is no conserved charge associated with the scalar. Hence, the thermodynamic potential is simply $S \equiv S(M)$ in the microcanonical ensemble and searching for positive eigenvalues in $\mathrm{Hess}(S)$ is equivalent to identifying a regime where $S(M)$ is convex. However, for AdS black objects, there is no simple expression for the entropy [76, 77]. Rather, assuming strictly positive temperatures (which is reasonable for SAdS_{d-1} black strings), the stability requirement may be rephrased in terms of finding negative eigenvalues in the Hessian of $M(S)$ which is simply the statement that the heat capacity becomes negative. We find in $d = 4$, $M(S) = (S/4\pi\ell_{d-1})^2$ and in $d > 4$,

$$M(S) = (d-3)\left(\frac{S}{4\pi}\right)^{\frac{d-4}{d-3}}\left[1 + \frac{(S/4\pi)^{\frac{2}{d-3}}}{\ell_{d-1}^2}\right]. \tag{3.5}$$

A routine computation of the heat capacity $C = T(\partial_S^2 M)^{-1}$ where $T = V'(r_+)/4\pi$, shows that $M(S)$ is concave in $d > 4$ for $r_+ < r_+^c = \sqrt{(d-4)/(d-2)}\ell_{d-1}$. Hence, sufficiently thin UBSs with $S(r_+) < S(r_+^c) = 4\pi r_+^c$ are thermodynamically unstable in $d > 4$. In $d = 4$, the solution is a uniform BTZ_3 string with a mass gap $M \geq 0$ separating the black string from the AdS_3 ($M = -1$) background which has a strictly positive heat capacity [47, 49]. Via correlated stability, this naively suggests tachyonic modes condense in $\mathrm{Spec}(\Box, \Delta_{\mathrm{L}})$ for horizons $r_+ < r_+^c$ in $d > 4$ whereas the BTZ_3 UBS is stable regardless of the horizon size. Hence, the GL instability should have a lower critical dimension of $d = 5$. Some evidence of this is observed for BTZ_3 black strings which are locally conformal to $\mathrm{AdS}_3 \times \mathbb{R}$ [64–66]. In $4 \geq d$, Einstein-(A)dS_{d-1} gravity is topological. Thus metric perturbations will not contain propagating degrees of freedom and should reduce to a pure gauge transformation. We study these expectations analytically and numerically shortly.

3.4 Classical Stability Analysis

We show that tachyonic modes in $\mathrm{Spec}(\Box, \Delta_{\mathrm{L}})$ are uncorrelated on the AdS_{d-1} UBS background and the BTZ_3 UBS is stable. We consider perturbing the metric and scalar field around the background Eqn. (3.1)

$$g_{ab}(x^a) = \bar{g}_{ab}(x^a) + \epsilon H_{ab}(x^a) + \mathcal{O}(\epsilon^2) \tag{3.6}$$

$$\sigma(x^a) = \bar{\sigma}(z) + \epsilon\Phi(x^a) + \mathcal{O}(\epsilon^2) \tag{3.7}$$

where $(\bar{g}_{ab}, \bar{\sigma})$ satisfies the equations of motion (3.2). To $\mathcal{O}(\epsilon)$, the perturbations on the AdS_{d-1} UBS background satisfy

$$\Box\Phi \equiv -\frac{1}{V}\frac{\partial^2\Phi}{\partial t^2} + \frac{1}{r^{d-3}}\frac{\partial}{\partial r}\left(r^{d-3}V\frac{\partial\Phi}{\partial r}\right) + \frac{\partial^2\Phi}{\partial z^2} = 0 \tag{3.8}$$

$$\Delta_{\mathrm{L}} H_{ab} = -\frac{4\Lambda}{d-2}H_{ab} + 2\,\partial_{(a}\bar{\sigma}\partial_{b)}\Phi \tag{3.9}$$

where the Lichnerowicz operator in the transverse gauge is

$$\Delta_{\mathrm{L}} H_{ab} \equiv \Box H_{ab} + 2\bar{R}_{acbd}H^{cd} - 2\bar{R}^{c}_{(a}H_{b)c}. \tag{3.10}$$

Now, identifying tachyonic modes in $\mathrm{Spec}(\Box, \Delta_{\mathrm{L}})$ is tantamount to finding regular solutions (H_{ab}, Φ) which have a growing mode instability [58–62]. As the UBS solution is spherically symmetric and has a Killing isometry along the flat direction, we search for growing modes in the s-wave gauge with the expansion

$$\Phi(x^a) = e^{im_n z + \Omega t}\phi(r), \tag{3.11}$$

$$H_{ab}(x^a) = e^{im_n z + \Omega t}\begin{pmatrix} h_{tt} & h_{tr} & h_{tz} & \mathbf{0} \\ h_{tr} & h_{rr} & h_{rz} & \mathbf{0} \\ h_{tz} & h_{rz} & h_{zz} & \mathbf{0} \\ \mathbf{0} & \mathbf{0} & \mathbf{0} & \boldsymbol{h}_{ij} \end{pmatrix}. \tag{3.12}$$

Here $m_n = (n/L_z)$, $\boldsymbol{h}_{ij}\mathrm{d}\theta^i\mathrm{d}\theta^j \equiv K(r)\mathrm{d}s^2_{S^{d-3}}$, and $h_{\mu\nu} \equiv h_{\mu\nu}(r)$ along the directions transverse to S^{d-3}. In the presence of matter, we are allowed to work in the transverse gauge $H^{ab}{}_{;b} = \frac{1}{2}H^{;a}$ where $H = \bar{g}^{ab}H_{ab}$. Lastly, in order for the initial value problem to be well posed, the domain of dependence will include $\mathscr{I}^+$ on the conformal boundary of the SAdS_{d-1} BH when prescribing data [58, 59, 62].

3.4.1 Matter Perturbations.

It is straightforward to show that no tachyonic modes may be found in $\mathrm{Spec}(\Box)$ obeying regularity conditions near horizon $r \approx r_+$ and asymptotically $r \to \infty$ [55]. Evaluating Eqn. (3.8) on the ansatz Eqn. (3.11), one finds

$$V\phi'' + \left[\frac{d-3}{r}V + V'\right]\phi' - \left[m_n^2 + \frac{\omega^2}{V}\right]\phi = 0. \tag{3.13}$$

Regularity conditions enforce the behavior $\phi \sim (r - r_+)^\alpha$ near horizon and $\phi \sim r^{-\beta}$ asymptotically with $\alpha, \beta \in \mathbb{R}^+$ [89]. As a result, the only way to achieve this behavior is if $\phi(r)$ possesses a maximum at some radial position $r_\star > r_+$. At the turning point, $\phi'(r_\star) = 0$ and hence we have

$$V(r_\star)\phi''(r_\star) = \left[m_n^2 + \frac{\omega^2}{V(r_\star)}\right]\phi(r_\star). \tag{3.14}$$

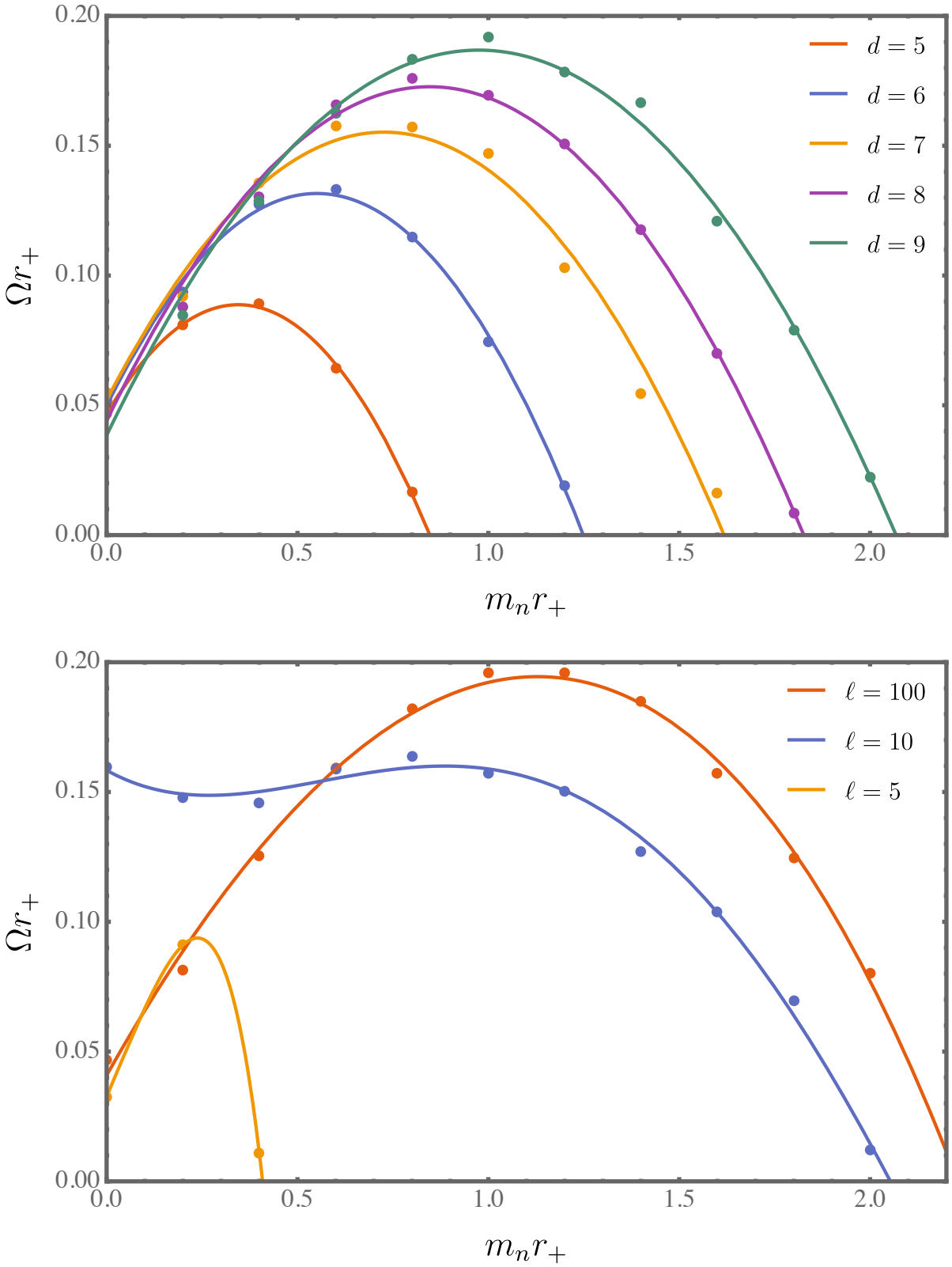

Figure 3.1: Top: Plot of (m_n, Ω) with $r_+ = 2.0$ and $\ell = 50$ for which the ratio $\mathcal{R}$ changes sign in $9 \leq d \leq 5$. The points correspond to values calculated numerically indicating an instability. The lines are polynomial fits to illustrate the trend. Bottom: The instability in $d = 10$ for various values of ℓ. As $\mu_+ \sim \mu_+^c$, the instability is terminated.

However, for this to be a maximum $V(r_\star)\phi''(r_\star) < 0$ but no maximum may exist as $V(r_\star) > 0$ for $r_\star > r_+$.

We generalize the stability argument given in [55] by performing a KK compactification of the flat direction. One would then find a tower of masses $(\Box^{\mathrm{SAdS}_{d-1}} - m_n^2)\Phi = 0$ from which it is direct to see the Breitenlöhner-Freedman stability condition $m_n^2 = (n/L_z)^2 > -\frac{(d-2)^2}{4\ell_{d-1}^2}$ is satisfied [87, 88]. Hence, the AdS_{d-1} UBS solution is indeed stable to scalar perturbations in $d \geq 4$ independent of the coordinate gauge. As such, we eliminate this perturbation in our search for an instability [59].

3.4.2 Metric Perturbations

The metric perturbations are quite involved. Nonetheless, it is possible to present the salient arguments, detailed in the supplementary files, which identify the growing mode instability. As the scalar perturbation decouples, the metric perturbations become tracefree $\bar{g}^{ab}H_{ab} = 0$. Then gauge conditions, in conjunction with eliminating stable perturbations, can be used to reduce Eqn. (3.9) to a single ODE

$$A_{m_n,\Omega}(r)h_{tr}''(r) + B_{m_n,\Omega}(r)h_{tr}'(r) + C_{m_n,\Omega}(r)h_{tr}(r) = 0. \tag{3.15}$$

The conditions on the radial boundary and the horizon are sensitive to the dimension and on Λ_{bdy}. The qualitative difference between $d = 4$ and $d > 4$ is best understood in the limit $(\Lambda_{\mathrm{bulk}}, \Lambda_{\mathrm{bdy}}) \to 0$ where one is supposed to recover the instability of $\mathrm{Schwarzschild}_{d-1}$ uniform black strings [2]. In $d = 4$, no $\mathrm{Schwarzschild}_3$ UBS exist in the spectrum of Einstein gravity, where as the same is not true in $d > 4$. Next, the dependence of the regularity condition on Λ_{bdy} may be inferred in terms of the control parameter $\mu_+ = r_+/\ell_{d-1}$. For $\mu_+ \gg 1$, the radius of the AdS_{d-1} UBS is large and requires sharply growing regular perturbations to destabilize the solution where as $\mu_+ \ll 1$ correspond to thin UBS solutions which are easier to perturb. We perform the parameter search in the latter regime in order to make contact with correlated stability. The conditions on the horizon and radial boundary may be found by solving Eqn. (3.15) on the various asymptotics. We find

$$r \to r_+ : \begin{cases} \mathcal{A}_\pm(m_n)(r-r_+)^{-1\pm\frac{r_+\Omega}{d-4}\sqrt{1-\varepsilon}}, & d > 4 \\ \mathcal{C}_\pm(m_n)(r-r_+)^{-1\pm\frac{r_+\Omega}{2\mu_+^2}}, & d = 4 \end{cases} \tag{3.16}$$

$$r \to \infty : \begin{cases} \mathcal{B}_\pm(m_n)e^{\pm m_n^2 r/\sqrt{m_n^2-\Omega^2}}, & d > 4 \\ \mathcal{D}_\pm(m_n)e^{\pm \mathrm{i}\, m_n^2 r/\sqrt{\mu_+^2 m_n^2+\Omega^2}}, & d = 4 \end{cases} \tag{3.17}$$

where $\varepsilon = \frac{(d-2)}{(d-4)}\mu_+^2$. In $d > 4$, the near horizon condition suggests a real regular solution exists provided $\varepsilon < 1$ and $\Omega < (d-4)/r_+\sqrt{1-\varepsilon}$. The condition on ε is analytic evidence

[2] We thank Matthew Headrick for bringing this to our attention

of correlated stability as the control parameter is bounded above precisely by the thermodynamic instability $\mu_+^2 < \frac{(d-4)}{(d-2)} \equiv (r_+^c/\ell_{d-1})^2$. Near horizon, one recovers the familiar Schwarzschild$_{d-1}$ UBS behavior when $\mu_+ = 0$ [58, 59]. In the far horizon, the solution differs due to the conformal structure on the asymptotically AdS$_{d-1}$ surface.

In $d = 4$, it is evident the perturbation is pure gauge – the asymptotic solutions are oscillatory rather than smoothly damped. Near horizon, instabilities are exponentially damped out from the spectrum as regular solutions require $\Omega < \frac{2\mu_+^2}{r_+} \ll 1$. We believe this behavior to be related to the lack of propagating gravitational degrees of freedom in lower dimensions. It is natural to understand this as analytic evidence suggesting the classical stability of BTZ$_3$ UBSs which agrees with the expectations provided from correlated stability.

The goal is now to perform a parameter search on (m_n, Ω) which yields regular solutions, i.e., tachyonic modes in Spec$(\Delta_{\rm L})$. We numerically integrate Eqn. (3.15) (see the supplementary files) to compute the instability pairs (m_n, Ω) using an adaptive Runge-Kutta-Fehlberg (RK45) routine in *Mathematica*. A backwards integration is carried out between $r_1 = 200.0$ and $r_2 = r_+ + 10^{-5}$ with the seed solution set by the decaying branch $h_{tr} \sim e^{-m_n^2 r/\sqrt{m_n^2-\Omega^2}}$. The existence of an instability is detected with a sign change in the ratio $\mathcal{R} = \mathcal{A}_-/\mathcal{A}_+$ [58, 59] where

$$\mathcal{R} = \frac{\left(\frac{r_+\Omega}{d-4}\sqrt{1-\varepsilon}-1\right)h_{tr} - (r-r_+)h'_{tr}}{\left(\frac{r_+\Omega}{d-4}\sqrt{1-\varepsilon}-1\right)h_{tr} + (r-r_+)h'_{tr}}(r-r_+)^{\frac{2r_+\Omega}{d-4}\sqrt{1-\varepsilon}}. \tag{3.18}$$

We confirm the AdS$_{d-1}$ UBS solution is indeed unstable in $10 \geq d \geq 5$, and in $d = 10$ we studied the threshold of this instability for various control parameters. We found no such instability in $d = 4$ or beyond r_+^c/ℓ_{d-1}; the results are summarized in Fig. [3.1].

3.5 Comments on Weak Cosmic Censorship Violation

Naturally, one may ask which geometry arises at the end state of this instability, an Schwarzschild-AdS$_d$ black hole (SAdS$_d$ BH) or a novel non-uniform AdS$_d$ black string (AdS$_d$ nUBS) configuration, and if a violation of weak cosmic censorship occurs during the transition, especially in $d = 4$. As it turns out, the existence of a GL mode is insufficient to provide a violation of weak cosmic censorship [3] (see [71, 72] where GL points exist but a tunneling event is not expected to occur). One is further required to compute the entropy of the nUBS solution and determine its dominance in the phase diagram. It is then reasonable to conjecture that weak cosmic censorship is violated, if (i) a GL mode exists, and (ii) the non-uniform solution has a subdominant entropy relative to the uniform solution ($S_{\rm nUBS} < S_{\rm UBS}$).

[3] We would like to thank Jorge Santos for valuable communications on this matter.

In the absence of a dynamical scalar, a suggestive set of non-uniform saddles can be constructed by foliating AdS_d in terms of AdS_{d-1} slices and then replacing each slice with SAdS_{d-1} black holes (BH). The resulting solutions to Eqn. (3.1) are exact AdS_d black funnels (BF) [73, 74]

$$\begin{aligned} \mathrm{d}s^2_{\mathrm{BF}} &= \frac{(L_d/\ell_{d-1})^2}{\cos(z/\ell_{d-1})^2}\left[\mathrm{d}z^2 - V(\hat{r})\mathrm{d}\hat{t}^2 + \frac{\mathrm{d}\hat{r}^2}{V(\hat{r})} + \hat{r}^2\mathrm{d}s^2_{S^{d-3}}\right], \\ V(\hat{r}) &= 1 - \hat{m}\hat{r}^{4-d} - \hat{r}^2\ell^2_{d-1}, \quad \sigma(z) = \sigma_0 \end{aligned} \tag{3.19}$$

which are locally conformal to $\mathrm{AdS}_{d-1}\times\mathbb{R}$. The phase diagram now contains (at least [71]) three black objects with distinct horizon topologies $\mathcal{H}$ and scalar minima; SAdS_d BH with $(\sigma = \sigma_0, \mathcal{H} = S^{d-2})$, AdS_d BF with $(\sigma = \sigma_0, \mathcal{H} = \Omega^2_z(S^{d-3}\times\mathbb{R}))$, and AdS_{d-1} UBS with $(\sigma \propto z, \mathcal{H} = S^{d-3}\times\mathbb{R})$. On thermodynamic grounds, transitions between these geometries is expected at a critical point $M_\star$ [71]. Clearly, a violation of weak cosmic censorship is expected in any first order transition between black string and black hole phases, whereas fragmentation does not occur during transitions between black string phases which share conformally equivalent horizon topologies. If the BF phase is entropically dominant, then an energy barrier will separate the UBS and BH phases. Hence, the statement of weak cosmic censorship violation amounts to finding regimes where $S_{\mathrm{BF}} < S_{\mathrm{UBS}}$ so that transitions between black strings and black holes occur. Such a regime will depend on the control parameter $\mu_z = L_z/\ell_{d-1}$. One should expect that area difference of the UBS and BF strips, with length $z \in [-\pi L_z/2, \pi L_z/2]$, should be negative for sufficiently small μ_z (see Fig. 3.2). We confirm this via entropy estimates in $d \geq 5$. The thermodynamics read

$$M_{\mathrm{BF}} = (d-3)\hat{r}_+^{d-4}\left[E_{S^{d-3}} + \frac{\hat{r}_+^2}{\ell^2_{d-1}}\right] I_d(\mu_z), \tag{3.20}$$

$$S_{\mathrm{BF}} = 4\pi\hat{r}_+^{d-3} I_d(\mu_z), \tag{3.21}$$

where $I_d(\mu_z) = (2\pi)^{-1}(\frac{d-1}{d-2})^{(d-2)/2}\int_{-\pi/2}^{\pi/2}\cos(\mu_z x)^{2-d}\mathrm{d}x$ which is convergent for $\mu_z < 1$ (see Eqn. (3.3)). Along the line $M_{\mathrm{BF}} = M_{\mathrm{UBS}}$, the entropy difference may be estimated in the stable regime $(\mu_+, \hat{\mu}_+) \gg E_{S^{d-3}}$ via

$$\Delta S(\mu_z) = S_{\mathrm{UBS}} - S_{\mathrm{BF}} \approx S_{\mathrm{UBS}}\left(1 - I_d(\mu_z)^{\frac{1}{d-2}}\right). \tag{3.22}$$

The UBS and BF phases exchange dominance when $I_d(\mu_z^c) = 1$. Under these conditions, it is reasonable to conjecture that *weak cosmic censorship is violated provided the non-uniform saddle corresponds to an exact AdS_d black funnel geometry.*

3.6 Conclusions

We find the spectra of scalar operators on Locally $\mathrm{AdS}_{d-1}\times\mathbb{R}$ uniform black strings supported by a massless scalar [55, 86] are indeed uncorrelated in $d \geq 5$, contrary to prior

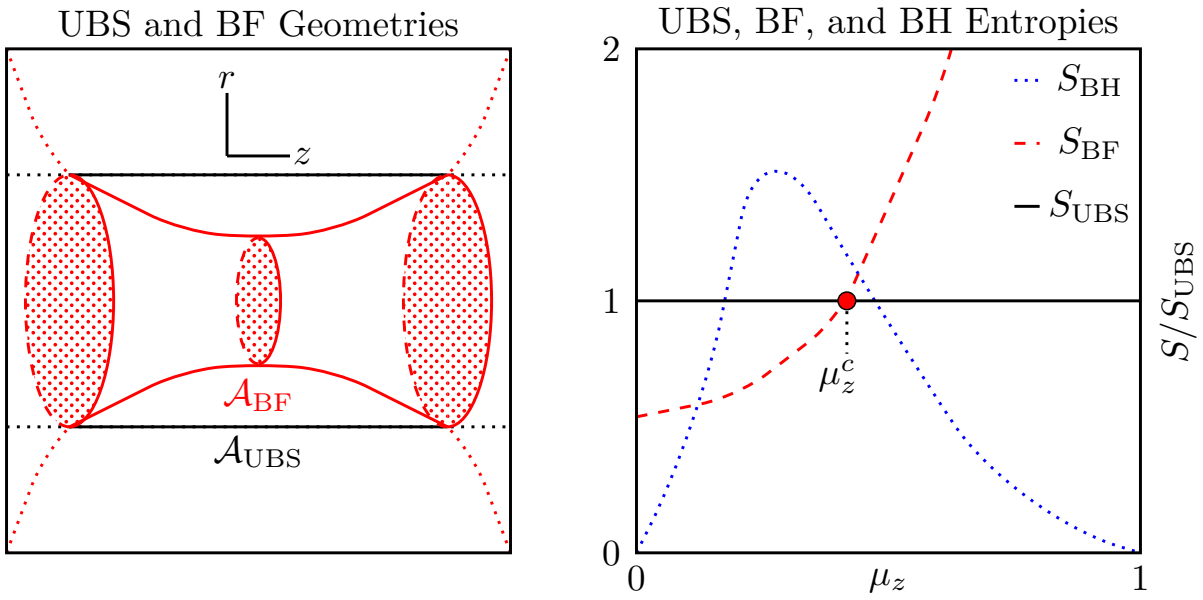

Figure 3.2: Left: Diagram of coincident UBS and BF geometries within the strip $z \in [-\pi L_z/2, \pi L_z/2]$ at equal mass. Right: The UBS is entropically dominant over the BF solution for $\mu_z < \mu_z^c$. The BH entropy is observed to follow the above trend.

expectations [75–78], and this solution falls into the class of black strings covered by correlated stability in $d \geq 4$. Tachyonic modes in the Laplace-Beltrami spectrum appear to be only sufficient to generate classical instabilities. This suggests that black string instabilities are triggered only if there exist tachyonic modes in $\mathrm{Spec}(\Delta_{\rm L})$. Lastly, we have found a regime of intermediate AdS_{d-1} UBS solutions which are entropically favorable over exact AdS_d BF and compete directly with Schwarzschild-AdS_d BHs. Although a complete numerical study of the Einstein-Dilaton-AdS_d model is needed to elucidate if weak cosmic censorship is violated, the thermodynamic argument presents some preliminary evidence that the instability can tunnel a UBS to a BH. In AdS_d with a constant scalar, it is well known that additional black objects, such as black droplets, exist in the thermodynamic phase space [71]. These black objects do not change the qualitative argument given here as the horizons in such cases are partitioned, and hence it is reasonable to conjecture a violation of weak cosmic censorship in $d \geq 5$. It is of interest to understand which configuration the AdS_{d-1} UBS will ultimately converge onto.

Acknowledgments

The authors acknowledge the use of the **diffgeo** Mathematica package for their symbolic tensor calculations [90]. We thank Jorge Santos, Robie Hennigar, Robert Mann, and Matthew Headrick for discussions and hospitality. We are supported by the University of Minnesota Doctoral Dissertation Fellowship. A. D. is supported by the National Science

Foundation Graduate Research Fellowship under Grant No. 00039202.

Note Added. After the completion of the present analysis, we were made aware of similar work carried out independently in $d = 5$ [91]. The analysis of the AdS_4 UBS solution there involved a power series expansion of the metric perturbation h_{tr} in order to search for an instability. We would like to thank the authors of [55] for sharing their preprint along with their helpful insights on the subject.

Part II

Holography: Encoding Information via Dualities

Chapter 4

A Primer on Dualities

Dualities are prevalent in the history of physics. The first well known classical duality was the electromagnetic duality. Indeed, one can show that Maxwell's equations remain invariant under a transformation in which the electric and magnetic fields are swapped [92]. As is often the case, the fundamental structure which permits this duality is spacetime geometry and its isometries. In particular, for electromagnetism formulated on manifolds respecting Lorentz covariance, a Lorentz transformation on the electric field maps it onto the magnetic field. In this way, the existence of the duality is predicated on the underlying spacetime geometry and its isometry group.

Another duality, though often not discussed in this way, is the Fourier transform [93] encountered in Sec. 1.1. Suppose we wished to solve a linear differential equation in the form

$$\sum_n c_n(\partial_x)^n \Phi(x) = 0$$

where the constants c_i are unknown. Provided initial and boundary data, the theory of ordinary differential equations guarantees the existence of a solution though it may be hard to find. If, however, there exists a function $\phi(p)$ related to $\Phi(x)$ by a Fourier transform, the problem of solving the above PDE is reduced to finding roots of the complex polynomial equation

$$\sum_n c_n(\mathrm{i}p)^n = 0$$

which is a much simpler. In this sense, we say that differential equations in $\mathbb{R}_x$ (and more generally $\mathbb{R}^n_x$) are dual to polynomial equations in $\mathbb{R}_p$ (similarly $\mathbb{R}^n_p$). Note, this is only possible for manifolds which admit a well-defined notion of a Fourier transform, i.e., manifolds with well-defined Poyntragin duals. Again we see that manifolds require a high degree of symmetry which can be used to construct such dualities. We now turn to dualities in general.

Dualities are mathematical correspondences; an isomorphism between two seemingly disparate systems which share an underlying symmetry. Often, dualities translate hard problems from one system into more tractable problems in another. Hence, by searching

for dualities one can derive rich physical insights and possibly solve intractable problems. In general, non-trivial dualities provide more information as one is able to both explore known physical regimes and unknown landscapes of the theory space.

Here, we are primarily concerned with quantum/classical dualities. Such dualities are quite powerful as they provide a sharp dictionary encoding observables, correlation functions, and (non-)equilibrium quantum behavior into the equations of motion, geodesics, and geometries in the dual classical theory.

In order to build intuition for such a duality, we focus on a simpler example. Here, we first show how one can map the $(d+1)$-dimensional classical Ising model onto a d-dimensional qubit Ising model in an external magnetic field. Along the way, we will write a formal statement of what justifies this duality, establish a dictionary between the two systems ($\tilde{J}_{ij} \leftrightarrow (J, g)$), and identify the physical insights one can draw when utilizing dualities.

Once built, this intuition can then be applied to the gauge/gravity duality. In particular, we discuss the holographic gauge/gravity which offers a powerful description of strongly coupled d-dimensional $SU(N_c)$ gauge theories in terms of a weakly coupled $(d+1)$-dimensional gravitational theory in AdS. We will then explore various applications of the gauge/gravity duality to deformations of $4d$ $SU(N_c)$ Yang-Mills theory.

4.1 Dualities of the Ising Model

The $2d$ Ising model is perhaps the most well recognized model in condensed matter and statistical physics and described by the Hamiltonian

$$H = -\sum_{\langle i,j \rangle} \tilde{J}_{ij} S_i S_j \tag{4.1}$$

where classical spins $S_k \in \{-1, 1\}$ rest on each lattice site $i \in \Lambda_2$ and interact with their nearest neighbors $\langle i, j \rangle$ with strength $\tilde{J}_{ij}$. In this primer to dualities, we demonstrate that the above Hamiltonian for the $2d$ classical Ising model is dual to the quantum transverse field Ising chain (TFIC)

$$\hat{H} = -J\left[\sum_{\langle i,j \rangle} Z_i Z_j + g \sum_k X_k\right] \tag{4.2}$$

where g denotes the magnetic moment of the transverse magnetic field, J sets the overall energy scale, and X, Z are the Pauli spin matrices in the denoted directions.

4.1.1 Encoding the $1d$ Classical Ising Model onto a Qubit

Let us consider this duality in one spatial dimension. The $1d$ classical Ising model is either a line or chain of classical spins depending if one has free or periodic boundary

conditions. Here, we assume periodic boundary conditions on a chain of N spins, denoted by $\bigcirc$. This can be modeled by the Hamiltonian

$$H^{\bigcirc} \equiv H_{\text{Ising}_{1d}} = -\tilde{J}\sum_{i=1}^{N} S_i S_{i+1} \tag{4.3}$$

where the interaction strength has been assumed to be uniform $\tilde{J}_{i,i+1} = \tilde{J}$. The 2^N configurations can be represented by the following partition function

$$\mathcal{Z}^{\bigcirc} \equiv \mathcal{Z}_{\text{Ising}_{1d}} = \sum_{\{S\}} e^{-\beta_{\text{Ising}} H(S)} = \sum_{\{S\}} \exp\left(K\sum_{i=1}^{N} S_i S_{i+1}\right) \tag{4.4}$$

where $K = \beta_{\text{Ising}}\tilde{J}$. Now the goal is to show that the partition function is equivalent to the partition function for a single qubit. Observe that the duality is at the level of the partition functions, and not the individual Hamiltonians. This will come up again in the holographic gauge/gravity duality.

To establish the equivalence, we employ the transfer matrix method. The trick is to write $\mathcal{Z}^{\bigcirc}$ as a trace over a matrix product. To facilitate this, we first complete the square

$$\mathcal{Z}^{\bigcirc} = e^{KN}\sum_{\{S\}} \exp\left(-\frac{K}{2}\sum_{i=1}^{N}[S_i - S_{i+1}]^2\right) = e^{KN}\sum_{\{S\}}\prod_{i=1}^{N} e^{-\mathcal{L}(i,i+1)} \tag{4.5}$$

where we have used that the residual term $\sum_i (S_i^2 + S_{i+1}^2) = 2N$ since each spin belongs to $S_i \in \{-1, 1\}$.

We now make a conceptual leap in logic. Imagine, rather than the spins lying on a line, consider a single spin (say S_1) evolving in Euclidean time τ. That is, we think of the spatial circle instead as a time direction in Euclidean signature. If so, then the difference of the spins may be treated as a time derivative, or a matrix operator, acting on S_1 and evolving it to a final state S_N. This operator $e^{-\mathcal{L}(i,i+1)} = T(i, i+1)$ as a 2×2 matrix repeated acting on S_1. The matrix elements of the transfer matrix are determined by the value of the spin at the lattice site. For $S_i = S_{i+1}$, one obtains $T(i, i+1) = 1$ whereas when $S_i = -S_{i+1}$, one obtains $T(i, i+1) = e^{-2K}$. The upshot is then that

$$T(i, i+1) = \begin{pmatrix} 1 & e^{-2K} \\ e^{-2K} & 1 \end{pmatrix}_{i,i+1} = \langle S_i|\mathbf{T}|S_{i+1}\rangle \tag{4.6}$$

where in the last equality, we identify $\mathbf{T}$ as an quantum operator acting on a two level quantum system. Hence, one obtains

$$\begin{aligned}
\mathcal{Z}^{\bigcirc} &= e^{KN}\sum_{\{S\}}\prod_{i=1}^{N} e^{-\mathcal{L}(i,i+1)} = e^{KN}\sum_{\{S\}}\prod_{i=1}^{N} T(i, i+1) \\
&= e^{KN}\sum_{S_1=\pm 1}\cdots\sum_{S_N=\pm 1}\langle S_1|\mathbf{T}|S_2\rangle\cdots\langle S_N|\mathbf{T}|S_{N+1}\rangle \\
&= \sum_{S_1=\pm 1}\langle S_1|(e^K\mathbf{T})^N|S_{N+1}\rangle = \text{tr}\Big(\mathbf{t}^N\Big).
\end{aligned}$$

The Qubit Hamiltonian

The last step to encode the classical Ising chain is to demand that $\mathbf{t}^N$ is equal to the new Hamiltonian $\hat{H}^{\odot}$ for a single qubit, denoted by $\odot$, evolving in Euclidean time $\beta = N\delta\tau$ in a transverse field. First, note that $\mathbf{t}$ is Hermitian, hence

$$\mathbf{t} = e^{K}(\mathbb{I} + e^{-2K}X) \tag{4.7}$$

where X is the Pauli matrix. This is possible as the Pauli matrices $(\mathbb{I}, X, Y, Z)$ form an orthonormal basis in the vector space of 2×2 Hermitian matrices. Then we ask, under what conditions can one construct a Hamiltonian $\hat{H}^{\odot}$ which satisfies

$$\mathbf{t} = \exp\left(-\delta\tau \hat{H}^{\odot}\right)? \tag{4.8}$$

Since the Hamiltonian for an isolated qubit is also Hermitian, and since the Y and Z operators do not appear in the transfer matrix, we can start with the ansatz

$$-\delta\tau \hat{H}^{\odot} = a\mathbb{I} + bX. \tag{4.9}$$

Recalling that $e^{a\mathbb{I}} = e^{a}\mathbb{I}$ and that $e^{bX} = (\cosh(b)\mathbb{I} + \sinh(b)X)$, Eqn. (4.8) reads

$$e^{K}(\mathbb{I} + e^{-2K}X) = \begin{pmatrix} e^{K} & e^{-K} \\ e^{-K} & e^{K} \end{pmatrix} = e^{a}(\cosh(b)\mathbb{I} + \sinh(b)X)$$

which can be solved to set $e^{-2K} = \tanh(b)$ and $e^{a} = 2\sinh(K)\cosh(K)$. Hence we arrive at the Hamiltonian

$$\boxed{\hat{H}^{\odot} = -E_g\mathbb{I} - \frac{\Delta}{2}X} \tag{4.10}$$

where $E_g = a/\delta\tau$ is identified as the ground state energy, $\Delta = 2b/\delta\tau$ is the energy gap, and the magnetic moment is set by $\Delta = 2Jg$.

We started with the 1D Ising model and claimed that we can map it onto a Hamiltonian for a single qubit. If so, then there should be no Z_iZ_{i+1} interaction terms in the quantum Hamiltonian as there are no other qubits. Therefore, all on-site interactions are self interactions which contribute to the ground state energy. We can identify the ground state energy using the Ising temperature $K = \beta_{\text{Ising}}\tilde{J}$. By sending, $K \to \infty$ ($\beta_{\text{Ising}} = (T_{\text{Ising}})^{-1} \to \infty$), one sends $b \to 0$ and $a \to \infty$ in which case we have

$$\hat{H}^{\odot} \approx -E_g\mathbb{I}. \tag{4.11}$$

Hence, at zero Ising temperature, we see that E_g must be the correct ground state energy and there is no magnetic field. In the presence of a magnetic field, i.e., finite Ising temperature, there is an energy gap set by Δ. The absence of any finite Ising temperature phase transition for the qubit is clearly related to the lack of a transition for the $1d$ Ising model.

Thus, we have a precise statement of the duality between the $1d$ Classical Ising chain and the $0d$ single qubit evolving in Euclidean time, namely

$$\mathcal{Z}^{\bigcirc} = \mathrm{Tr}(\mathbf{t}^N) = \mathrm{Tr}(e^{-\beta\hat{H}^{\bigodot}}) \equiv \mathcal{Z}^{\bigodot}$$
$$e^{-2K} = \tanh(Jg\delta\tau)$$

Furthermore, it is straightforward to evaluate the partition function in this case by diagonalizing $\mathbf{t}$ and using the cylicity of the trace:

$$\mathrm{Tr}(\mathbf{t}^N) = \lambda_+^N + \lambda_-^N = 2^N\Big(\cosh(K)^N + \sinh(K)^N\Big). \tag{4.12}$$

4.1.2 Encoding the $2d$ Classical Ising Model onto Qubit Chains

The calculations for the $2d/1d$ are somewhat involved but are quite similar in spirit. We sketch the duality heuristically here (see McGreevy's lecture notes for detailed calculations and Tim Hsieh's high level exposition, which discusses other lattice dualities). Essentially, the argument is as follows. Starting with the $2d$ Ising Hamiltonian, where i, j span the τ, x directions respectively,

$$H_{2d\ \mathrm{Ising}} = \sum_{\langle i,j\rangle} K_x S_j(i)S_{j+1}(i) + K_\tau S_j(i)S_j(i+1) \tag{4.13}$$

suppose we partitioned the $2d$ $n \times n$ lattice, say verticially, into several chains which are weakly interacting spatially $K_x \ll 1$. We can then treat each vertical line of spins as a Euclidean timeline for a single spin. Once again, we construct a $2^n \times 2^n$ transfer matrix T between any two successive time slices defined by

$$T^{x,x}_{\tau,\tau+1} = \exp(-\mathcal{L}(\tau, x; \tau+1, x))$$

which takes a spin at site x at Euclidean time τ to $\tau+1$. Here $\mathcal{L}$ is shifted by a constant from $H_{2d\mathrm{Ising}}$ upon completing the square as above. Applying the transfer matrix successively to each spin site $x = 1, 2, \ldots, n$ one can show that

$$\mathcal{Z}_{2d\ \mathrm{Ising}} = \sum_S e^{-H_{2d\ \mathrm{Ising}}} = \sum_S \prod_{\tau=1}^{n} T^{x,x}_{\tau,\tau+1} = \mathrm{tr}_{\mathcal{H}}(\mathbf{t})$$

where the Hilbert space consists of a two-state system at every site $\mathcal{H} = \bigotimes_j \mathcal{H}_j$. Next, we suppose that there exists a quantum Hamiltonian $\hat{H}$ on each site for which

$$\mathbf{t} = \exp\Big(-\delta\tau\hat{H}\Big).$$

This time, however, appealing to the Hermiticity is not enough to determine the relation between parameters in $\hat{H}$ and $H_{2d\ \mathrm{Ising}}$. Rather, we will have to expand assuming $\delta\tau \ll 1$. In the approximation, one would find the relations $K_x \sim \delta\tau$ and $e^{-2K_\tau} \sim \delta\tau$ and hence,

there exists a fixed ratio $g = e^{-2K_\tau}/K_x$ which can be used to study the transfer matrix perturbately. Using these relations, we may write the Hamiltonian ansatz for a $1d$ qubit chain as

$$\hat{H} \equiv \hat{H}_{1d\ \mathrm{QC}} = -J\left(\sum_i Z_i Z_{i+1} + g\sum_i X_i\right). \tag{4.14}$$

Repeating the calculation from the quantum to classical side fixes the precise relations as

$$K_x = J\delta\tau \qquad e^{-2K_\tau} = \tanh(gK_x) \tag{4.15}$$

and thus we arrive at the statement of the equivalence of partition functions

$$\mathcal{Z}_{2d\ \mathrm{Ising}} = \mathcal{Z}_{1d\ \mathrm{QC}}. \tag{4.16}$$

The duality is established again at the level of the partition function. Furthermore, the duality provides a mapping between a statistical system that is one spatial dimension higher than the quantum system. However, the total number of dimensions have not changed, one spatial dimension in the Ising model has been repurposed as a Euclidean time direction. Lastly, observe that the duality holds along a special curve in the moduli space of (K_τ, K_x). Specifically, (K_τ, K_x) are not free parameters since $e^{-2K_\tau} = \tanh(gK_x)$ for some g.

Phase Transitions

Let us check the robustness of the duality by studying the thermal behavior of both theories. For a square lattice, Onsager found the mean magnetization for the $2d$ Ising model to be

$$M = (1 - [\sinh(2K_\tau)\sinh(2K_x)]^{-2})^{1/8} \tag{4.17}$$

With the phase transition occurring at $\sinh(2K_\tau)\sinh(2K_x) = 1$. If the duality written above is to be believed, then we can compute the free energy of the $1d$ qubit chain as

$$F_{1d\ \mathrm{QC}} = -\log(\mathcal{Z}_{1d\ \mathrm{QC}}) = -\log(\mathcal{Z}_{2d\ \mathrm{Ising}})$$

and hence any phase transitions in $\mathcal{Z}_{2d\ \mathrm{Ising}}$ should also be present in $\mathcal{Z}_{1d\ \mathrm{QC}}$ in the thermodynamic limit $n \to \infty$. We can check this by studying the mean magnetization for finite sized qubit chains

$$M_Q = \frac{1}{N}\langle \mathrm{gs}|\hat{M}|\mathrm{gs}\rangle \tag{4.18}$$

where $\hat{M}$ is the magnetization operator and $|\mathrm{gs}\rangle$ refers to the ground state of the spin chain. From the duality, since $K_\tau = -\frac{1}{2}\log(\tanh(gK_x))$ the phase transition should occur when $\sinh(2K_x)\mathrm{csch}(2gK_x) = 1$, i.e., $g = 1$.

As can be checked from my code here, there appears to be a phase transition around $g \approx 1$. For small coupling values, the spins are all anti-aligned with the external magnetic

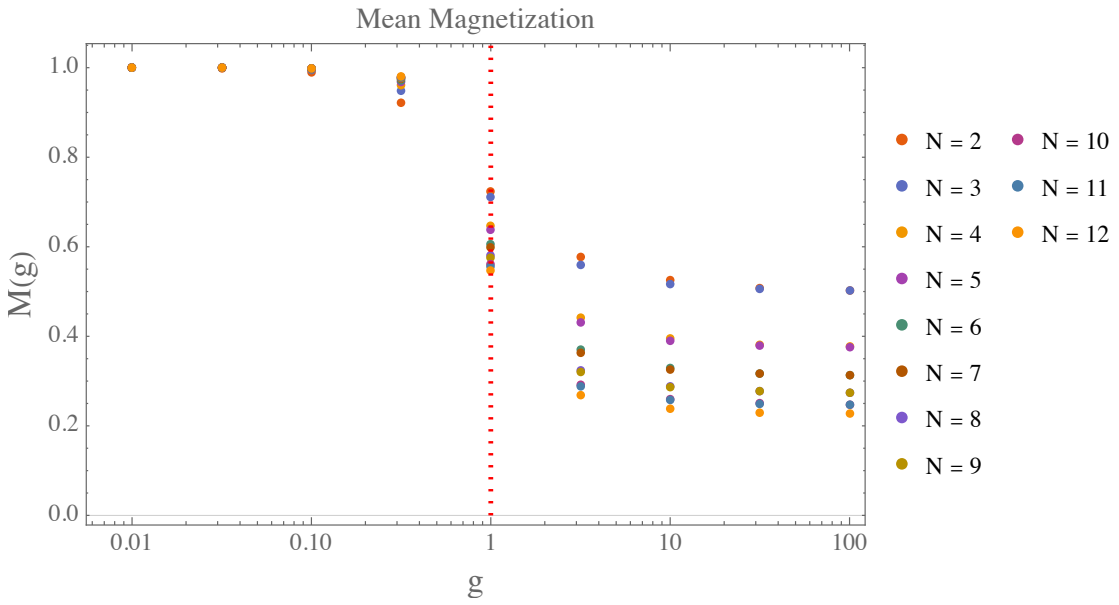

Figure 4.1: The mean magnetization as a function of coupling g.

field hence $M_Q \approx 1$. At larger couplings, the spins flip to be aligned with the external field thereby becoming paramagnetic with $M_Q \to 0$ in the large N limit. The trend can be confirmed for larger qubit chains, but the computational time is prohibitive.

4.1.3 Generalizing the Classical/Quantum Correspondence

The dualities discussed above can be generalized into higher dimensions via the following protocol:

1. Absorb the thermodynamic temperature β_{Ising} of the Ising model into the interaction strengths $\tilde{J}_{ij}$. Assume that the interaction strenths are uniform along their respective axis.

2. Denote one of the $(d+1)$ spatial directions as Euclidean time, τ, and consider the partition $N\delta\tau = \beta$ as the quantum temperature.

3. Apply the transfer matrix to convert the partition function of a statistical system into the partition of a quantum system evolving in Euclidean time.

4. Perform a perturbative analysis to establish a dictionary between the coupling parameters of both systems.

Obviously, the third step is the tricky leap in intution, but in the cases where this can be applied, we arrive at the formal equivalence between the partition functions of the two systems:

$$\mathcal{Z}_{(d+1)\ \text{Ising}}(K_\tau, K_{x^d}) = \mathcal{Z}_{d\ \text{TFIC}}(J_{x^d}, g) \tag{4.19}$$

where K_τ is the interaction strength along the Euclidean time direction and K_{x^d} in the remaining spatial directions. The precise map between these parameters and those in the TFIC are given by the following dictionary.

Classical	**Quantum**
$(d+1)$ spatial dimensions	d spatial dimensions, 1 time dimension
Transfer Matrix $\mathbf{t}$	Euclidean-time Propagator $e^{-\Delta\tau \mathbf{H}}$
Ising Temperature β_{Ising}	Lattice Couplings Strengths (J_{x^d}, g)
Periodicity of Euclidean time τ	Quantum Temperature: $\beta = \delta\tau N$
Equilibrium State	Ground State

Table 4.1: The dictionary between the $(d+1)$-dimensional Ising model and the d-dimensional quantum transverse field Ising chain.

Building A Dictionary for Dualities

When mapping the $1d$ Ising model onto a qubit, we found that the coupling constant $K = \beta_{\text{Ising}}\tilde{J}$ was related to the parameters (J, g) via $e^{-2K} = e^{-2\beta_{\text{Ising}}\tilde{J}} = \tanh(Jg\delta\tau)$. Since in the $1d$ Ising model, there are no other spatial directions, we must have that $K = K_\tau$ in the notation above. In higher dimensions ($J \to J_{x^d}$), this still holds true so $K = K_\tau$ and the remaining spatial lattice parameters can be shown to satisfy $K_{x^d} = J_{x^d}\delta\tau$. Finally, the duality only holds along the line in moduli space $K_\tau = -\frac{1}{2}\log(\tanh(gK_{x^d}))$ (see these notes for details).

4.2 The Gauge/Gravity Duality

In exploring the Ising model, we learned several features of quantum/classical dualities. Broadly, such dualities have a classical theory in one spatial dimension higher than the quantum theorem, display an equivalence between the partition functions of each theory, and contains a dictionary providing a precise map between parameters. In the next step towards exploring the intersections between classical gravity and quantum information, we discuss briefly the gauge/gravity duality. For a comprehensive review of the duality, see [94].

The gauge/gravity duality is a holographic duality which offers a powerful window into the physics of certain quantum field theories at finite temperature with the thermodynamics of classical geometry (see Part I). Specifically, we are interested in using the gauge/gravity duality to study strongly coupled $SU(N)$ gauge theories at finite temperature. For these theories, the partition function, $\mathcal{Z}_{\text{GT}}$, cannot be analytically computed using perturbative methods. Rather, the duality provides a framework for asking sharp questions about the behavior of gauge theories at strong coupling and finite temperature

by encoding these properties into the partition function of certain quantum gravity theories, $\mathcal{Z}_{\rm QG}$, at weak coupling. This strong-weak relationship between the parameters is analogous to anisotropic couplings found in the Ising model duality.

Akin to the quantum/classical duality of the Ising model, the gauge/gravity duality rests on the holographic principle which asserts that the information stored in a volume V_{d+1} is encoded in its boundary area A_d. Hence, we can think of a strongly coupled gauge theory as living on the codimension one boundary of a weakly coupled quantum gravity theory in a bulk and relates $\mathcal{Z}_{\rm GT} = \mathcal{Z}_{\rm QG}$. To be more precise, the strongest form of the gauge/gravity duality states that

$\mathcal{N} = 4$ Super Yang-Mills (SYM) theory with gauge group $SU(N)$ and Yang-Mills coupling constant $g_{\rm YM}$
is *dynamically equivalent* to
type IIB superstring theory with string length $\ell_S = \sqrt{\alpha'}$ and coupling constant g_s on $\mathrm{AdS}_5 \times S^5$ with radius of curvature L and N units of $F_{(5)}$ flux on S^5.

The two free parameters on the field theory side, $g_{\rm YM}$ and N, are mapped to the free parameters g_s and $L/\sqrt{\alpha'}$ on the string theory side by $g^2_{\rm YM} = 2\pi g_s$ and $2g^2_{\rm YM}N = L^4/(\alpha')^2$. More compactly, the partition functions of both theories satisfy [13, 95, 96]

$$\mathcal{Z}_{\mathcal{N}=4} = \mathcal{Z}_{\rm IIB} \tag{4.20}$$

for arbitrary couplings. Although the strongest form of the gauge/gravity duality is conceptually interesting, it remains difficult to perform explicit calculations with arbitrary values of the parameters. However, in the 't Hooft limit, which is $N \to \infty$, $g_s \ll 1$, $g_{\rm YM} \ll 1$, and $g^2_{\rm YM}N$ fixed, the gauge theory is strongly coupled, and the dual gravity theory may be treated as classical and weakly curved. In this regime, otherwise intractable non-perturbative analyses at strong coupling and finite temperature becomes tractable calculations of the thermodynamics of classical saddle points, i.e., tree level contributions, of the IIB action to the partition function. The duality has passed several nontrivial consistency checks, and provided some motivation that the QGP phase behaves as a perfect fluid rather than a free gas.

The most promising application of the duality lies in the identification of a gravitational model which replicates features of QCD at strong coupling. There are two ways to approach this problem; bottom-up or top-down. In a bottom-up approach, one builds a particular gravity model by introducing 3-branes in conjunction with additional bulk fields thereby deforming the boundary gauge theory towards QCD. These AdS/QCD models faithfully reproduce certain phenomenological features such as electroweak or chiral symmetry breaking, bulk/shear viscosities, and dynamical confinement. In a top-down approach, one uses the facts that Yang-Mills is a closely related cousin of QCD, and that the 't Hooft limit behaves as a thermodynamic limit when the boundary gauge theory

lives on the compact manifold S^d in order to study thermal aspects of QCD such as the deconfinement/confinement phase transition. Both approaches provide valuable information and insight into the strong coupling, finite temperature properties of gauge theories. In the following chapters, we explore applications of holographic quantum/classical dualities to deformations of $4d$ $SU(N_c)$ Yang-Mills (a closely related cousin of QCD).

Chapter 5

Dynamical AdS/Yang-Mills

This chapter is a faithful reproduction of the published work **S. P. Bartz, A. Dhuntarao, and J. I. Kapusta, Phys. Rev. D, 98(2), 0236019, (2018)** with minor edits [97].

Abstract

The AdS/CFT correspondence has provided new and useful insights into the nonperturbative regime of strongly coupled gauge theories. We construct a class of models meant to mimic Yang-Mills theory using the superpotential method. This method allows us to efficiently address the problem of solving all the equations of motion. The conformal symmetry is broken in the infrared by a dilaton field. Using a five-dimensional action we calculate the mass spectrum of scalar glueballs. This spectrum contains a tachyon, indicating an instability in the theory. We stabilize the theory by introducing a cosmological constant in the bulk and a pair of 3-branes, as in the Randall-Sundrum model. The scalar glueball masses computed by lattice gauge theory are then described very well by just a few parameters. Prospects for extending the model to other spins and parities and to finite temperature are considered.

5.1 Introduction

The AdS/CFT correspondence has proven to be a useful mathematical tool for the analysis of certain strongly coupled gauge theories. This correspondence establishes a connection between a d-dimensional super-Yang Mills (SYM) theory and a weakly coupled gravitational theory in d+1 dimensions [13, 95, 96]. Perturbation theory can be used to solve SYM at small coupling but it fails at large coupling, whereas the reverse is true in the gravity dual. QCD is a strongly-coupled gauge theory at hadronic scales, making it a prime candidate for the application of the gauge/gravity correspondence. However, it is still not known whether a gravitational dual to QCD exists. The so-called bottom-up

approach assumes the existence of such a dual, modeling features of QCD by an effective five-dimensional gravity theory. Linear confinement in QCD provides a scale that is embodied in an IR cut-off of the fifth dimension in the AdS/QCD model [98, 99]; these are referred to as hard-wall models. Soft-wall models use a dilaton field as an effective IR cutoff [100]. The simplest of these uses a dilaton quadratic in the fifth dimensional coordinate to provide linear radial Regge trajectories. Others modify the UV behavior of the dilaton to more accurately model the ground state masses as well [101–104].

Typically, soft-wall models of QCD use parametrizations for the background dilaton and chiral fields that are not derived as the solution to any equations of motion. The problem is that there is always one more equation than there are independent fields, causing a severe self-consistency condition on the potential. Previously, two of us expanded upon previous work [105–112] to find a suitable potential for the background fields of a soft-wall AdS/QCD model [113]. A glueball field was added, and a potential was constructed which led to a dynamical dilaton and a good description of the mass spectra of vector, axial-vector, and pseudoscalar mesons. A shortfall of that approach was that there was a special term in the potential, dependent on the dilaton field, that could only be determined numerically *a posteriori* and that did not appear to have a natural functional form. It remains an open problem to find a well-defined, natural action that provides a set of background equations from which these fields can be derived. A solution to that problem may suggest how it can be derived from a top-down approach. A well-defined action with good phenomenology is necessary to provide access to the thermal properties of the model through perturbation of the geometry [108, 114, 115].

Our goal is to find a relatively simple analytic potential for Yang-Mills theory which is self-consistent, which satisfies the basic requirements of the gauge/gravity correspondence, and which reproduces the scalar glueball mass spectrum as computed in lattice gauge theory. This would be useful not only for hadron phenomenology but might point towards a ten-dimensional string model from which it arises. In addition, an analytic potential would greatly simplify the task of applying the model at finite temperature, such as the equation of state and the transport coefficients. This task suggests using the tools of supersymmetry. We will therefore follow Ref. [105] which used two fields and a superpotential method. In what follows one of the fields is the dilaton and the other is a scalar glueball.

We can illustrate the enduring interest in the relationship between Yang-Mills theory and the gauge/gravity correspondence with two papers separated by two decades. Csáki *et al.* [116] calculated the scalar glueball masses by solving supergravity wave equations in a black hole geometry and compared the results to the then-available lattice calculations. Ballon-Bayona *et al.* [117] investigated effective holographic models for QCD and proposed semianalytic interpolations between the UV and the IR to obtain a spectrum for scalar and tensor glueballs consistent with current lattice QCD calculations. In that

approach the dilaton was identified as the glueball. A UV cutoff has been a persistent issue, which we will address directly in our paper.

The outline of our paper is as follows. In Sec. 5.2 we review the results for scalar glueball masses computed in lattice gauge theory. In Sec. 5.3 we give the basic setup for the five-dimensional action. Some possible potentials which incorporate the proper behavior are given in Sec. 5.4. A specific example is worked out in detail in Sec. 5.5. We solve a Schrödinger equation for the glueball mass spectrum in Sec. 5.6 where it is found that the lowest state is a tachyon, which seems to be a generic result. In order to stabilize the theory we consider the Randall-Sundrum model, which is briefly reviewed in Sec. 5.7. The dilaton and glueball fields are added to the Randall-Sundrum model in Sec. 5.8 and the glueball mass spectrum is recalculated in Sec. 5.9 with excellent results. Our summary and conclusion is presented in Sec. 5.10.

5.2 Lattice Results

The 0^{++} glueball mass spectrum, as calculated by lattice gauge theory [118, 119], is shown in Fig. 5.1. The radial quantum number is n and the masses are expressed in terms of the string tension $\sigma = (440\,\mathrm{MeV})^2$. The error bars include statistical uncertainties only. It is apparent that the spectrum is linear at large n. A linear fit to the states $n = 2, 3, 4$ of the form $m_n^2/\sigma = an + b$ results in $a = 20.37 \pm 1.142$ and $b = -1.666 \pm 2.713$. For later use we express this as

$$m_n^2 = 8\lambda(n - 0.082 \pm 0.133) \tag{5.1}$$

with $\sqrt{\lambda} = 702$ MeV. Here we are not interested in the small uncertainty in the slope, only the intercept which is consistent with zero.

We can also make a linear fit to all states including $n = 1$ as shown in Fig. 5.2. The form $m_n^2/\sigma = an + b$ results in $a = 25.178 \pm 1.483$ and $b = -13.859 \pm 1.703$. Then

$$m_n^2 = 8\lambda(n - 0.550 \pm 0.075) \tag{5.2}$$

with $\sqrt{\lambda} = 781$ MeV. In this fit the intercept is clearly negative and the fit is not nearly as good.

5.3 Setup

We assume that the four-dimensional strongly coupled field theory can be modeled by the following five-dimensional action, written in the string frame:

$$\mathcal{S} = \frac{1}{16\pi G_5}\int d^5x\sqrt{g}e^{-2\Phi}\left(R + 4g^{MN}\partial_M\Phi\partial_N\Phi - \tfrac{1}{2}g^{MN}\partial_M G\partial_N G - V(\Phi, G)\right). \tag{5.3}$$

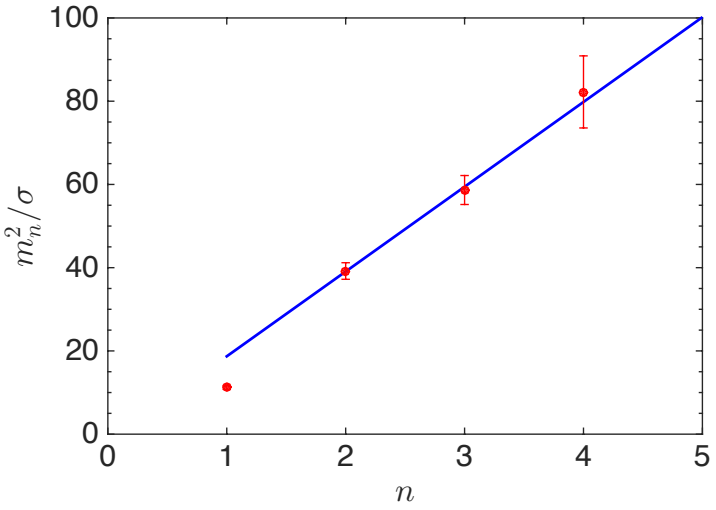

Figure 5.1: The scalar glueball mass spectrum as computed on the lattice in pure SU(3) gauge theory. The linear fit includes $n \geq 2$.

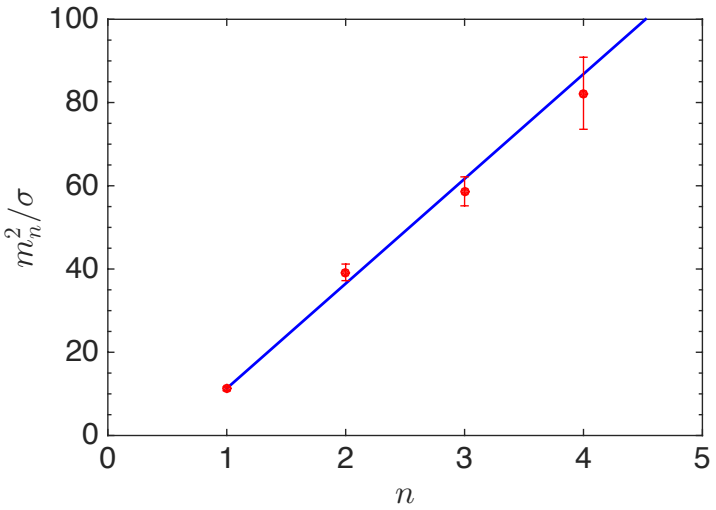

Figure 5.2: The scalar glueball mass spectrum as computed on the lattice in pure SU(3) gauge theory. The linear fit includes $n \geq 1$.

Here Φ is the dilaton and G is the glueball field; these fields are dimensionless. The metric is pure anti-de Sitter (AdS), $g_{MN} = (l/z)^2 \eta_{MN}$ with AdS curvature $R = -30/l^2$ and $g = -\det g_{MN}$.

It is easier to search for the background fields in the Einstein frame, which is obtained from the string frame via the conformal transformation

$$g_{MN} = e^{4\Phi/3} \tilde{g}_{MN} \,. \tag{5.4}$$

where the tilde distinguishes the two frames. Rescaling the dilaton by $\phi = \sqrt{8/3}\Phi$ puts the vacuum action in canonical form

$$\mathcal{S}_E = \frac{1}{16\pi G_5} \int d^5x \sqrt{\tilde{g}} \left(\tilde{R} - \tfrac{1}{2} \tilde{g}^{MN} \partial_M \phi \partial_N \phi - \tfrac{1}{2} \tilde{g}^{MN} \partial_M G \partial_N G - \tilde{V}(\phi, G) \right) , \tag{5.5}$$

with $\tilde{V} = e^{4\Phi/3} V = e^{2\phi/\sqrt{6}} V$.

To apply the superpotential method [120, 121] requires switching from (x^μ, z) to (x^μ, y) coordinates such that

$$ds^2 = e^{-2A(y)} dx^2 + dy^2 \,. \tag{5.6}$$

We look for a background solution with $\phi = \phi(y)$ and $G = G(y)$. The equations of motion are

$$3A'' - 6A'^2 = \tfrac{1}{4}\phi'^2 + \tfrac{1}{4}G'^2 + \tfrac{1}{2}\tilde{V} \,, \tag{5.7}$$

$$6A'^2 = \tfrac{1}{4}\phi'^2 + \tfrac{1}{4}G'^2 - \tfrac{1}{2}\tilde{V} \,, \tag{5.8}$$

$$\phi'' - 4A'\phi' = \frac{\partial \tilde{V}}{\partial \phi} \,, \tag{5.9}$$

$$G'' - 4A'G' = \frac{\partial \tilde{V}}{\partial G} \,. \tag{5.10}$$

Here a prime means differentiation with respect to y. Since there is one more equation than there are independent fields, these equations would not have a solution for an arbitrarily chosen potential $\tilde{V}(\phi, G)$. To solve these equations we convert them to a set of first order differential equations by use of a "superpotential" $W(\phi, G)$ such that

$$A' = W \,, \tag{5.11}$$

$$\phi' = 6 \frac{\partial W}{\partial \phi} \,, \tag{5.12}$$

$$G' = 6 \frac{\partial W}{\partial G} \,. \tag{5.13}$$

Then the original set of equations is satisfied when

$$\tilde{V} = 18 \left[\left(\frac{\partial W}{\partial \phi} \right)^2 + \left(\frac{\partial W}{\partial G} \right)^2 \right] - 12 W^2 \,. \tag{5.14}$$

The challenge is to find a function $W(\phi, G)$ which gives the desired behavior of the fields. But it must be emphasized that any appropriately smooth function W will allow for all the original differential equations to be satisfied, which is our goal.

As discussed above, good hadron phenomenology suggests that A, ϕ, y and z are related in the following ways.

$$\mathrm{e}^{-A} = \frac{l}{z}\,\mathrm{e}^{-a\phi} \tag{5.15}$$

$$dy = \frac{l}{z}\,\mathrm{e}^{-a\phi}\,dz \tag{5.16}$$

Here a is an arbitrary constant. From the first of these equations we clearly have $A = \ln(z/l) + a\phi$. Now the differential equation for A becomes

$$A' = \frac{1}{z}\frac{dz}{dy} + a\phi' = W\,. \tag{5.17}$$

Using the relationship between y and z and the differential equation for ϕ we get a differential equation for W.

$$\frac{\partial W}{\partial \phi} = \frac{1}{6a}\left(W - \frac{1}{l}\,\mathrm{e}^{a\phi}\right) \tag{5.18}$$

As we know from previous studies [106] the constant $a = 1/\sqrt{6}$ in order to have linear radial Regge trajectories; we shall henceforth fix it at that value. Then the most general solution to the differential equation for W is

$$W(\phi, G) = \frac{1}{l}\left[U(G) + 1 - \frac{\phi}{\sqrt{6}}\right] e^{\phi/\sqrt{6}}\,. \tag{5.19}$$

Here U is any function of G; the $+1$ is added for future convenience. The resulting differential equations can be written simply as

$$z\frac{dG}{dz} = 6\frac{dU}{dG}\,, \tag{5.20}$$

$$\frac{d}{dz}(z\phi) = \sqrt{6}\,U\,. \tag{5.21}$$

Alternatively the first equation can be inserted in the second to obtain

$$6\frac{dU}{dG}\frac{d\phi}{dG} + \phi = \sqrt{6}\,U\,. \tag{5.22}$$

This is a remarkable simplification from previous studies of phenomenologically relevant AdS-inspired approaches.

The potential resulting from this analysis is

$$l^2 V(\phi, G) = -12 + 4\sqrt{6}\phi - \tfrac{3}{2}\phi^2 + 3\sqrt{6}\phi U - 24U - 9U^2 + 18\left(\frac{dU}{dG}\right)^2\,. \tag{5.23}$$

One might wonder about the term linear in ϕ, but really it should be viewed in the Einstein frame. Assuming that U has no constant terms

$$l^2\tilde{V} = -12 + \tfrac{5}{2}\phi^2 + \cdots . \tag{5.24}$$

The first term is just the usual negative cosmological constant, while the second term suggests that the mass of the dilaton is $m_\phi^2 l^2 = 5$. If one wants to relate this to an operator it would have dimension 5. However, as pointed out in [106], the AdS/CFT correspondence between dimension of the operator and mass of the field does not generally apply to the dilaton field for the reasons presented there.

5.4 Possible Potentials

The AdS/CFT dictionary sets the mass for the fields according to the dimension Δ of the dual operator,

$$m^2 l^2 = \Delta(\Delta - 4)\,, \tag{5.25}$$

where l is related to the AdS curvature. The glueball mass is 0 since the dimension of the gluon condensate is 4. The dilaton mass is undetermined and is not connected to the dimension of the corresponding operator, as discussed in [106].

In the UV limit, $z \to 0$, the glueball field is proportional to z^4. In the IR limit, $z \to \infty$, the glueball field must be proportional to z in order that the dilaton field be proportional to z^2 so that the mesons have linear radial Regge trajectories. As a consequence $U \to \frac{1}{12}G^2$ in the IR limit. In the UV limit $U \to \frac{1}{3}G^2$.

One possible potential which yields the correct UV and IR behavior is

$$U = \tfrac{1}{12}G^2\left[1 + 3\mathrm{e}^{-\gamma G^2}\right]. \tag{5.26}$$

Here the only free parameter is γ which controls the transitional behavior of G between the IR and the UV.

A second possible potential is

$$U = \tfrac{1}{12}G^2\left[4 - 3\tanh\gamma G^2\right]. \tag{5.27}$$

The free parameter γ controls the transitional behavior.

A third possible potential is

$$U = \tfrac{1}{12}G^2 + \frac{1}{4\gamma}\ln\left(1 + \gamma G^2\right). \tag{5.28}$$

Again the transitional behavior is fixed by the numerical value of γ.

5.5 Log Potential

Let us focus on the logarithmic potential because we can find some analytical results straightaway. The differential equation for G

$$z\frac{dG}{dz} = 6\frac{dU}{dG} = \frac{\gamma G^2 + 4}{\gamma G^2 + 1} G \tag{5.29}$$

has the solution

$$G^2 \left(\gamma G^2 + 4\right)^3 = \left(\frac{z}{z_0}\right)^8 . \tag{5.30}$$

Here z_0 is a constant of integration. In the large z limit the solution is

$$\gamma G^2 = \gamma^{1/4} \left(\frac{z}{z_0}\right)^2 - 3 + \cdots . \tag{5.31}$$

In the small z limit the solution is

$$G = \frac{1}{8}\left(\frac{z}{z_0}\right)^4 - 3\gamma \left(\frac{z}{2z_0}\right)^{12} + \cdots . \tag{5.32}$$

The field is plotted as a function of z in Fig. 5.3 (see Eq. (5.38) for the relationship among z_0, γ and λ). The power-law behavior in the UV and IR limits is evident.

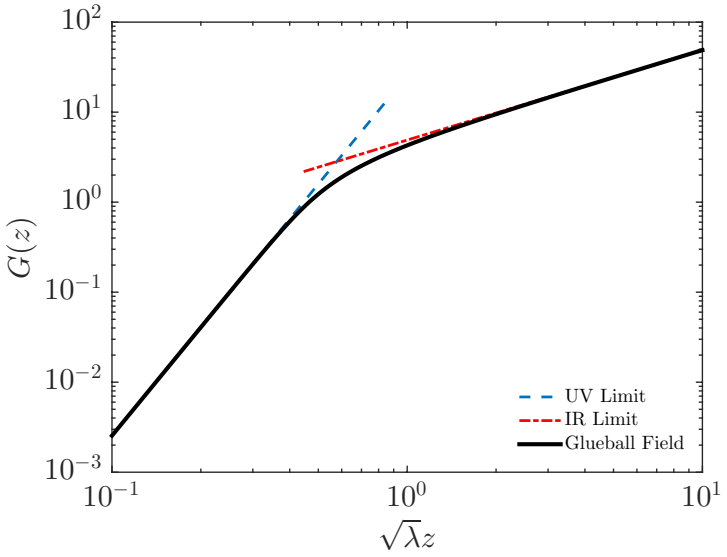

Figure 5.3: The glueball field as a function of the dimensionless variable $\sqrt{\lambda}z$. Plotted this way it only depends on the parameter γ which here is chosen to be $1/2$.

We have not found a solution $\phi(G)$ in terms of elementary functions. The solution can be expressed in terms of an integral with the proper boundary conditions as

$$\phi(G) = \sqrt{6}\left\{U(G) - \frac{z_0}{z(G)}\int_0^G \frac{z(G')}{z_0}\frac{dU}{dG'}dG'\right\} \tag{5.33}$$

where

$$\frac{dU}{dG} = \frac{G}{6}\frac{4+\gamma G^2}{1+\gamma G^2} \tag{5.34}$$

and z/z_0 is given by Eq. (5.30). It is straightforward to find the limits as $G \to \infty$

$$\begin{aligned}\phi &= \sqrt{6}\left[\frac{1}{36}G^2 + \frac{1}{4\gamma}\ln\gamma G^2 - \frac{2}{3\gamma} + \cdots\right] \\ &= \sqrt{6}\left[\frac{1}{36\gamma^{3/4}}\left(\frac{z}{z_0}\right)^2 + \frac{1}{4\gamma}\ln\left(\frac{z}{z_0}\right)^2 + \frac{1}{16\gamma}\ln\gamma - \frac{3}{4\gamma} + \cdots\right]\end{aligned} \tag{5.35}$$

and as $G \to 0$

$$\begin{aligned}\phi &= \frac{\sqrt{6}}{9}\left[\frac{1}{3}G^2 + \frac{7}{136}\gamma G^4 + \cdots\right] \\ &= \frac{2\sqrt{6}}{9}\left[\frac{2}{3}\left(\frac{z}{2z_0}\right)^8 - \frac{27\gamma}{17}\left(\frac{z}{2z_0}\right)^{16}\cdots\right].\end{aligned} \tag{5.36}$$

The requirement of linear confinement requires a solution in the large z limit of the form

$$\phi = \sqrt{\frac{8}{3}}\lambda z^2\,. \tag{5.37}$$

Using the above limiting forms we find that the constant of integration in the differential equation for $G(z)$ is

$$\frac{1}{z_0^2} = 24\gamma^{3/4}\lambda\,. \tag{5.38}$$

This also determines the magnitude of the gluon condensate, defined by $G = G_4 z^4$, to be

$$G_4 = 72\gamma^{3/2}\lambda^2\,. \tag{5.39}$$

Only γ remains as an undetermined parameter. The field is plotted as a function of z in Fig. 5.4. The power-law behavior in the UV and IR limits is evident.

5.6 Glueball Mass Spectrum

Suppose that the metric has the form

$$ds^2 = b^2(z)\left(-dt^2 + d\mathbf{x}^2 + dz^2\right) \tag{5.40}$$

and that the action has the canonical form of Eq. (5.5). The equation of motion which determines the mass spectrum for the field $G = G(z) + \Delta G(z,x)$ is

$$-b^3\eta^{\mu\nu}\partial_\mu\partial_\nu\Delta G - \partial_z(b^3\partial_z\Delta G) + b^5\frac{\partial^2\tilde{V}}{\partial G^2}\Delta G = 0\,. \tag{5.41}$$

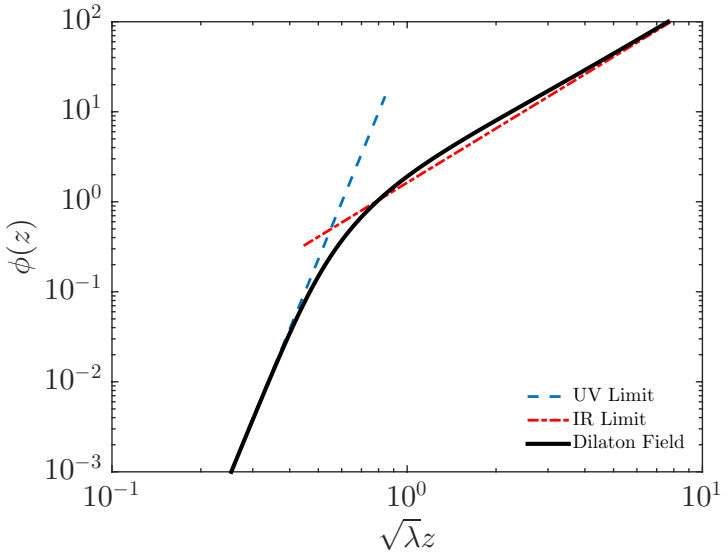

Figure 5.4: The dilaton field as a function of the dimensionless variable $\sqrt{\lambda}z$. Plotted this way it only depends on the parameter γ which here is chosen to be 1/2.

Here $\Delta G(z,x) = \Delta G_n(z)\mathrm{e}^{ip\cdot x}$ so that $\eta^{\mu\nu}\partial_\mu\partial_\nu \to m^2$. This leads to the eigenvalue equation

$$-\partial_z^2\Delta G_n(z) - b^{-3}\left(\partial_z b^3\right)\partial_z\Delta G_n(z) + b^2\frac{\partial^2\tilde{V}}{\partial G^2}\Delta G_n(z) = m_n^2\Delta G_n(z)\,. \tag{5.42}$$

It can be put in the form of the Schrödinger equation by the transformation $\Delta G_n = \mathrm{e}^{\omega_s/2}H_n$ with $\omega_s = -3\ln b$. Hence

$$-\ddot{H}_n + \left[\tfrac{1}{4}\dot{\omega_s}^2 - \tfrac{1}{2}\ddot{\omega}_s + \frac{l^2}{z^2}\frac{\partial^2 V}{\partial G^2}\right]H_n = m_n^2 H_n \tag{5.43}$$

where a dot means differentiation with respect to z.

In the present case $\omega_s = \sqrt{\frac{3}{2}}\phi + 3\ln z$. From the equations of motion one can write

$$\begin{aligned} z\dot{\phi} &= \sqrt{6}U - \phi \\ z^2\ddot{\phi} &= 2\phi - 2\sqrt{6}U + 6\sqrt{6}\left(\frac{\partial U}{\partial G}\right)^2 . \end{aligned} \tag{5.44}$$

These can be used in

$$\dot{\omega}_s = \frac{1}{z}\left(3 + \sqrt{\frac{3}{2}}z\dot{\phi}\right) \tag{5.45}$$

and in

$$\ddot{\omega}_s = \frac{1}{z^2}\left(-3 + \sqrt{\frac{3}{2}}z^2\ddot{\phi}\right) \tag{5.46}$$

without having to numerically calculate the first or second derivatives of ϕ with respect to z. This combines to give

$$\tfrac{1}{4}\dot{\omega_s}^2 - \tfrac{1}{2}\ddot{\omega}_s = \frac{1}{z^2}\left[\frac{15}{4} - \frac{5}{4}\sqrt{6}\phi + \frac{15}{2}U + \frac{9}{4}U^2 - \frac{3}{4}\sqrt{6}\phi U + \frac{3}{8}\phi^2 - 9\left(\frac{dU}{dG}\right)^2\right] . \quad (5.47)$$

The potential in Eq. (5.23) gives

$$l^2\frac{\partial^2 V}{\partial G^2} = 3\sqrt{6}\phi\frac{d^2U}{dG^2} - 24\frac{d^2U}{dG^2} - 18U\frac{d^2U}{dG^2} - 18\left(\frac{dU}{dG}\right)^2 + 36\left(\frac{d^2U}{dG^2}\right)^2 + 36\frac{dU}{dG}\frac{d^3U}{dG^3} \quad (5.48)$$

which does not specify the function $U(G)$.

For the specific example of the logarithmic form of U we find

$$\frac{dU}{dG} = \frac{G}{6}\left[\frac{\gamma G^2+4}{\gamma G^2+1}\right] \quad (5.49)$$

$$\frac{d^2U}{dG^2} = \frac{1}{6}\left[\frac{(\gamma G^2)^2 - \gamma G^2 + 4}{(\gamma G^2+1)^2}\right] \quad (5.50)$$

$$\frac{d^3U}{dG^3} = \frac{\gamma G(\gamma G^2-3)}{(\gamma G^2+1)^3} . \quad (5.51)$$

The Schrödinger equation can be put in dimensionless form by changing to the dimensionless variable $x = \sqrt{2\lambda}z$. Then

$$-\frac{d^2H_n}{dx^2} + V_H\left(\phi(x), G(x)\right)H_n = \frac{m_n^2}{2\lambda}H_n . \quad (5.52)$$

where

$$V_H = \frac{1}{x^2}\left[\frac{15}{4} - \frac{5}{4}\sqrt{6}\phi + \frac{15}{2}U + \frac{9}{4}U^2 - \frac{3}{4}\sqrt{6}\phi U + \frac{3}{8}\phi^2 - 9\left(\frac{dU}{dG}\right)^2 + l^2\frac{\partial^2 V}{\partial G^2}\right] . \quad (5.53)$$

It is straightforward to compute the limits of V_H in the UV and IR limits. In the IR $V_H \to x^2$ and in the UV $V_H \to 15/4x^2$. These are independent of the parameter γ.

Now the parameter γ should be used to obtain the best fit to the glueball mass spectrum. Some results are plotted in Fig. 5.5 for a representative range of γ. It shows the existence of a tachyon when $n = 1$. Very similar results are obtained with the other forms of U discussed in Sec. 5.4.

In fact this can be anticipated analytically by consideration of the limit $\gamma >> 1$. Then the mass spectrum is obtained from

$$-\frac{d^2H_{n'}}{dx^2} + \left[x^2 - 6 + \frac{3}{4x^2}\right]H_{n'} = \frac{m_{n'}^2}{2\lambda}H_{n'} . \quad (5.54)$$

This may be compared to the radial equation for the harmonic oscillator in the form

$$-\frac{d^2H_{n'}}{dx^2} + \left[x^2 + \frac{l^2-1/4}{x^2}\right]H_{n'} = \frac{2E_{n'}}{\hbar\omega}H_{n'} \quad (5.55)$$

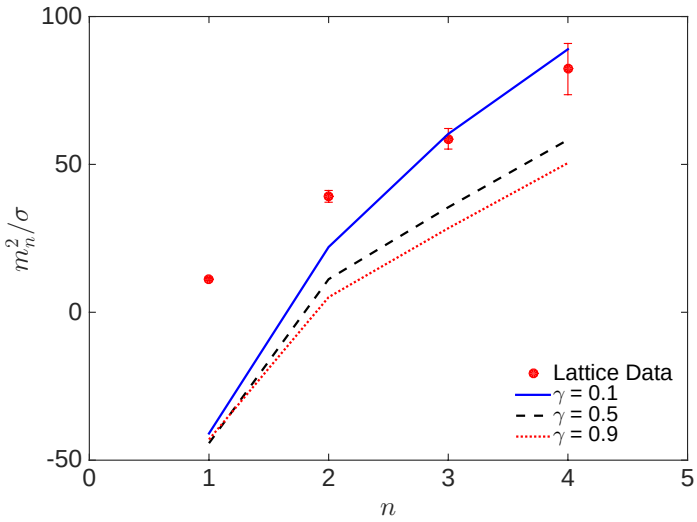

Figure 5.5: The mass spectra with $\sqrt{\lambda} = 700$ MeV for several values of the parameter γ.

with radial quantum number $n' = 0, 1, 2...., l = \frac{1}{2}, \frac{3}{2}, ...$ and energy eigenvalue

$$E_{n'} = \hbar\omega \left[2n' + l + 1\right] . \tag{5.56}$$

Switching to the radial quantum number $n = n' + 1$ to be consistent with the notation used earlier results in

$$m_n^2 = 8\lambda \left[n - \frac{3}{2}\right] . \tag{5.57}$$

This has exactly one tachyonic state.

5.7 Randall-Sundrum Model

There is a tachyon in the versions of the AdS model considered above which indicates an instability. In an attempt at stabilization we turn to the Randall-Sundrum model [122]. The goal of Ref. [122] was to obtain a more natural explanation of the hierarchy between the weak scale and the fundamental scale of gravity. Here we have more mundane considerations.

The Randall-Sundrum model introduces a cosmological constant Λ in the bulk and two 3-branes, one located at $y = 0$ and the other at $y = L$. The 3-branes have constant energy densities V_0 and V_L, respectively. There is an assumed symmetry $y \to -y$ so that only positive values of y are needed. The action is

$$\mathcal{S} = 2M^3 \int d^4x dy \sqrt{g} \left(R + \frac{\Lambda}{2M^3}\right) - \int d^4x \sqrt{g(y=0)} V_0 - \int d^4x \sqrt{g(y=L)} V_L \, . \tag{5.58}$$

Here M is the five-dimensional gravity scale ($M^3 = 1/32\pi G_5$). The metric has the form

$$ds^2 = \mathrm{e}^{-2A(y)}(-dt^2 + d\mathbf{x}^2) + dy^2 \, , \tag{5.59}$$

with indices running from 0 through 4, 4 representing the fifth dimension y. Note that we have dropped the tildes in this section even though we are working in the Einstein frame. The sign in front of Λ in the action is chosen so that in this model it turns out positive. The formulas for the components of the Ricci tensor are given in the Appendix. For this metric they are

$$R_{00} = -(A'' - 4A'^2)\mathrm{e}^{-2A} = -R_{ii} \tag{5.60}$$

with no sum on $i = 1,2,3$ and

$$R_{yy} = 4A'' - 4A'^2 \,. \tag{5.61}$$

The scalar curvature is

$$R = 8A'' - 20A'^2 \,. \tag{5.62}$$

Einstein's equations give the following pair of scalar equations.

$$A'^2 = \frac{\Lambda}{24M^3} \equiv k^2 \tag{5.63}$$

$$A'' - 2A'^2 = -\frac{\Lambda}{12M^3} + \frac{V_0}{12M^3}\delta(y) + \frac{V_L}{12M^3}\delta(y - L) \tag{5.64}$$

The solution to Eq. (5.63) is simply

$$A(y) = k|y|\theta(L - |y|) \tag{5.65}$$

when making using of the symmetry $y \to -y$. Also from Eq. (5.63) we have

$$A' = k\left[\theta(y)\theta(L - y) - \theta(-y)\theta(L + y)\right] . \tag{5.66}$$

Differentiating this expression, using the symmetry, and comparing to Eq. (5.64), we find the requirements that $V_0 = \sqrt{24M^3\Lambda}$ and $V_L = -\sqrt{24M^3\Lambda}$. These requirements are equivalent to demanding that the four-dimensional cosmological constant be zero. For this, we need

$$\begin{aligned}
\int_{-L}^{L} dy\sqrt{g(y)} &= \frac{1}{2k}\left(1 - \mathrm{e}^{-4kL}\right) , \\
\int_{-L}^{L} dy\sqrt{g(y=0)} &= \frac{1}{2k} , \\
\int_{-L}^{L} dy\sqrt{g(y=L)} &= \frac{1}{2k}\mathrm{e}^{-4kL} , \\
\int_{-L}^{L} dy\sqrt{g(y)}\, R(y) &= -6k\left(1 - \mathrm{e}^{-4kL}\right) .
\end{aligned} \tag{5.67}$$

Then the four-dimensional action is

$$\int d^4x \left[12M^3k\left(1 - \mathrm{e}^{-4kL}\right) + \frac{\Lambda}{2k}\left(1 - \mathrm{e}^{-4kL}\right) - \left(V_0 + V_L\mathrm{e}^{-4kL}\right)\right] \tag{5.68}$$

which is zero if V_0 and V_L take on the values mentioned above.

5.8 Randall-Sundrum Model with Scalar Fields

Now we add the scalar fields ϕ and G as in Sec. III. We assume that $V_L = -V_0$ but V_0, Λ, and M are unrelated; k is still defined as $\sqrt{\Lambda/24M^3}$. The equations of motion are

$$3A'' - 6A'^2 + \frac{\Lambda}{4M^3} = \tfrac{1}{4}\phi'^2 + \tfrac{1}{4}G'^2 + \tfrac{1}{2}\tilde{V} + \frac{V_0}{4M^3}[\delta(y) - \delta(y-L)]\,, \tag{5.69}$$

$$6A'^2 - \frac{\Lambda}{4M^3} = \tfrac{1}{4}\phi'^2 + \tfrac{1}{4}G'^2 - \tfrac{1}{2}\tilde{V}\,, \tag{5.70}$$

$$\phi'' - 4A'\phi' = \frac{\partial\tilde{V}}{\partial\phi}\,, \tag{5.71}$$

$$G'' - 4A'G' = \frac{\partial\tilde{V}}{\partial G}\,. \tag{5.72}$$

Based on previous results we look for a solution of the following form:

$$A' = W + k\left[\theta(y)\theta(L-y) - \theta(-y)\theta(L+y)\right]\,, \tag{5.73}$$

$$\phi' = 6\frac{\partial W}{\partial\phi}\,, \tag{5.74}$$

$$G' = 6\frac{\partial W}{\partial G}\,. \tag{5.75}$$

Then the original set of equations are satisfied when

$$\tilde{V} = 18\left[\left(\frac{\partial W}{\partial\phi}\right)^2 + \left(\frac{\partial W}{\partial G}\right)^2\right] - 12W^2 - 24k\left[\theta(y)\theta(L-y) - \theta(-y)\theta(L+y)\right]W\,, \tag{5.76}$$

and $V_0 = \sqrt{24M^3\Lambda}$, as before.

5.8.1 Change of coordinate

Reference [123] studied tensor fluctuations in the absence of scalar fields. The authors found it convenient to make the change of variables from y to z via

$$z = \mathrm{sign}(y)\left[\mathrm{e}^{k|y|} - 1\right]/k\,. \tag{5.77}$$

With the inclusion of scalar fields it suggests that we choose

$$A(y) = \ln\left(k|z| + 1\right) + a\phi(|z|)\,, \tag{5.78}$$

valid for both positive and negative values of z including $z = 0$. Then $y = 0$ corresponds to $z = 0$. Along with this we assume that

$$dy = \frac{\mathrm{e}^{-a\phi(|z|)}}{k|z|+1}dz\,. \tag{5.79}$$

This gives the metric

$$ds^2 = \frac{\mathrm{e}^{-2a\phi(|z|)}}{(k|z|+1)^2}\left(-dt^2 + d\mathbf{x}^2 + dz^2\right) . \tag{5.80}$$

The equation for A is now

$$A' = \frac{\mathrm{sign}(z)}{|z|+l}\frac{dz}{dy} + a\phi' = W + k\,\mathrm{sign}(z)\,. \tag{5.81}$$

Unless otherwise stated we shall assume that L becomes arbitrarily large so that we may ignore any singularities at $y = \pm L$ in the equations of motion.

Using the equations above we can readily find a differential equation which determines the ϕ dependence of W.

$$6a\frac{\partial W}{\partial \phi} = W + k\,\mathrm{sign}(z)\left(1 - \mathrm{e}^{a\phi}\right) \tag{5.82}$$

The solution is

$$W = k\,\mathrm{sign}(z)\left\{[U(G) + 1 - a\phi]\,\mathrm{e}^{a\phi} - 1\right\} . \tag{5.83}$$

Compare this to Eq. (5.19). Therefore we can write the potential $\tilde{V}$ as

$$\tilde{V} = 18\left[\left(\frac{\partial W}{\partial \phi}\right)^2 + \left(\frac{\partial W}{\partial G}\right)^2\right] - 12W^2 - 24k|W|\,. \tag{5.84}$$

The potential V for non-negative values of z is nearly the same as before.

$$V(\phi, G)/k^2 = -12\left(1 - \mathrm{e}^{-2a\phi}\right) + 4\sqrt{6}\phi - \tfrac{3}{2}\phi^2 + 3\sqrt{6}\phi U - 24U - 9U^2 + 18\left(\frac{dU}{dG}\right)^2 \tag{5.85}$$

The only difference is the term proportional to $\mathrm{e}^{-2a\phi}$ which arises on account of the brane at $z = 0$.

In terms of the z coordinate the equations for the fields are now ($z \geq 0$)

$$(z+l)\frac{dG}{dz} = 6\,\frac{dU}{dG} \tag{5.86}$$

$$(z+l)\frac{d\phi}{dz} + \phi = \sqrt{6}\,U\,. \tag{5.87}$$

The l acts as a UV cutoff. Compare these to Eqs. (5.20) and (5.21). The solutions with the 3-brane, $G(z,l)$ and $\phi(z,l)$, can be obtained from the solutions without the 3-brane, $G(z,0)$ and $\phi(z,0)$, simply by shifting the coordinate, specifically $G(z,l) = G(z+l,0)$ and $\phi(z,l) = \phi(z+l,0)$.

5.8.2 Vacuum energy density in four dimensions with scalar fields

Let us calculate the vacuum energy density in four dimensions with the inclusion of the fields ϕ and G. The action is now a combination of Eqs. (5.5) and (5.58) with

$$\tilde{\mathcal{L}} = -\tfrac{1}{2}\tilde{g}^{MN}\partial_M\phi\partial_N\phi - \tfrac{1}{2}\tilde{g}^{MN}\partial_M G\partial_N G - \tilde{V}(\phi, G) \tag{5.88}$$

and

$$\tilde{R} = 8A'' - 20A'^2\,. \tag{5.89}$$

From Eqs. (5.69) and (5.70) we may infer that

$$\tilde{\mathcal{L}} = -6A'' + 12A'^2 - \frac{\Lambda}{2M^3} + \frac{V_0}{2M^3}[\delta(y) - \delta(y-L)] \tag{5.90}$$

when the solutions are plugged back into the Lagrangian. Then the action is

$$\mathcal{S}_E = 4M^3\int d^4x\int dy\,\mathrm{e}^{-4A}(A'' - 4A'^2)\,. \tag{5.91}$$

Again using the same equations we have

$$A'' - 4A'^2 = \tfrac{1}{3}\tilde{V} - 4k^2 + \frac{V_0}{12M^3}\left[\delta(y) - \delta(y-L)\right]\,. \tag{5.92}$$

The last pair of terms integrates to zero leaving

$$\mathcal{S}_E = \frac{4}{3}M^3\int d^4x\int dy\,\mathrm{e}^{-4A}\tilde{V}\,. \tag{5.93}$$

Is this action finite? Switching from y to z involves the change

$$dy\,\mathrm{e}^{-4A} = dz\frac{\mathrm{e}^{-5a\phi}}{(k|z|+1)^5}\,. \tag{5.94}$$

The action is thus proportional to

$$\int_0^\infty \frac{dz}{(kz+1)^5}\,\mathrm{e}^{-3a\phi}\,V \tag{5.95}$$

In the IR, $V \to -6\phi^2(z)$, while in the UV, $V \to$ constant. Hence the action is finite and so is the four-dimensional vacuum energy density. This is due to the UV cutoff k in the Randall-Sundrum model.

5.9 Glueball Mass Spectrum Revisited

In this section we calculate the glueball mass spectrum with the Randall-Sundrum modified action described above. From Eqs. (5.40)-(5.42) we find the Schrödinger equation

$$-\ddot{H}_n + \left[\tfrac{1}{4}\dot{\omega_s}^2 - \tfrac{1}{2}\ddot{\omega}_s + \frac{1}{(k|z|+1)^2}\frac{\partial^2 V}{\partial G^2}\right]H_n = m_n^2 H_n \tag{5.96}$$

where

$$\begin{aligned}
\omega_s &= 3\ln(k|z|+1) + \sqrt{\frac{3}{2}}\phi(|z|) \\
\dot{\omega}_s &= \left\{ \frac{3k}{k|z|+1} + \sqrt{\frac{3}{2}}\frac{d}{d|z|}\phi(|z|) \right\} \mathrm{sign}(z) \\
\ddot{\omega}_s &= -\frac{3k^2}{(k|z|+1)^2} + \sqrt{\frac{3}{2}}\ddot{\phi} + 6k\delta(z)\,.
\end{aligned} \tag{5.97}$$

Restricting z to positive values only results in the following equation.

$$\begin{aligned}
\ddot{H}_n = &\left[\frac{15}{4}\frac{k^2}{(kz+1)^2} + \frac{3}{2}\sqrt{\frac{3}{2}}\frac{k\dot{\phi}}{kz+1} + \frac{3}{8}\dot{\phi}^2 - \frac{1}{2}\sqrt{\frac{3}{2}}\ddot{\phi} - \frac{3}{2}k\delta(z) + \frac{1}{(kz+1)^2}\frac{\partial^2 V}{\partial G^2} \right] H_n \\
&- m_n^2 H_n
\end{aligned} \tag{5.98}$$

Note the appearance of an attractive δ-function potential. Its coefficient is 3/2 instead of 3 because we are restricting the space to non-negative values of z. We can express $\dot{\phi}$ and $\ddot{\phi}$ in terms of the background fields and z as before using Eq. (5.44)

$$-\ddot{H}_n + V_H H_n = m_n^2 H_n \tag{5.99}$$

where now

$$V_H = \frac{k^2}{(kz+1)^2}\left[\frac{15}{4} + \frac{15}{2}(U - a\phi) + \frac{9}{4}(U-a\phi)^2 - 9\left(\frac{dU}{dG}\right)^2 + \frac{1}{k^2}\frac{\partial^2 V}{\partial G^2} \right] - \frac{3}{2}k\delta(z)\,. \tag{5.100}$$

The Schrödinger equation may be solved for positive values of z by neglecting the Dirac δ-function but imposing the boundary condition $\dot{H}_n(\epsilon) = -\frac{3}{2}kH_n(0)$ with $\epsilon \to 0^+$. This condition follows in the usual way; see the Appendix.

The original AdS/Yang-Mills (YM) model contained three parameters: l, a physically irrelevant parameter representing the AdS curvature; λ, representing the slope of the mass spectrum; and γ, representing the transition from the UV to the IR behavior. None of the results depended upon l. The lack of a UV cutoff in that model resulted in an instability manifested by an infinite action and a tachyon. The AdS/YM model which includes the Randall-Sundrum 3-branes replaces the parameter l with the parameter $l = 1/k$ which is relevant: it shifts the variable z by an amount l, and it enters into the Schrödinger equation for the glueball mass spectrum. It is related to the tension on the 3-branes. It also renders the action finite, hence we do not expect a tachyon.

Figure 6 shows a best fit to the glueball mass spectrum as calculated on the lattice. The best-fit parameters are: $\sqrt{\lambda} = 581.8$ MeV, $k = 0.951\sqrt{\lambda}$, and $\gamma = 0.2725$. Not only is the linearity achieved at large n but also the departure from linearity for the ground state $n = 1$. The potential entering the Schrödinger equation with these parameters is shown in Fig. 7. Note that it does not have the $1/x^2$ behavior exhibited in Eqs. (5.53) and (5.54) as $x \to 0$ because of the UV cutoff $l = 1/k$.

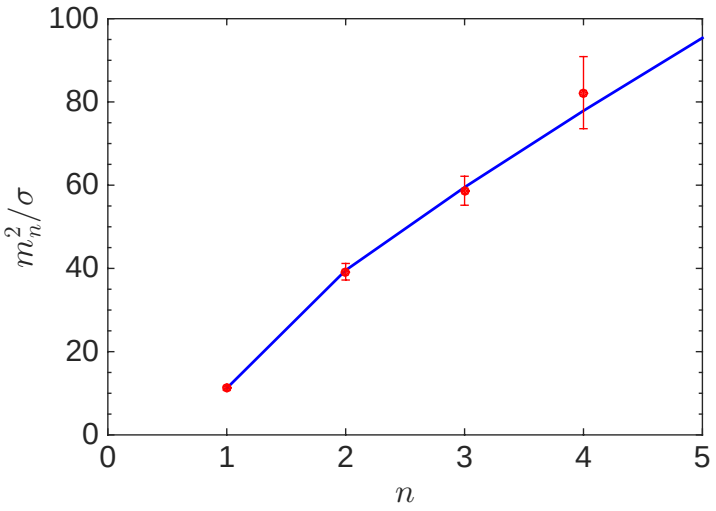

Figure 5.6: Glueball mass spectrum calculated with the AdS/YM model including the Randall-Sundrum 3-brane. The best-fit parameters are given in the text.

5.10 Conclusion

Our goal in this paper was to construct a fully dynamical AdS-type model that could reproduce the scalar glueball mass spectrum as calculated by lattice gauge theory. The model should respect the gauge/gravity duality correspondence. The first hurdle in doing so is the fact that there is always one more equation of motion for the background fields than there are independent fields. This hurdle was overcome by using the superpotential method, whereby one function $U(G)$ determines the full potential $V(\phi, G)$ in the Lagrangian. Then it is straightforward to parametrize $U(G)$ such that the correspondence is satisfied and that the scalar glueball spectrum has a linear trajectory for the radial excitations. The theory has two parameters: λ, which arises as a constant of integration in the differential equations determining the background fields and which introduces an overall energy scale (there is no such scale in the Lagrangian), and a dimensionless parameter γ which determines the scale at which the theory switches from the IR to the UV behavior. Unfortunately any such theory has a tachyon, which indicates an instability.

The model is stabilized by merging the AdS approach with the Randall-Sundrum model. In that model a cosmological constant is introduced in the bulk and 3-branes are introduced at $y = 0$ and $y = L$. The length L can be taken as large as desired and hence is an irrelevant parameter. It introduces one new parameter, k, with dimensions of energy which provides a UV cutoff and renders the action finite. This eliminates the tachyon. An excellent fit to the 4 scalar glueball states calculated by lattice gauge theory is obtained.

The next step in our program is to study the theory at finite temperature. Nonzero

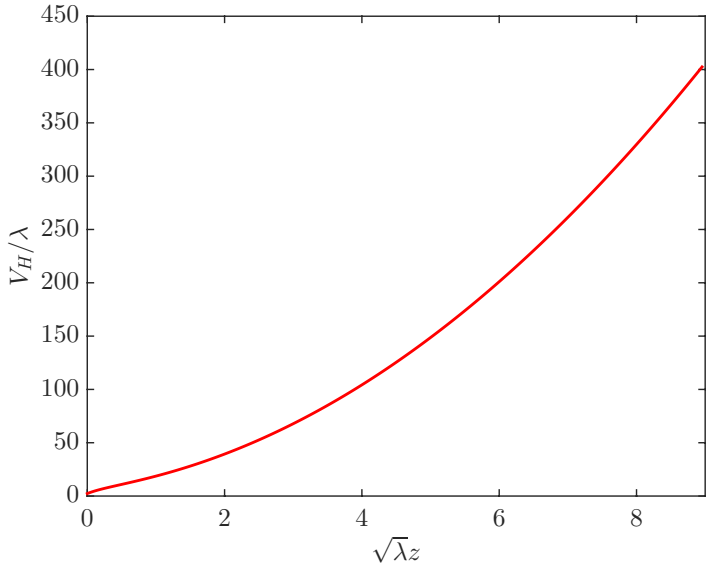

Figure 5.7: The Schrödinger potential for the AdS/YM model including the Randall-Sundrum 3-brane.

temperature will modify the background fields $\phi(z)$ and $G(z)$. The outcome would be the equation of state and the transport coefficients, such as the shear and bulk viscosities and various relaxation times that appear in higher order viscous fluid dynamics. One can also study the spectra of the $J^{PC} = 0^{-+}, 1^{+-}$ and 1^{--} states. Finally, one may consider applying this approach to the full bottom-up AdS/QCD phenomenology. There is much work yet to be done!

Acknowledgments

We thank T. Gherghetta for very insightful discussions. This work was supported by the U.S. DOE Grant No. DE-FG02-87ER40328. A. D. is supported by the National Science Foundation Graduate Research Fellowship Program under Grant No. 00039202.

Chapter 6

RS Branes at Finite Temperature

This chapter is a faithful reproduction of the published work **A. Dhumuntarao, J. I. Kapusta, and C. Plumberg, Phys. Rev. D, 101, 066023, (2020)** with minor edits [124].

Abstract

We find exact finite temperature solutions to $d = 5$ Einstein-dilaton gravity with black branes and a Randall–Sundrum 3-brane. We show that there exists a unique generating superpotential for these models. The location of the black brane and the associated Hawking temperature depend on the value of the 3-brane tension while other parameters are held fixed. The thermodynamics of these solutions are presented, from which we show that the entropy satisfies $S < \mathrm{Vol}(\mathbb{R}^3)/4G_5$. We demonstrate that in a certain limit the gauge dual of this theory effectively reduces to $\mathcal{N} = 4$ SYM at finite temperature on $S^1 \times \mathbb{R}^3$.

6.1 Introduction

The gauge/gravity conjecture has provided insights into the phenomenology of large N_c, strongly coupled gauge theories at finite temperature [13, 95, 125]. The holographic duality encodes finite temperature properties of d-dimensional gauge theories on $S^1 \times \mathbb{R}^d$ (or S^d) into the thermodynamics of $(d+1)$-dimensional gravitational theories. In these non-perturbative regimes, the behavior of the strongly coupled plasma state may be inferred by calculating geometric properties of black brane (hole) solutions in the gravitational dual.

The identification of a gravitational dual to Quantum Chromodynamics (QCD), the standard model, or extensions of the standard model would be a novel application of the conjecture and remains an open problem. A bottom-up approach to realize the holographic construction, known as AdS/QCD [98, 100, 126], deforms the boundary Conformal Field Theory (CFT) towards QCD by introducing 3-branes in conjunction with

additional bulk fields. These "soft wall" AdS/QCD models are used to reproduce certain phenomenological features such as electroweak or chiral symmetry breaking [99, 101, 127], bulk/shear viscosities [128–131], and dynamical confinement [105].

Recently two of us proposed a dynamical two field model in order to reproduce the scalar glueball mass spectrum determined by lattice calculations at zero temperature [118, 132]. After incorporating backreactions, we found a tachyonic mode in the spectrum. To remove this mode, we introduced a Randall–Sundrum (RS) 3-brane with nonzero tension which acted as a mode cutoff in the putative dual field theory [122, 123, 133, 134]. The junction conditions at the brane regularized this mode and allowed for a good description of the scalar glueball mass spectrum.

At finite temperature, few extensions to the canonical $\mathrm{AdS}_5/\mathrm{CFT}_4$ program are analytically tractable. A certain subset, referred to as Einstein-dilaton models, permits a single bulk scalar field, making it amenable to analytically extract rich thermodynamic behavior [135–139]. In these models, the finite temperature supergravity background is often fixed to be SAdS_5 or thermal AdS, and the spectrum of bulk matter is calculated in the absence of backreactions. The aim of this work is to provide an analytically tractable, solvable model which incorporates changes induced by a codimension one 3-brane and a bulk scalar field on the thermodynamics of bulk gravity at finite temperature.

We study Einstein-dilaton gravity with a bulk RS 3-brane situated at the $\mathbb{R}/\mathbb{Z}_2$ orbifold fixed point with finite tension. The tension of the codimension one brane combined with the dilaton provides a rich structure. In Sec. 6.2 we show that this model is sufficiently constrained to provide a unique generating superpotential. We solve the resulting nonlinear coupled equations of motion exactly in Sec. 6.3. We identify the range of parameters which admit stable black brane formation in Sec. 6.4. We find the formation of black branes is contingent upon a simple lower bound

$$\omega = \frac{3}{4\pi}\frac{k}{\sigma G_5} > 1 \tag{6.1}$$

where $\sigma > 0$ refers to the brane tension, k^2 is proportional to the bulk cosmological constant Λ, G_5 is the bulk gravitational constant. When the bound is satisfied, black branes simultaneously form on either side of the RS 3-brane. When the parameter λ (to be defined later) takes the value 0, the scalar field decouples and the pure Randall–Sundrum model is recovered. When $\lambda = \pm 1$ the scalar field may be identified as a tachyon, and black branes exist only above a certain minimum temperature.

In Sec. 6.5 we explore the thermodynamics of these finite temperature solutions. We find that, as long as the RS 3-brane is present, the black brane entropy is bounded above by

$$0 \leq S < \frac{V_3}{4G_5} \tag{6.2}$$

where $V_3 = \mathrm{Vol}(\mathbb{R}^3)$. The upper bound is saturated only in the limit of a vanishing brane tension, $\sigma \to 0$. Examples of other systems which have a limiting entropy are recalled

in Sec. 6.6. As shown in Sec. 6.7, carefully taking the limit of vanishingly small tension and cosmological constant effectively reduces the model to Type IIB string theory on $AdS_5 \times S^5$ of which the conjectured dual field theory is $\mathcal{N} = 4$ SYM on $S^1 \times \mathbb{R}^3$ at finite temperature with broken supersymmetry.

Our conclusions are presented in Sec. 6.8. The results presented in this paper may have applications in holographic QCD, physics beyond the standard model, and models of the early universe.

6.2 Action and Generating Superpotential

We will study the following $5d$ Einstein-Hilbert action minimally coupled to a single dimensionless bulk scalar field,

$$\mathcal{S} = 2M^3 \int d^5x \sqrt{|g|} \left[R + 12k^2 - \frac{1}{2}(\partial\phi)^2 - V(\phi) \right] . \tag{6.3}$$

The (negative) cosmological constant is $\Lambda = -6k^2$, $2M^3 = (16\pi G_5)^{-1}$ with G_5 being the bulk gravitational constant, and $(\partial\phi)^2 = g^{MN}(\partial_M\phi)(\partial_N\phi)$. Conformal invariance is broken by the scalar field.

In addition to the bulk action, we introduce an RS 3-brane Σ with tension σ in the following way. We extend the compactification radius of the $S^1_{r_c}/\mathbb{Z}_2$ orbifold to the real line [122]. The RS 3-brane is then situated at the orbifold fixed point of $\mathbb{R}/\mathbb{Z}_2$, and we expect to recover $4d$ Poincaré invariance at Σ. Let $\gamma = g_\Sigma$ be the induced metric; then we work with the boundary action

$$\mathcal{S}_\partial = \mathcal{S}_{\text{GHY}} - \int_\Sigma d^4x \sqrt{|\gamma|}\sigma. \tag{6.4}$$

where $\mathcal{S}_{\text{GHY}}$ is the Gibbons-Hawking-York boundary term which is required for a well-posed variational principle. Often the background needs to be identified and subtracted in order to render the total action finite. Here the presence of the RS brane provides a natural counterterm which, as noted in [31], we identify as the surface term responsible for yielding a finite action.

To search for static black brane/thermal solutions, we employ the domain wall ansatz for the bulk metric

$$ds^2 = e^{-2A(y)} \left[-f(y)dt^2 + d\boldsymbol{x}^2 \right] + \frac{dy^2}{f(y)} . \tag{6.5}$$

Here $f(y)$ is the blackening function whose zero indicates a horizon and $A(y)$ is the warp function. In these coordinates, Σ is located at $y = 0$, and junction conditions on $A(y)$ and $f(y)$ will have to be imposed. See Fig. 6.1. Note that in the special case where the RS brane is absent and $f(y) = 1$, this metric arises from considering the near horizon asymptotics of N_c coincident D3 branes and is equivalent to a warped AdS_5 with the deep IR located at $y \to \infty$ (see [95, 100, 101, 131, 132] for motivations and references therein).

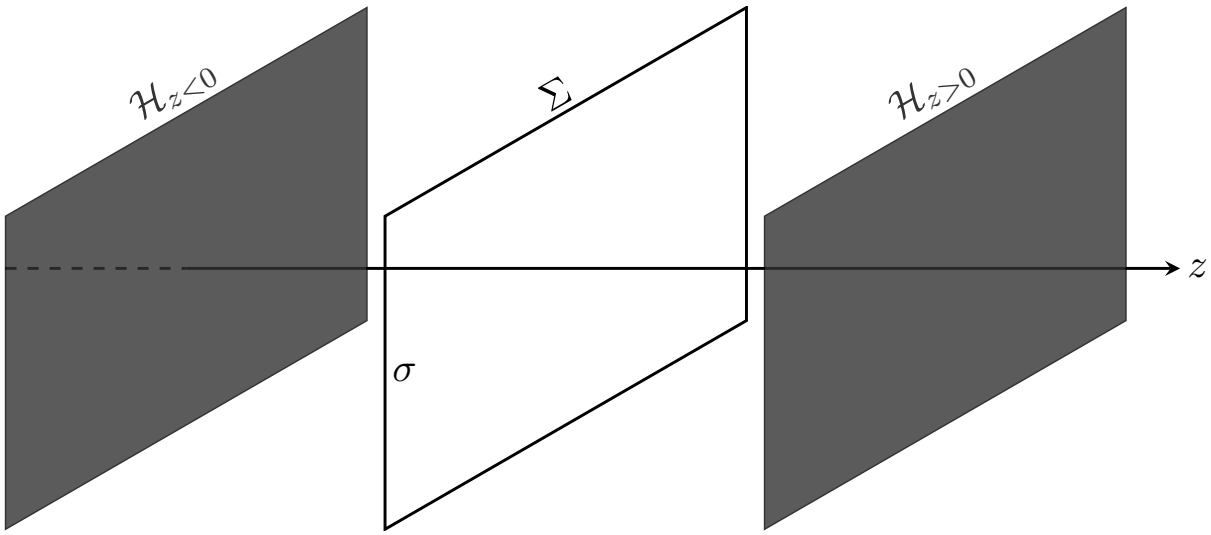

Figure 6.1: The setup: two horizons form equidistantly on either side of Σ when the tension σ satisfies the bound $\omega > 1$.

At zero temperature, the RS brane exhibits a $\mathbb{Z}_2$ orbifold symmetry which is expected to be preserved at finite temperature [140][1]. We search for solutions which respect the orbifold symmetry. A straightforward calculation of the Ricci tensor and the Ricci scalar yields

$$\begin{aligned} R_{tt} &= f\left[\frac{1}{2}f'' - fA'' + 4fA'^2 - 3f'A'\right]e^{-2A} \\ R_{\boldsymbol{xx}} &= \left[f'A' - 4fA'^2 + fA''\right]e^{-2A} \\ R_{yy} &= 4A'' - 4A'^2 + \frac{3f'}{f}A' - \frac{f''}{2f} \\ R &= 8fA'' - 20fA'^2 + 9f'A' - f'' \end{aligned} \tag{6.6}$$

where the prime notation denotes a derivative with respect to y. The resulting linearly independent equations of motion are

$$6A'' = \phi'^2 + 12q\delta(y) \tag{6.7}$$

$$12fA'^2 - 3f'A' = \frac{f}{2}\phi'^2 + 12k^2 - V \tag{6.8}$$

$$(f\,\phi')' - 4fA'\phi' = \frac{dV}{d\phi}\,. \tag{6.9}$$

where $q \equiv \sigma/24M^3$. In the Randall-Sundrum model the vacuum solution requires $q = k$. The first equation may be solved provided that there exists a continuous function $B(y)$

[1] In Ref. [141] a perturbative analysis suggested an explicit breaking. However, the equations of motion are not linearly independent as the authors have claimed. Thus their analysis of the orbifold symmetry breaking is suspect.

satisfying the following system of differential equations

$$A' = B + q[\theta(y) - \theta(-y)] \tag{6.10}$$

$$B' = \frac{1}{6}\phi'^2 \,. \tag{6.11}$$

The Heaviside functions appear as a consequence of respecting the orbifold symmetry. Moreover, the delta function may be interpreted as a domain wall in the gravitational theory or, equivalently, as a mode cutoff in the putative dual field theory.

In the rest of this work we look for solutions to the following coupled nonlinear differential equations,

$$B' = \frac{1}{6}\phi'^2 \tag{6.12}$$

$$V - 12k^2 = 3\left[f(B+q)\right]' - 12f(B+q)^2 \tag{6.13}$$

$$\frac{dV}{d\phi} = (f\phi')' - 4f(B+q)\phi' \tag{6.14}$$

where we have eliminated the warp function in favor of $B(y)$. Although we have restricted to $y > 0$, the deformation $y \to |y|$ and $q \to q\,\Theta(y)$, where $\Theta(y) \equiv \theta(y) - \theta(-y)$, recovers the orbifold symmetry. We still need to find the junction conditions for these functions on Σ.

A common issue with Einstein-dilaton theories is the internal consistency of the nonlinear differential equations. To remedy this issue, we construct the following algorithm which solves the system uniquely up to boundary conditions on the 3-brane.

1. Introduce $W(\phi)$ as a superpotential [120, 121] which generates the potential $V(\phi)$.
2. Promote the metric function $B(y)$ to $B(\phi)$.
3. Introduce a function $D(\phi) \equiv e^{-a\phi}\left[B(\phi) + q\right]$.
4. Transform the coordinates via $du = e^{a\phi(y)}dy$.
5. Impose consistency on Eqs. (6.13) and (6.14).

Superpotential methods are often used to introduce a holographic RG flow from the UV to the IR along the bulk direction and reduce the order of the differential equations [135, 142]. These auxiliary superpotentials are tasked to generate the potential at zero temperature by a first order gradient flow along ϕ via

$$V(\phi) = 18\left(\frac{dW}{d\phi}\right)^2 - 12W^2 - 24kW\Theta(y)\,, \tag{6.15}$$

where the discontinuity $\Theta(y)$ arises from the junction condition [132]. At zero temperature, the superpotential is identified with the metric function $B(y)$. At finite temperature,

the situation is more subtle. Though the relation (6.15) holds at finite temperature since the potential should be temperature independent, the coupling between f and B via Eqs. (6.12) to (6.14) breaks the identification between $W(\phi)$ and $B(\phi)$. In this case, $W(\phi) \propto B(\phi)$ with the factor being set by the brane tension σ and the bulk constants Λ and G_5.

While the superpotential $W(\phi)$ uniquely generates the potential $V(\phi)$, the function $B(\phi)$ reduces the non-linear equation (6.12) to a first order gradient flow along ϕ

$$\frac{dB}{d\phi} = \frac{1}{6}\frac{d\phi}{dy}\,, \tag{6.16}$$

provided that ϕ' has no critical points in the bulk. A unique solution for the dilaton may be constructed from

$$\frac{dD}{d\phi} + aD = \frac{1}{6}\frac{d\phi}{du}\,. \tag{6.17}$$

We henceforth set the parameter $a = 1/\sqrt{6}$. This value is determined by the conformal transformation from the string to Einstein frame in order to obtain a canonical kinetic term [105] and separately was found to give rise to linear Regge trajectories in certain AdS/QCD contexts [98, 118].

Next, note that both Eqs. (6.13) and (6.14) are differential equations containing f and f'. Steps 3 and 4 of the algorithm reduce to

$$18D\left[\frac{dD}{d\phi} + aD\right]\frac{df}{d\phi} + 9\left[2\left(\frac{dD}{d\phi}\right)^2 + 4aD\frac{dD}{d\phi} - D^2\right]f = \left(V - 12k^2\right)e^{-2a\phi} \tag{6.18}$$

and

$$36\left[\frac{dD}{d\phi} + aD\right]^2\frac{df}{d\phi} + 18\left[\frac{dD}{d\phi} + aD\right]\left[2\frac{d^2D}{d\phi^2} + 4a\frac{dD}{d\phi} - D\right]f = \frac{dV}{d\phi}\,e^{-2a\phi}\,. \tag{6.19}$$

One may ask whether these two equations are consistent with each other. These can be put in the form

$$\begin{aligned} f + P_1\frac{df}{d\phi} &= Q_1 \\ f + P_2\frac{df}{d\phi} &= Q_2\,. \end{aligned} \tag{6.20}$$

Then $P_1 = P_1$ results in the differential equation

$$D\frac{d^2D}{d\phi^2} = \left(\frac{dD}{d\phi}\right)^2 \tag{6.21}$$

whose only solution is

$$D = D_0\exp((\lambda - 1)a\phi) \tag{6.22}$$

where D_0 and λ are any real constants. Setting $Q_1 = Q_2$ results in

$$\frac{d}{d\phi}\left(V - 12k^2\right) = 2\lambda a\left(V - 12k^2\right) \tag{6.23}$$

with solution

$$V - 12k^2 = V_0\, e^{2\lambda a\phi} \tag{6.24}$$

We may conclude that expression (6.24) is the only potential for a single scalar field that admits a black brane. Note however that a constant blackening function $f = 1$ places no restrictions on the potential because, after multiplication by $e^{2a\phi}$, Eq. (6.19) just becomes the derivative with respect to ϕ of Eq. (6.18).

The superpotential which generates this V and satisfies the junction condition is

$$W = k\left(e^{\lambda a\phi} - 1\right)\Theta(y) \tag{6.25}$$

where we used the fact that $\Theta^2(y)$ is continuous at $y = 0$. It follows that $V_0 = 3(\lambda^2 - 4)k^2$. It also follows that

$$B = q\left(e^{\lambda a\phi} - 1\right)\Theta(y) \tag{6.26}$$

so that $W = \omega B$ where $\omega \equiv k/q$.

6.3 Exact Solutions

Using the solutions $D(\phi)$ and $V(\phi)$ found in the previous section, the functions $P(\phi)$ and $Q(\phi)$ reduce to constants

$$\begin{aligned} P &= -\frac{6a\lambda}{4 - \lambda^2} \\ Q &= \frac{k^2}{q^2} = \omega^2\,. \end{aligned} \tag{6.27}$$

Then the differential equation for the blackening function has a simple closed form

$$f(\phi) = \omega^2 - \left(\omega^2 - 1\right)e^{-\phi/P}\,. \tag{6.28}$$

The dilaton profile may be obtained from Eq. (6.17). The solution in the original y coordinate is

$$\phi(y) = -\frac{1}{a\lambda}\ln\left(1 - q\lambda^2|y|\right)\,. \tag{6.29}$$

Equipped with the profile $\phi(y)$, the functions f, V B, and by extension A, obtain analytic forms in terms of y. Thus we have uniquely solved the system of Eqs. (6.12) to (6.14) incorporating the backreactions of the scalar field and the codimension one hypersurface on the background geometry.

In order to facilitate the analysis of the parameter space of solutions, we perform a coordinate transformation $dy = e^{-A(y(z))}dz$ where

$$A(y) = -\frac{1}{\lambda^2}\ln\left(1 - q\lambda^2|y|\right) \tag{6.30}$$

is the solution to Eq. (6.10). The metric then takes the canonical thermal form with an overall conformal (warp) factor

$$ds^2 = e^{-2A(y(z))}\left[-f(z)dt^2 + d\boldsymbol{x}^2 + \frac{dz^2}{f(z)}\right] \tag{6.31}$$

with the coordinates related by

$$1 - \lambda^2 q|y(z)| = \left[1 + (1-\lambda^2)q|z|\right]^{-\lambda^2/(1-\lambda^2)} . \tag{6.32}$$

In these coordinates the functions respecting the orbifold symmetry are

$$f(z) = \omega^2 - (\omega^2 - 1)\left[1 + (1-\lambda^2)q|z|\right]^{(4-\lambda^2)/(1-\lambda^2)} \tag{6.33}$$

$$A(z) = \frac{1}{1-\lambda^2}\ln\left[1 + (1-\lambda^2)q|z|\right] \tag{6.34}$$

$$\phi(z) = \frac{\lambda}{a(1-\lambda^2)}\ln\left[1 + (1-\lambda^2)q|z|\right] \tag{6.35}$$

$$V(z) = 12k^2 - 3(4-\lambda^2)k^2\left[1 + (1-\lambda^2)q|z|\right]^{2\lambda^2/(1-\lambda^2)} . \tag{6.36}$$

6.4 Parameter Space Constraints

We now consider the conditions in which a horizon forms and study the parameter space of finite temperature solutions. Heuristically, λ characterizes the dilaton content while ω parameterizes the metric content of the theory. We will study the parameter space generated by (λ, ω) and illustrate certain extremal values in preparation for a finite temperature analysis.

To constrain λ, note that the dilaton profile contains a logarithmic singularity at finite z when $|\lambda| > 1$. To prevent this, the relevant domain which provides nonsingular ϕ and real $V(\phi)$ for all z is given by $-1 \leq \lambda \leq 1$. Though the edge cases of the parameter domain of λ have to be studied with care, the limits of the functions f, A, ϕ and V exist and respect the orbifold symmetry.

First, consider the limit $\lambda \to 0$ when the dilaton decouples

$$\begin{aligned} \phi(z) &= 0 \\ V(z) &= 0 \\ A(z) &= \log(1 + q|z|) \\ f(z) &= \omega^2 - (\omega^2 - 1)(1 + q|z|)^4 , \end{aligned} \tag{6.37}$$

so that only the metric degrees of freedom remain. In this case, we see that the action reduces to an Einstein-Hilbert action with a cosmological constant and a boundary term from the brane tension. This limit will provide useful thermodynamic consistency checks between this spacetime and AdS_5.

Alternatively, consider the limits $\lambda \to \pm 1$

$$\begin{aligned} \phi(z) &= \pm\sqrt{6}q|z| \\ V(z) &= 3k^2(4 - 3e^{2q|z|}) \\ A(z) &= q|z| \\ f(z) &= \omega^2 - (\omega^2 - 1)e^{3q|z|}\,. \end{aligned} \tag{6.38}$$

In these limits the dilaton profiles actually match the tachyonic profiles considered in Ref. [105].

For a tension $\sigma > 0$, the first constraint we may impose is $\omega > 0$. The coefficient $1-\omega^2$ in Eq. (6.33) then determines the existence of a black brane. For $0 < \omega < 1$ ($\omega > 1$), $f(z)$ is a monotonically increasing (decreasing) function with respect to $|z|$. Hence, for a real solution to $f(z_h) = 0$ at some $|z_h| > 0$ to exist, the tension must satisfy $\omega > 1$. As a consequence of the orbifold symmetry, when this condition is satisfied, two black branes surrounding the 3-brane form. Alternatively, this bound may be interpreted as the necessary condition[2] for the system to be in equilibrium. Furthermore, one can check that the Kretschmann invariant $R_{abcd}R^{abcd}$ is finite at $|z_h|$. See Figs. 6.2 and 6.3.

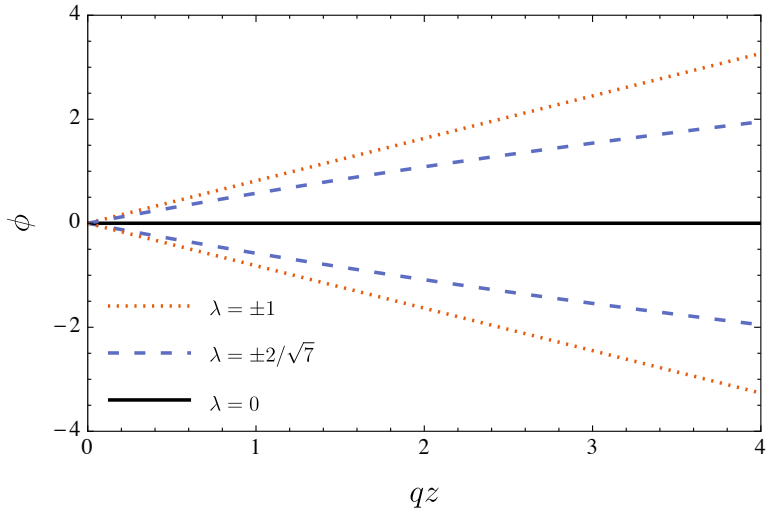

Figure 6.2: The scalar field as a function of the dimensionless variable qz for representative values of $-1 \leq \lambda \leq 1$.

The second set of solutions are extremal, i.e., when the tension of the 3-brane is such that $q = k$. As $q \to k$ from below, the horizons $\mathcal{H}_{z<0}$ and $\mathcal{H}_{z>0}$ are pushed to their

[2]We thank Robert Myers for bringing this to our attention.

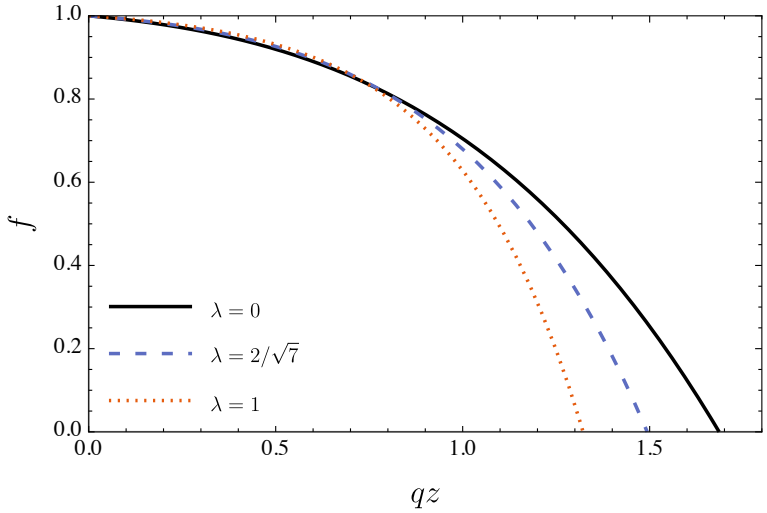

Figure 6.3: The blackening function f as a function of the dimensionless variable qz for representative values of λ.

respective asymptotics, and black brane formation is prohibited when the equality holds. As we will subsequently show, in the extremal case $T = 0$, and these solutions are similar to AdS in Poincaré coordinates with the Killing horizon replaced with the 3-brane.

Lastly, we remark that solutions with $\omega < 1$ are forbidden as valid thermodynamic solutions. In these cases, f diverges as $|z| \to \infty$. Without a horizon to contain these singularities, these spacetimes are wormhole–like solutions and thus are excluded from our finite temperature study.

6.5 Thermodynamics

In this section the entropy is calculated from the Bekenstein-Hawking formula with the temperature identified from the periodicity of Euclidean time [2, 8, 143].

We begin by deriving the Hawking temperature associated with the metric in z coordinates Eq. (6.31). We initially focus on theories which are non-tachyonic, i.e., $|\lambda| < 1$. Since $\omega > 1$ in order for black branes to exist, it is convenient to solve $f(z_h) = 0$, Eq. (6.33), for z_h and relate it to the tension via

$$\left[1 + (1-\lambda^2)q|z_h|\right]^{(4-\lambda^2)/(1-\lambda^2)} = \frac{\omega^2}{\omega^2 - 1} = \left[1 - q^2/k^2\right]^{-1} \tag{6.39}$$

where we have used the definition of ω. Note that as $q \to k$ from below, the location of the horizons are taken to their respective asymptotics, $|z_h| \to \infty$. This justifies the explanation given earlier. Further, note that black brane formation is prohibited in the extremal case $\omega = 1$ since $f(z) = 1$.

From the periodicity in Euclidean time, the Hawking temperature reads

$$T = -\frac{1}{4\pi}\dot{f}(z_h) = \frac{k}{4\pi}(4-\lambda^2)\left(\frac{\omega^2-1}{\omega}\right)\left(\frac{\omega^2}{\omega^2-1}\right)^{3/(4-\lambda^2)} \tag{6.40}$$

Note that the extremal case $q = k$ precisely corresponds to $T = 0$ unless the theory has

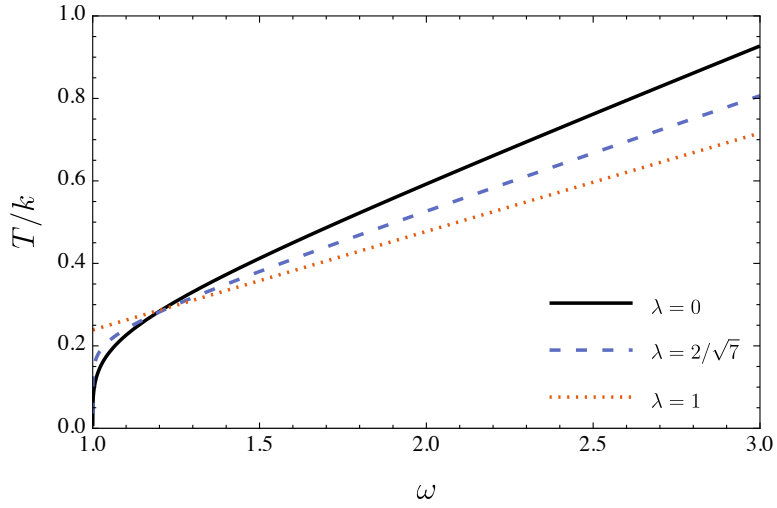

Figure 6.4: The temperature in units of k as a function of the dimensionless variable ω for several values of λ. It depends only on $|\lambda|$ and not on its sign. For $|\lambda| = 1$ there is a minimum temperature below which a black brane solution emerges.

tachyonic scalars, in which a minimum temperature develops at $T_{\rm min} = 3k/4\pi$. See Fig. 6.4.

The entropy can be found from the Bekenstein-Hawking area law $S = \text{Area}(\mathcal{H})/4G_5$ [2, 8]. For the area of the horizon we have $dt = dz = 0$. The area is computed from $\text{Area}(\mathcal{H}) = \int \sqrt{g_3(z_h)}\, d^3x$, where g_3 is the determinant of the metric for the 3-dimensional space. It is

$$g_3(z_h) = \mathrm{e}^{-6A(z_h)} = \left(1 - \frac{q^2}{k^2}\right)^{6/(4-\lambda^2)} \tag{6.41}$$

The entropy density is therefore

$$s = 8\pi M^3 \left(\frac{\omega^2-1}{\omega^2}\right)^{3/(4-\lambda^2)} \tag{6.42}$$

Interestingly, the entropy density is bounded from above: $0 \le T < \infty$ and $0 \le s < 8\pi M^3$. See Fig. 6.5. In the low temperature limit the entropy grows like $s \sim M^3 (T/k)^{3/(1-\lambda^2)}$.

6.6 Examples of Systems with Limited Entropy

One may wonder how unusual it is for a system to have a limiting entropy with increasing temperature. It typically happens when two conditions are met: There is a restriction on

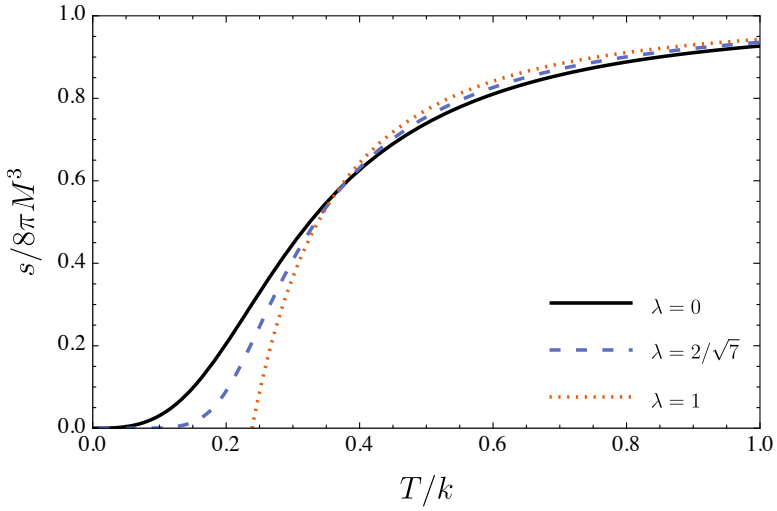

Figure 6.5: The entropy density, in units of $8\pi M^3$, as a function of the temperature, in units of k, for several values of λ. It depends only on $|\lambda|$ and not on its sign. For $|\lambda| = 1$ the entropy goes to zero at a non-zero temperature.

the allowed phase space, and there is a relevant energy scale apart from the temperature. We will illustrate this with two examples. The first involves a restriction on the allowed energies, and the second involves a restriction on the volume available to a gas of extended particles.

6.6.1 Two level system of fermions

Consider a system of N noninteracting fermions, each of which can be in a state with zero energy or energy E_0. The partition function is

$$\ln Z = N \ln \left(1 + e^{-E_0/T}\right) . \tag{6.43}$$

The total entropy is

$$S = \frac{d}{dT} \left(T \ln Z\right) = \ln Z + N \, \frac{E_0/T}{e^{E_0/T} + 1} \, . \tag{6.44}$$

When $T/E_0 \to \infty$, $S \to N \ln 2$. This is well known. Since the entropy is the logarithm of the number of available states, and at high temperature the two states are equally occupied, one obtains the $\ln 2$.

Next, consider a gas of massless, noninteracting spin $\frac{1}{2}$ fermions (including anti-particles) which have a maximum allowed momentum p_0. This is analogous to a gas of phonons in a solid. The entropy density is

$$s = \frac{2T^3}{\pi^2} \int_0^{p_0/T} dx \, x^2 \left[-n \ln n - (1-n) \ln(1-n)\right] \tag{6.45}$$

where the occupation number is $n = 1/(e^x + 1)$. When $T \ll p_0$ the entropy density goes to $s \to (7\pi^2/45)T^3$. When $T \gg p_0$ it goes to $s \to p_0^3 \, (2 \ln 2)/(3\pi^2)$.

When bosons are considered instead of fermions, the entropy grows logarithmically as $\ln(E_0/T)$ and $\ln(p_0/T)$, respectively. The difference, of course, is the fact that an arbitrary number of bosons can occupy any given quantum state.

6.6.2 Excluded volume model of a hadron gas

Another example is a Van der Waals type of excluded volume model for a hadron gas. In one version of the model, the volume occupied by a hadron is approximated by $E(p)/\epsilon_0$, where $E(p)$ is the energy of the hadron with momentum p and ϵ_0 is a constant with units of energy/volume [144, 145]. The equation of state is expressed in parametric form.

$$\begin{aligned} P(T) &= \frac{P_{\rm pt}(T_*)}{1 - P_{\rm pt}(T_*)/\epsilon_0} \\ s(T) &= \frac{s_{\rm pt}(T_*)}{1 + \epsilon_{\rm pt}(T_*)/\epsilon_0} \\ \epsilon(T) &= \frac{\epsilon_{\rm pt}(T_*)}{1 + \epsilon_{\rm pt}(T_*)/\epsilon_0} \end{aligned} \tag{6.46}$$

The subscript "pt" refers to the pressure, entropy, or energy density of a gas of hadrons treated as point particles. The temperature is obtained from the parameter T_* by the formula

$$T = \frac{T_*}{1 - P_{\rm pt}(T_*)/\epsilon_0}\,. \tag{6.47}$$

It can be readily verified that the thermodynamic identities $s = dP/dT$ and $\epsilon = -P + Ts$ are satisifed.

The temperature $T \to \infty$ at a finite value of T_* determined by $P_{\rm pt}(T_{*\rm max}) = \epsilon_0$. The pressure P is unbounded but the entropy and energy densities have finite upper limits. Consider, for example, a gas of massless bosons and fermions with the equation of state $P_{\rm pt}(T_*) = cT_*^4$. Then, when the excluded volumes are taken into account, the entropy density is

$$s(T) = \frac{4cT_*^3}{1 + 3cT_*^4/\epsilon_0} \tag{6.48}$$

with

$$T = \frac{T_*}{1 - cT_*^4/\epsilon_0}\,. \tag{6.49}$$

Thus $T_{*\rm max} = (\epsilon_0/c)^{1/4}$ and

$$s(T) < c(\epsilon_0/c)^{3/4}\,. \tag{6.50}$$

On the other hand, when $T \ll T_{*\rm max}$, the entropy density is unaffected by the excluded volume, and $s \to 4cT^3$. The reason for an upper limit on the entropy in this excluded volume model is the restriction in coordinate space, not momentum space.

6.7 Recovering AdS/CFT

In order to make comparison with SAdS_5 black branes, we write the metric in the form

$$ds^2 = H^{-1/2}(r)\left[-f(r)dt^2 + d\boldsymbol{x}^2\right] + H^{1/2}(r)\frac{dr^2}{f(r)}\,. \tag{6.51}$$

There is no scalar field so $\lambda = 0$. The z and r coordinates are related by

$$H = 1 + \frac{L^4}{r^4} = (1+qz)^4\,. \tag{6.52}$$

In the far IR ($z \to \infty$, $r \to 0$) we identify $L = 1/q$. The blackening and warp functions become

$$f(r) = 1 - \left(\frac{r_h}{r}\right)^4 \tag{6.53}$$

$$A(r) = \frac{1}{4}\ln\left(1 + \frac{L^4}{r^4}\right) \tag{6.54}$$

where the warp function may be identified as an overall conformal factor. The horizon is given by

$$\frac{r_h}{L} = \left(\frac{\omega^2-1}{\omega^2}\right)^{1/4}\,. \tag{6.55}$$

In the near horizon limit the metric takes the form

$$ds^2 = \left(\frac{r}{L}\right)^2\left[-f(r)dt^2 + d\boldsymbol{x}^2 + \left(\frac{L}{r}\right)^4\frac{dr^2}{f(r)}\right]. \tag{6.56}$$

The finite temperature AdS/CFT result is obtained by taking the limit $\omega \to 1$ with r_h held fixed. In a sense this is a low temperature limit because, with $L = 1/q \to \infty$, we have $r_h/L \to \pi T L \to (\omega^2-1)^{1/4}$. The AdS/CFT dictionary says that

$$8\pi M^3 = \frac{1}{4G_5} \equiv \frac{N_c^2}{2\pi L^3} \tag{6.57}$$

where N_c is the number of colors of the gauge field. Hence the entropy density becomes

$$s = \frac{\pi^2 N_c^2}{2}T^3 \tag{6.58}$$

which is the canonical result.

6.8 Conclusion

In this paper we studied Einstein-dilaton gravity with a bulk Randall–Sundrum 3-brane situated at the $\mathbb{R}/\mathbb{Z}_2$ orbifold fixed point. We looked for solutions to the equations of motion which incorporated a black brane, including backreaction of the dilaton field on

the metric. A black brane can only form if the potential has a particular functional form. With this potential we discovered exact solutions to the equations of motion. The temperature and entropy density are readily determined from these solutions. The temperature is controlled by varying the tension on the RS 3-brane. It turns out that the entropy has an upper bound given simply by $\mathrm{Vol}(\mathbb{R}^3)/4G_5$. Examples of other systems which also have a limiting entropy were provided. Typically they require some restriction in the allowed phase space along with a relevant dimensional parameter, apart from the temperature, to provide a scale.

Further lines of inquiry naturally present themselves. Why is it that the functional form of the potential is restricted in order that a black brane can be formed? Formation of a black brane and its associated Hawking temperature and Bekenstein entropy, following from the area law, are the usual means to study such theories. There is no analogous restriction at zero temperature.

Extensions of the model to include more scalar fields, such as glueball and chiral fields, might provide better descriptions of pure Yang–Mills theory and QCD. Extensions to include physics beyond the standard model of particle physics and general relativity might be very relevant to the physics of the early universe.

Acknowledgments

We thank T. Gherghetta for comments on the manuscript. This work was supported by the U.S. DOE Grant No. DE-FG02-87ER40328. A. D. is supported by the National Science Foundation Graduate Research Fellowship Program under Grant No. 00039202. C. P. acknowledges support from the CLASH project (KAW 2017-0036).

Chapter 7

Confinement and Graded Partition Functions for $\mathcal{N} = 4$ SYM

This chapter is a faithful reproduction of the published work **A. Cherman and A. Dhumuntarao, Phys. Rev. D 103, 066013 (2021)** with minor edits [146].

Abstract

Gauge theories with confining phases at low temperatures tend to deconfine at high temperatures. In some cases, for example in supersymmetric theories, confinement can persist for all temperatures provided the partition function includes a grading by $(-1)^F$. When it is possible to define partition functions which smoothly interpolate between no grading and $(-1)^F$ grading, it is natural to ask if there are other choices of grading that have the same effect as $(-1)^F$ on confinement. We explore how this works for $\mathcal{N} = 4$ SYM on $S^1 \times S^3$ in the large N limit at both small and large coupling. We find evidence for a continuous range of grading parameters that preserve confinement for all temperatures at large coupling, while at small coupling only a discrete set of gradings preserves confinement.

7.1 Introduction

Gauge theories tend to deconfine at high temperatures. This statement can be made precise in theories that have a center symmetry, such as $SU(N)$ Yang-Mills theory, see e.g. [147, 148]. Studying the properties of a $4d$ theory on a spatial manifold M_3 at finite temperature is equivalent to asking about the behavior of the Euclidean path integral on $M_3 \times S^1_\beta$ with periodic boundary conditions for bosons and anti-periodic boundary conditions for fermions. This path integral gives the thermodynamic partition function

$$Z(\beta) = \mathrm{tr}\, e^{-\beta H} \tag{7.1}$$

where $\beta = 1/T$. Wilson loops that wind around the thermal circle, $\operatorname{tr}\Omega = \mathcal{P}e^{i\int_{S^1} A}$ transform by a $\mathbb{Z}_N$ phase under center symmetry, $\operatorname{tr}\Omega \to e^{2\pi i/N}\operatorname{tr}\Omega$. In pure $SU(N)$ YM theory, it is known that $\langle \operatorname{tr}\Omega\rangle = 0$ at low temperatures, see e.g. [149], but it is non-zero at high temperatures [147]. This implies that the high and low temperature regimes are separated by a phase transition in the thermodynamic limit. Note however that there are actually two physically distinct ways to take the thermodynamic limit for $SU(N)$ YM theory. The standard way is take the volume of M_3 to infinity. Alternatively, one can take $N \to \infty$ with the 't Hooft coupling $\lambda = g^2_{\rm YM}N$ and other parameters such as the spatial volume held fixed [150–152]. There is a temperature-driven deconfinement transition in both of these two thermodynamic limits. In this paper we will discuss the deconfinement phase transition in the the large N thermodynamic limit.

The deconfinement phase transition is rather difficult to evade by, e.g., varying parameters controlling the matter content. Indeed, in the large N limit, the deconfinement transition is forced by the fact that the confining phase features a Hagedorn density of states. This means that the density of states, $\rho(E)$, grows exponentially with the energy $\rho(E) \sim e^{+\beta_H E}$, where it is assumed that $E \sim N^0$ is large compared to the characteristic mass scale of the theory, and $\beta_H > 0$, the Hagedorn temperature, depends on the matter content of the theory, but can be estimated as $\beta_H \sim \min(\Lambda^{-1}, R)$ where Λ is the large scale and R is the characteristic size of the spatial box. Given this density of states, the thermodynamic partition function cannot be analytic at $\beta = \beta_H$. Thus the theory must have deconfinement transition at some $\beta_c \geq \beta_H$ at large N.

However, the deconfinement phase transition can be evaded if one considers some *graded* partition functions. The most famous example is

$$\tilde{Z}(\beta) = \operatorname{tr}(-1)^F e^{-\beta H} \tag{7.2}$$

where F is fermion parity. This partition function is calculated by a path integral with periodic boundary conditions for all fields on S^1_β. If the distribution of bosonic and fermionic states are uncorrelated, a $(-1)^F$-graded partition function will also exhibit phase transitions as a function of β in the thermodynamic limit. However, if the spectra of bosonic and fermionic states are related in a sufficiently precise way, there will be large cancellations and the graded density of states $\tilde{\rho}(E)$ can have sub-exponential growth at large E at arbitrary β. Then $\tilde{Z}(\beta)$ can avoid the Hagedorn instability and the deconfinement phase transition.

This naturally occurs in supersymmetric gauge theories, where the bosonic and fermionic states with energies $E > 0$ necessarily come in degenerate multiplets in the infinite-volume limit. Surprisingly, deconfinement phase transitions of (7.2) can sometimes be avoided even without supersymmetry. Indeed, this is the case for adjoint QCD, YM theory coupled to $N_f > 1$ adjoint fermions [153–157], and even in some theories with fundamental fermions, which require more complicated gradings [158]. In such theories, $\tilde{Z}(\beta)$ is smooth, and hence the theory remains confining at all temperatures.

In this paper, we want to study what happens to deconfinement transition in theories where it is possible to smoothly interpolate between (7.1) and (7.2), both at large and small 't Hooft coupling. This is most easily done for the large N limit of $4d$ $\mathcal{N}=4$ super Yang-Mills theory, formulated in Euclidean signature on $S^3_R \times S^1_\beta$, where R is the radius of S^3. Indeed, it is known that without any grading, large N, $\mathcal{N}=4$ SYM has a deconfinement as a function of β/R, and the critical value of β/R is known both at small [150–152] and large [13, 95, 96, 125] 't Hooft coupling[1] due to the AdS/CFT correspondence. Supersymmetry suggests that the theory should be in a confined phase for all β/R if the partition function includes a grading by $(-1)^F$, and indeed this has been verified at large coupling in Ref. [125]. Finally, $\mathcal{N}=4$ SYM has a continuous internal global symmetry, $SO(6)_R$, which, as we will show, can be used to define a grading that smoothly interpolates between (7.1) and (7.2). We define this grading below and study the resulting phase structure at small and large 't Hooft coupling.

7.2 Graded partition functions

In a conformal field theory (such as $\mathcal{N}=4$ SYM) on $S^3_R \times S^1_\beta$, the partition function can be viewed as $Z(\beta/R) = \sum_\Delta e^{-\Delta\beta/R}$, where the sum runs over the scaling dimensions of local operators, so that the Hamiltonian is related to the dilation operator $H = D/R$. In theories with global symmetries it is also possible to turn on chemical potentials μ_i associated to conserved charges Q_i, yielding

$$Z(\beta,\mu_i) = \operatorname{tr} e^{\beta\sum_i \mu_i Q_i} e^{-\beta H}\,. \tag{7.3}$$

In the specific case of $\mathcal{N}=4$ SYM, there is an $SO(6)$ R-symmetry, and so one can turn on three independent chemical potentials associated with the three Cartan generators of $SO(6)_R$. We can consider $\mathcal{N}=4$ SYM as $\mathcal{N}=1$ SYM coupled to three adjoint chiral supermultiplets, then the three complex scalar fields ϕ_1,ϕ_2,ϕ_3 in $\mathcal{N}=4$ SYM are the lowest components of the three chiral supermultiplets. The three scalars transform in the **6** representation of $SO(6)_R$, and following the conventions of Ref. [161], we assemble the three scalars into a six-dimensional vector $(\phi_1,\phi_1^*,\phi_2,\phi_2^*,\phi_3,\phi_3^*)^T$, and write the Cartan generators in the **6** representation as

$$Q_1^{\mathbf{6}} = \operatorname{diag}(+1,-1,0,0,0,0) \tag{7.4}$$

$$Q_2^{\mathbf{6}} = \operatorname{diag}(0,0,+1,-1,0,0) \tag{7.5}$$

$$Q_2^{\mathbf{6}} = \operatorname{diag}(0,0,0,0,+1,-1)\,, \tag{7.6}$$

Then $2Q_i^{\mathbf{6}}$ acts with charge 2 on ϕ_i, and the superconformal R-charge r can be written as $r = \frac{2}{3}(Q_1+Q_2+Q_3)$, see e.g. [162]. We will set $\mu_1=\mu_2=\mu_3=2\mathrm{i}\theta/\beta$ and study the

[1] More generally, the critical value of β/R is bounded from below by the Hagedorn temperature, which is known for all λ [159, 160].

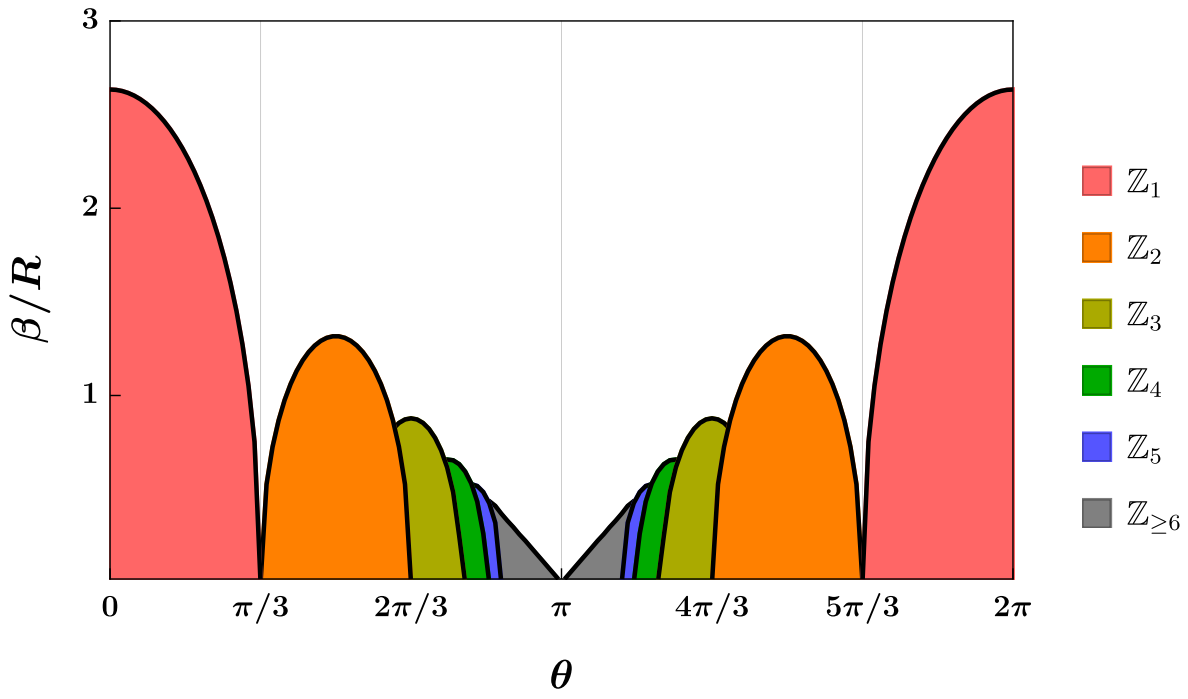

Figure 7.1: Large N phase diagram of $\mathcal{N}=4$ SYM theory on S^3_R for $\lambda \to 0$ as a function of inverse temperature β and grading θ. The theory is in a confined phase in the white region, and is partially confined in the colored regions. In between $\theta = \pi/3$ and $\theta = 5\pi/3$ center symmetry is only partially broken, with the unbroken subgroup of $\mathbb{Z}_N$ indicated by the color scheme in the legend. The theory confines at all β/R when $\theta = \pi/3, \pi, 5\pi/3$.

partition function

$$Z(\beta,\theta) = \mathrm{tr}\, e^{2i\theta \sum_{i=1}^{3} Q_i} e^{-\beta H} = \mathrm{tr}\, e^{3i\theta r} e^{-\beta H} \,. \tag{7.7}$$

This graded partition function is periodic in θ with period 2π. It implements a simple interpolation from (7.1) at $\theta = 0$ to (7.2) at $\theta = \pi$, thanks to the fact that in $\mathcal{N}=4$ SYM there is a spin-charge relation $e^{3\pi i r} = (-1)^F$, see e.g. [163]. Charge conjugation symmetry further relates r to $-r$, so that the θ periodicity is reduced to $\theta \simeq \theta + \pi$.

As we already mentioned, $\mathcal{N}=4$ SYM confines for all β/R when $\theta = \pi$, which is natural since this corresponds to working with a $(-1)^F = e^{3\pi i r}$ graded partition function in a supersymmetric theory. However, it is also true that in any supermultiplet, the r charge of the bosons and fermions differs by 1. This means that grading by $e^{i\pi r}$ should produce cancellations that are as strong as with $(-1)^F$, and one should expect to find confinement for all β/R when $\theta = \pi/3, 5\pi/3$. The calculations below show that these expectations are satisfied.

7.3 Zero Coupling Analysis

Let us determine the β and θ dependence of Z in (7.7) in the zero coupling limit $\lambda \to 0$, at large N. The partition function is given by a matrix integral which can be interpreted as an integral over the holonomy Ω [151], which implements the Gauss law constraint [147]. The matrix integral can be reduced to an integral over the eigenvalues of the holonomy

$$Z(\beta/R, \{\mu_i\}) = \int \left(\prod_k d\lambda_k\right) e^{-\mathcal{S}_{\text{eff}}(\lambda_k; \frac{\beta}{R}, \{\mu_i\})} \tag{7.8}$$

where λ_k are the eigenvalues, $\{\mu_i\}$ are the three independent chemical potentials for mutually commuting charges in $SO(6)_R$, and $\mathcal{S}_{\text{eff}}$ is an effective action. The holonomy eigenvalues take values on a circle, and the effective action can be written in terms of Fourier coefficients ρ_n of the eigenvalue distribution ρ

$$\mathcal{S}_{\text{eff}} = N_c^2 \sum_{n=1}^{\infty} V_n \rho_n^2 \tag{7.9}$$

where $\rho_n \equiv \int_{-\pi}^{\pi} \mathrm{d}\alpha \rho(\alpha) \cos(n\alpha)$ and the V_n coefficients are given by

$$V_n \equiv \frac{1}{n}\left(1 - z_B(x^n, \{\mu_i\}) + (-1)^n z_F(x^n, \{\mu_i\})\right]). \tag{7.10}$$

The parameter $x = e^{-\beta/R}$, and the functions $z_B = z_V + z_S, z_F$ are related to the single-particle partition functions for the massless vector, scalar, and fermion fields of $\mathcal{N} = 4$ SYM on S^3 [161]:

$$z_V(x) = \frac{6x^2 - 2x^3}{(1-x)^3}, \tag{7.11}$$

$$z_S(x, \{\mu_i\}) = \frac{x + x^2}{(1-x)^3} \sum_{a=1}^{3} (x^{R\mu_i} + x^{-R\mu_i}), \tag{7.12}$$

$$z_F(x, \{\mu_i\}) = \frac{2x^{3/2}}{(1-x)^3} \prod_{a=1}^{3} (x^{\frac{1}{2}R\mu_i} + x^{-\frac{1}{2}R\mu_i}). \tag{7.13}$$

We now set $\mu_i = \frac{2\mathrm{i}\theta}{\beta}$, so that

$$z_S = 6\frac{x + x^2}{(1-x)^3} \cdot [\cos(2\theta)], \tag{7.14a}$$

$$z_F = 16\frac{x^{3/2}}{(1-x)^3} \cdot [\cos(\theta)]^3. \tag{7.14b}$$

So long as all of the coefficients V_n are positive, the matrix integral is dominated by the center-symmetric $\rho_n = 0$ minimum. When there is value of n for which V_n becomes negative there is a phase transition. We can interpret these phase transitions as

center-breaking phase transitions where $\mathbb{Z}_N$ is spontaneously broken to an (approximate) subgroup $\mathbb{Z}_n$. (For an early discussion of partial deconfinement see e.g. [164].) For large β/R, corresponding to $x \ll 1$, it is easy to verify that $V_n > 0$ for all n, but for small β/R some V_n generically become negative. Figure 7.1 is a plot of the phase diagram as a function of θ and β/R. Center symmetry is preserved above the black curve, and is broken either completely or to a subgroup of $\mathbb{Z}_N$ below the black curve.

There are two interesting features in Fig. 7.1. First, the lack of deconfinement for any β at $\theta = \pi$ is consistent with our original expectations: it amounts to working with a $(-1)^F$ graded partition function. Second, the theory also remains confining for all β/R if $\theta = \pi/3, 5\pi/3$. In the region $(\pi/3, \pi) \cup (\pi, 5\pi/3)$ the system is in a (partially) center-broken phase for sufficiently small values of β/R. The dependence of the deconfinement temperature on θ is highly non-monotonic.

What should we expect as λ is increased from zero? At a heuristic level, increasing the coupling λ should increase the fluctuations of the Polyakov loop eigenvalues, and it is natural to expect such fluctuations to increase the range of β/R values where all traces of powers of the Polyakov loop vanish. It would be interesting but challenging to directly compute corrections to our results in powers of λ, see e.g. [152, 165] for the challenges that arise already in pure YM theory. However, one of the special features of $\mathcal{N} = 4$ SYM is that the $\lambda \to \infty, N \to \infty$ limit is just as calculable as the $\lambda \to 0, N \to \infty$ limit thanks to the AdS/CFT correspondence [13, 95, 96, 125]. In what follows, we take advantage of AdS/CFT and study the θ dependence of the phase diagram at large 't Hooft coupling.

7.4 Infinite coupling

At large N and λ, $\mathcal{N} = 4$ $SU(N)$ SYM is believed to have a dual gravitational description [13, 95, 96, 125]. The dependence of the theory on R-charge chemical potentials has been extensively explored in the literature, see e.g. [32, 33, 96, 125, 161]. The AdS/CFT dictionary for conserved charges implies that to study $\mathcal{N} = 4$ SYM with chemical potentials for R symmetry, we should consider the truncation of Type IIB supergravity on $\mathrm{AdS}_5 \times S^5$ to a $5d$ Einstein gravity theory coupled to three $U(1)$ gauge fields (A_I), $I = 1, 2, 3$, associated with the $U(1)^3$ Cartan subgroup of $SO(6)_R$ [166–170]:

$$\mathcal{I} = -\frac{1}{2\kappa^2} \int \mathrm{d}^5x \sqrt{-g} \left[R + \frac{12}{\ell^2} - \frac{\ell^2}{4} \sum_{I=1}^{3} (F_I)^2 \right] \tag{7.15}$$

where $(F_I)_{MN} = \partial_M (A_I)_N - \partial_N (A_I)_M$ are the field strengths of the three gauge fields, $M, N = 1, \ldots, 5$, κ is related to the $5d$ Newton constant G_5 via $\kappa = 8\pi G_5$, and the cosmological constant is $\Lambda = -6/\ell^2$.

The boundary values of bulk gauge fields act as sources for conserved currents in the boundary theory, and our goal is to turn on equal chemical potentials for each of the

three Cartan charges. For this purpose we can simply set $A^I = A$ above, and then the bulk action reduces to an Einstein-Maxwell-AdS$_5$ theory

$$\mathcal{I} = -\frac{1}{2\kappa^2}\int \mathrm{d}^5x\sqrt{-g}\left[R + \frac{12}{\ell^2} - \frac{3\ell^2}{4}F_{MN}F^{MN}\right]. \tag{7.16}$$

The Einstein-Maxwell-AdS$_5$ system has been extensively explored in [32, 33], and has Reissner-Nordstrom-AdS$_5$ black hole solutions[2] with parameters (L_m, L_q) which are related to the ADM mass and the charge density respectively. The charged black hole solution reads

$$\mathrm{d}s^2 = -f(r)\mathrm{d}t^2 + \frac{\mathrm{d}r^2}{f(r)} + r^2\mathrm{d}\Omega_3^2, \tag{7.17}$$

$$f(r) = 1 + \frac{r^2}{\ell^2} - \frac{L_m^2}{r^2} + \frac{L_q^4}{r^4}, \tag{7.18}$$

$$A_t(r) = \left(\mu - \frac{L_q^2}{\ell r^2}\right). \tag{7.19}$$

This non-supersymmetric family of non-rotating solutions is expected to correspond to spatially-homogeneous equilibrium states of the dual field theory.

We briefly review how the thermodynamic parameters of the bulk solution, i.e., the inverse temperature and chemical potential, map to the corresponding field theory parameters. First, we recall that ℓ can be identified with the radius of the S^3 spatial manifold in the dual field theory [161]. To identify β, we pass to Euclidean signature $t \to \mathrm{i}\tau$, and recall that the metric is free of conical singularities provided τ is periodic with period

$$\beta = \frac{4\pi}{\partial_r f(r)}\Big|_{r_+} = \frac{2\pi\ell^2 r_+}{\ell^2(1-(L_q/r_+)^4) + 2r_+^2} \tag{7.20}$$

where r_+ is the outer horizon corresponding to the largest positive root of $f(r_+) = 0$. The Hawking temperature $T = 1/\beta$ is then identified with the temperature of the dual field theory. Next, the chemical potential is determined by the asymptotic value of the field strength along the $\tau - r$ disk, D_2:

$$\int_{D_2} F = \int_0^\beta \mathrm{d}\tau \int_{r_+}^\infty \mathrm{d}r\, F_{r\tau} = \mathrm{i}\beta\mu. \tag{7.21}$$

The gauge field must be regular at r_+, meaning that $A_\tau(r_+) = 0$, which yields the identification

$$\mu = \frac{L_q^2}{\ell r_+^2}. \tag{7.22}$$

The confinement/deconfinement phase transition is mapped onto a gravitational phase transition in the following way. The solution with $L_m = L_q = 0$ should be thought of

[2] Our normalization convention is different from [32, 33], so that $A_{\text{there}} = \sqrt{4/3\ell^2}A_{\text{here}}$.

as thermal AdS_5, and is dual to the confining phase of the dual gauge theory, whereas solutions with $L_m^2 \in \mathbb{R}_+$ are dual to the deconfined phase [125]. The difference of the free energies of these two phases is [31–33]

$$\mathcal{F}_{\text{deconfined}} - \mathcal{F}_{\text{confined}} = \frac{\pi r_+^2}{8G_5}\left(1 - (\ell\mu)^2 - \frac{r_+^2}{\ell^2}\right). \tag{7.23}$$

When this quantity changes sign, there is a deconfinement phase transition from the point of view of the field theory [96, 125], which is realized as a Hawking-page phase transition in the gravitational theory [171].

To map out the dependence of the phase transition temperature on the parameter θ in (7.7), we study how (7.23) behaves as a function of an appropriate imaginary chemical potential. We take $\mu \to \mathrm{i}\tilde{\mu} = \frac{2\mathrm{i}\theta}{\beta}$ while keeping r_+, which requires sending $L_q^2 \to \mathrm{i}\tilde{L}_q^2$. Then A_τ is real and continues to satisfy $A_\tau(r_+) = 0$. The on-shell Euclidean action becomes

$$\mathcal{F}_{\text{deconfined}} - \mathcal{F}_{\text{confined}} = \frac{\pi r_+^2}{8G_5}\left(1 + \left(\frac{2\ell\theta}{\beta}\right)^2 - \frac{r_+^2}{\ell^2}\right). \tag{7.24}$$

This expression is manifestly invariant under $\theta \to -\theta$. In addition, we should understand the θ dependence in this formula and the ones that follow mod 2π. In field theory, this basic fact follows from charge quantization. To see how this is matched in the bulk, we recall that Type IIB string theory has an NS-NS two-form gauge field B. One can turn on a flat B potential (that is, obeying $dB = 0$) in the solutions discussed above at no cost in energy, with an arbitrary value of the 2π periodic parameter α [125, 172, 173]:

$$\alpha = \int_{D_2} B. \tag{7.25}$$

The periodicity of the chemical potential under shifts of $2\pi\mathrm{i}/\beta$ is ensured by the shift freedom of $\alpha \to \alpha + 2\pi$.

It is now straightforward to determine the phase transition temperature as a function of θ. The critical temperature, T_c, is determined by the solution of $\mathcal{F}_{\text{deconfined}} - \mathcal{F}_{\text{confined}} = 0$, which reduces to

$$1 = \frac{\ell^2}{r_+^2}\left[1 + \left(\frac{2\ell\theta}{\beta_c}\right)^2\right]. \tag{7.26}$$

Using (7.20), we may trade r_+ for β_c, replace ℓ by R, and find the transition temperature in field theory variables

$$\beta_c(\theta) = \frac{2\pi R}{3}\sqrt{1 - \left(\frac{\theta}{\pi/3}\right)^2}. \tag{7.27}$$

When $\theta = 0$, corresponding to conventional thermal field theory we recover the standard Hawking-Page phase transition for uncharged $SAdS_5$ black holes $\beta_c = 2\pi R/3$ [171]. As θ is increased the deconfinement temperature decreases. At $\theta = \pi/3$ mod 2π the critical temperature becomes infinite, and there are no sensible Reissner-Nordstrom-AdS_5 black

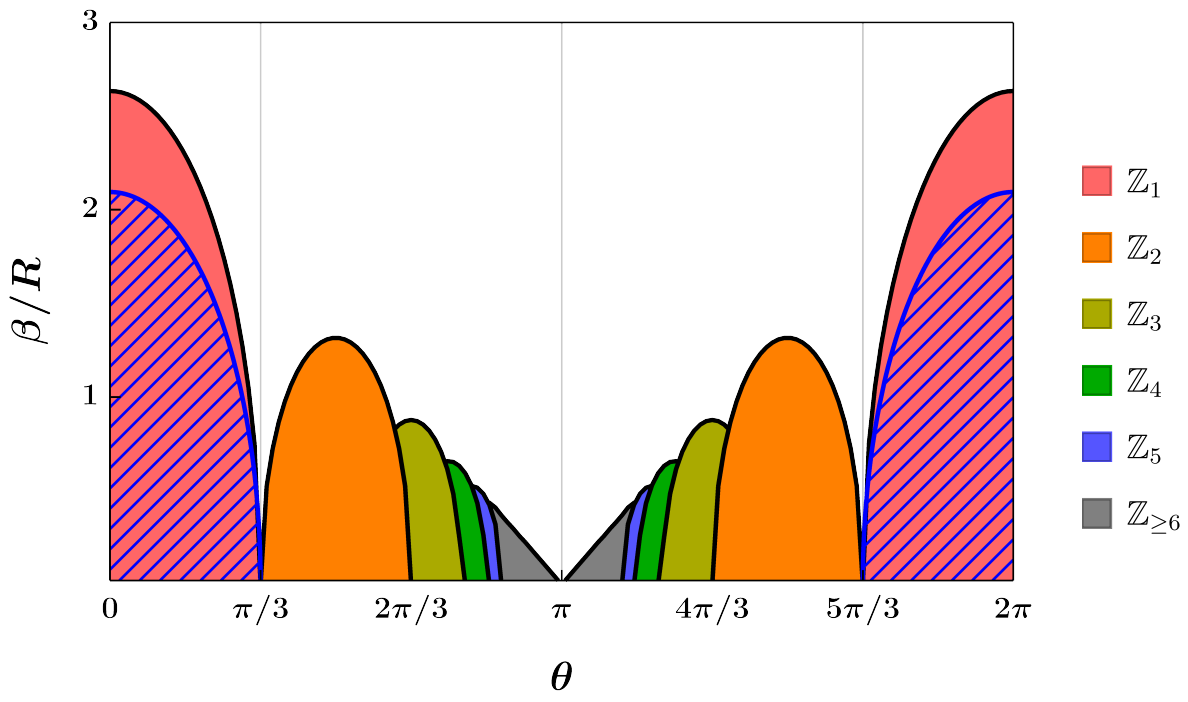

Figure 7.2: Large N phase diagram of $\mathcal{N}=4$ SYM theory on S^3_R as a function of inverse temperature β and grading θ at zero and infinite 't Hooft coupling λ. The grading θ interpolates between the thermal and $(-1)^F$ graded partition functions. At $\lambda=0$ the theory has a deconfinement phase transition along the black curve, and has at least partially broken center symmetry everywhere in the colored regions. The analogous phase transition curve due to known bulk solutions at large coupling $\lambda\to\infty$ is shown in blue, with center symmetry broken everywhere in the hatched region. Note that the deconfined region at large-coupling is a subset of the deconfined region at zero coupling.

hole solutions because β_c becomes complex. The fact that $\mathcal{N}=4$ SYM is confined for all β when $\theta=\pi$, corresponding to $(-1)^F$ graded partition function, has been known since Ref. [125]. But our analysis here suggests that there is actually a whole window of θ values, namely

$$\theta\in\left[\frac{\pi}{3},\frac{5\pi}{3}\right] \tag{7.28}$$

where $\mathcal{N}=4$ $SU(N)$ SYM apparently remains confined for all values of β/R at large λ. We compare the zero and large coupling phase diagrams in Fig. 7.2.

We should emphasize that to reach (7.27) we have only studied the known (analytically-continued) solutions that correspond to homogeneous equilibrium states in the dual field theory. It would be very interesting to see whether there might be some sort of previously unknown (perhaps multi-center) black objects which would be associated to the partially-confined phases[3] we saw at small coupling, see e.g. [181] for a discussion in the context of the superconformal index.

[3]There is another notion of 'partial deconfinement/sub-matrix deconfinement' recently discussed in

7.5 Conclusions

In $\mathcal{N} = 4$ SYM theory, it is possible to smoothly interpolate from the standard thermodynamic partition function to a $(-1)^F$-graded partition function by taking advantage of the $SO(6)$ R-symmetry. We studied the simplest such generalized partition function, where the grading factor is $e^{3i\theta r}$ uses the superconformal R-charge r. We found that the large N theory is in the confined phase on $S^3_R \times S^1_\beta$ when $\theta = \pi/3, \pi, 5\pi/3$ both at small and large coupling. The result for $e^{3\pi i r} = (-1)^F$ was already known. The other two points with complete confinement for all temperatures at both small and large 't Hooft coupling correspond to the more complicated grading $(-1)^F e^{\pm 2\pi i r}$. The small coupling and large coupling corners of parameter space differ in the behavior for $\theta \in (\pi/3, \pi) \cup (\pi, 5\pi/3)$. At small coupling, the phase transition temperature depends non-monotonically on θ in the region $\theta \in (\pi/3, \pi) \cup (\pi, 5\pi/3)$, with center symmetry partially broken for high enough temperatures, with the critical temperature diverging as $\theta \to \pi$. At large coupling, on the other hand, we found no evidence of such rich behavior: the theory appears to be in the confined phase for all temperatures for $\theta \in [\pi/3, 5\pi/3]$.

It is interesting to connect our results to some recent studies of deconfinement in the superconformal index of $\mathcal{N} = 4$ SYM. At the outset, however, we should stress that our graded partition function is quite different from the superconformal index of $\mathcal{N} = 4$ SYM [182], see e.g. Refs. [183, 184] for recent reviews. The partition function we focus on here receives contributions from all of the states in the theory and depends non-trivially on the 't Hooft coupling. On the other hand, the superconformal index is a special $S^3_R \times S^1_\beta$ partition function which is designed to only receive contributions from 1/4 BPS states (in $\mathcal{N} = 1$ language). It is independent of the 't Hooft coupling, so that its exact form for all values of λ and N can be determined in terms of a matrix integral. The superconformal index involves two chemical potentials (and corresponding fugacities p, q) built out of appropriate combinations of Δ R-charge r and the left and right moving angular momenta j_1, j_2. When the fugacities are real, the superconformal index $\mathcal{I}$ is always in the 'confining phase', meaning that $\log \mathcal{I} \sim \mathcal{O}(1)$ [182]. It was recently discovered that $\log \mathcal{I}$ can become $\mathcal{O}(N^2)$ if the fugacities are rotated into the complex plane, so that the superconformal index can be used to study deconfinement and black holes, see Ref. [162, 163, 181, 185–204]. While the superconformal index and our partition functions are distinct, they do share an interesting parallel: the grading $(-1)^F e^{\pm 2\pi i r}$ plays the same role in both cases as being on the boundary between deconfinement for some β/R and confinement for all β/R. This was recently shown in Ref. [163], which studied the superconformal index as a function of $p = q = ye^{i\psi}$, finding a deconfined region for $\psi \in (-4\pi, -3\pi) \cup (-3\pi, -2\pi)$, with e.g. $\psi = -2\pi$ corresponding to a grading by $(-1)^F e^{-2\pi i r}$.

Our large-coupling results are less complete than our results at small coupling, be-

Refs. [174–180].

cause we do not know how to exclude the possibility that there are some presently unknown black objects which correspond to partially confined phases at large coupling. One might guess that increasing the 't Hooft coupling should increase eigenvalue fluctuations, and heuristically this could be expected to increase the deconfinement temperature and (naively) wipe out partially confined phases. This simple picture is consistent with our results. However, Ref. [181] recently also found evidence for partially-confined phases within the superconformal index, which is independent of the 't Hooft coupling. So, from the viewpoint of field theory, partially confined phases appear to be fairly ubiquitous. It would be very interesting to find new black objects dual to partially-confined phases, or to prove that none exist at least within the supergravity approximation.

Acknowledgements

We are grateful to M. Ünsal for conversations that inspired this work and collaboration at an initial stage, as well as to E. Poppitz and J. Sonner for helpful discussions, and the anonymous referee for a very helpful observation. A. C. is supported by startup funds from the University of Minnesota, and A. D. is supported by the National Science Foundation Graduate Research Fellowship under Grant No. 00039202.

Part III

Quantum Information and Geometric Flows

Chapter 8

Aspects of Information, Geometry, and Entanglement

In Part I, we established the connection between classical geometry and thermodynamics. This connection hinged on the behavior of ingoing and outgoing modes of quantum fields residing on an ambient curved spacetime geometry, often near a horizon. When the ambient spacetime is anti-de Sitter, a black hole deep in the interior can be in thermal equilibrium with its outgoing Hawking radiation. Hence, spacetime geometry can be understood as a thermodynamic system and is capable of rich behavior, including van der Waals phase transitions, existence of non-trivial topological configurations, and thermodynamic instabilities.

In Part II, we explored applications of holographic dualities. Such dualities provide a concrete mathematical map between a quantum field theory and a gravitational theory in one higher spatial dimension. Specifically, holographic dualities encode the thermodynamics of strongly coupled gauge theories into the thermodynamics of weakly coupled gravitational theories – a feat not possible if classical geometry and thermodynamics were not connected.

These parts served to form the first links between geometry, entropy, and quantum thermodynamic systems. These links rest on a fundamental observation; the Bekenstein-Hawking entropy for black hole geometries scales with the area of the horizon. Holographic dualities utilize the Bekenstein-Hawking area law to match the entropy of horizon geometries with the usual volume law scaling of thermodynamic entropy observed in quantum field theories. However, a microscopic origin of Bekenstein-Hawking area law from counting black hole microstates in the microcanonical ensemble is not well understood, except in special cases [205].

Another type of entropy measure, important in quantum information theory, which obeys an area law is the entanglement (or von Neumann) entropy. Given an arbitrary quantum state $|\Psi\rangle$ over a bipartite system, the entanglement entropy S_{EE} provides a measure of how far the state is from a pure state. This entropy computes the amount

of entanglement between degrees of freedom across the partition and is known to scale with an area law when the states considered are ground states of CFTs and gapped many-body quantum systems [206]. Since holographic dualities relate CFTs, which have discrete eigenstates, to gravitational theories in one higher dimension, it is natural to wonder if the Bekenstein-Hawking entropy for black holes may be understood as an entanglement entropy for CFTs.

In this part, we finalize the relationship between quantum information and classical geometry via holographic dualities. In the following chapter, we first provide a primer on entanglement entropy, focusing on generalized Bell states and the thermofield double state. We then discuss area-law entanglement in continuum quantum systems, specifically in massive scalar field theories and briefly return to the Ising duality discussed in Sec. 4.1. We conclude this chapter with a review of the Ryu-Takayanagi conjecture [207–209] which asserts that the entanglement entropy, or quantum information, in a reduced quantum system can be holographic encoded into the area of classical extremal surfaces in AdS spacetime.

In the following chapter, we use this conjecture to prove novel bounds on the growth rate of entanglement entropy.

8.1 An Introduction to Entanglement Entropy

The entanglement entropy is a measure of how quantum information is stored in a quantum state. In particular, the entanglement entropy measures the amount of entanglement between two subsystems of a composite quantum system. Here, we provide an overview of the entanglement entropy focusing primarily on generalized Bell states. For a comprehensive review, see [210].

Consider a bipartite system with regions A and B, see Fig. 8.1 below reproduced from [210]. The system Σ is said to be bipartite if its Hilbert space $\mathcal{H}_\Sigma$ can be expressed by the tensor product $\mathcal{H}_\Sigma = \mathcal{H}_I \otimes \mathcal{H}_{I^c}$ over the individual subsystems where $I = A$ or B. To see if the two subsystems are entangled, we need further technologies: a density matrix ρ_Σ and an operation tr_I which isolates a subsystem. The first is easy, the density matrix, by definition, is constructed from the (pure) quantum state $|\Psi\rangle \in \mathcal{H}_\Sigma$ of the system

$$\rho_\Sigma = |\Psi\rangle \langle\Psi| \,. \tag{8.1}$$

For the second, let $\{|i\rangle_I, i = 1, 2, \cdots, \dim(\mathcal{H}_I)\}$ be an orthonormal basis for $\mathcal{H}_I$. The partial trace tr_I of an operator $\mathcal{O}$ is then defined by

$$\mathrm{tr}_I(\mathcal{O}) \equiv \sum_i {}_I \langle i| \mathcal{O} |i\rangle_I \,. \tag{8.2}$$

The partial trace can be used to isolate a subsystem I by "tracing out" the complement

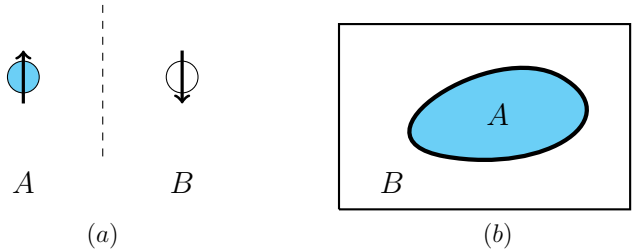

Figure 8.1: A bipartite system with subsystems A, shown in blue, and complement B. (a) Two discrete spin systems. The subsystems are the left and right spins. (b) A continuum quantum field theory. At a given timeslice, the spatial continuum is split into the subsystems A and B whose common boundary $\partial A = \partial B$ is always a codimension-two hypersurface.

I^c. To be concrete, the reduced density matrix of the subsystem I is obtained via

$$\rho_I \equiv \mathrm{tr}_{I^c}(\rho_\Sigma). \tag{8.3}$$

We now have the necessary ingredients to compute the entropy stored in the entanglement between I and I^c. The entanglement entropy of the subsystem I is computed by

$$S_I = -\,\mathrm{tr}_I[\rho_I \log(\rho_I)]. \tag{8.4}$$

This entropy satisfies the following statements:

1. The entanglement entropy is non-zero only if the complement of the subsystem is non-empty. In other words, $S_I = 0$ when $\mathrm{Area}(I^c) = 0$. To see this, first note that $\mathrm{Area}(I^c) = 0$ is the same as saying $I^c = \emptyset$. Next, we have $\Sigma = I \cup I^c = I \cup \emptyset = I$. And finally, it is well known that the entanglement entropy of the total system always vanishes for a pure state. Proof:

$$S_I = -\,\mathrm{tr}_I[\rho_I \log(\rho_I)] = -\,\mathrm{tr}_\Sigma[\rho_\Sigma \log(\rho_\Sigma)] = -\,\mathrm{tr}_\Sigma[ODO^{-1} \log\Big(ODO^{-1}\Big)] \tag{8.5}$$

$$= -\,\mathrm{tr}_\Sigma[D \log(D)] = 0 \tag{8.6}$$

   where we have used that the density matrix (i) can be diagonalized, i.e., $\rho_\Sigma = ODO^{-1}$ and (ii) the ground state is pure so $\rho_\Sigma = (\rho_\Sigma)^2$ implying that the eigenvalues $\lambda_i \in \{0, 1\}$.

2. The entanglement entropy is finite for finite-dimensional quantum systems, such as on a lattice. However, S_I suffers from UV divergences in quantum field theory (necessarily infinite dimensional) due to short range interactions near the boundary of I, denoted ∂I.

3. It is possible to show that the entanglement entropy vanishes only if the pure ground state is **separable** which means that the quantum state admits the decomposition $|\Psi\rangle = |\Psi\rangle_I \otimes |\Psi\rangle_{I^c}$. In the case where $\mathrm{Area}(I^c) = 0$, there exists no states in $\mathcal{H}_{I^c}$ and hence the bipartition is simple $|\Psi\rangle = |\Psi\rangle_I \otimes 1 = |\Psi\rangle_\Sigma$.

8.1.1 Entanglement in Generalized Bell States

Let us now turn to computing the entanglement entropy. The simplest example is the two spin system (see Fig. 1(a)). Let A and B be two particles with spin $s = 1/2$. Each particle has two states in their respective Hilbert spaces $H_I = \text{span}(\{|\uparrow\rangle_I, |\downarrow\rangle_I\})$ where $I = A$ or B and the bases are orthonormal $\langle i|j\rangle = \delta_{ij}$ for $i, j \in \{\uparrow, \downarrow\}$. The total Hilbert space is then straightforward to build

$$\mathcal{H}_\Sigma = \mathcal{H}_I \otimes \mathcal{H}_{I^c} = \{|\downarrow\downarrow\rangle, |\downarrow\uparrow\rangle, |\uparrow\downarrow\rangle, |\uparrow\uparrow\rangle\} \tag{8.7}$$

where $|ij\rangle \equiv |i\rangle_I \otimes |j\rangle_{I^c}$. Now, suppose the ground state is given as $|\Psi\rangle = \frac{1}{\sqrt{2}}(|\downarrow\uparrow\rangle + |\uparrow\downarrow\rangle)$ then the density matrix of the total system reads

$$\rho_\Sigma = |\Psi\rangle\langle\Psi| = \frac{1}{2}(|\downarrow\uparrow\rangle + |\uparrow\downarrow\rangle)^2. \tag{8.8}$$

Tracing out, say $I^c = B$, we arrive at the reduced density matrix for $I = A$

$$\rho_A = \frac{1}{2}(|\downarrow\rangle_{AA}\langle\downarrow| + |\uparrow\rangle_{AA}\langle\uparrow|) = \begin{pmatrix} 1/2 & 0 \\ 0 & 1/2 \end{pmatrix}. \tag{8.9}$$

As the logarithm of a diagonal matrix is the same as a matrix formed from the logarithm of each diagonal element, the entropy of entanglement for the ground state $|\Psi\rangle$ is

$$\begin{aligned} S_A &= -\,\text{tr}_A \left[\begin{pmatrix} 1/2 & 0 \\ 0 & 1/2 \end{pmatrix} \cdot \begin{pmatrix} \log(1/2) & 0 \\ 0 & \log(1/2) \end{pmatrix} \right] \\ &= \log(2) \end{aligned} \tag{8.10}$$

This value is in fact the maximum amount of quantum information stored between two entangled particles. To prove this statement, let us consider a more general Bell state

$$|\Psi\rangle = \cos(\theta)\,|\downarrow\uparrow\rangle - \sin(\theta)\,|\uparrow\downarrow\rangle\,. \tag{8.11}$$

A routine computation then shows the entanglement entropy stored in the generalized entangled state is

$$S_A(\theta) = -2\left[\cos(\theta)^2 \log(\cos(\theta)) + \sin(\theta)^2 \log(\sin(\theta))\right]. \tag{8.12}$$

The entanglement entropy is clearly maximized at $\theta_c = (\pi/4)$ which yields $S_A(\theta_c) = \log(2)$ justifying the earlier claim. The states for which $\theta = 0, \pi/2$ are pure product states as the entanglement entropy vanishes.

8.1.2 Entanglement in the Thermofield Double State

Here, we consider a more nontrivial example; the thermofield double state. The purpose of this example is to highlight how the entanglement entropy can be a measure fo the

thermal entropy for a subsystem A. The thermofield double state $|\Psi\rangle$ is an entangled state defined by

$$|\Psi\rangle = \frac{1}{\sqrt{\mathcal{Z}}} \sum_n e^{-\beta E_n/2} |n\rangle_A \otimes |n\rangle_B, \tag{8.13}$$

where the state is normalized by the partition function $\mathcal{Z} = \sum_n e^{-\beta E_n}$. Consider the partial trace of the density matrix ρ_Σ over the subsystem B. The reduced density matrix of A is

$$\begin{aligned} \rho_A &= \frac{1}{Z} \sum_n e^{-\beta E_n} |n\rangle_{AA}\langle n|, \\ &= \frac{1}{Z} e^{-\beta H_A} \ . \end{aligned} \tag{8.14}$$

Clearly, we can interpret the reduced density matrix as one that is constructed for a Gibbs state with an inverse temperature β and a (modular) Hamiltonian H_A satisfying $H_A|n\rangle_A = E_n|n\rangle_A$.

One additional peculiarity of the thermofield double state is that one can purify the thermal system A by extending the Hilbert space to $\mathcal{H}_A \otimes \mathcal{H}_B$. In doing so, one copies the state vectors $\{|n\rangle_B\}$ from $\mathcal{H}_A$ to $\mathcal{H}_B$ and assigning Boltzmann weights $p_i = e^{-\beta E_i}/\mathcal{Z}$ to the state vector

$$|\Phi\rangle \equiv \sum_i \sqrt{p_i}\, |i\rangle_A \otimes |i\rangle_B \tag{8.15}$$

In doing so, expectation values of local operators belonging to the subsystem A are thereby promoted to operators in thermofield double state Eqn. (8.13) over the enlarged system. Again, a routine computation of the entanglement entropy shows

$$\begin{aligned} S_A &= -\operatorname{tr}_A \left[\rho_A \left(-\beta H_A - \log Z\right)\right], \\ &= \beta \left(\langle H_A\rangle - F\right), \end{aligned} \tag{8.16}$$

where in the last line we have used that $\beta F = -\log(\mathcal{Z})$. Clearly, the entanglement entropy and the thermal entropy for the subsystem A are identical.

8.2 Entanglement Entropy and Area Laws

In this section, we present an overview of the area law behavior exhibited by the entanglement entropy of continuum quantum systems. Specifically, we broadly study the area law entanglement exhibited by massive scalar field theory, discussed earlier Sec. 1.1. We use these results to motivate numerical calculations of the entanglement entropy for the Ising chains discussed in Sec. 4.1. We show that quantum/classical dualities indeed preserve the entanglement structure non-trivally by encoding the entanglement into correlations. This overview largely follows the excellent discussion in [210] and we will henceforth leave out the technical details.

For continuum quantum systems, computing the entanglement entropy is quite non-trivial. One useful technique, known as the replica trick, allows one to reliably compute the entanglement entropy so long as one knows the reduced density matrix of a subsystem to its higher moments:

$$S_A = -\lim_{n\to 1} \partial_n \log \mathrm{tr}_A(\rho_A^n). \tag{8.17}$$

To understand this expression, consider a partition function $\mathcal{Z}$ of a manifold $\mathcal{M}$ with a punctured region A. The idea is to construct a new spacetime by stitching together these spacetimes n-times. These spacetimes are glued together in such a way that operators to the left and right of the puncture form a cyclic ladder. This last step essentially amounts to repeated insertions of identity operators for the density matrix of the spacetime stack. It follows that $\mathrm{tr}_A(\rho_A^n)$ can be expressed by the partition function on the n-fold cover $\mathcal{M}_n$ with a cut along A [206, 211]. To be clear, see the following figure reproduced from [210]

$$\mathrm{tr}_A(\rho_A^n) = \frac{1}{(\mathcal{Z})^n}$$

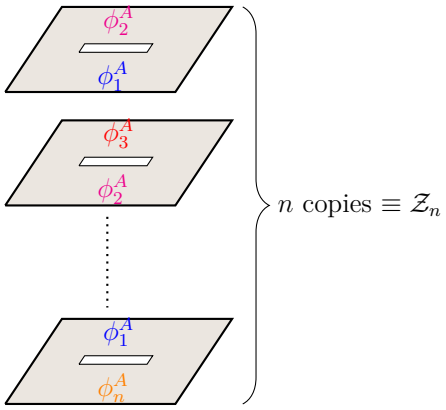

$$= \frac{\mathcal{Z}_n}{(\mathcal{Z})^n}, \tag{8.18}$$

where $\mathcal{Z}_n$ denotes the partition function on $\mathcal{M}_n$. Performing this replica yields an alternative definition for the entropy of entanglement

$$S_A = -\lim_{n\to 1} \partial_n (\log \mathcal{Z}_n - n \log \mathcal{Z}) \ . \tag{8.19}$$

Observe that the stack of spacetimes are glued together at A and hence the punctured region, or entangling surface, is a codimension-two surface $\Sigma = \partial A$ with a deficit angle of $2\pi(1-n)$.

We can directly apply this form of the entanglement entropy to consider continuum field theories, specifically for a massive scalar field theory. Consider the Euclidean action for a free massive scalar field

$$I_E = \frac{1}{2}\int \mathrm{d}^d x \left[(\partial_\mu \phi)^2 + m^2 \phi^2\right], \tag{8.20}$$

where the space and Euclidean time coordinates are $x_i \, (i = 1, \cdots, d-1)$ and x_0 respectively. Take A and B to be the regions in $x_1 > 0$ and $x_1 \leq 0$. We choose the entangling

surface Σ to a codimension two hyperplane located at $x_1 = 0$: $\Sigma = \{(x_0, x_i) | \, x_0 = x_1 = 0\}$. On the manifold $\mathcal{M}_n$, we can install the following metric

$$\begin{aligned} \mathrm{d}s^2 &= \mathrm{d}x_0^2 + \mathrm{d}x_1^2 + \sum_{i=2}^{d-1} \mathrm{d}x_i^2, \\ &= \mathrm{d}r^2 + r^2 \mathrm{d}\tau^2 + \sum_{i=2}^{d-1} \mathrm{d}x_i^2, \end{aligned} \tag{8.21}$$

where polar coordinates were used for the (x_0, x_1) plane, $0 \leq r$, and $0 \leq \tau \leq 2\pi$. Observe that the manifold stack is decomposable as a direction product of a $2d$ cone $\mathcal{C}_n$ and $\mathbb{R}^{d-2}$. This makes the calculations of the partition function much easier. For the partition function $\mathcal{Z}_n$ on $\mathcal{M}_n$, we can compute the one-loop determinant of a massive scalar field in the standard way using the Schwinger representation

$$\begin{aligned} \log \mathcal{Z}_n &= -\frac{1}{2} \log \det\Big(-\nabla^2 + m^2\Big), \\ &= -\frac{1}{2} \operatorname{tr} \log\Big(-\nabla^2 + m^2\Big), \\ &= \frac{1}{2} \int_{\epsilon^2}^{\infty} \frac{\mathrm{d}s}{s} \operatorname{tr}\left[e^{-s(-\nabla^2 + m^2)} - e^{-s}\right], \\ &= \frac{1}{2} \int_{\epsilon^2}^{\infty} \frac{\mathrm{d}s}{s} \times \left[\frac{\mathrm{Vol}(\mathbb{R}^{d-2})}{12\, n} \frac{e^{-sm^2}}{(4\pi s)^{(d-2)/2}} - \operatorname{tr}\Big[e^{-s}\Big]\right], \end{aligned} \tag{8.22}$$

where the covariant derivative ∇ is over $\mathcal{M}_n$ and the last step was performed by appealing to the decomposition of the Laplacian into $\nabla^2 = \nabla^2_{\mathcal{C}_n} + \nabla^2_{\mathbb{R}^{d-2}}$ and solving the eigenvalue problem on each space. Observe that the n-fold dependence is localized entirely on the conical base, and therefore we can directly compute the partition function of a single spacetime as

$$\log \mathcal{Z} = \lim_{n \to 1} \log \mathcal{Z}_n. \tag{8.23}$$

Hence, we can directly calculate the entanglement entropy across the entangling region for the massive scalar field. Inserting these expressions into Eqn. (8.19) and expanding around $\epsilon \approx 0$ leaves us with

$$\begin{aligned} S_A &= \frac{\pi \,\mathrm{Vol}(\mathbb{R}^{d-2})}{3} \int_{\epsilon^2}^{\infty} \mathrm{d}s \, \frac{e^{-sm^2}}{(4\pi s)^{d/2}} \\ &= \frac{\mathrm{Vol}(\mathbb{R}^{d-2})}{6(4\pi)^{d-1}} \left[\frac{1}{(d-2)\epsilon^{d-2}} - \frac{m^2}{(d-4)\epsilon^{d-4}} + \cdots\right]. \end{aligned} \tag{8.24}$$

The leading term scales as $\mathrm{Vol}(\mathbb{R}^{d-2})/\epsilon^{d-2}$ which is precisely a dimensional factor going as the area of the entangling surface $\Sigma = \mathbb{R}^{d-2}$. This completes our calculation of the area law of entanglement entropy. For $d = 2$, the entanglement entropy is actually logarithmically divergent. In the next section, we quote the logarithmic divergence for $2d$ CFTs and refer to a numerical calculation checking the entanglement entropy.

8.2.1 Ising Dualities and Entanglement in Qubit Chains

One of the most important tests for any duality is to be able to recover the entanglement entropy from calculations on both sides. At its critical point $g = 1$, the $2d$ Ising model belongs to the same universality class of a $2d$ conformal field theories with central charge $c = 1/2$ [212]. The entanglement entropy for such theories is [206],

$$S_{2d\ \mathrm{CFT}} = A + \frac{c}{3} \log\left(\frac{N}{\pi} \sin\left(\frac{\pi x}{N}\right)\right). \tag{8.25}$$

Furthermore, one can compute the entanglement entropy of a qubit chain by first finding the ground state of the chain, tracing out a subsystem containing some number of qubits, and using the reduced density matrix to calculate the ordinary entanglement entropy:

$$S_I = -\operatorname{tr}_I[\rho_I \log(\rho_I)]. \tag{8.26}$$

Via the quantum/classical duality, the $2d$ Ising model is dual to the $1d$ qubit chain (see Sec. 4.1). Hence, the goal here is to explore if we can recover a central charge of $c = 1/2$ purely by numerically finding the ground state of the qubit chain at the $g = 1$ critical point. The arbitrary normalization A in the entanglement entropy of $2d$ CFTs will have to be calibrated against the numerical calculations.

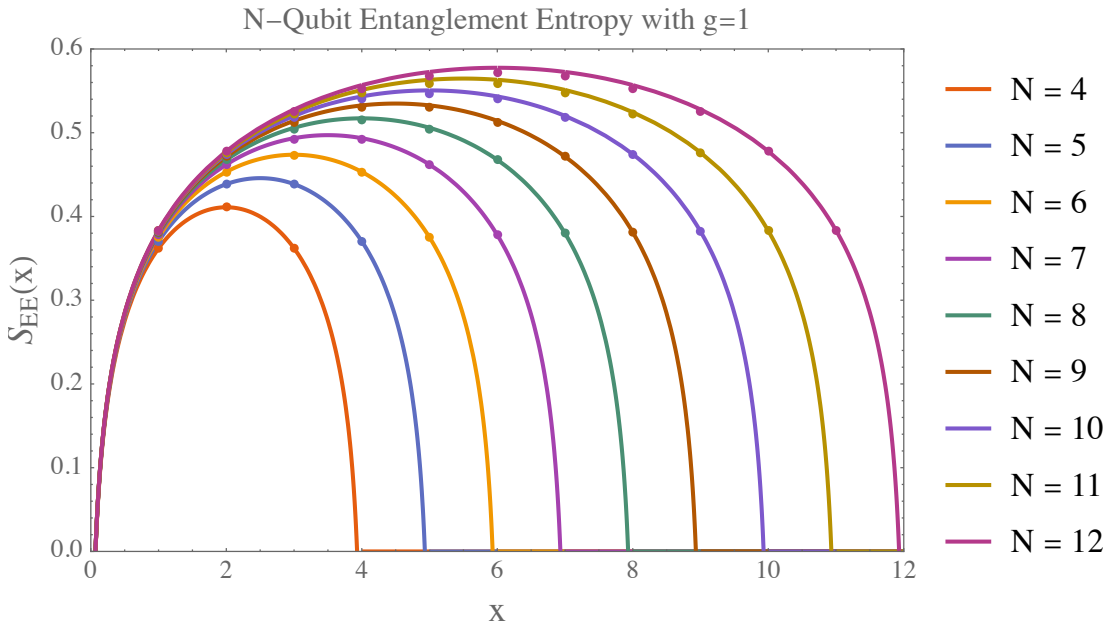

Figure 8.2: The entanglement entropy as a function of "temperature".

In the above, we plot the entanglement entropy for $2d$ CFTs and compare this against numerical calculations performing partial traces at locations x on a qubit chain in its ground state. After calibrating the shift, we see that the CFT result matches precisely with the entanglement entropy calculated for $g = 1$. For short qubit chains of length

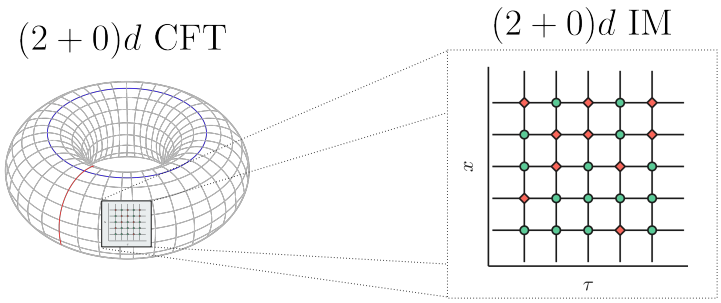

Figure 8.3: A $2d$ CFT with periodic boundary condition and a $2d$ Ising model. In the near critical limit, the $2d$ Ising model becomes conformally invariant and the lattice spacing shrinks simulating a continuum.

$N = 4, 5$, the numerical central charge differed moderately from the predicted value sitting around $c \approx .578$. However, in the large qubit limit, the central charge approached the expected CFT result and was calculated to be $c \approx .518$ at $N = 12$ qubits.

Though larger chains are expensive to simulate, this examples presents an interesting observation and experimental opportunity. The first check is that dualities indeed preserve the entanglement structure. In this case, the entanglement in qubit chain is encoded into the $2d$ Ising model at its critical point. The entanglement of the qubit chain is stored classically in the correlations between spins across the entangling surface or quantum mechanically in the CFT degrees of freedom across the fiducial barrier. From either perspective, entanglement is preserved. The second opportunity presented by this example is an experimental test of holography. That both the CFT entanglement entropy and the von Neumann entropy of qubit chains are the same presents a unique opportunity to test if modern quantum computers can reproduce the same phenomena under similar conditions of criticality. The difficult but rewarding challenge is to understand how to directly measure entanglement in a quantum system. Understanding to what extent quantum entanglement can be a resource for computational purposes remains an outstanding challenge.

8.3 Holographic Entanglement Entropy

The road to understanding a holographic dual of entanglement entropy begins with understanding the thermal aspect of black hole as an entanglement entropy for fields across the horizon. Returning to the metric used in the calculation of the entanglement entropy for massive scalar field theory, an analytic continuation on the manifold $\mathcal{M}$ yields

$$\mathrm{d}s^2 = -r^2 \mathrm{d}\eta^2 + \mathrm{d}r^2 + \sum_{i=2}^{d-1} \mathrm{d}x_i^2 \ , \tag{8.27}$$

with the new time $\eta = -\mathrm{i}\tau$ ranging $-\infty < \eta < \infty$. Observe that we are not considering the n-fold manifold but instead a single copy. The above spacetime is the Minkowski spacetime encountered in Sec. 1.1. We can restrict further to the Rindler wedge which covers the portion $x_1 \geq |T|$ (see Fig. 8.4 from [210] below),

$$\mathrm{d}s^2 = -\mathrm{d}T^2 + \mathrm{d}x_1^2 + \sum_{i=2}^{d-1} \mathrm{d}x_i^2 \ , \tag{8.28}$$

as seen from the coordinate transformation

$$T = r \sinh \eta \ , \qquad x_1 = r \cosh \eta \ . \tag{8.29}$$

This is precisely the same transformation which transforms an inertial observer in Rindler to an accelerated observer in Minkowski spacetime in the presence of a horizon at $r = 0$. The Rindler horizon leads an observer to encounter the Unruh effect discussed earlier.

From the perspective of entanglement entropy, the Unruh effect is a manifestation of an observer confined to region A with a reduced density matrix ρ_A which is in a mixed thermal ensemble at temperature $\beta = 2\pi$ though the system $A \cup B$ is in a pure state. The reduced density matrix is thermal in the same sense as in the thermofield double state Eqn. (8.13). Hence, the entanglement entropy is precisely equal to the thermal entropy for a Rindler observer.

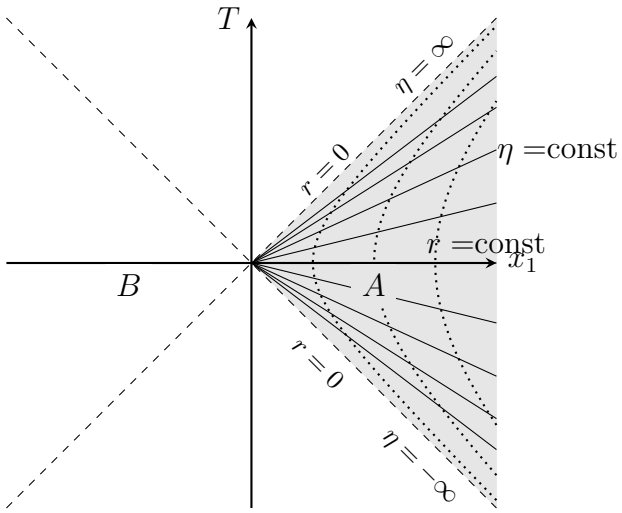

Figure 8.4: Inertial observers in the Rindler wedge (shaded region) see a thermal state. Whereas inertial observers in Minkowski spacetime see a pure state. Relative to the observers in Minkowski spacetime, the Rindler observers are accelerating.

As discussed in Sec. 1.1, the Unruh and Hawking effects are deeply intertwined with the presence of accelerated or apparent horizons. This suggests that the thermal aspects of black holes can instead be thought of in terms of the entanglement. If we consider a black hole event horizon as an entangling surface, then the Hawking temperature is

simply the temperature observed by an accelerated observer. In general, inertial observers in black hole geometries are infalling and hence the accelerated observer must be at the asymptotic boundary (in agreement with the flux of Hawking radiation approaching asymptotic infinity). Secondly, and more importantly, the entanglement entropy must be related to the thermal entropy of the black hole. From a holographic perspective, the thermal entropy of black hole geometries must be related to the entanglement entropy of codimension one CFTs. These observations lead us to the Ryu-Takayanagi conjecture.

8.3.1 The Ruy-Takayanagi Conjecture

In their paper, Ryu and Takayani proposed a conjecture deeply connecting quantum information science with classical gravity via holography [207–209]. The conjecture provides a concrete description for calculating the entanglement entropy in conformal field theories by utilizing special surfaces in ambient AdS geometries. Their theorem, along with suitable covariant generalizations, is as follows;

Theorem 4. *Consider a spatial slice Σ of an AdS spacetime on whose boundary we define the dual CFT. Define the entanglement entropy S_A in a CFT on $\mathbb{R}^{d,1}$ (or $\mathbb{R} \times S^d$) for a subsystem A that has an arbitrary $d-1$ dimensional boundary $\partial A \in \mathbb{R}^d$ (or S^d). Let γ_A be a surface satisfying*

- *γ_A has the same boundary as A.*
- *γ_A is homologous to A.*
- *γ_A is a stationary point of the area functional, i.e., extremal.*

Then, the entanglement entropy for the subsystem A is given by

$$S_A = -\operatorname{tr}[\rho_A \log(\rho_A)] = \frac{Area[\gamma_A]}{4G_N}. \tag{8.30}$$

Thus far, this conjecture has passed several non-trivial consistency checks and has motivated deep connections between gravity, thermodynamics and entanglement (explored below shortly). One immediate connection is the similarity to the Bekenstein-Hawking entropy. Indeed, when the extremal surface γ_A is the black hole horizon, the holographic entanglement entropy recovers the Bekenstein-Hawking entropy. Following this trail of discoveries, we are lead to a profound realization that spacetime emerges from entanglement [213] and that classical gravity and quantum information science are holographically equivalent.

In the following chapter, we explore the holographic entanglement entropy, derive novel bounds on the growth of entanglement in time-evolving conformal field theories, and find an interesting Bekenstein bound on entanglement itself.

Chapter 9

Maximal Entangling Rates from Holography

This chapter is a faithful reproduction of the submitted work **Å. Folkestad and A. Dhumuntarao, arxiv:2211.07654 (2022)**. One distinguishing feature of this chapter which is not included in the submitted work [214] is the inclusion of the novel results in 9.5.

Abstract

We prove novel speed limits on the growth of entanglement, equal time correlators, and spacelike Wilson loops in spatially uniform time-evolving states in strongly coupled CFTs with holographic duals. These bounds can also be viewed as quantum weak energy conditions. Several of the speed limits are valid for regions of arbitrary size and with multiple connected components, and our findings imply new bounds on the effective entanglement velocity of small subregions. In 2d CFT, our results prove a conjecture by Liu and Suh for a large class of states. We also bound spatial derivatives of entanglement and correlators. Key to our findings is a momentum-entanglement correspondence, showing that entanglement growth is computed by the momentum crossing the HRT surface. In our setup, we prove a number of general features of boundary-anchored extremal surfaces, such as a sharp bound on the smallest radius that a surface can probe, and that the tips of extremal surfaces cannot lie in trapped regions. Our methods rely on novel global GR techniques, including a delicate interplay between Lorentzian and Riemannian Hawking masses. While our proofs assume the dominant energy condition in the bulk, we provide numerical evidence that our bounds are true under less restrictive assumptions.

9.1 Introduction

Entanglement is one of the key features unique to quantum mechanics, and its effects are ubiquitous in modern physics. It is now clear that entanglement and entanglement

entropy is a central quantity across a diverse range of fields, such as quantum many-body physics [215–217], quantum information theory [218–220], quantum gravity [6, 14, 15, 207, 209, 213, 221–229], and quantum field theories and their RG flows [212, 230–237].

A central question relevant to all of the above subjects is how entanglement behaves dynamically. In this paper, we address the following questions: are there general bounds on the entanglement entropy in time-dependent states? Does there exist speed limits on how fast it can grow? The latter question is relevant to understanding how rapidly quantum information can propagate, how long it takes a many-body system to thermalize, or, in quantum gravity, for constraining the dynamics of spacetime itself.

While calculating entanglement entropies is notoriously hard, many lessons have been learned over the last two decades. Quantum quenches in particular have received considerable interest. In a quantum quench, the Hamiltonian is abruptly changed, or a source is turned on over a small time interval δt. In either case, there is an abrupt injection of energy into the system, kicking the state out of equilibrium. The subsequent approach to equilibrium can then be computed in various setups. In the seminal paper by Calabrese and Cardy [212], the entanglement entropy S_R of an interval R of length ℓ in a $(1+1)$-dimensional conformal field theory (CFT) after a uniform quench was computed, and for large times and interval lengths, it was found to behave as

$$S_R(t) - S_R(t=0) = \begin{cases} 2s_{\text{th}}t & t < \ell/2 \\ s_{\text{th}}\ell & t \geq \ell/2 \end{cases}, \tag{9.1}$$

where s_{th} the thermal entropy density of the final state. Linear growth of entanglement for large regions R after uniform quenches has also been found in higher dimensional holographic CFTs [238–241]. In particular, after local equilibration and before late time saturation, the entanglement entropy of a region R after a quench was found to behave as [240, 241]

$$S_R(t) - S_R(t=0) = v_E s_{\text{th}} \text{Area}[\partial R] t + \dots \tag{9.2}$$

with v_E the so-called entanglement velocity, which satisfies $v_E \leq 1$.

While quenches provide useful insights on entanglement dynamics, they do not cover all kinds of states, and it would be useful to have more general constraints. Some such results do exist. Consider two quantum systems $A \cup a$ and $B \cup b$ coupled by an interaction Hamiltonian H acting only on A and B. In [242] (building on [243]) it was proven that

$$\left| \frac{\mathrm{d}S_{A\cup a}}{\mathrm{d}t} \right| \leq \eta \|H\| \log d, \tag{9.3}$$

where $d = \min\{\dim A, \dim B\}$, and where η is an order 1 constant. While this bound has broad generality for finite-dimensional systems, it is not useful in QFT, where d is infinite. Even if we UV-regulate to make d finite, $\|H\|$ is infeasible to compute. Furthermore, the bound is state-independent, and it is natural to suspect there exists stronger bounds that depend on the conserved charges of the state.

A bound more useful in QFT was conjectured [240, 241], based on the findings in holographic quenches. It was proposed that a normalized instantaneous entanglement growth $\mathfrak{R}$ in relativistic quantum field theory satisfies the bound

$$\mathfrak{R} \equiv \frac{1}{\text{Area}[\partial R] s_{\text{th}}} \left| \frac{\mathrm{d}S_R}{\mathrm{d}t} \right| \leq 1. \tag{9.4}$$

In [244] relativistic QFT was used to prove that $\mathfrak{R} \leq 1$ for large convex regions R in spatially uniform states, neglecting contributions to S_R not scaling with volume.[1] However, it was found in [241] that the largest values for $\mathfrak{R}$ were obtained for intermediate sized regions, where it could exceed v_E (for $d > 2$), and where existing proofs of $\mathfrak{R} \leq 1$ do not apply. Thus, the validity of (9.4) for general regions is still an open question.[2]

In this work, for holographic CFTs with large coupling and large$-N$ (large effective central charge), we prove novel bounds that imply $\mathfrak{R} \leq 1$ for a large class of situations not covered by [244, 245]. We also prove several bounds that to our knowledge have not been previously discussed, including growth bounds on correlators and Wilson loops. We will see that our growth bounds can be seen as new types of quantum energy conditions, valid for uniform states. We also derive absolute bounds on entanglement entropy and equal time correlators.

Let us now summarize our results. Consider first a 2d CFT on $S^1 \times \mathbb{R}$ or Minkowski space in a homogeneous and isotropic state undergoing time-evolution. Let t label the timeslices on which the state is uniform. Let R be a union of n finite intervals of any size. Assuming an energy condition and certain falloff conditions on the matter fields in the bulk, which we assume for all bounds presented in the following, we prove that

$$\left| \frac{\mathrm{d}S_R}{\mathrm{d}t} \right| \leq n \sqrt{\frac{8\pi c}{3} \Big(\langle T_{tt} \rangle - \langle T_{tt} \rangle_{\text{vacuum}} \Big)}, \tag{9.5}$$

where c is the central charge and $\langle T_{tt} \rangle$ the CFT energy density one-point function, which is the same everywhere in a uniform state. If we work with uncharged states, (9.5) implies that $\mathfrak{R} \leq 1$. Thus, for the $2d$ theories under consideration, we have given a proof of $\mathfrak{R} \leq 1$ to regions of arbitrary finite size and with any number of connected components.[3]

Next, consider $d \geq 2$-dimensional holographic CFTs on Minkowski space, again in a time-evolving uniform state. Taking R to be either a single ball or strip of characteristic

[1] A proof was also given in [245] for half-planes, taking linear growth of entanglement as an assumption. For quenches, it was proven for large regions holographically in [246], together with many other properties of quenches.

[2] In fact, since generic QFTs can have state-dependent divergences in S_R [247], $\partial_t S_R$ can be divergent in some theories, and so (9.4) cannot be true in all relativistic QFTs. This means that a generalization of the proofs of [244, 245] to include contributions not scaling with volume impossible without more input on the theories under consideration.

[3] For holographic CFTs, (9.5) also improves on a bound proven for single intervals of any size in all $2d$ CFTs by [244], which can be written as $\mathfrak{R} \leq \coth\left(\pi \ell \sqrt{\frac{\pi c}{6\langle T_{tt} \rangle}}\right)$.

size ℓ, we prove that

$$\left|\frac{\mathrm{d}S_R}{\mathrm{d}t}\right| \leq \kappa \mathrm{Vol}[R] \langle T_{tt}\rangle \left[1 + \mathcal{O}\left(\frac{\ell^d \langle T_{tt}\rangle}{c_{\text{eff}}}\right)\right], \tag{9.6}$$

where κ is an $O(1)$ numerical constant given in (9.31), and which depends on d and the shape of R. c_{eff} is the effective central charge, to be defined in the following. For small regions this bound is much stronger than $\mathfrak{R} \leq 1$.[4] If β is the effective inverse temperature at which the thermal energy density equals $\langle T_{tt}\rangle$, we get

$$\mathfrak{R} \leq \mathcal{O}(\ell/\beta) \ll 1. \tag{9.7}$$

We also prove a higher-dimensional analogue of (9.5), although the proof is more limited. We prove for states that are somewhat more general than quench states that

$$\left|\frac{\mathrm{d}S_R}{\mathrm{d}t}\right| \leq \frac{1}{4}\mathrm{Area}[\partial R] c_{\text{eff}} \left[\frac{16\pi}{(d-1)c_{\text{eff}}} \langle T_{tt}\rangle\right]^{\frac{d-1}{d}}, \tag{9.8}$$

where R either is a single ball, or the union of any number of strips. Considering a neutral state, (9.8) translates into $\mathfrak{R} \leq 1$. While our proof of (9.8) applies to a smaller class of states, we give substantial numerical evidence that (9.8) holds more generally for all uniform states.

For strips, we also prove bounds on the entanglement entropy itself. For R_ℓ a strip of width ℓ at fixed time t, we prove that the vacuum subtracted entropy $\Delta S(\ell)$ satisfies

$$\partial_\ell \Delta S(\ell) \geq 0, \tag{9.9}$$

which in particular implies $\Delta S \geq 0$.

In the special dimensions of $d = 2, 3, 4$, we prove additional bounds. Assuming the geodesic approximation for correlators [249], we prove that the equal time two-point function of a scalar operator O of large scaling dimension Δ in $d = 2$ satisfies

$$\left|\frac{\mathrm{d}}{\mathrm{d}t} \log \langle O(x)O(0)\rangle_{\rho(t)}\right| \leq \sqrt{\frac{96\pi\Delta^2}{c}\Big(\langle T_{tt}\rangle - \langle T_{tt}\rangle_{\text{vac}}\Big)}, \tag{9.10}$$

where $\rho(t)$ is the state under consideration. This bound is saturated in the global CFT_2 quenches studied in [250, 251] (for any Δ). We also prove a tighter bound when x is small:

$$\left|\frac{\mathrm{d}}{\mathrm{d}t} \log \langle O(x)O(0)\rangle_{\rho(t)}\right| \leq \frac{12\pi\Delta|x|}{c}\Big(\langle T_{tt}\rangle - \langle T_{tt}\rangle_{\text{vac}}\Big)\left[1 + \ldots\right], \tag{9.11}$$

where dots indicate $\mathcal{O}\left(x^2 \langle T_{tt}\rangle / c\right)$ corrections. We furthermore prove a bound on the correlator itself. Letting $x > 0$, we have

$$\frac{\mathrm{d}}{\mathrm{d}x} \ln \langle O(x)O(0)\rangle_{\rho(t)} \leq \frac{\mathrm{d}}{\mathrm{d}x} \ln \langle O(x)O(0)\rangle_{\text{vacuum}} = -\frac{2\Delta}{x}, \tag{9.12}$$

[4] See [248] for a discussion of a different definition of $\mathfrak{R}$, where s_{th} is replaced by the vacuum-subtracted entanglement entropy per volume in the final state. With this definition, $\mathfrak{R}$ is $O(1)$ for small subregions, but it can exceed 1.

which shows that for the states covered by our assumptions, correlations between heavy scalars must die off faster than in the vacuum.

When $d = 3, 4$, we prove bounds on Wilson loops $\mathcal{W}(C)$ of spacelike circles C, assuming we can compute these using classical worldsheets in the bulk. Assuming $\mathcal{N} = 4$ SYM with gauge group $SU(N)$ and 't Hooft coupling λ on the boundary, we show that[5]

$$\left|\frac{\mathrm{d}}{\mathrm{d}t}\log\langle\mathcal{W}(C)\rangle_{\rho(t)}\right| \leq \mathrm{Length}[C]\sqrt{\frac{2\lambda}{3N^2}\langle T_{tt}\rangle}, \qquad d = 4. \tag{9.13}$$

In $d = 3$, we prove a similar result, but for the more restricted set of states which includes global quenches (see (9.131)). For small Wilson loops, we also have stricter bounds, which we give in the main text (see (9.126)).

How are these bounds proven? Let us give the broad picture, restricting to the time-derivative of the entanglement entropy of a strip for concreteness. For CFTs dual to classical Einstein gravity, the von Neumann entropy of the reduced state ρ_R on a subregion R is given by the HRT formula [207–209], which says that

$$S_R = \frac{\mathrm{Area}[X]}{4G_N}, \tag{9.14}$$

where X is the HRT surface, which roughly means a codimension 2 spacelike surface that has stationary area under perturbations of X in the bulk interior. Bounding $\partial_t S_R$ in uniform states now corresponds to bounding $\partial_t \mathrm{Area}[X_t]$, where X_t is a one-parameter family of HRT surfaces living in general time-dependent spacetimes with planar symmetry. Key to our proofs then is carrying out the analysis locally on a planar symmetric spatial slice Σ that contains X_t. We then show that the change in entanglement entropy is given by

$$\frac{\mathrm{d}S_R}{\mathrm{d}t} = \int_X GP, \tag{9.15}$$

where P is the matter momentum density in a direction orthogonal to HRT surface, and G essentially a propagator that only depends on the smallest radius probed by X, and not any other details of the spacetime. We thus see that the flux of matter falling out of the entanglement wedge is directly responsible for the increase of entanglement entropy. The formula (9.15) can be seen as momentum-entanglement correspondence, analogue to the momentum-complexity correspondence proposed in [252] and given a precise form in [253–255]. To further leverage this formula to get our proofs, we study two quasilocal masses and find in certain dimensions the integral in (9.15) is exactly encoded in the difference between these two quasilocal masses at infinity. A detailed analysis of the monotonicity properties of these masses under various flows then lets us prove our final bounds, essentially using a combination of Lorentzian and Riemannian inverse mean

[5]For other potential $d = 4$ holographic CFTs, our result can be written in terms of the effective central charge and effective coupling – see main text.

curvature flows. We emphasize that beyond our assumed symmetries, we do not need to assume a particular form of the spacetimes we are considering, and we are certainly not restricted to quenches.

Along the way we derive various general properties of the HRT surfaces of strips and spheres in planar symmetric spacetimes. For example, for $d = 2$ we prove that the radius r_0 of the tip of the HRT surface of a strip of width ℓ satisfies

$$r_0 \geq \frac{2L^2}{\ell}, \tag{9.16}$$

where L the AdS radius. We prove similar bounds in higher dimensions. We also prove that the tip of an HRT surface of a sphere or a strip can never lie in a trapped region in spacetime. The same is shown for boundary anchored extremal surfaces of dimension $q + 1$ anchored at q-spheres.

This paper is organized as follows. In Sec. 9.2 we set up our assumptions and prove all our entanglement growth bounds for strip subregions R. In Sec. 9.3 we prove the entanglement growth bounds for ball shaped regions R and furthermore derive general properties $(q + 1)$-dimensional extremal surfaces anchored at q-dimensional spheres on the boundary, leading to our results for correlators and Wilson lines. In Sec. 9.4 we prove bounds on spatial derivatives of the entanglement entropy of strips and equal time two-point correlators in $d = 2$. In Sec. 9.6, for a subset of our bounds, we give significant numerical evidence that the dominant energy condition, which was assumed for our proofs, can be replaced by less restrictive assumptions. Finally, in Sec. 9.7, we conclude with a discussion of the implications of our findings, together with future directions. For a reader only wanting to understand the results without getting into the details of the proofs, it is possible to only read sections 9.2.1, 9.3.1, 9.4, 9.6, and 9.7.

Note added in v3: In previous versions of this paper, stronger growth bounds were given for strips in the case when $S - S_{\text{vac}} \leq 0$. However, these bounds were vacuous, since for strips, we now have a proof that $S - S_{\text{vac}} \geq 0$ under our assumptions. Furthermore, the bounds (9.9), and (9.12) were added in v3.

9.2 Maximal Entanglement Rates for Strips

9.2.1 Setup and summary of results

Consider a d-dimensional holographic CFT in Minkowski space dual to classical Einstein gravity. Consider now some general time-evolving state $\rho(t)$ possessing a geometric dual, and having spatially homogeneous and isotropic one-point functions for local operators dual to bulk fields, such as the CFT stress tensor T_{ij}. Homogeneity and isotropy ensures that the dual asymptotically AdS_{d+1} spacetime $(\mathcal{M}, g)$ has planar symmetry. We allow $\rho(t)$ to live on either one or two copies of Minkowski space, so that the dual spacetime

can have either one or two asymptotic boundaries. For a single system, we allow $\rho(t)$ to be mixed.[6]

Our goal in this section is to use the HRT entropy formula in this setup to derive a speed limit on the growth of the entanglement for a strip, and in some cases the union of any number of strips, provided they all live on the same connected component of the conformal boundary. In Sec. 9.3 we will generalize to spherical subregions, and to Wilson lines and two-point correlators. However, we will present the results on entanglement growth for spherical regions in this section, since they naturally are presented together with the results for strips.

Before presenting our results, let us set up our assumptions. We will assume that our spacetimes are AdS-hyperbolic, meaning that we can foliate $(\mathcal{M}, g_{ab})$ with spacelike hypersurfaces Σ_t that all have the same topology and are geodesically complete as Riemannian manifolds. These represent moments of time. Next, letting L be the asymptotic AdS radius, we assume that $(\mathcal{M}, g_{ab})$ satisfies the Einstein equations

$$R_{ab} - \frac{1}{2} g_{ab} R - \frac{d(d-1)}{2L^2} g_{ab} = 8\pi G_N \mathcal{T}_{ab}, \tag{9.17}$$

and that the dominant energy condition (DEC) holds for the bulk stress tensor $\mathcal{T}_{ab}$, meaning that

$$\mathcal{T}_{ab} u^a v^b \geq 0 \qquad \text{for all timelike } u^a, v^b. \tag{9.18}$$

Next, we assume that the Balasubramanian-Kraus [257] boundary stress tensor $\langle T_{ij} \rangle$ is finite. When it is finite, it corresponds to the one-point function of the CFT stress tensor. To specify falloff assumptions more explicitly, let Ω be any defining function, meaning any function on the conformal compactification of $\mathcal{M}$ such that the pullback of $\Omega^2 g_{ab}|_{\partial\mathcal{M}}$ to the conformal boundary is a Lorentzian metric. We then require that the bulk stress tensor satisfies

$$\mathcal{T}_{ab} u^a v^b \sim o\left(\Omega^d\right), \qquad \forall \text{ unit vectors } v^a, u^a, \tag{9.19}$$

near the conformal boundary $\partial\mathcal{M}$. In the radial coordinate r introduced below, this means the stress tensor in an orthonormal basis falls off as $o(r^{-d})$. Matter fields with falloffs sufficiently slow to require modifications of the definition of the spacetime mass are not covered by our results.[7] To avoid having to repeat the same assumptions in every theorem, let us define the following:

Definition 1. *We say that an $AAdS_{d+1}$ spacetime $(\mathcal{M}, g_{ab})$ is regular if it is AdS-hyperbolic, has falloffs (9.19), and g_{ab} is C^2.*

[6] Allowing two-sided spacetimes means that automatically allow mixed states on a single CFT, since we can always find a purification dual to a wormhole, simply by gluing a second CPT-conjugate copy of the spacetime to itself along the HRT surface [256].

[7] In this case, depending on how slow the falloffs are, subleading divergences in the entropy might become state dependent [247], in which case $\mathfrak{R} \leq 1$ cannot remain true. See discussion in Sec. 9.7.

For index conventions, we will take $a, b, \ldots$ to be abstract spacetime indices, and $\alpha, \beta, \ldots$ to be abstract indices on spacelike hypersurfaces Σ. We take $\mu, \nu, \ldots$ to be coordinate indices on Σ. Other indices should be clear in the context. Furthermore, whenever intrinsic tensors on submanifolds are written with spacetime indices, we mean the pushforward/pullback to spacetime using the embedding map.

To describe the boundary regions covered by our results, we select a Minkowski conformal frame on the conformal boundary with coordinates

$$\mathrm{d}s^2|_{\partial\mathcal{M}} = -\mathrm{d}t^2 + L^2(\mathrm{d}\phi^2 + \mathrm{d}\boldsymbol{x}^2), \qquad \phi \in \mathbb{R}, \quad \boldsymbol{x} \in \mathbb{R}^{d-2}, \tag{9.20}$$

where the constant t-slices are the ones on which we have uniform one-point functions for local operators. For $d = 2$ we can allow ϕ to be periodically identified, in which case we say that $\mathcal{M}$ has spherical symmetry. If $\partial\mathcal{M}$ has two connected components, we focus on a particular one. We define $R_{t'}$ to be the one-parameter family of boundary regions given by

$$-\frac{\ell}{2L} \leq \phi \leq \frac{\ell}{2L}, \qquad t = t', \tag{9.21}$$

which just corresponds to a strip or interval of length ℓ at time t'. In this section, when we talk about strips or refer to a one-parameter family, we always mean the family (9.21). We will abbreviate $R_{t=0} \equiv R$, and define

$$\mathrm{Area}[\partial R_t] = \mathrm{Area}[\partial R] = L^{d-2}\int_{\mathbb{R}^{d-2}} \mathrm{d}^{d-2}\boldsymbol{x}, \qquad d > 2, \tag{9.22}$$

while for $d = 2$, we have $\mathrm{Area}[\partial R] = 2$. For $d > 2$ this is of course divergent, but since it always appears as an overall prefactor it causes no difficulties.

Next, the HRT formula [207–209] states that the von Neumann entropy of the reduced CFT state on R_t, $\rho_R(t) \equiv \mathrm{tr}_{R^c}\,\rho(t)$, is given by

$$S_R(t) = -\,\mathrm{tr}\,[\rho_R(t)\ln\rho_R(t)] = \frac{\mathrm{Area}[X_t]}{4G_N}, \tag{9.23}$$

where X_t is the minimal codimension-2 spacelike surface in $(\mathcal{M}, g_{ab})$ that is (1) a stationary point of the area functional (i.e. extremal), (2) anchored at ∂R_t on the conformal boundary ($\partial X_t = \partial R_t$), and (3) homologous to R_t. The latter means that there exists spacelike hypersurface Σ with $\partial\Sigma = X_t \cup R_t$, where we here mean the boundary in the conformal completion. We will use the gravitational description to derive an upper bound on

$$\left|\frac{\mathrm{d}}{\mathrm{d}t}\left(\frac{\mathrm{Area}[X_t]}{4G_N}\right)\right| \tag{9.24}$$

purely in terms of quantities that have a known interpretation in the CFT. While $\mathrm{Area}[X_t]$ is formally divergent, since we (1) work with spacetimes with falloffs (9.19) and (2) $\mathrm{Area}[\partial R_t]$ is time-independent, (9.24) is in fact finite up to the $\mathrm{Area}[\partial R]$ prefactor.

Let us now summarize our main results, which are broadly divided into two categories. The first class of bounds scales like Area$[\partial R]$, and they are strongest when R is large. The second class of bounds scales like Vol$[R]$, and they are consequently the strongest for small subregions. For intermediate sized regions, where the entanglement entropy is about the enter the volume-scaling regime, we expect the two types of upper bounds to be roughly comparable.

First, for a three-dimensional bulk, we obtain the following

Theorem 5. *Let $(\mathcal{M}, g_{ab})$ be a regular asymptotically AdS_3 spacetime with planar or spherical symmetry satisfying the DEC. Assume that X_t is the HRT surface of a finite interval R_t. Then*

$$\left|\frac{\mathrm{d}}{\mathrm{d}t}\left(\frac{\mathrm{Area}[X_t]}{4G_N}\right)\right| \leq \sqrt{\frac{8\pi c}{3}\Big(\langle T_{tt}\rangle - \langle T_{tt}\rangle_{\mathrm{vac}}\Big)}, \tag{9.25}$$

where $c = \frac{3L}{2G_N}$.

Since the HRT surface of a union of strips is just the union of HRT surfaces of a collection of individual strips, this bound immediately implies that if R is a union of n intervals contained in a single moment of time on one of the connected components of $\partial\mathcal{M}$, then

$$\left|\frac{\mathrm{d}}{\mathrm{d}t}S_R\right| \leq n\sqrt{\frac{8\pi c}{3}\Big(\langle T_{tt}\rangle - \langle T_{tt}\rangle_{\mathrm{vac}}\Big)}. \tag{9.26}$$

While we are not able to give a general proof of the analogue of Theorem 5 in higher dimensions, we prove a generalization in thin-shell spacetimes:

Theorem 6. *Let $(\mathcal{M}, g)$ be an asymptotically $AdS_{d+1\geq 3}$ spacetime with planar symmetry satisfying the DEC. Assume that X_t is the HRT surface of a region R_t corresponding to either a finite width strip or a ball. Assume that the bulk matter consists of $U(1)$ gauge fields and a thin shell of matter:*

$$\mathcal{T}_{ab} = \mathcal{T}^{\mathrm{shell}}_{ab} + \mathcal{T}^{\mathrm{Maxwell}}_{ab}, \tag{9.27}$$

where $\mathcal{T}^{\mathrm{shell}}_{ab}$ has delta function support on a codimension-1 worldvolume that is timelike or null, and with $\mathcal{T}^{\mathrm{shell}}_{ab}$ separately satisfying the DEC. Assume $(\mathcal{M}, g_{ab})$ is regular, except we do not require g to be C^2 at the shell. Then

$$\left|\frac{\mathrm{d}}{\mathrm{d}t}\left(\frac{\mathrm{Area}[X_t]}{4G_N}\right)\right| \leq \frac{1}{4}\mathrm{Area}[\partial R]c_{\mathrm{eff}}\left[\frac{16\pi}{(d-1)c_{\mathrm{eff}}}\langle T_{tt}\rangle\right]^{\frac{d-1}{d}}, \tag{9.28}$$

where $c_{\mathrm{eff}} = L^{d-1}/G_N$.

This theorem applies to thin-shell Vaidya spacetimes and charged generalizations. These spacetimes (and related setups) have been studied extensively [238–241, 246, 248, 258–298] as holographic models CFT quenches. However, more general cases than Vaidya are

allowed, where the shell might correspond to some brane in the bulk, propagating in a timelike direction. Using the duality between radius and scale in the CFT, thin shell spacetimes correspond to CFT states where all dynamics is happening at a single scale (that evolves with time). We also should note that (9.28) holds if R is a union of any number of strips on the same conformal boundary, due to the fact that the HRT surface of n strips is just equal to n HRT surfaces of n (generally different) strips. One can hope that this might also be true for multiple spheres, but this does not follow from our current analysis. Also, while we do not have a proof, we conjecture that (9.28) is valid in all DEC respecting regular planar symmetric AAdS_{d+1} spacetimes, and we provide strong numerical evidence for this in Sec. 9.6.

Also, note that c_{eff} can be defined purely in CFT in terms of a universal prefactor of the sphere vacuum entanglement entropy [207, 208], or in terms of the renormalized entanglement entropy [299, 300]. So our final bounds on $|\partial_t S|$ make no reference to the bulk.

The previous two results give upper bounds scaling like $\mathrm{Area}[\partial R]$. Now let us turn to bounds scaling like $\mathrm{Vol}[R]$. We prove the following bound on small regions, valid for all $d \geq 2$:

Theorem 7. *Let $(\mathcal{M}, g_{ab})$ be a regular asymptotically $AdS_{d+1\geq 3}$ spacetime with planar symmetry satisfying the DEC. Assume that X_t is the HRT surface of a region R_t corresponding to either a strip or a ball. Let ℓ be either the strip width or ball radius, and assume that*

$$\frac{\ell^d \langle T_{tt}\rangle}{c_{\mathrm{eff}}} \ll 1. \tag{9.29}$$

Then

$$\left|\frac{\mathrm{d}}{\mathrm{d}t}\left(\frac{\mathrm{Area}[X_t]}{4G_N}\right)\right| \leq \kappa_d \mathrm{Vol}[R]\,\langle T_{tt}\rangle \left[1+\mathcal{O}\left(\frac{\langle T_{tt}\rangle\,\ell^d}{c_{\mathrm{eff}}}\right)\right]. \tag{9.30}$$

where

$$\kappa_d = \frac{\Gamma\left(\frac{1}{2(d-1)}\right)}{\Gamma\left(\frac{d}{2(d-1)}\right)} \begin{cases} 2\pi & R \text{ is an interval and } d=2, \\ \frac{\sqrt{\pi}}{d-1} & R \text{ is a strip and } d>2, \\ 2\sqrt{\pi} & R \text{ is a ball and } d>2. \end{cases} \tag{9.31}$$

Next, for thin shell spacetimes, volume-type bounds can be proven exactly for subregions of any size, at the cost of a slightly larger prefactor:

Theorem 8. *Consider the same setup as in Theorem 6. Then*

$$\left|\frac{\mathrm{d}}{\mathrm{d}t}\left(\frac{\mathrm{Area}[X_t]}{4G_N}\right)\right| \leq \kappa'_d \mathrm{Vol}[R]\,\langle T_{tt}\rangle\,, \tag{9.32}$$

with

$$\kappa'_d = d^{-\frac{d}{2(d-1)}} \frac{\Gamma\left(\frac{1}{2(d-1)}\right)}{\Gamma\left(\frac{d}{2(d-1)}\right)} \begin{cases} 2\pi & R \text{ is an interval and } d=2, \\ \sqrt{\frac{4\pi}{(d-1)}} & R \text{ is a strip and } d>2, \\ \sqrt{16\pi(d-1)} & R \text{ is a ball and } d>2. \end{cases} \tag{9.33}$$

We will now outline the strategy used to obtain these bounds. First, we observe that there exists exactly one homology hypersurface Σ_t that both contains X_t, and which respects the planar symmetry of $(\mathcal{M}, g_{ab})$. Then we show that the location of X_t on Σ_t can be solved for exactly in terms of the intrinsic geometry on Σ_t. Together with the DEC, this fact allows us to lower bound the radius of the tip of the HRT surface. Next, we use the fact that since X_t is extremal, the first order variation of its area is a pure boundary term located at ∂X_t [301], and we show that this boundary term is simply given by a particular component of the extrinsic curvature of Σ_t as $r \to \infty$. Then we work out the form of Einstein constraint equations on Σ_t, and show that the relevant extrinsic curvature component can be written as an integral of the matter flux over the HRT surface. Finally, essentially relying on inverse mean curvature flow of Lorentzian and Riemannian Hawking masses, and their monotonicity properties under these flows, we bound the integrated matter flux across the HRT surface from above in terms of the mass of the spacetime.

Now, before we dive in, we should clarify the meaning of radii in planar symmetric spacetimes. Since we have planar symmetry, spacetime has a two-parameter foliation where each leaf is a codimension-2 spacelike plane that has the usual flat intrinsic metric. When we talk about a plane, we always mean one of these leafs. These planes can all be assigned an "area radius" r, and it is possible to view r as a scalar function on spacetime which is not tied to any coordinate. Nevertheless, unlike in spherical symmetry, there is an overall scaling ambiguity in this function, since the non-compactness of the planes means we cannot normalize r to some area – there is no "unit plane". However, if we choose some Minkowski conformal frame on the boundary, we can fix the overall normalization of r by demanding that the defining function Ω that takes us to the chosen conformal frame is $\Omega = r/L$. We will implicitly assume such a choice, and refer to *the* radius of a plane.

9.2.2 An explicit solution for the HRT surface location

Without loss of generality, we will bound the time-derivative at $t = 0$ and use the shorthands $X_{t=0} = X$ and $R_{t=0} = R$. Since R is a strip contained in a canonical time slice of Minkowski, and since the ambient spacetime has planar symmetry, there exists a homology hypersurface $\hat{\Sigma}$ of X respecting the planar symmetry – see Figure 9.1. We can pick coordinates on $\hat{\Sigma}$ so that its induced metric $H_{\alpha\beta}$ reads

$$H_{\mu\nu}\mathrm{d}y^\mu \mathrm{d}y^\nu = B(r)\mathrm{d}r^2 + r^2(\mathrm{d}\phi^2 + \mathrm{d}\boldsymbol{x}^2), \quad r \in [r_0, \infty), \quad \phi \in [-\Phi(r), \Phi(r)], \tag{9.34}$$

where $\phi = \Phi(r)$ is the coordinate embedding function of (half of) the HRT surface in $\hat{\Sigma}$, as illustrated in Figure 9.1. r_0 is the smallest value of r probed by the HRT surface, corresponding to its tip. $\hat{\Sigma}$ can naturally be extended to include all $\phi \in \mathbb{R}$ by planar symmetry, and this choice turns out to be convenient for us. We denote the corresponding

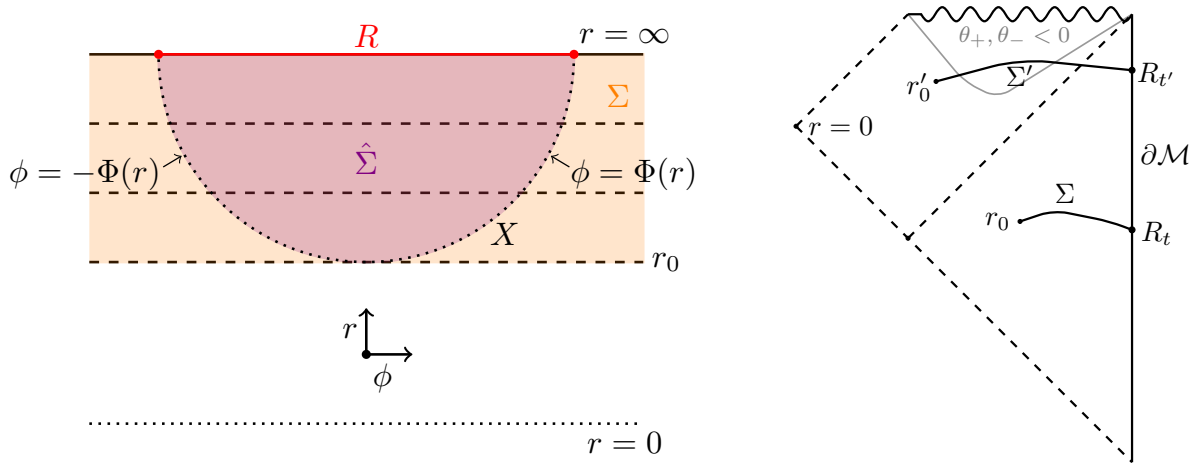

Figure 9.1: Left: the planar symmetric homology hypersurface $\hat{\Sigma}$ with respect to the HRT surface X. Σ is the extended homology hypersurface, whose boundary is the plane at $r = r_0$. Dashed lines are planes – i.e. constant r surfaces. Right: example conformal diagram indicating possible embeddings of two extended homology hypersurfaces Σ and Σ'. The grey line is an apparent horizon, with vanishing outwards null expansion, $\theta_+ = 0$.

hypersurface as Σ, and refer to it as the extended homology hypersurface.[8] See Figure 9.1. The boundary of Σ (in the bulk proper) is a plane of radius r_0.

Relying on the formulas derived in the remainder of this section, we prove the following Lemma in appendix A.3.5:

Lemma 1. *Let Σ be the extended homology hypersurface of an HRT surface X anchored at a strip region given by (9.21). Then a single coordinate system of the form*

$$\mathrm{d}s^2 = B(r)\mathrm{d}r^2 + r^2\mathrm{d}\boldsymbol{x}^2 \tag{9.35}$$

is enough to cover all of Σ. Furthermore, X has only one turning point, meaning that embedding function $r(\phi)$ is monotonically increasing for $\phi \geq 0$.

This means one function $\Phi(r)$ contains all the information about the embedding of X in Σ – we do not need multiple branches. It also means that Σ cannot have any locally stationary planes – that is – no planes of vanishing mean curvature, where $B(r)$ would blow up. The means we never need to worry about patching across coordinate systems when working on Σ. Geometrically, it implies that Σ has no "throats".

Now, taking $(r, \boldsymbol{x})$ to be coordinates on X, the induced metric on X reads

$$\mathrm{d}s^2|_X = \left[B(r) + r^2\Phi'(r)^2\right]\mathrm{d}r^2 + r^2\mathrm{d}\boldsymbol{x}^2. \tag{9.36}$$

[8] $\hat{\Sigma}$ and Σ are unique. Planar symmetry means that $(\mathcal{M}, g_{ab})$ can be foliated by planes, and every point $p \in X$ lies in some plane in this foliation. Demanding planar symmetry of Σ requires that the full leaf intersected by p is included in Σ, and so we have a one-parameter family of codimension-2 surfaces picked out by X, which thus fully specifies Σ, and similarly for $\hat{\Sigma}$.

Since X is an extremal surface, its area is stationary under all variations, including under variations within Σ. Enforcing this gives an ODE for $\Phi(r)$ in terms of $B(r)$. To find it, we compute the mean curvature $\mathcal{K}$ of X viwed as a submanifold of Σ and demand it to be zero. This gives the equation (see appendix A.3.1 for a computation)

$$rB\Phi'' + (d-1)r^2\left(\Phi'\right)^3 + \Phi'\left(dB - \frac{r}{2}B'\right) = 0. \tag{9.37}$$

The relevant boundary conditions are

$$\Phi'(r_0) = \infty, \quad \Phi(r_0) = 0, \tag{9.38}$$

where the former says that r_0 is the radius of the plane tangent to the tip of the HRT surface (i.e. where $\frac{\mathrm{d}r}{\mathrm{d}\phi} = 0$), while the latter implements that $\phi = 0$ corresponds to the center of the strip. It turns out that equation (9.37) can be integrated, and the solution with the correct boundary condition is

$$\Phi(r) = \int_{r_0}^{r} \mathrm{d}\rho \frac{\sqrt{B(\rho)}}{\rho\sqrt{(\rho/r_0)^{2d-2}-1}}. \tag{9.39}$$

This gives the location of the HRT surface within Σ explicitly in terms of the geometry of Σ. We now use this solution to determine the Einstein constraint equations on Σ, and to derive a formula for the rate of change of the entanglement growth.

9.2.3 A momentum-entanglement correspondence

Since X_t is extremal, its first order variation reduces to a pure boundary term given by (see for example the appendix of [301, 302]):

$$\left.\frac{\mathrm{dArea}[X_t]}{\mathrm{d}t}\right|_{t=0} = \int_{\partial X} N^a \eta_a, \tag{9.40}$$

where η^a is the translation vector generating the flow of ∂X_t at conformal infinity at $t = 0$, while N^a is the normal to ∂X that is also tangent to X, and that points towards the conformal boundary. In writing this formula, we implicitly assume that it is evaluated with some near-boundary cutoff that is subsequently removed. As is well known, given some choice of boundary conformal frame, a canonical choice of cutoff exists [303–305], which in our case reduces to a cutoff in the radial coordinate r. With a cutoff adapted to the Minkowski conformal frame and the falloffs (9.19), (9.40) is finite, even though $\mathrm{Area}[X_t]$ diverges.

Now we write (9.40) in a more useful form. We will give all the main steps, but relegate tedious but straight forward computations to the appendix.

Using the planar symmetry of Σ, the extrinsic curvature $K_{\alpha\beta}$ of Σ is given by

$$K_{\mu\nu}\mathrm{d}y^\mu \mathrm{d}y^\nu = K_{rr}(r)\mathrm{d}r^2 + K_{\phi\phi}(r)\left[\mathrm{d}\phi^2 + \mathrm{d}\boldsymbol{x}^2\right], \tag{9.41}$$

where we take the extrinsic curvature to be defined with respect to the future directed normal. Using this, we show in appendix (A.3.3), retracing the steps of [306], that

$$\left.\frac{\mathrm{dArea}[X_t]}{\mathrm{d}t}\right|_{t=0} = -\frac{\mathrm{Area}[\partial R]}{L^{d-2}} \lim_{r\to\infty} r^{d-3} K_{\phi\phi}. \tag{9.42}$$

Physically, $\lim_{r\to\infty} r^{d-3} K_{\phi\phi}$ measures the boost angle at which X hits the conformal boundary, or rather, the subleading part of the angle, since extremality implies that X hits $\partial\mathcal{M}$ orthogonally. This can be seen by studying extremal surfaces in a near-boundary expansion. Thus, we see that the entanglement growth is, up to a factor, identically given by the (subleading) boost angle at which the HRT surface hits the boundary. The same was found for maximal volume slices in [306].

Next we want to find a more explicit expression for $\lim_{r\to\infty} r^{d-3} K_{\phi\phi}$. To do this, we need to use the Einstein constraint equations, which read

$$\begin{aligned} \mathcal{R} + K^2 - K^{\alpha\beta} K_{\alpha\beta} + \frac{d(d-1)}{L^2} &= 16\pi G_N \mathcal{T}_{ab} t^a t^b, \\ D_\alpha K^\alpha{}_\beta - D_\beta K &= 8\pi G_N \mathcal{T}_{ab} t^a e^b_\beta, \end{aligned} \tag{9.43}$$

where $\mathcal{R}$ is the Ricci scalar of the metric on Σ, t^a the future unit normal to Σ, $K = H^{\alpha\beta} K_{\alpha\beta}$, and e^a_α a set of tangent vectors to Σ. To write these equations in coordinate form, it is convenient to introduce the function $\omega(r)$ as

$$B(r) = \frac{1}{\frac{r^2}{L^2} - \frac{\omega(r)}{r^{d-2}}}. \tag{9.44}$$

We will call $\omega(r)$ the Riemannian Hawking mass.[9] It will play a central role in our work. Whether or not $\omega(\infty)$ is proportional to the spacetime mass for some general spacelike hypersurface Σ depends on the behavior of the extrinsic curvature Σ at large r. It turns out that for $d \geq 3$, and with Σ being the extended homology hypersurface of an HRT surface, it has the property that it is proportional to the CFT energy density:

$$\langle T_{tt} \rangle = \frac{d-1}{16\pi G_N L^{d-1}} \omega(\infty), \qquad d \geq 3. \tag{9.45}$$

For $d = 2$, the right hand side is a lower bound on $\langle T_{tt} \rangle - \langle T_{tt} \rangle_{\mathrm{vac}}$, where the vacuum energy must be subtracted when we allow ϕ to be periodic. We will explain these facts in Sec. 9.2.5.

It is also convenient to redefine $K_{rr}(r)$ in terms of a function $F(r)$ which is the rr-component of the extrinsic curvature in an orthonormal basis

$$K_{rr}(r) \equiv B(r) F(r). \tag{9.46}$$

[9] For $d = 3$ it is also known as the Geroch-Hawking mass [307–310], and its was used to prove the Riemannian Penrose inequality [310].

In terms of these functions, the constraint equations in coordinate form read

$$(d-1)\frac{\omega'(r)}{r^{d-1}} = 2\mathcal{E}(r) - \frac{(d^2-3d+2)}{r^4}K_{\phi\phi}(r)^2 - \frac{2(d-1)}{r^2}F(r)K_{\phi\phi}(r), \tag{9.47}$$

$$K'_{\phi\phi}(r) - \frac{K_{\phi\phi}(r)}{r} = rF(r) - \frac{r^2}{d-1}\mathcal{J}(r), \tag{9.48}$$

where we introduced the notation

$$\begin{aligned}\mathcal{E} &= 8\pi G_N \mathcal{T}_{ab}t^a t^b,\\ \mathcal{J} &= 8\pi G_N \mathcal{T}_{ab}(\partial_r)^a t^b.\end{aligned} \tag{9.49}$$

These are (proportional to) the energy density and radial momentum density of the matter with respect to the frame t^a. $\mathcal{J} > 0$ corresponds to matter falling into the bulk towards smaller r. From (9.19) and the fact that $B(r) \sim \mathcal{O}(r^{-1})$, we find that

$$\mathcal{E} \sim o\left(1/r^d\right), \qquad \mathcal{J} \sim o\left(1/r^{d+1}\right), \tag{9.50}$$

where we use that $\frac{1}{\sqrt{B}}(\partial_r)^a$ is a unit vector.

To turn (9.47) and (9.48) into a closed system, we will eliminate $F(r)$. We do this by imposing extremality of X in the direction of t^a. To do this, note that the inwards (outwards) null expansion θ_+ (θ_-) of X can be written as (see for example the appendix of [306])

$$\sqrt{2}\theta_\pm[X] = \pm\mathcal{K}[X] + K - n^\alpha n^\beta K_{\alpha\beta}, \tag{9.51}$$

where n^α is the outwards normal to X within Σ,[10] and where we remind that $\mathcal{K}[X]$ is the mean curvature of X within Σ. Extremality means $\theta_+ = \theta_- = 0$, which implies that $\mathcal{K} = 0$ and

$$K|_X = n^\alpha n^\beta K_{\alpha\beta}|_X. \tag{9.52}$$

This equation holds at $\phi = \Phi(r)$, which by planar symmetry means it holds everywhere on Σ. Writing out this equation in coordinates, carried out in appendix A.3.2, we find

$$F + \frac{(d-2)K_{\phi\phi}}{r^2} + (d-1)K_{\phi\phi}\frac{(\Phi')^2}{B} = 0. \tag{9.53}$$

Plugging in the solution for $\Phi(r)$, given in (9.39), we get that

$$F(r) = -\frac{K_{\phi\phi}(r)}{r^2}\left(\frac{(d-2)r^{2d-2} + r_0^{2d-2}}{r^{2d-2} - r_0^{2d-2}}\right), \tag{9.54}$$

which upon insertion into the constraints, gives a closed system of ODEs

$$\frac{\omega'(r)}{r^{d-1}} = \frac{2}{d-1}\mathcal{E}(r) + \frac{K_{\phi\phi}^2}{r^4}h_1(r), \tag{9.55}$$

$$K'_{\phi\phi}(r) + \frac{K_{\phi\phi}}{r}h_2(r) = -\frac{r^2}{d-1}\mathcal{J}(r), \tag{9.56}$$

[10] We have here taken the outwards and inwards null vectors, k_+^a and k_-^a, respectively, to be $k_\pm^a = 2^{-1/2}(t^a \pm n^a)$.

where

$$h_1(r) = \frac{(d-2)\,(r/r_0)^{2d-2} + d}{(r/r_0)^{2d-2} - 1}, \qquad h_2(r) = \frac{(d-3)\,(r/r_0)^{2d-2} + 2}{(r/r_0)^{2d-2} - 1}. \tag{9.57}$$

Now, $F(r)$ is a component of the extrinsic curvature in an orthonormal basis, so it must be finite at r_0. Using this to fix an integration constant, we find that the solutions of (9.55) and (9.56) are

$$K_{\phi\phi}(r) = -\frac{r^2}{(d-1)\sqrt{(r/r_0)^{2d-2}-1}} \int_{r_0}^{r} \mathrm{d}\rho \mathcal{J}(\rho) \sqrt{(\rho/r_0)^{2d-2}-1}, \tag{9.58}$$

$$\omega(r) = \omega(r_0) + \int_{r_0}^{r} \mathrm{d}\rho \left[\rho^{d-5} h_1(\rho) K_{\phi\phi}(\rho)^2 + \frac{2\rho^{d-1}}{d-1} \mathcal{E}(\rho) \right], \tag{9.59}$$

where $K_{\phi\phi}(r_0) = 0$ since $\mathcal{J}(\rho)$ must be bounded.[11] Inserting (9.58) into (9.42) and multiplying by $(4G_N)^{-1}$, we get that

$$\left.\frac{\mathrm{d}S_R}{\mathrm{d}t}\right|_{t=0} = \frac{\mathrm{Area}[\partial R]}{4G_N L^{d-2}(d-1)} \int_{r_0}^{\infty} \mathrm{d}r \mathcal{J}(r) \sqrt{r^{2d-2} - r_0^{2d-2}}. \tag{9.60}$$

Since $\mathcal{J} > 0$ corresponds to a flux of energy density towards decreasing r, we see that matter falling out of the entanglement wedge and deeper into the bulk is directly responsible for the increase of entanglement. Conversely, outgoing matter is responsible for decrease in entanglement. We can also rewrite this formula in a covariant way. In appendix A.3.3 we show that

$$\left.\frac{\mathrm{d}S_R}{\mathrm{d}t}\right|_{t=0} = \int_X G \mathcal{T}_{ab} n^a t^a \tag{9.61}$$

where n^a is the outwards unit normal to X that is tangent to Σ, and

$$G(r) = \frac{2\pi r^d}{(d-1) r_0^{d-1}}. \tag{9.62}$$

The formulas (9.42), (9.58)–(9.62) are the main results of this section. These results together with the theorems proven in the following section are crucial pieces to our proven bounds.

9.2.4 Geometric constraints on the HRT surface

In this section, we prove the following

[11] For thin-shell spacetimes $\mathcal{J}(\rho)$ can be a delta function, but we can safely assume this delta function does not have support exactly at $r = r_0$.

Theorem 9. *Let $(\mathcal{M}, g_{ab})$ be a regular asymptotically $AdS_{d+1\geq 3}$ spacetime with planar symmetry satisfying the DEC. Let X be the HRT surface of a strip R of width ℓ, and let be r_0 be the smallest radius probed by X. Then*

$$\frac{L^2}{r_0} \leq \frac{\Gamma\left(\frac{1}{2(d-1)}\right)}{2\sqrt{\pi}\Gamma\left(\frac{d}{2(d-1)}\right)}\ell. \tag{9.63}$$

Furthermore, if $r_{0,\text{vac}}$ is the smallest radius probed by the HRT surface X_0 of a strip of width ℓ in pure AdS_{d+1}, then

$$r_0 \geq r_{0,\text{vac}}. \tag{9.64}$$

We now give the proof assuming that $\omega(r_0) \geq 0$, and then we will spend most of the rest of this section proving this assertion.

Proof. By Lemma 3, proven below, we have that $\omega(r_0) \geq 0$. Furthermore, the DEC implies that $\mathcal{E}$ is positive. Hence, (9.59) gives that $\omega(r)$ is everywhere positive. But this means that

$$B(r) = \frac{1}{\frac{r^2}{L^2} - \frac{\omega(r)}{r^{d-2}}} \geq \frac{L^2}{r^2}, \tag{9.65}$$

which allows us to lower bound the strip width as follows:

$$\begin{aligned}
\ell = 2L\Phi(\infty) &= 2L\int_{r_0}^{\infty} \mathrm{d}\rho \frac{\sqrt{B(\rho)}}{\rho\sqrt{(\rho/r_0)^{2d-2}-1}} \\
&\geq 2L^2 \int_{r_0}^{\infty} \mathrm{d}\rho \frac{1}{\rho^2\sqrt{(\rho/r_0)^{2d-2}-1}} \\
&= \frac{2L^2}{r_0}\frac{\sqrt{\pi}\Gamma\left(\frac{d}{2(d-1)}\right)}{\Gamma\left(\frac{1}{2(d-1)}\right)}.
\end{aligned} \tag{9.66}$$

Finally, if we are in pure AdS, we must have have that the spacetime mass is vanishing, implying that $\omega(\infty) = 0$, and so by $\omega'(r) \geq 0$ and the fact that $\omega(r_0) \geq 0$, we must have $\omega(r) = 0$ everywhere. But that means that the above inequalities become equalities, giving $\frac{L^2}{r_0} \geq \frac{L^2}{r_{0,\text{vac}}}$, which implies (9.64). □

Now we turn to proving that $\omega(r_0)$ is non-negative. The crucial tool is a planar-symmetric AdS_{d+1} version of the Lorentzian Hawking mass [311], which we define for a planar surface σ as

$$\mu[\sigma] = \frac{r^d}{L^2} - \frac{2r^d\theta_+\theta_-}{k_+\cdot k_-(d-1)^2}, \tag{9.67}$$

where k^+ and k^- are the outwards and inwards null vectors orthogonal to σ, respectively, and $\theta_\pm$ the corresponding null expansions. In [312], generalizing the results of [313] to planar symmetry and AAdS_{d+1} spacetimes, it was shown that the DEC implies that $\mu[\sigma]$ is monotonically non-decreasing when σ is moving in an outwards spacelike direction,

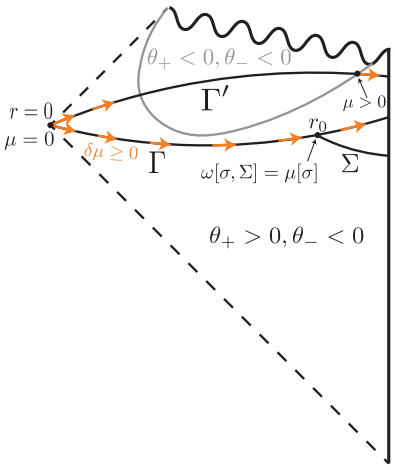

Figure 9.2: Example of two complete hypersurfaces Γ and Γ'. The Lorentzian Hawking mass is vanishing at $r = 0$ and positive at marginally trapped surfaces, given by the planes contained in the gray line. μ is monotonically non-decreasing along spacelike outwards flows in the untrapped region, where $\theta_+ \geq 0, \theta_- \leq 0$. At the boundary σ of the extended homology hypersurface Σ, the Riemannian Hawking mass ω with respect to Σ agrees with the Lorentzian Hawking mass μ.

provided we are in a normal region of spacetime, meaning that $\theta_+ \geq 0, \theta_- \leq 0$ when we take k_+^a and k_-^a to be future directed.[12]

Furthermore, it is useful to rewrite the Riemannian Hawking mass $\omega(r)$ in a different way. ω can be thought of as a function of a planar surface σ together with a hypersurface Σ containing it, and in [306] it is shown that we can write ω as

$$\omega[\sigma, \Sigma] = \frac{r^d}{L^2} - \frac{\mathcal{K}[\sigma]^2}{(d-1)^2}, \tag{9.68}$$

where $\mathcal{K}$ is the mean curvature of σ in Σ. Using (9.51), which assumes the normalization $k_+ \cdot k_- = -1$, we see that $2\theta_+\theta_- = (K - n^\alpha n^\beta K_{\alpha\beta})^2 - \mathcal{K}^2$, and so we get the following relation between the Hawking masses

$$\mu[\sigma] = \omega[\sigma, \Sigma] + \frac{r^d}{(d-1)^2}(K - n^\alpha n^\beta K_{\alpha\beta})^2. \tag{9.69}$$

With this in hand, we prove the following Lemma.

Lemma 2. *Let Γ be a complete planar symmetric hypersurface with one conformal boundary. Let σ_r be a one-parameter family of planes in Γ with radius r, and with $r \in (0, \epsilon]$ for any $\epsilon > 0$. Then*

$$\lim_{r \to 0} \mu[\sigma_r] \geq 0. \tag{9.70}$$

[12] This monotonicity is a planar-symmetric Lorentzian version of the monotonicity the Riemannian Hawking mass under inverse mean curvature flow, which has been used to prove Riemannian Penrose inequalities [307–310]. A Lorentzian flow with a monotonic Lorentzian Hawking mass for compact surfaces in three dimensions, without any symmetry assumptions, was studied in [314].

Proof. Let us pick coordinates

$$\mathrm{d}s^2|_\Gamma = \left[\frac{r^2}{L^2} - \frac{\omega(r)}{r^{d-2}}\right]^{-1} \mathrm{d}r^2 + r^2 \mathrm{d}\boldsymbol{x}^2 \tag{9.71}$$

on Γ in a neighborhood of $r = 0$. Since Γ is complete and we only have one conformal boundary, arbitrarily small r must be part of Γ. Since Γ is spacelike, we must have $\omega(r) \leq r^d/L^2$, which means that $\omega(r) \sim \mathcal{O}(r^d)$ at small r. Now, from (9.69) we see that $\mu[\sigma_r] \geq \omega[\sigma_r, \Gamma]$ and so

$$\mu[\sigma_r] \geq \mathcal{O}(r^d). \tag{9.72}$$

Taking $r \to 0$ proves our assertion. □

Now we are ready to prove that $\omega(r_0) \geq 0$, together with the fact that the tip of the HRT surface cannot lie in a trapped region.

Lemma 3. *Let $(\mathcal{M}, g_{ab})$ be a planar-symmetric regular asymptotically AdS_{d+1} spacetime. Let X be the HRT surface of a strip. Then the tip of X lies in an untrapped region of spacetime, meaning the future null expansions of the plane σ tangent to X at the tip satisfies*

$$\theta_+[\sigma] \geq 0, \quad \theta_-[\sigma] \leq 0. \tag{9.73}$$

Furthermore, if the DEC holds and $(\mathcal{M}, g)$ is regular, the Riemannian Hawking mass of σ is non-negative:

$$\omega[\sigma, \Sigma] = \omega(r_0) \geq 0. \tag{9.74}$$

Proof. Let Σ be the unique planar symmetric extended homology hypersurface containing X. Let σ be the boundary of Σ in the bulk, having radius r_0. Its null expansion is

$$\sqrt{2}\theta_\pm[\sigma] = \pm\mathcal{K}[\sigma] + K - r^\alpha r^\beta K_{\alpha\beta}, \tag{9.75}$$

where $r^\alpha = \frac{1}{\sqrt{B}}(\partial_r)^\alpha$. An explicit computation gives

$$\begin{aligned} \mathcal{K}[\sigma] &= \frac{d-1}{r_0\sqrt{B(r_0)}}, \\ K &= \frac{1}{B}K_{rr} + \frac{K_{\phi\phi}(d-1)}{r^2}, \end{aligned} \tag{9.76}$$

and so we find

$$\sqrt{2}\theta_\pm[\sigma] = \pm\frac{d-1}{r_0\sqrt{B(r_0)}} - \frac{K_{\phi\phi}(r_0)(d-1)}{r_0^2}. \tag{9.77}$$

From (9.58) we have that $K_{\phi\phi}(r_0) = 0$, and so we get that

$$\pm\theta_\pm \geq 0, \tag{9.78}$$

proving the first assertion.

Next, since $K_{\phi\phi}(r_0) = 0$ we see that $2\theta_+\theta_-|_\sigma = -\mathcal{K}^2|_\sigma$, implying that $\mu[\sigma] = \omega[\sigma, \Sigma]$. Now, since our spacetime is AdS-hyperbolic, we can embed σ in a complete hypersurface with planar symmetry Γ, see Figure 9.2. Since σ lies in an untrapped region of spacetime, and since Γ is spacelike, $\mu[\sigma]$ is monotonically non-increasing as we deform σ in inwards along Γ while preserving its planar symmetry. Since the g_{ab} is C^2, $\theta_\pm$ are continuous, and so as we deform σ inwards, one of two things happen. Either we hit a marginally trapped surface, where $\theta_+\theta_- = 0$ and where μ is manifestly positive, or we approach $r = 0$, where we again have that μ is non-negative by Lemma 2. See Figure 9.2. But since μ is non-increasing along this deformation, and since it ends up somewhere non-negative, we must have $\mu[\sigma] \geq 0$. But $\mu[\sigma] = \omega[\sigma, \Sigma]$, completing the proof. □

We have illustrated the fact that the tip cannot lie in a trapped region of spacetime in Figure 9.1 – the tip cannot lie behind the gray line. Note that the proof of this fact does not rely on the DEC. This result improves on the findings of [315] in the special case where we have planar symmetry. In [315], they showed without any symmetry assumptions that the tip of an HRT surface in a $(2+1)$–dimensional spacetime can never lie in the so-called umbral region, which is a special subset of the trapped region that lies behind regular holographic screens [315, 316]. They also showed this result with planar symmetry in all dimensions. Here we extend this result to show that the whole trapped region is forbidden, although our result is more limited in that it always requires planar symmetry and a strip (or spherical) boundary region. Note also that this result does not forbid X to probe inside trapped regions – it is only the tip that is forbidden to lie there (see Figure 9.1). For example, for early times after a quench, the HRT surface will have portions threading through the trapped region [240, 241].

9.2.5 Proofs

Proof of $d = 2$ bound

We are now ready to prove Theorem 5. Evaluating the Lorentzian Hawking mass on a sphere at large r in a planar symmetric AAdS_{d+1} spacetime with falloffs (9.19), we get that

$$\langle T_{tt} \rangle = \frac{d-1}{16\pi G_N L^{d-1}} \mu(\infty). \tag{9.79}$$

This is valid also for $d = 2$, except if ϕ is periodically identified, we must replace the left hand side with $\langle T_{tt} \rangle - \langle T_{tt} \rangle_{\text{vac}}$. It can be seen to be true by evaluating $\mu(\infty)$ near the boundary in the usual Fefferman-Graham expansion [303–305]. Now, from (9.69) and (9.76) we have that

$$\mu(r) = \omega(r) + r^{d-4} K_{\phi\phi}(r)^2. \tag{9.80}$$

From (9.58), we see that $K_{\phi\phi}$ has asymptotic falloff $K_{\phi\phi} \sim \mathcal{O}(r^{3-d})$. Thus, we get that for $d \geq 3$, $\mu(\infty) = \omega(\infty)$, while for $d = 2$, we have

$$\mu(\infty) = \omega(\infty) + \left(\lim_{r\to\infty} r^{-1} K_{\phi\phi}\right)^2 . \tag{9.81}$$

Since $\omega(\infty) \geq 0$ by the DEC, when $d = 2$ we obtain

$$\left|\lim_{r\to\infty} r^{-1} K_{\phi\phi}\right| \leq \sqrt{\mu(\infty)} = \sqrt{16\pi G_N L \langle T_{tt}\rangle}. \tag{9.82}$$

Using that $\text{Area}[\partial R_t] = 2$, and combining (9.82) and (9.42) then yields

$$\left|\frac{\mathrm{d}S_R}{\mathrm{d}t}\right|_{t=0} \leq \frac{1}{2G_N}\sqrt{16\pi G_N L \langle T_{tt}\rangle} = \sqrt{\frac{8\pi c}{3}\langle T_{tt}\rangle}, \tag{9.83}$$

where we used the known Brown-Henneaux expression for the central charge: $c = \frac{3L}{2G_N}$ [317]. This proves Theorem 5.

Proof of bound for small ℓ

Now let us consider the result for small subregions, given by Theorem 7. The following Lemma is what we need:

Lemma 4. *Let $(\mathcal{M}, g_{ab})$ be a regular asymptotically $AdS_{d+1\geq 3}$ spacetime with planar symmetry satisfying the DEC. Let X be the HRT surface of a strip R of width ℓ, and let be r_0 be the smallest radius probed by X. Assume that*

$$\frac{\ell^d \langle T_{tt}\rangle}{c_{\text{eff}}} \ll 1. \tag{9.84}$$

Then

$$\left|\lim_{r\to\infty} r^{d-3} K_{\phi\phi}\right| \leq \frac{L}{2r_0}\omega(\infty)\left[1 + \mathcal{O}\left(\frac{\ell^d \langle T_{tt}\rangle}{c_{\text{eff}}}\right)\right]. \tag{9.85}$$

Proof. Let us for convenience define $W = -\lim_{r\to\infty} r^{d-3} K_{\phi\phi}$, and assume without loss of generality that $W > 0$ (otherwise, just reverse the time direction). Using the solutions (9.58) and (9.59), we have that

$$\begin{aligned}\frac{W}{\omega(\infty)} &= \frac{1}{d-1}\frac{\int_{r_0}^\infty \mathrm{d}r \mathcal{J}(r)\sqrt{r^{2d-2} - r_0^{2d-2}}}{\omega(r_0) + \int_{r_0}^\infty \mathrm{d}r\left[r^{d-5}h_1(r)K_{\phi\phi}(r)^2 + \frac{2r^{d-1}}{d-1}\mathcal{E}(r)\right]} \\ &\leq \frac{\int_{r_0}^\infty \mathrm{d}r r^{d-1}\mathcal{J}(r)}{2\int_{r_0}^\infty \mathrm{d}r r^{d-1}\mathcal{E}(\rho)}.\end{aligned} \tag{9.86}$$

The DEC requires that

$$0 \leq 8\pi G_N \mathcal{T}_{ab}\left[t^a \pm \frac{1}{\sqrt{B}}(\partial_r)^a\right] t^b = \mathcal{E} \pm \frac{1}{\sqrt{B}}\mathcal{J}, \tag{9.87}$$

and so we have that

$$\mathcal{E} \geq \frac{1}{\sqrt{B}}|\mathcal{J}|. \tag{9.88}$$

Writing B in terms of ω, and enforcing the DEC, we get

$$\frac{W}{\omega(\infty)} \leq \frac{\int_{r_0}^{\infty} \mathrm{d}r r^{d-1}\mathcal{J}(r)}{\frac{2}{L}\int_{r_0}^{\infty}\mathrm{d}r r^d\sqrt{1-\frac{\omega(r)L^2}{r^d}}|\mathcal{J}(r)|}. \tag{9.89}$$

Let us now for a moment assume that we are perturbatively close to the vacuum, where ϵ is a perturbative parameter parametrizing the magnitude of $\omega(\infty)$. By monotonicity and positivity of $\omega(r)$, $\omega(r) \sim \mathcal{O}(\epsilon)$ as well, and so the $\omega(r)$ appearing in the square root gives higher order contributions:

$$\begin{aligned}
\frac{W}{\omega(\infty)} &\leq \frac{\int_{r_0}^{\infty}\mathrm{d}r r^{d-1}|\mathcal{J}(r)|}{\frac{2}{L}\left[\int_{r_0}^{\infty}\mathrm{d}r r^d|\mathcal{J}(r)| - \frac{L^2}{2}\int_{r_0}^{\infty}\mathrm{d}r\omega(r)|\mathcal{J}(r)| + \ldots\right]} \\
&= \frac{L}{2}\frac{\int_{r_0}^{\infty}\mathrm{d}r r^{d-1}|\mathcal{J}(r)|}{\int_{r_0}^{\infty}\mathrm{d}r r^d|\mathcal{J}(r)|}\left[1+\frac{L^2}{2}\frac{\int_{r_0}^{\infty}\mathrm{d}r\omega(r)|\mathcal{J}|}{\int_{r_0}^{\infty}\mathrm{d}r r^d|\mathcal{J}|}+\ldots\right] \\
&\leq \frac{L}{2r_0}\left[1+\frac{L^2}{r_0^d}\omega(\infty)+\ldots\right] \\
&\leq \frac{L}{2r_0}\left[1+\frac{L^{2d}}{r_0^d}\frac{\mu(\infty)}{L^{2d-2}}+\ldots\right] \\
&= \frac{L}{2r_0}\left[1+\frac{16\pi\eta_d}{d-1}\frac{\ell^d\langle T_{tt}\rangle}{c_{\text{eff}}}+\ldots\right]
\end{aligned} \tag{9.90}$$

where η_d is the $O(1)$ number coming from using (9.63). We see that the effective expansion parameter is the dimensionless quantity $\frac{\ell^d\langle T_{tt}\rangle}{c_{\text{eff}}}$. So the expansion is not really in small mass, which is dimensionful, but in small strip width relative to the inverse energy density per CFT degree of freedom. □

From (9.42) and (9.63), we get, up to the perturbative corrections,

$$\begin{aligned}
\left|\frac{\mathrm{d}S_R}{\mathrm{d}t}\right| &\leq \frac{\text{Area}[\partial R]}{4G_N L^{d-2}}\frac{L}{2r_0}\omega(\infty) \leq \frac{\sqrt{\pi}}{d-1}\frac{\Gamma\left(\frac{1}{2(d-1)}\right)}{\Gamma\left(\frac{d}{2(d-1)}\right)}\ell\text{Area}[\partial R]\langle T_{tt}\rangle \\
&= \text{Vol}[R]\langle T_{tt}\rangle\begin{cases}2\pi & d=2\\ \frac{\sqrt{\pi}}{d-1}\frac{\Gamma\left(\frac{1}{2(d-1)}\right)}{\Gamma\left(\frac{d}{2(d-1)}\right)} & d>2\end{cases},
\end{aligned} \tag{9.91}$$

where we used (9.63) and (9.45) in the second inequality. This also holds for $d = 2$, since $\omega(\infty) \leq \mu(\infty)$, provided we replace $\langle T_{tt}\rangle \to \langle T_{tt}\rangle - \langle T_{tt}\rangle_{\text{vac}}$ if ϕ is compact. Also, note that for $d = 2$ we have that $\ell\text{Area}[\partial R] = 2\text{Vol}[R]$. This completes the proof of Theorem 7 for strip regions.

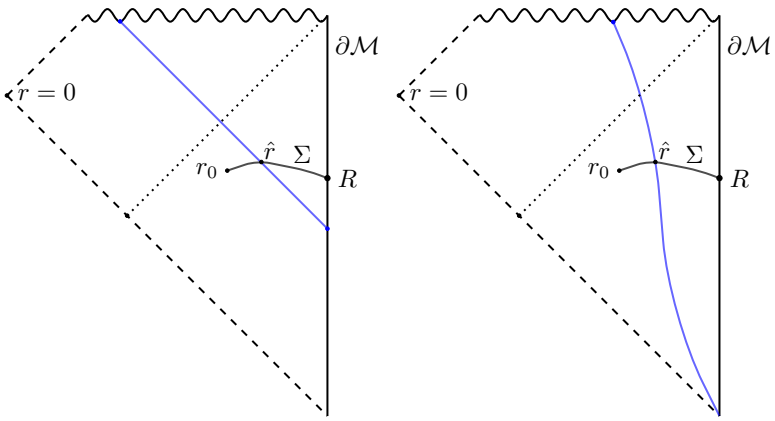

Figure 9.3: Examples of thin-shell spacetimes, where the blue lines correspond to the shells. The left space is dual to a uniform quench, where matter is thrown in from the boundary, while the right is a spacetime with a brane in the bulk interior.

Proof of bounds in thin-shell spacetimes

We now turn our attention to thin-shell spacetimes, where we will be able to establish that a bound of the form $|\partial_t S| \leq \#\text{Vol}[R]\,\langle T_{tt}\rangle$ holds for any ℓ. Furthermore, in this class of spacetimes we will prove our conjectured generalization of Theorem 5 to $d > 2$, i.e. Theorem 6.

Consider a spacetime where the matter consists of a single thin shell of matter that separately satisfies the DEC, together with a possible contribution from any number of $U(1)$ gauge fields:

$$\begin{aligned} \mathcal{E} &= \kappa\delta(r-\hat{r}) + \mathcal{E}^{\text{Maxwell}}, \\ \mathcal{J} &= \eta\delta(r-\hat{r}), \end{aligned} \tag{9.92}$$

for some $\eta, \kappa, \hat{r} > r_0$. See Figure 9.3. Here we used that in planar symmetry, Maxwell fields give no contribution to the radial momentum density $\mathcal{J}$ (see for example Sec. 3 of [306]). In fact, we can add to the $U(1)$ gauge fields any matter that has a positive contribution to $\mathcal{E}$ but no contribution to $\mathcal{J}$.

The DEC, through (9.88), imposes that $\mathcal{J}$ only can have support at $\hat{r}$. Without loss of generality, we take $\eta > 0$. Let us in this section also use our scaling freedom in r to set $r_0 = L$ and choice of units to set $L = 1$.

Define again $W = -\lim_{r\to\infty} r^{d-3} K_{\phi\phi}$. Plugging (9.92) into (9.58), the solution for $K_{\phi\phi}$ is

$$K_{\phi\phi}(r) = -\frac{r^2}{d-1}\eta\sqrt{\frac{\hat{r}^{2d-2}-1}{r^{2d-2}-1}}\theta(r-\hat{r}), \tag{9.93}$$

and so

$$\eta = \frac{(d-1)W}{\sqrt{\hat{r}^{2d-2}-1}}, \tag{9.94}$$

which gives

$$K_{\phi\phi}(r) = -\frac{r^2 W}{\sqrt{r^{2d-2}-1}}\theta(r-\hat{r}). \tag{9.95}$$

Next, let us solve for the contribution to $\omega(r)$ from the squared extrinsic curvature term in (9.59):

$$\begin{aligned} Q(r) &\equiv \int_1^r \mathrm{d}\rho \rho^{d-5} K_{\phi\phi}(\rho)^2 h_1(\rho) \\ &= \theta(r-\hat{r}) W^2 \int_{\hat{r}}^r \mathrm{d}\rho \rho^{d-1} \frac{h_1(\rho)}{[\rho^{2d-2}-1]} \\ &= W^2 \theta(r-\hat{r}) \left[\frac{\hat{r}^d}{\hat{r}^{2d-2}-1} - \frac{r^d}{r^{2d-2}-1} \right]. \end{aligned} \tag{9.96}$$

To proceed, we need to understand what happens to ω as we cross the shock. Restricting attention to a small neighborhood of $\hat{r}$, where we can treat explicit occurrences of r not appearing in delta functions as constant, the equation for ω reads

$$(d-1)\frac{\omega'(r)}{\hat{r}^{d-1}} = 2\mathcal{E}^{\text{shell}} + \dots, \tag{9.97}$$

where the terms indicated with dots will make no contribution to the discontinuity. Remembering that the DEC implies that $\sqrt{B}\mathcal{E} \geq |\mathcal{J}|$, imposing the DEC on the shell means that

$$\mathcal{E}^{\text{shell}} \geq \sqrt{\hat{r}^2 - \frac{\omega(r)}{\hat{r}^{d-2}}}\eta\delta(r-\hat{r}). \tag{9.98}$$

Inserting (9.98) into (9.97), dividing by the prefactor of the delta function, and integrating from $\hat{r}-\varepsilon$ to $\hat{r}+\varepsilon$ for some small positive ε, we find

$$\sqrt{\hat{r}^2 - \frac{\omega_-}{\hat{r}^{d-2}}} - \sqrt{\hat{r}^2 - \frac{\omega_+}{\hat{r}^{d-2}}} \geq \frac{\hat{r}}{d-1}\eta + \mathcal{O}(\varepsilon), \tag{9.99}$$

where we defined $\omega_\pm = \omega(\hat{r}\pm\varepsilon)$. We only have a sensible solution when $B(r)$ is real and positive everywhere, which requires

$$\frac{1}{d-1}\eta \leq \sqrt{1-\frac{\omega_-}{\hat{r}^d}}. \tag{9.100}$$

Solving for ω_- from (9.99) and inserting our expression for η, we get that

$$\omega_+ \geq \omega_- + \frac{\hat{r}^d}{\sqrt{\hat{r}^{2d-2}-1}} W \left[\sqrt{1-\frac{\omega_-}{\hat{r}^d}} - \frac{W}{\sqrt{\hat{r}^{2d-2}-1}} \right]. \tag{9.101}$$

Using this and (9.80), the Lorentzian Hawking mass at infinity has the lower bound

$$\begin{aligned} \mu(\infty) &= \omega(\infty) + \delta_{d2} W^2 \\ &\geq \omega_- + \frac{\hat{r}^d}{\sqrt{\hat{r}^{2d-2}-1}} W \left[\sqrt{1-\frac{\omega_-}{\hat{r}^d}} - \frac{W}{\sqrt{\hat{r}^{2d-2}-1}} \right] + Q(\infty) + \delta_{d2} W^2 \\ &= \omega_- + \frac{\hat{r}^d}{\sqrt{\hat{r}^{2d-2}-1}} W \sqrt{1-\frac{\omega_-}{\hat{r}^d}}, \end{aligned} \tag{9.102}$$

where δ_{ij} is the Kronecker delta. Thus, for any real n, we have that

$$\frac{W^n}{\mu(\infty)} \leq \frac{W^n}{\omega_- + \frac{\hat{r}^d}{\sqrt{\hat{r}^{2d-2}-1}} W \sqrt{1-\frac{\omega_-}{\hat{r}^d}}} \equiv U_n, \tag{9.103}$$

together with the constraints

$$0 \leq \omega_- \leq \hat{r}^d, \tag{9.104}$$

$$W \leq \sqrt{\hat{r}^{2d-2}-1}\sqrt{1-\frac{\omega_-}{\hat{r}^d}}. \tag{9.105}$$

Our goal will now be to upper bound U_n for all legal triplets $(W, \hat{r}, \omega_-)$ for $n = 1$ and $n = \frac{d}{d-1}$, which turns out to be values that will give interesting growth bounds.

Note first that we have

$$\partial^2_{\omega_-} U_n \geq 0, \tag{9.106}$$

so any local extremum of U_n with respect to ω_- is a minimum. Thus, for any given W and $\hat{r}$, U_n is maximized when ω_- is on the boundary of its domain. First, take $\omega_- = 0$. Then, assuming that $1 \leq n \leq \frac{d}{d-1}$,

$$U_n = \frac{W^{n-1}\sqrt{\hat{r}^{2d-2}-1}}{\hat{r}^d} \leq \frac{\left[\hat{r}^{2d-2}-1\right]^{\frac{n}{2}}}{\hat{r}^d} \leq \frac{\hat{r}^{n(d-1)}}{\hat{r}^d} \leq 1, \tag{9.107}$$

where we used (9.105) in the second inequality. For $n = 1$, we get the stronger bound

$$U_1 \leq \frac{\sqrt{\hat{r}^{2d-2}-1}}{\hat{r}^d} \leq \sqrt{\frac{d-1}{d^{\frac{d}{d-1}}}} \equiv \alpha_d, \tag{9.108}$$

where the upper bound is found by maximizing with respect to $\hat{r}$. Next, let us look at the maximal value for ω_-, where we have the equality

$$W = \sqrt{\hat{r}^{2d-2}-1}\sqrt{1-\frac{\omega_-}{\hat{r}^d}}. \tag{9.109}$$

Neglecting the first ω_- in the denominator of U_n and using $W \leq \sqrt{\hat{r}^{2d-2}-1}$, we get

$$U_n \leq \frac{\left[\hat{r}^{2d-2}-1\right]^{n/2}}{\hat{r}^d}. \tag{9.110}$$

But this is just the expression bounded earlier, and so (9.107) and (9.108) holds generally. Restoring factors of L, r_0, we have the following true bounds

$$W \leq L^{\frac{d-2}{d}} \omega(\infty)^{\frac{d-1}{d}}, \tag{9.111}$$

$$W \leq \alpha_d \frac{L}{r_0} \omega(\infty). \tag{9.112}$$

Redoing the steps in (9.91) with the numerical factor from in (9.112), we get Theorem 8 for strip regions. Next, inserting (9.111) into (9.42), we find

$$\left|\frac{\mathrm{d}S_R}{\mathrm{d}t}\right| \leq \frac{\mathrm{Area}[\partial R]}{4G_N L^{d-2}} L^{\frac{d-2}{d}} \left[\frac{16\pi G_N L^{d-1}}{d-1}\langle T_{tt}\rangle\right]^{\frac{d-1}{d}} = \frac{1}{4}\mathrm{Area}[\partial R] c_{\mathrm{eff}} \left[\frac{16\pi}{(d-1)c_{\mathrm{eff}}}\langle T_{tt}\rangle\right]^{\frac{d-1}{d}}, \tag{9.113}$$

proving Theorem 6 for strip regions.

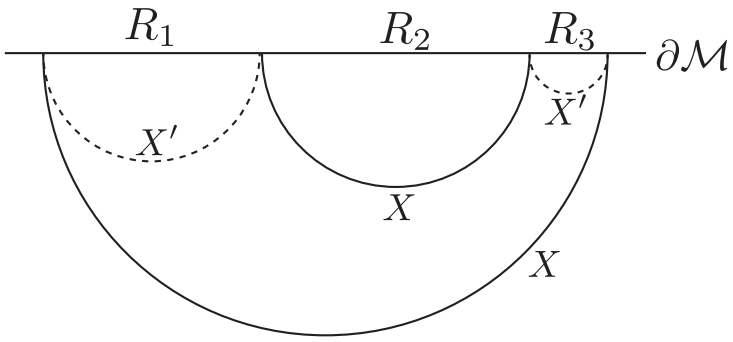

Figure 9.4: Possible HRT surfaces X and X' of the region $R_1 \cup R_3$, projected onto a timeslice.

9.2.6 Multiple strips and mutual information

Our results not scaling with Vol$[R]$ can be generalized to regions R consisting of n disjoint finite strips by simply applying the same argument to each connected component of the HRT surface separately. For $d = 2$ this results in

$$\left|\frac{\mathrm{d}S_R}{\mathrm{d}t}\right| \leq n\sqrt{\frac{8\pi c}{3}\langle T_{tt}\rangle}. \tag{9.114}$$

It is easy to see that (9.113) also holds true for n strips. No modification is needed, since Area$[\partial R]$ implicitly contains the factor of n present in the $d = 2$ case.

For the bounds scaling like volume, the behavior is different, since the upper bound depends on the connectivity properties of the entanglement wedge. Consider for example $d = 2$ and the three intervals R_1, R_2, R_3 in Figure 9.4, and let $R = R_1 \cup R_3$ be the region under consideration. We then see that

$$\left|\frac{\mathrm{d}S_R}{\mathrm{d}t}\right| \leq \kappa \langle T_{tt}\rangle \begin{cases} \mathrm{Vol}[R] & \text{the entanglement wedge is disconnected,} \\ \mathrm{Vol}[R] + 2\mathrm{Vol}[R_2] & \text{the entanglement wedge is connected,} \end{cases} \tag{9.115}$$

where κ is the relevant numerical prefactor of either Theorem 7 or 8. We get this result by adding the different volume factors from each connected component of the HRT surface. Similar games can be played for n strips in d dimensions.

Next, lets us consider $d = 2$ and the mutual information between two subsystems R_1 and R_2 consisting of n_1 and n_2 finite intervals, respectively. We then have

$$\begin{aligned} \left|\partial_t I(R_1, R_2)\right| &= |\partial_t S_{R_1} + \partial_t S_{R_2} - \partial_t S_{R_1 R_2}| \leq |\partial_t S_{R_1}| + |\partial_t S_{R_2}| + |\partial_t S_{R_1 R_2}| \\ &\leq (2n_1 + 2n_2)\sqrt{\frac{8\pi c}{3}\langle T_{tt}\rangle}. \end{aligned} \tag{9.116}$$

Using (9.28), the generalization to higher d is obvious.

9.3 Maximal rates for Balls, Wilson Loops and Correlators

9.3.1 Setup and summary of results

In this section we will consider extremal surfaces X_t of dimension $q+1$ anchored at q-dimensional spheres ∂R_t at time t on the conformal boundary, where extremal means that all the mean curvatures of X_t are zero.[13] We take the spheres to have radius $\mathcal{R}$. For $q=0$, ∂R_t just consists of two points, and X_t is a one-parameter family of geodesics. For $q=d-2$, X_t is a one-parameter family of HRT surfaces anchored at spheres. For $q=1$, X_t are two-dimensional spacelike worldsheets anchored at circles.

As before we are working with planar symmetric spacetimes, subject to the same assumptions described in Sec. 9.2.1. The logical steps will be mostly identical to Sec. 9.2, but with extra technicalities coming from the curvature of ∂R_t. Note that since we now have submanifolds of varying dimensions, we will use the symbol $\|\cdot\|$ to indicate the measure of the surface in the natural induced volume form. For quantities on the conformal boundary, $\|\cdot\|$ means with respect to the induced metric from the Minkowski conformal frame. We will use Length[], Area[] and Vol[] to refer to the measure of surfaces of dimension 1, codimension 2, and codimension 1, respectively.

To describe the relevant subregions in our results, let $\boldsymbol{z}$ be Cartesian coordinates in the direction transverse to the sphere ∂R_t. We now choose coordinates for our Minkowski conformal frame on the boundary to be

$$\mathrm{d}s^2 = -\mathrm{d}t^2 + L^2\left(\mathrm{d}\phi^2 + \phi^2 \mathrm{d}\Omega_q^2 + \mathrm{d}\boldsymbol{z}^2\right), \tag{9.117}$$

with $\mathrm{d}\Omega_q^2$ the metric of a round unit q-sphere, and with the constant$-t$ slices the ones on which one-point functions of local operators are constant. For $q=0$ there is no $\mathrm{d}\Omega_q^2$–term, while for $q=d-2$ there is no $\mathrm{d}\boldsymbol{z}^2$ term. ϕ is a dimensionless radial coordinate on the boundary, and $R_{t'}$ is given by

$$0 \le \phi \le \frac{\mathcal{R}}{L}, \qquad t=t', \qquad \boldsymbol{z}=0. \tag{9.118}$$

We now have

$$\|\partial R_t\| = \|\partial R\| = \Omega_q \mathcal{R}^q, \tag{9.119}$$

where Ω_q is the volume of a unit q-sphere.

Let us now summarize the results proven in this section. For entanglement entropy, we will prove the parts Theorems 6, 7 and 8 that refer to spherical ∂R. For extremal surfaces of other dimensionalities, the following theorem applies to the most general class of spacetimes and subregions:

[13] This means that the generalized volume of X_t is stationary under perturbations with compact support.

Theorem 10. *Let $(\mathcal{M}, g_{ab})$ be a regular asymptotically AdS_{d+1} spacetime with planar symmetry satisfying the DEC. Assume that d is even, and let be X_t be an extremal surface of dimension $d/2$, anchored on the conformal boundary at the sphere ∂R_t. Then*

$$\left|\frac{\mathrm{d}}{\mathrm{d}t}\|X_t\|\right| \leq \|\partial R\| L^{\frac{d}{2}} \sqrt{\frac{16\pi}{c_{\text{eff}}(d-1)} \langle T_{tt}\rangle}. \tag{9.120}$$

Of course, for $d = 2$, this just reduces to Theorem 5. For $d = 4$ this can be converted to the growth bound on circular Wilson loops, given by (9.13). Next, for surfaces X_t anchored at small spheres on the boundary, we get the following:

Theorem 11. *Let $(\mathcal{M}, g_{ab})$ be a regular asymptotically AdS_{d+1} spacetime with planar symmetry satisfying the DEC. Let be X_t be an extremal surface of dimension $q+1$, anchored on the conformal boundary at the sphere ∂R_t having radius $\mathcal{R}$. Assume that*

$$q \geq \frac{d-2}{2} \tag{9.121}$$

and

$$\frac{\mathcal{R}^d \langle T_{tt}\rangle}{c_{\text{eff}}} \ll 1. \tag{9.122}$$

Then

$$\left|\frac{\mathrm{d}}{\mathrm{d}t}\|X_t\|\right| \leq \eta_{d,q} \|\partial R\| L^{q+1} \mathcal{R}^{d-q-1} \frac{\langle T_{tt}\rangle}{c_{\text{eff}}} \left[1 + \mathcal{O}\left(\frac{\mathcal{R}^d \langle T_{tt}\rangle}{c_{\text{eff}}}\right)\right], \tag{9.123}$$

where

$$\eta_{d,q} = \frac{8\pi}{d-1} \left[\frac{\Gamma\left(\frac{1}{2(q+1)}\right)}{\sqrt{\pi}\Gamma\left(\frac{q+2}{2(q+1)}\right)}\right]^{d-q-1}. \tag{9.124}$$

Using well known dictionary entries, described in Sec. 9.3.6, this converts to growth bounds on the entanglement of small balls, small circular Wilson loops, and heavy two-point functions at small separations. Specifically, for the latter two, we get

$$\left|\frac{\mathrm{d}}{\mathrm{d}t} \log |\langle O(x)O(0)\rangle_{\rho(t)}|\right| \leq \frac{8\pi\Delta}{c_{\text{eff}}} |x| \langle T_{tt}\rangle \left[1 + \mathcal{O}\left(\frac{|x|^2 \langle T_{tt}\rangle}{c_{\text{eff}}}\right)\right], \quad d = 2, \tag{9.125}$$

and

$$\left|\frac{\mathrm{d}}{\mathrm{d}t} \log |\langle \mathcal{W}(C)\rangle_{\rho(t)}|\right| \leq \frac{8\pi\sqrt{\lambda_{\text{eff}}}}{(d-1)c_{\text{eff}}} \eta_{d,1} \mathcal{R}^{d-1} \langle T_{tt}\rangle \left[1 + \mathcal{O}\left(\frac{\mathcal{R}^d \langle T_{tt}\rangle}{c_{\text{eff}}}\right)\right], \quad d \in \{3, 4\}, \tag{9.126}$$

where $\sqrt{\lambda_{\text{eff}}} = L^2/\ell^2_{\text{string}}$ is the effective 't Hooft coupling, and ℓ_{string} the bulk string length. Finally, for thin-shell spacetimes, we prove the following:

Theorem 12. *Let $(\mathcal{M}, g_{ab})$ be an asymptotically AdS_{d+1} spacetime with planar symmetry satisfying the DEC. Assume that X_t is an extremal surface anchored at a boundary sphere of dimension*

$$q \geq \frac{d-2}{2}. \tag{9.127}$$

Next, assume that the bulk matter consists of $U(1)$ gauge fields and a thin shell of matter:

$$\mathcal{T}_{ab} = \mathcal{T}^{\text{shell}}_{ab} + \mathcal{T}^{\text{Maxwell}}_{ab}, \tag{9.128}$$

where $\mathcal{T}^{\text{shell}}_{ab}$ has delta function support on a codimension−1 worldvolume that is timelike or null, and that separately satisfies the DEC. Assume $(\mathcal{M}, g)$ is regular, except we do not require g_{ab} to be C^2 at the shell. Then

$$\left|\frac{\mathrm{d}}{\mathrm{d}t}\|X_t\|\right| \leq \|\partial R\| L^{q+1} \left[\frac{16\pi}{(d-1)c_{\text{eff}}} \langle T_{tt}\rangle\right]^{\frac{q+1}{d}} \tag{9.129}$$

and

$$\left|\frac{\mathrm{d}}{\mathrm{d}t}\|X_t\|\right| \leq \kappa_{d,q} \|\partial R\| L^{q+1} \mathcal{R}^{d-q-1} \frac{\langle T_{tt}\rangle}{c_{\text{eff}}} \tag{9.130}$$

with $\kappa_{d,q}$ given by (9.191).

The main application of (9.129) is to bound Wilson loops in $d = 3$, where we get

$$\left|\frac{\mathrm{d}}{\mathrm{d}t} \log |\, \langle \mathcal{W}(C)\rangle_{\rho(t)}\, |\right| \leq \frac{\sqrt{\lambda_{\text{eff}}}\text{Length}[C]}{2\pi} \left[\frac{8\pi}{c_{\text{eff}}} \langle T_{tt}\rangle\right]^{2/3}. \tag{9.131}$$

Let us now turn to the proofs.

9.3.2 An implicit solution for the extremal surface location

As earlier, let Σ be the extended planar symmetric homology hypersurface containing X. For the exact same reason as earlier, there is a unique choice of Σ. We can now pick coordinates on Σ given by

$$\mathrm{d}s^2|_\Sigma = H_{\mu\nu}\mathrm{d}y^\mu \mathrm{d}y^\nu = B(r)\mathrm{d}r^2 + r^2\left(\mathrm{d}\phi^2 + \phi^2 \mathrm{d}\Omega_q^2 + \mathrm{d}\boldsymbol{z}^2\right). \tag{9.132}$$

Again, one such coordinate system covers all of Σ, as shown in appendix A.3.5.

We take our intrinsic coordinates on X to be (r, Ω^i), where Ω^i are coordinates on the sphere. The embedding coordinates of X in Σ reads

$$X^\mu = (r, \phi = \Phi(r), \Omega^i, \boldsymbol{z} = 0), \tag{9.133}$$

where the symmetries of the problem dictate $\boldsymbol{z} = 0$. The induced metric on X is

$$\mathrm{d}s^2|_X = \left[B(r) + r^2\Phi'(r)^2\right]\mathrm{d}r^2 + r^2\Phi(r)^2\mathrm{d}\Omega_q^2. \tag{9.134}$$

Now we must implement the condition that X is extremal, which requires us to compute all its mean curvatures and demand them to be vanishing. To do this, let n_a^I be an orthonormal basis of normal forms to X that are tangent to Σ, labeled by I. Let t_a be

the future timelike normal orthogonal to Σ. A complete basis of mean curvatures of X now is

$$\begin{aligned}\mathcal{K}^I &= h^{ab}\nabla_a n_b^I,\\ \mathcal{K}^0 &= h^{ab}\nabla_a t_b,\end{aligned} \tag{9.135}$$

where $h^{ab} = g^{ab} + t^a t^b - \delta^{IJ} n_I^a n_J^b$. All of these quantities must vanish. Considering the $\mathcal{K}^I$ corresponding the $\boldsymbol{z}$ directions, we just get 0 by our symmetries. Letting $I = n$ denote the remaining normal direction in Σ, we get by direct computation that (see appendix (A.3.6) for some of the required ingredients)

$$\begin{aligned}\mathcal{K}^n = \frac{1}{r\sqrt{B}\left[B + r^2(\Phi')^2\right]^{3/2}}\Bigg[&r^2 B\Phi'' + (q+1)r^3(\Phi')^3\\ &+ \left((q+2)B - \frac{1}{2}rB'\right)r\Phi' - \frac{qB}{\Phi}\left(B + r^2(\Phi')^2\right)\Bigg].\end{aligned} \tag{9.136}$$

If it was not for the last term, we would reproduce (9.37) by setting $q = d-2$. The new term is caused by the curvature of ∂R. Now, with this last term, we no longer have an explicit analytical solution (when $q > 0$). However, we can find an implicit solution that lets us proceed. Define

$$\chi(r) = \frac{qB}{\Phi\Phi'}\left(\frac{B}{\Phi'^2} + r^2\right), \tag{9.137}$$

so that our equation for extremality reads

$$(q+1)r^3(\Phi')^3 + \left((q+2)B - \frac{1}{2}rB'\right)r\Phi' + r^2 B\Phi'' - (\Phi')^3\chi(r) = 0. \tag{9.138}$$

Imposing $\Phi(r_0) = 0$, where r_0 is the tip of the extremal surface, we have the implicit solution

$$\Phi(r) = \int_{r_0}^{r} \mathrm{d}\rho \frac{\sqrt{B(\rho)}}{\rho\sqrt{\mathcal{C}\rho^{2q+2}h(\rho) - 1}}, \tag{9.139}$$

where

$$h(r) = 1 - \frac{2}{\mathcal{C}}\int_{r_0}^{r} \mathrm{d}\rho\chi(\rho)\rho^{-6-2q}, \tag{9.140}$$

for some $\mathcal{C}$ that is fixed by imposing $\Phi'(r_0) = \infty$. Assuming $h(r_0)$ is finite, we get that $\mathcal{C} = r_0^{-2q-2}$. This is indeed correct, even though $\chi(r_0)$ looks superficially divergent. Since we are near a minimum of $r(\Phi)$ we have that $r = r_0 + \mathcal{O}(\Phi^2)$ near r_0, and so for r close to r_0 we get $\Phi = \alpha\sqrt{r - r_0}$ for some α. Even though Φ goes to zero at r_0 we find that

$$\chi(r) \sim \mathcal{O}(1) \tag{9.141}$$

near r_0, and so $h(r_0) = 1$. Next, reality of $\Phi(r)$ demands that $h(\rho) \geq (r_0/r)^{2q+2}$, while

positivity of Φ and Φ' ensures that $h(r) \leq 1$, and so in total we know that[14]

$$\Phi(r) = \int_{r_0}^{r} \mathrm{d}\rho \frac{\sqrt{B(\rho)}}{\rho\sqrt{(\rho/r_0)^{2q+2}h(\rho) - 1}}, \qquad 0 < (r_0/r)^{2q+2} < h(r) \leq 1. \tag{9.142}$$

9.3.3 The relation between the Hawking masses

Take $K_{\alpha\beta}$ to be the extrinsic curvature of the extended homology hypersurface. Like in the case of the strip, we have that

$$\mu(r) = \omega(r) + r^{d-4} K_{\phi\phi}(r)^2, \tag{9.143}$$

which follows from the same computation as in the previous section, together with (A.54) in appendix A.3.6. We have that $K_{\phi\phi} \sim \mathcal{O}(1/r^{q-1})$, as becomes clear in the next section. Thus, at large r we have

$$\mu(r) = \omega(r) + \mathcal{O}\left(r^{d-2-2q}\right). \tag{9.144}$$

Consequently, $\omega(\infty)$ is proportional to spacetime mass if and only if

$$q > \frac{d-2}{2}. \tag{9.145}$$

If $2q = d-2$, $\omega(\infty)$ is smaller than $\mu(\infty)$ by some finite number. For $2q < d-2$, we get $\omega(\infty) = -\infty$ by (9.144) and the fact that $\mu(\infty)$ is finite and positive. We will see below that this comes out of the constraint equations, since exactly when $2q < d-2$, $\omega(r)$ is neither positive nor monotonically increasing. We will not be able to say anything about the case $2q < d-2$.

9.3.4 $\partial_t \|X_t\| \leq$ momentum on X_t

The time-derivative of the generalized volume satisfies [301, 302]

$$\frac{\mathrm{d}}{\mathrm{d}t}\|X_t\| = \int_{\partial X_t} N^a \eta_a, \tag{9.146}$$

where $\eta^a = (\partial_t)^a$ generates the deformation of ∂X_t, while N^a is the unit vector that is (1) tangent to X_t, (2) orthogonal to ∂X_t, and (3) pointing towards the conformal boundary. A computation in appendix A.3.4 shows that (9.146) can be written as

$$\frac{\mathrm{d}}{\mathrm{d}t}\|X_t\|\Big|_{t=0} = \frac{\|\partial R\|}{L^q} \lim_{r\to\infty} r^{q-1} K_{\phi\phi}(r). \tag{9.147}$$

Now we again reach the stage where we must write the Einstein constraint equations as a closed system, which requires us to impose extremality in the timelike direction.

[14] By the same kind of analysis as in appendix A.3.5, we cannot have additional turning points where $\Phi'(r)$ diverges, and so we have strict inequality in the lower bound.

First, note that from the planar symmetry of Σ, if $\boldsymbol{x}$ are Cartesian coordinates on the plane containing R, then we have that the extrinsic curvature of Σ reads

$$\begin{aligned} K_{\mu\nu}\mathrm{d}y^\mu \mathrm{d}y^\nu &= K_{rr}(r)\mathrm{d}r^2 + K_{\phi\phi}(r)\left(\mathrm{d}\boldsymbol{x}^2 + \mathrm{d}\boldsymbol{z}^2\right) \\ &= K_{rr}(r)\mathrm{d}r^2 + K_{\phi\phi}(r)\left(\mathrm{d}\phi^2 + \phi^2\mathrm{d}\Omega_q^2 + \mathrm{d}\boldsymbol{z}^2\right). \end{aligned} \tag{9.148}$$

Thus, the components of the extrinsic curvature with indices in the sphere directions reads

$$K_{ij} = K_{\phi\phi}(r)\phi^2 w_{ij}, \tag{9.149}$$

where w_{ij} is the unit metric on the q-sphere. Define again $F(r)$ through the relation $K_{rr}(r) = F(r)B(r)$. Computing $\mathcal{K}^0 = 0$, using (9.149), and solving for $F(r)$ (see Appendix A.3.6), we get, after substituting our expression for $\Phi(r)$, that

$$F(r) = -\frac{K_{\phi\phi}(r)}{r^2}H(r), \tag{9.150}$$

where we for convenience defined the function

$$H(r) = \frac{q(r/r_0)^{2q+2}h(r) + 1}{(r/r_0)^{2q+2}h(r) - 1}. \tag{9.151}$$

Since $\partial_h H < 0$ and $h(r) \leq 1$, we get the lower bound

$$H(r) \geq \frac{q(r/r_0)^{2q+2} + 1}{(r/r_0)^{2q+2} - 1} \equiv H_L(r). \tag{9.152}$$

The constraint equations (9.47) and (9.48) are unchanged, except now the expression for $F(r)$ is different. Plugging it in we get

$$(d-1)\frac{\omega'(r)}{r^{d-1}} = 2\mathcal{E} + \frac{(d-1)}{r^4}K_{\phi\phi}(r)^2\left[2H(r) - d + 2\right], \tag{9.153}$$

$$K'_{\phi\phi} + \left[H(r) - 1\right]\frac{K_{\phi\phi}}{r} = -\frac{r^2}{d-1}\mathcal{J}(r). \tag{9.154}$$

Now, using the lower bound $H_L(r)$, let us note the following:

$$2H(r) - d + 2 \geq \frac{(2q - d + 2)(r/r_0)^{2q+2} + d - 1}{(r/r_0)^{2q+2} - 1}. \tag{9.155}$$

This is positive definite for all r only when $q \geq \frac{d-2}{2}$, so for geodesics ($q = 0$), we only have monotonicity of $\omega(r)$ when $d = 2$. But this is just the case studied in the previous section. For ($q = 1$), which is the relevant case for Wilson loops, we have monotonicity of $\omega(r)$ only for $d \leq 4$. For an HRT surface we have $q = d-2$, and so we have monotonicity in all dimensions. It is in fact quite surprising that we have monotonicity for any q whatsoever, since when looking at the Einstein constraint equations in covariant form, monotonicity of the Riemannian Hawking mass is only manifest on hypersurfaces that have vanishing mean curvature.

Let us assume $2q \geq d-2$ going forward, and let us bound $K_{\phi\phi}$ and μ at infinity. Fixing an integration constant by demanding that $F(r_0) = \text{finite}$, the solution to the momentum constraint is

$$K_{\phi\phi}(r) = -\frac{1}{d-1}\int_{r_0}^{r} \mathrm{d}\rho\rho^2 \mathcal{J}(\rho) e^{-\int_\rho^r \mathrm{d}\frac{1}{z}(H(z)-1)}. \tag{9.156}$$

We have that

$$\begin{aligned} |K_{\phi\phi}(r)| &\leq \frac{1}{d-1}\int_{r_0}^{r} \mathrm{d}\rho\rho^2 |\mathcal{J}(\rho)| e^{-\int_\rho^r \mathrm{d}\frac{1}{z}(H_L(z)-1)} \\ &= \frac{r^2}{(d-1)\sqrt{(r/r_0)^{2q+2}-1}}\int_{r_0}^{r} \mathrm{d}\rho |\mathcal{J}(\rho)| \sqrt{(\rho/r_0)^{2q+2}-1}. \end{aligned} \tag{9.157}$$

We see from this expression that $K_{\phi\phi} \sim \mathcal{O}(1/r^{q-1})$. Also, in this last expression, if we replace $|\mathcal{J}| \to -\mathcal{J}$, we just get the solution of (9.154) with $H(r)$ replaced by $H_L(r)$. We will use this fact later.

Inserting (9.157) in (9.147), we finally get

$$\left|\frac{\mathrm{d}}{\mathrm{d}t}\|X_t\|\right| \leq \frac{(d-1)\|\partial R\|}{L^q}\int_{r_0}^{\infty} \mathrm{d}\rho |\mathcal{J}(\rho)| \sqrt{\rho^{2q+2}-r_0^{2q+2}}. \tag{9.158}$$

Unlike for an HRT surface anchored at a strip, we are here only able to write an inequality.

Next, let us turn to the second ingredient: the mass. Rewriting (9.153) in terms of $\mu(r)$, we get

$$(d-1)\frac{\mu'(r)}{r^{d-1}} = 2\mathcal{E} + \frac{(d-1)}{r^4}K_{\phi\phi}(r)^2\left[2H(r)+d-6\right] + \frac{2(d-1)}{r^3}\frac{\mathrm{d}}{\mathrm{d}r}K_{\phi\phi}^2. \tag{9.159}$$

After an integration by parts and using $H(r) \geq H_L(r)$, we get that

$$\mu(\infty) \geq \mu(r_0) + \frac{2}{d-1}\int_{r_0}^{\infty} \mathrm{d}\rho\rho^{d-1}\mathcal{E}(\rho) + \int_{r_0}^{\infty} \mathrm{d}\rho\rho^{d-5}K_{\phi\phi}(r)^2\left[2H_L(r)+d\right] \tag{9.160}$$

where

$$2H_L(r)+d = \frac{(d+2q)(r/r_0)^{2q+2}+(d-2)}{(r/r_0)^{2q+2}-1} \geq 0. \tag{9.161}$$

Possessing now an upper bound on $\partial_t\|X_t\|$ and a lower bound on mass, we next need an upper bound on L^2/r_0.

9.3.5 Constraints on boundary anchored extremal surfaces

It turns out that generalizations of Lemmata 2 and 3 remain true for the surfaces considered in this section. The proof of Lemma 2 is unchanged, while from the discussion in appendix A.3.5 and A.3.6, together with the proof of Lemma 3, we get the following constraints on the tip of X:

Lemma 5. *Let $(\mathcal{M}, g_{ab})$ be an asymptotically $AdS_{d+1\geq 3}$ spacetime with planar symmetry. Let X be a $(q+1)$-dimensional extremal surface anchored at a q-sphere on the conformal boundary. Then the tip of X lies in an untrapped region. Furthermore, if $(\mathcal{M}, g_{ab})$ is regular and satisfies the DEC, then $\omega(r_0) \geq 0$, where r_0 is the radius of the tip of X.*

With this in hand, we readily obtain the spherical dimension–$(q+1)$ version of Theorem 9:

Theorem 13. *Let $(\mathcal{M}, g_{ab})$ be a regular planar-symmetric asymptotically $AdS_{d+1\geq 3}$ spacetime satisfying the DEC. Let X be a dimension $q+1$ extremal surface anchored at a sphere of radius $\mathcal{R}$. Let be r_0 be the radius of the plane tangent to the tip of X. Then if*

$$q \geq \frac{d-2}{2}, \tag{9.162}$$

we have

$$\frac{L^2}{r_0} \leq \frac{\Gamma\left(\frac{1}{2(q+1)}\right)}{\sqrt{\pi}\Gamma\left(\frac{q+2}{2(q+1)}\right)}\mathcal{R}. \tag{9.163}$$

Proof. For $2q \geq d-2$, (9.153) implies $\omega'(r) \geq 0$. Combining with $\omega(r_0) \geq 0$, we get $\omega(r) \geq 0$. Using now $h(r) < 1$ and that $\omega(r) \geq 0$ implies $B(r) \geq L/r$, we get

$$\begin{aligned} \mathcal{R} = L\Phi(\infty) &= L\int_{r_0}^{\infty} \mathrm{d}r \frac{\sqrt{B(r)}}{r\sqrt{(r/r_0)^{2q+2}h(r)-1}} \\ &\geq L^2 \int_{r_0}^{\infty} \mathrm{d}r \frac{1}{r^2\sqrt{(r/r_0)^{2q+2}-1}} = \frac{L^2}{r_0}\frac{\sqrt{\pi}\Gamma\left(\frac{q+2}{2(q+1)}\right)}{\Gamma\left(\frac{1}{2(q+1)}\right)}. \end{aligned} \tag{9.164}$$

□

9.3.6 Proofs

Proof of bounds in $d = 2$ and $d = 4$

Consider the special dimension

$$q = \frac{d-2}{2}, \tag{9.165}$$

which can only happen when d is even. As seen previously, we have that $\omega(r) \geq 0$ in this case. Furthermore, (9.143) becomes

$$\mu(\infty) = \omega(\infty) + \left[\lim_{r\to\infty} r^{q-1}K_{\phi\phi}\right]^2, \tag{9.166}$$

and so

$$\left|\lim_{r\to\infty} r^{q-1}K_{\phi\phi}(\infty)\right| \leq \sqrt{\mu(\infty)}, \tag{9.167}$$

which gives

$$\left|\frac{\mathrm{d}}{\mathrm{d}t}\|X_t\|\right|_{t=0} \leq \frac{\|\partial R\|}{L^q}\sqrt{\mu(\infty)} \quad = \|\partial R\| L^{q+1}\sqrt{\frac{16\pi}{c_{\text{eff}}(d-1)}\langle T_{tt}\rangle}. \tag{9.168}$$

This proves Theorem 10. For $q = 0, d = 2$, this is just the formula we used to derive (9.25).

The above result implies a bound on correlators that can be computed using the geodesic approximation. The geodesic approximation says that the two-point function of a CFT scalar operator O of large scaling dimension $\Delta \gg 1$ can be computed as

$$\langle O(\boldsymbol{x})O(0)\rangle_{\rho(t)} = \eta e^{-\frac{\Delta}{L}\|X_t\|_{\text{reg}}}, \tag{9.169}$$

where η is some constant, and $\|X_t\|_{\text{reg}}$ is the regularized distance of a geodesic anchored at the points $(t, \boldsymbol{x})$ and $(t, 0)$ on the conformal boundary. We here adopted the Schrödinger picture. Combining (9.168) and (9.169) and taking $d = 2$, we get[15]

$$\left|\frac{\mathrm{d}}{\mathrm{d}t}\log\langle O(x)O(0)\rangle_{\rho(t)}\right| \leq \sqrt{\frac{96\pi\Delta^2}{c}\langle T_{tt}\rangle}, \qquad d = 2. \tag{9.170}$$

Next, for $d = 4$, (9.168) holds for $q = 1$, where the X_t are two-dimensional worldsheets anchored at circles on the boundary. If $\mathcal{W}(C)$ is a Wilson loop of a circle $C = S^1$, we have that [318, 319]

$$\langle \mathcal{W}(C)\rangle_{\rho(t)} = \eta e^{-\frac{1}{2\pi\alpha'}\|X_t\|}, \tag{9.171}$$

where $\alpha' = \ell^2_{\text{string}}$ and η again some constant. Combining (9.168) and (9.171) we get

$$\left|\frac{\mathrm{d}}{\mathrm{d}t}\log\langle \mathcal{W}(C)\rangle_{\rho(t)}\right| \leq \text{Length}[C]\sqrt{\frac{4\lambda_{\text{eff}}}{3\pi c_{\text{eff}}}\langle T_{tt}\rangle}, \qquad d = 4, \tag{9.172}$$

where $\text{Length}[C] = 2\pi\mathcal{R}$. With the precise dictionary for the duality between type IIB supergravity on $\text{AdS}_5 \times S^5$ and $\mathcal{N} = 4$ super Yang-Mills with gauge group $SU(N)$ and 't Hooft coupling λ, given by

$$\frac{G_N}{R^3} = \frac{\pi}{2N^2}, \quad \sqrt{\lambda} = \frac{L^2}{\alpha'}, \tag{9.173}$$

(9.172) can be written as (9.13).

Proof of bounds for small $\mathcal{R}$

Next we prove bounds that are strong at small radii $\mathcal{R}$. We have:

Lemma 6. *Consider the same assumptions as in Theorem 13. Assume furthermore that* $\mathcal{R}^d \langle T_{tt}\rangle / c_{\text{eff}} \ll 1$ *and* $2q \geq d - 2$. *Then*

$$\left|\lim_{r\to\infty} r^{d-3}K_{\phi\phi}\right| \leq \frac{L}{2r_0^{d-q-1}}\omega(\infty)\left[1 + \mathcal{O}\left(\frac{\mathcal{R}^d\langle T_{tt}\rangle}{c_{\text{eff}}}\right)\right]. \tag{9.174}$$

[15] Of course, we could have derived this in Sec. 9.2, given that that geodesics coincide with the HRT surface when $d = 2$.

Proof. Define $W = -\lim_{r\to\infty} r^{q-1} K_{\phi\phi}$, and assume without loss of generality that $W > 0$. Using (9.58) and (9.153) and the exact same logic as in the proof of Lemma 4, we get

$$\begin{aligned}\frac{W}{\omega(\infty)} &\leq \frac{L\int_{r_0}^{\infty} \mathrm{d}r r^{q+1}|\mathcal{J}(r)|}{2\int_{r_0}^{\infty} \mathrm{d}r r^{d}\sqrt{1-\frac{\omega(r)L^2}{r^d}}|\mathcal{J}(r)|} \\ &\leq \frac{L\int_{r_0}^{\infty} \mathrm{d}r r^{q+1}|\mathcal{J}(r)|}{2\int_{r_0}^{\infty} \mathrm{d}r r^{d}|\mathcal{J}(r)|}\left[1+\frac{L^2\omega(\infty)}{2r_0^d}+\ldots\right] \\ &\leq \frac{L}{2r_0^{d-q-1}}\left[1+\mathcal{O}\left(\frac{\mathcal{R}^d\langle T_{tt}\rangle}{c_{\text{eff}}}\right)\right].\end{aligned} \tag{9.175}$$

□

Inserting now (9.174) into (9.147), we get

$$\begin{aligned}\left|\frac{\mathrm{d}}{\mathrm{d}t}\|X_t\|\right|_{t=0} &\leq \frac{8\pi\|\partial R\|L^{1+q}}{(d-1)c_{\text{eff}}}\frac{L^{2(d-q-1)}}{r_0^{d-q-1}}\langle T_{tt}\rangle \\ &\leq \frac{\|\partial R\|L^{1+q}}{c_{\text{eff}}}\eta_{d,q}\mathcal{R}^{d-q-1}\langle T_{tt}\rangle\end{aligned} \tag{9.176}$$

where

$$\eta_{d,q} = \frac{8\pi}{d-1}\left[\frac{\Gamma\left(\frac{1}{2(q+1)}\right)}{\sqrt{\pi}\Gamma\left(\frac{q+2}{2(q+1)}\right)}\right]^{d-q-1}. \tag{9.177}$$

We can convert this to bounds on two-point functions and circular Wilson loops. Combining (9.176) with (9.169) and (9.171), we get the bounds (9.125) and (9.126).

Finally, with $q = d-2$ and $d > 2$, the entanglement entropy of small spheres is bounded as

$$\left|\frac{\mathrm{d}S_R}{\mathrm{d}t}\right| \leq \frac{2\sqrt{\pi}\Gamma\left(\frac{1}{2(d-1)}\right)}{\Gamma\left(\frac{d}{2(d-1)}\right)}\mathrm{Vol}[R]\langle T_{tt}\rangle + \ldots \tag{9.178}$$

where we used that $\mathrm{Vol}[R] = \mathrm{Area}[\partial R]\mathcal{R}/(d-1)$. The proves the part of Theorem 7 where ∂R is a sphere.

Proof of bounds for thin-shell spacetimes

Finally, let us prove our thin-shell results valid all for $\mathcal{R}$, assuming $2q \geq d-2$. Since we already have general bounds for two-point correlators in $d = 2$ and Wilson loops in $d = 4$, this section is mostly relevant for entanglement in medium or large balls in general d, and for medium and large Wilson loops in $d = 3$. We consider the same setup as in Sec. 9.2.5, and use the same notation. Again, we choose $r_0 = L = 1$.

Now, let us consider the solutions (9.153) and (9.154) with the replacement $H(r) \to H_L(r)$. As discussed in Sec. 9.3.4, this gives a smaller value for $\mu(\infty)$ and larger value for $\left|\lim r^{q-1}K_{\phi\phi}\right|$ if $\mathcal{J}$ has a fixed sign, which is the case here. Since we will consider

bounds of the form $\lim r^{q-1}K_{\phi\phi} \leq \#\mu(\infty)^n$ for $n > 0$, the bounds we obtain with this replacement will be valid for the original spacetime.

Now, with a delta function shock, solution for $K_{\phi\phi}$ reads

$$K_{\phi\phi}(r) = -\frac{r^2}{d-1}\eta\sqrt{\frac{\hat{r}^{2q+2}-1}{r^{2q+2}-1}}\theta(r-\hat{r}) = -\frac{r^2 W}{\sqrt{r^{2q+2}-1}}\theta(r-\hat{r}). \tag{9.179}$$

From (9.160) we get that the contribution to $\mu(\infty)$ from the extrinsic curvature reads

$$\begin{aligned} Q(\infty) &\equiv \int_{r_0}^{\infty} \mathrm{d}\rho\rho^{d-5}K_{\phi\phi}(r)^2\frac{(d+2q)r^{2q+2}+(d-2)}{r^{2q+2}-1} \\ &= W^2\frac{\hat{r}^d}{\hat{r}^{2q+2}-1}. \end{aligned} \tag{9.180}$$

The analysis of how the DEC changes across the shock is unchanged from the strip case, except for a few exponents, and we find

$$\omega_+ = \omega_- + \frac{\hat{r}^d}{\sqrt{\hat{r}^{2q+2}-1}}W\left[\sqrt{1-\frac{\omega_-}{\hat{r}^d}} - \frac{W}{\sqrt{\hat{r}^{2q+2}-1}}\right]. \tag{9.181}$$

By the same logic as in Sec. 9.2.5 we get,

$$\frac{W^n}{\mu(\infty)} \leq \frac{W^n}{\omega_- + W\frac{\hat{r}^d}{\sqrt{\hat{r}^{2q+2}-1}}\sqrt{1-\frac{\omega_-}{\hat{r}^d}}} \equiv U_n \tag{9.182}$$

where

$$0 \leq \omega_- \leq \hat{r}^d, \tag{9.183}$$

$$W \leq \sqrt{r^{2q+2}-1}\sqrt{1-\frac{\omega_-}{\hat{r}^d}}. \tag{9.184}$$

Again, it now suffices to take ω_- at the boundary of its allowed domain. With $\omega_- = 0$ and $1 \leq n \leq \frac{d}{q+1}$ we get

$$U_n = \frac{W^{n-1}\sqrt{\hat{r}^{2q-2}-1}}{\hat{r}^d} \leq \frac{[r^{2q+2}-1]^{n/2}}{\hat{r}^d} \leq 1, \tag{9.185}$$

and for $n = 1$ we get the stronger bound

$$U_1 \leq \sqrt{\frac{q+1}{d}}\left(\frac{d}{d-1-q}\right)^{\frac{q+1-d}{2(q+1)}} \equiv \alpha_{d,q}. \tag{9.186}$$

For saturation of (9.184), neglecting the first ω_- in the denominator of U_n and using that $W \leq \sqrt{\hat{r}^{2q+q}-1}$, we get

$$U_n \leq \frac{[r^{2q+2}-1]^{n/2}}{\hat{r}^d} \leq 1. \tag{9.187}$$

Restoring factors of L, r_0, we have the following general bounds

$$W \leq \alpha_{q,d} \frac{L}{r_0^{d-q-1}} \omega(\infty), \tag{9.188}$$

$$W \leq L^{\frac{2q+2-d}{d}} \omega(\infty)^{\frac{q+1}{d}}. \tag{9.189}$$

Combining (9.188) with (9.147) and (9.162) now gives that

$$\left| \frac{\mathrm{d}}{\mathrm{d}t} \|X_t\| \right| \leq \kappa_{d,q} \|\partial R\| L^{1+q} \mathcal{R}^{d-q-1} \frac{\langle T_{tt} \rangle}{c_{\text{eff}}}, \tag{9.190}$$

where

$$\kappa_{d,q} = 2\alpha_{d,q}\eta_{d,q} = \frac{16\pi}{d-1}\sqrt{\frac{q+1}{d}} \left(\frac{d}{d-1-q} \right)^{\frac{q+1-d}{2(q+1)}} \left[\frac{\Gamma\left(\frac{1}{2(q+1)}\right)}{\sqrt{\pi}\Gamma\left(\frac{q+2}{2(q+1)}\right)} \right]^{d-q-1}. \tag{9.191}$$

This shows that the type of bounds derived in the small $\mathcal{R}$ limit holds in thin shell spacetimes for all $\mathcal{R}$, at price of a larger prefactor. For the entanglement entropy of balls, we get

$$\left| \frac{\mathrm{d}S_R}{\mathrm{d}t} \right| \leq 4\sqrt{\frac{\pi(d-1)}{d^{\frac{d}{d-1}}}} \frac{\Gamma\left(\frac{1}{2(d-1)}\right)}{\Gamma\left(\frac{d}{2(d-1)}\right)} \mathrm{Vol}[R] \langle T_{tt} \rangle . \tag{9.192}$$

For Wilson loops we get

$$\left| \frac{\mathrm{d}}{\mathrm{d}t} \log |\langle \mathcal{W}(C) \rangle_{\rho(t)}| \right| \leq \frac{\sqrt{\lambda_{\text{eff}}}}{c_{\text{eff}}} \mathcal{R}^{d-1} \langle T_{tt} \rangle \begin{cases} \frac{\sqrt{128\pi}\Gamma(1/4)}{3^{3/4}\Gamma(3/4)} \approx 26 & d=3 \\ \frac{8\Gamma(1/4)^2}{3\Gamma(3/4)^2} \approx 23 & d=4 \end{cases}. \tag{9.193}$$

Next, consider (9.189). This gives us that

$$\left| \frac{\mathrm{d}}{\mathrm{d}t} \|X_t\| \right|_{t=0} \leq \|\partial R\| L^{q+1} \left[\frac{16\pi}{(d-1)c_{\text{eff}}} \langle T_{tt} \rangle \right]^{\frac{q+1}{d}} \tag{9.194}$$

For $q = d-2$, corresponding to entanglement for ball subregions, this just gives (9.28), verifying that it holds for spheres as well, completing the proof of the part of Theorem 8 concerning spherical ∂R.

For $q = 0, d = 2$ and $q = 1, d = 4$ we just reproduce the bounds of Sec. 9.3.6, which are anyway proven with weaker assumptions there. For $q = 1, d = 3$ we get a new bound on Wilson loops, given by (9.131).

9.4 Bounding Spatial Derivatives

The technology we have developed to bound time derivatives also lets us bound spatial derivatives of extremal surface areas for strips.

Consider a one parameter family of strips R_ℓ of variable width ℓ at some fixed time boundary time, given by (9.21) with t' now held fixed. Let X_ℓ be the corresponding one-parameter family of HRT surfaces. A computation in appendix A.3.3 gives that

$$\frac{\mathrm{d}}{\mathrm{d}\ell}\mathrm{Area}[X_\ell] = \frac{\mathrm{Area}[\partial R]}{L^{d-1}} r_0^{d-1}. \tag{9.195}$$

For a strip, we thus see that the depth of the HRT surface tip uniquely determines $\partial_\ell S$. Using our lower bound on r_0 given by (9.63), we now immediately get the following:

Theorem 14. *Let $(\mathcal{M}, g_{ab})$ be a regular asymptotically $AdS_{d+1\geq 3}$ spacetime with planar symmetry satisfying the DEC. If X_ℓ is the HRT surface of a strip R_ℓ of width ℓ, then*

$$\frac{\mathrm{d}}{\mathrm{d}\ell}\left[\frac{\mathrm{Area}[X_\ell]}{4G_N}\right] \geq \frac{c_{\mathrm{eff}}}{4\ell^{d-1}}\mathrm{Area}[\partial R]\left[\frac{2\sqrt{\pi}\Gamma\left(\frac{d}{2(d-1)}\right)}{\Gamma\left(\frac{1}{2(d-1)}\right)}\right]^{d-1}. \tag{9.196}$$

The lower bound is equal to $\partial_\ell S_{\mathrm{vacuum}}$, and so we get

$$\frac{\mathrm{d}}{\mathrm{d}\ell}\Delta S[\rho_{R_\ell}] \geq 0 \tag{9.197}$$

where ΔS is the vacuum subtracted entropy. Since we get the vacuum entanglement entropy in the limit $\ell \to 0$, this implies that

$$\Delta S \geq 0. \tag{9.198}$$

It is easy to see that (9.197) and (9.198) applies to a subregion R corresponding to a union of any number of finite width strips, with ∂_ℓ now interpreted as the derivative with respect to increasing width of one or more of the connected components.

For $d = 2$, we also get a bound on correlators of heavy scalar single trace primaries. Working at a fixed moment of time with a homogeneous state ρ, the combination of (9.195), (9.63) and (9.169) for $x > 0$ gives

$$\frac{\mathrm{d}}{\mathrm{d}x}\ln\langle\mathcal{O}(x)\mathcal{O}(0)\rangle_\rho \leq \frac{\mathrm{d}}{\mathrm{d}x}\ln\langle\mathcal{O}(x)\mathcal{O}(0)\rangle_{\mathrm{vacuum}} = -\frac{2\Delta}{\ell} \tag{9.199}$$

which means that correlations must die of faster than the vacuum for the states and operators covered by our assumptions. This in particular implies that

$$\langle\mathcal{O}(x)\mathcal{O}(0)\rangle_\rho \leq \langle\mathcal{O}(x)\mathcal{O}(0)\rangle_{\mathrm{vacuum}}, \tag{9.200}$$

since we just get the vacuum correlator as $x \to 0$.

9.5 Bekenstein Bounds on Entanglement

In fact, much of the proof strategy use to establish Theorem. 7 can be adapted to prove a Bekenstein-type bound on the holographic entanglement entropy for reduced CFT states on small subregions. Here, we prove the following theorem, where we have left some details to the appendix A.3.

Theorem 15. *Let $(\mathcal{M}, g)$ be a planar-symmetric asymptotically AdS spacetime that is AdS hyperbolic and satisfying the DEC. Let X be the HRT surface of a strip R of width ℓ, and let ρ_R be the reduced CFT density matrix on R as a functional of the Riemannian mass ω. If $\rho_{R,vac}$ is the reduced CFT density matrix for a vanishing Riemannian mass, then the entanglement entropy is bounded above by*

$$0 \leq \Delta S[\rho_R] = S[\rho_R] - S[\rho_{R,vac}]. \tag{9.201}$$

Assume further that $\ell^d \langle T_{tt} \rangle / c_{eff} \ll 1$, then the entanglement difference is also bounded above

$$0 \leq \Delta S \leq \epsilon_d \ell^2 Area[\partial R] T_{tt} + \mathcal{O}\left(\frac{\ell^d \langle T_{tt} \rangle}{c_{eff}}\right) \tag{9.202}$$

where ϵ_d is

$$\epsilon_d = \frac{\sqrt{\pi}\Gamma\left(1 + \frac{1}{2(d-1)}\right)^2 \Gamma\left(\frac{1}{d-1}\right)}{\Gamma\left(\frac{1}{2} + \frac{1}{d-1}\right) \Gamma\left(\frac{d}{2(d-1)}\right)^2} \geq 0. \tag{9.203}$$

Proof. (Lower Bound) By Lemma. 3 and the DEC, the Riemannian mass is non-negative $\omega(r) \geq 0$ and consequently $B(r) \geq L/r = B(r, 0]$. Furthermore, Lemma. **??** furnishes a lower bound on the area functional γ_X for the HRT surface in a spacetime with non-vanishing Riemannian mass. Hence, the entanglement difference is

$$\begin{aligned} \Delta S[\rho_R] &= S[\rho_R] - S[\rho_{R,\text{vac}}]] \\ &= \frac{\text{Area}[\partial R]}{4G_N L^{d-2}} \int_{r_0}^{\infty} (\sqrt{\gamma_X} - \sqrt{\gamma_{X,\text{vac}}}) \geq 0 \end{aligned} \tag{9.204}$$

which completes the proof of the first part of the theorem. □

Now, we turn to proving the upper bound on the entanglement difference.

Proof. Let us first assume that we are perturbatively close to the vacuum, where ϵ is a small parameter specifying the magnitude of $\omega(\infty)$. Using that the Riemannian mass is non-negative, and by monotonicity $\omega(\infty) \geq \omega(r)$, we can perturbatively expand to find an upper bound on $B(r)$ via

$$\frac{L}{r} + L^3 \frac{\omega(\infty)}{2r^{d+1}} + \mathcal{O}(\omega^2) \geq \sqrt{B(r)} \approx \frac{L}{r}\left(1 + L^2 \frac{\omega(r)}{2r^d} + \mathcal{O}(\omega^2)\right). \tag{9.205}$$

Now, we consider the vacuum subtracted entanglement entropy again to find (up to quadratic corrections)

$$\begin{aligned} \Delta S[\rho_R(t)] &\leq \frac{\text{Area}[\partial R]}{4G_N L^{d-2}} \int_{r_0}^{\infty} r^{d-2} \left(L^3 \frac{\omega(\infty)}{2r^{d+1}} + \mathcal{O}(\omega^2)\right) \frac{(r/r_0)^{d-1}}{\sqrt{(r/r_0)^{2d-2} - 1}} \text{d}r \\ &= \frac{\sqrt{\pi}\Gamma\left(\frac{1}{d-1}\right)}{4(d-1)\Gamma\left(\frac{d}{2(d-1)}\right)} \frac{\text{Area}[\partial R]}{4G_N L^{d-2}} \frac{L^3 \omega(\infty)}{r_0^2} + \mathcal{O}(\omega^2) \\ &= \frac{\sqrt{\pi}\Gamma\left(\frac{1}{d-1}\right)}{4(d-1)\Gamma\left(\frac{d}{2(d-1)}\right)} \frac{\text{Area}[\partial R]}{4G_N L^{d-2}} \frac{L^3}{r_0^2} \left(\frac{16\pi G_N L^{d-1}}{d-1} \langle T_{tt} \rangle\right) + \mathcal{O}(\langle T_{tt} \rangle^2) \end{aligned} \tag{9.206}$$

Finally, using Eqn. (9.45) in conjunction with Thm. 9, some algebra reveals that

$$\Delta S \leq \epsilon_d \ell^2 \text{Area}[\partial R] T_{tt} + \mathcal{O}(\omega(\infty)^2) = \epsilon_d \ell E_R + \mathcal{O}((\ell E_R)^2) \tag{9.207}$$

where ϵ_d is

$$\epsilon_d = \frac{\sqrt{\pi}\Gamma\left(1+\frac{1}{2(d-1)}\right)^2 \Gamma\left(\frac{1}{d-1}\right)}{\Gamma\left(\frac{1}{2}+\frac{1}{d-1}\right)\Gamma\left(\frac{d}{2(d-1)}\right)^2} \geq 0. \tag{9.208}$$

Hence, we see the effective expansion parameter is the dimensionless quantity ℓE_R so the expansion is not exactly for small mass but for small strip length relative to the energy of the CFT. □

9.6 Evidence for Broader Validity of Bounds

In the previous sections, we have shown that the DEC allows us to prove several general bounds on the growth of entanglement, correlators and Wilson loops. However, the proofs crucially relied on the dominant energy condition. While the dominant energy condition holds in type IIA, IIB and eleven-dimensional supergravity (see for example the appendix of [320]), it is typically violated after dimensional reduction [321]. The prototypical example is a scalar field dual to a relevant CFT operator. This field has negative mass squared, leading to DEC violation.

Even though our proofs assumed the DEC, we will now provide strong evidence for a subset of the bounds that they hold when the DEC is violated in reasonable ways. That is, we provide evidence in scalar theories that violate the DEC, but which have proven positive mass theorems [322, 323] (so pure AdS is stable) and respect the null energy condition (NEC). This is evidence that our bounds are true even in CFTs with DEC-violating bulks, since the NEC and a stable vacuum are both necessary conditions for sensible bulk theories.[16]

In fact, we provide evidence not just that

$$\mathfrak{R} \leq 1, \tag{9.209}$$

but also that when $d > 2$,

$$\mathfrak{R} \leq v_E^{(\text{SAdS})} + \delta v_E < 1 \tag{9.210}$$

for some small δv_E that seems to depend on the scalar potential. Here

$$v_E^{(\text{SAdS})} = \sqrt{\frac{d}{d-2}}\left(\frac{d-2}{2(d-1)}\right)^{\frac{d-1}{d}} \tag{9.211}$$

[16] If we choose completely arbitrary bulk scalar theories, we have no positive mass theorem, so we can have $\langle T_{tt}\rangle < 0$ in a homogeneous state, and the bounds are clearly violated. But in these situations there is no sensible holographic dual.

is the entanglement velocity computed in a quench in holography, with the final state being neutral, dual to the AdS-Schwarzschild type black brane [240, 241].

The theories we will consider are neutral scalars minimally coupled to gravity,

$$8\pi G_N \mathcal{L} = \frac{1}{2}R - \frac{d(d-1)}{2L^2} - \frac{1}{2}|\mathrm{d}\phi|^2 - V(\phi), \tag{9.212}$$

where V is negative somewhere, leading to violation of the DEC (but not the NEC). These theories are common in consistent truncations and dimensional reductions of type IIA, IIB, and eleven-dimensional supergravity [324–327]. We consider these theories because, for standard forms of minimally coupled bosonic matter, neutral scalars appear to pose the biggest risk to our bounds. This is because gauge fields give no direct contribution to $\mathcal{J}$, and they have a manifestly positive contributions to the mass (they respect the DEC).

For free theories where $V = \frac{1}{2}m^2\phi^2$, in order to maximize the chance of violating our bounds, we choose potentials that are close to "maximally negative", meaning we pick m^2 just slightly above the Breitenlohner-Freedman [328, 329] bound:

$$m^2 L^2 \geq m_{\mathrm{BF}}^2 L^2 \equiv -(d/2)^2. \tag{9.213}$$

It is known that if $m^2 < m_{\mathrm{BF}}^2$, AdS is unstable, and so these theories cannot be dual to CFTs with a Hamiltonian that is bounded from below. Additionally, to have an example of an interacting potential, in $d = 3$ we consider a top down potential that becomes exponentially negative for large $|\phi|$.

The numerical method

Let us now explain our procedure. For a given $V(\phi)$ and spacetime dimension, we will construct an n-parameter family of initial data, parametrized by coefficients $\{f_i\}_{i=1}^n$. The data will be provided on an extended homology hypersurface of some HRT surface. Then we will define the function $\mathcal{A}(\{f_i\})$ to be equal to the ratio

$$\left|\lim_{r\to\infty} r^{d-3} K_{\phi\phi}\right| / \mu(\infty)^{\frac{d-1}{d}} \tag{9.214}$$

in the initial dataset specified by parameters $\{f_i\}$. Different initial datasets correspond to different moments of time in different spacetimes (with different sizes of R). The value of $\mathcal{A}$ in some particular initial dataset corresponds to the instantaneous entanglement velocity $\mathfrak{R}$ in that configuration, and we will do a numerical maximization of $\mathcal{A}$ with respect to the parameters $\{f_i\}$. If we find that $\mathcal{A}$ is upper bounded, and that the upper bound is $\mathcal{A}_{\max}$, we have provided evidence that

$$\left|\frac{\mathrm{d}S_R}{\mathrm{d}t}\right| \leq \frac{1}{4}\mathcal{A}_{\max}\mathrm{Area}[\partial R] c_{\mathrm{eff}} \left[\frac{16\pi}{(d-1)c_{\mathrm{eff}}}\langle T_{tt}\rangle\right]^{\frac{d-1}{d}}. \tag{9.215}$$

If $\mathcal{A}$ is not upper bounded, or if $\mathcal{A}_{\max} > 1$, we have a counterexample to $\mathfrak{R} \leq 1$ in the theory under consideration.

We will also evaluate the function $\mathcal{B}(\{f_i\})$, which we define as the value of

$$\frac{|\partial_t S_R|}{\mathrm{Vol}[R]\,\langle T_{tt}\rangle} = \frac{4\pi}{d-1}\frac{L}{\ell}\frac{\left|\lim r^{d-3}K_{\phi\phi}\right|}{\mu(\infty)} \times \begin{cases} 2 & d=2 \\ 1 & d>2 \end{cases} \tag{9.216}$$

for any given initial dataset. By the same logic as earlier, if $\mathcal{B}$ is upper bounded by $\mathcal{B}_{\max}$, we have evidence that

$$\left|\frac{\mathrm{d}}{\mathrm{d}t}S[\rho_R(t)]\right| \leq \mathcal{B}_{\max}\mathrm{Vol}[R]\,\langle T_{tt}\rangle\,. \tag{9.217}$$

If $\mathcal{B}$ is not upper bounded, then our volume-type bounds break without the DEC.

Assuming we work with strips R, for a single evaluation of $\mathcal{A}$ and $\mathcal{B}$, we need to numerically solve the ODEs given by (9.55) and (9.56). For simplicity we will restrict to strips, since for spheres we cannot solve for $\Phi(r)$ analytically. In this case we would need to solve a set of three coupled equations instead.

Let us now specify our family of initial data. An explicit computation gives that

$$\begin{aligned} \mathcal{E} &= \frac{1}{2}\dot{\phi}(r)^2 + \frac{1}{2}\left(\frac{r^2}{L^2} - \frac{\omega(r)}{r^{d-2}}\right)\phi'(r)^2 + V(\phi), \\ \mathcal{J} &= \dot{\phi}(r)\phi(r), \end{aligned} \tag{9.218}$$

where $\dot{\phi} = t^a\nabla_a\phi|_\Sigma$. Specifying an initial dataset now corresponds to specifying the two profiles $\phi(r)$ and $\dot{\phi}(r)$, together with the initial value of $\omega(r_0)$. Letting

$$\Delta = d/2 + \sqrt{(d/2)^2 + m^2L^2} \tag{9.219}$$

be the scaling dimension of the CFT operator dual O to ϕ, the profiles we consider are

$$\begin{aligned} \phi &= f_1 \exp\left[-\left(\frac{r-f_2}{f_3}\right)^2\right] + \frac{f_4}{r^\Delta} + \frac{f_5}{r^{\Delta+2}} \\ \dot{\phi} &= f_6 \exp\left[-\left(\frac{r-f_7}{f_8}\right)^2\right] + \frac{f_9}{r^{\Delta+1}} + \frac{f_{10}}{r^{\Delta+3}} \end{aligned} \tag{9.220}$$

which gives a ten-parameter family of initial data. The gaussians give localized lumps of matter, while the power law falloffs ensures that we can turn on a VEV of O in the CFT, with $\langle O\rangle \propto f_4$ and $\langle \partial_t O\rangle \propto f_8$. Note that the seemingly unusual $1/r^{\Delta+1}$ falloff in $\dot{\phi}$ is just caused by the fact that the time derivative is with respect to a unit normal rather than the more standard global time coordinate near the conformal boundary.

What remains is to pick $\omega(r_0)$. To minimize the CFT energy, we want $\omega(r_0)$ small. When the DEC holds, we know that AdS hyperbolicity implies that $\omega(r_0) \geq 0$, as proven in Lemma 3. However, without the DEC we can have that $\omega(r_0)$ is negative, but not

arbitrarily negative. If we pick $\omega(r_0)$ too negative, it will forbid an embedding of Σ in a complete slice. The difficulty is that how negative $\omega(r_0)$ can be depends on $\phi(r_0)$, $\dot{\phi}(r_0)$, and $V(\phi)$. We will thus restrict to $\omega(r_0) = 0$ and relegate a more complete study of the future. Even with $\omega(r_0) = 0$, it is far from obvious if our results survive breaking of the DEC, as we can easily obtain large regions of $\omega < 0$ even with $\omega(r_0) = 0$.

Finally, we need to deal with invalid datasets. For a given scalar profile, it could be that $\omega(r)$ overshoots r^d/L^2. In this case, the relevant solution does not correspond to a spacelike hypersurface, and so it must be discarded. In this case we conventionally define $\mathcal{A} = \mathcal{B} = 0$. Consequently, the functions we are maximizing will have discontinuities.

We are now ready to proceed to the numerical results.

$d = 2$

We now consider a free massive scalar field with mass

$$m^2 L^2 = 0.9 m_{\rm BF}^2 L^2 = -0.9, \tag{9.221}$$

dual to a relevant operator with $\Delta \approx 1.32$. We do not consider saturation of the BF bound, since this requires modification of the mass formula, and additionally causes $|\partial_t S|$ to be divergent (for any d). Furthermore, we do not want to go too close to the BF bound, since then $\omega(r)$ converges slowly at large r, and so the numerical maximization procedure becomes prohibitively expensive.

Using now Mathematica's built in `NMaximize` function, trying all methods for non-convex optimization implemented in Mathematica and picking the best result, we find that

$$\mathcal{A}_{\rm max} \approx 0.999 \leq v_E|_{d=2} = 1. \tag{9.222}$$

Thus, in $d = 2$ we have evidence that (9.25) holds without the DEC – at least in free tachyonic scalar theories.

Next, maximizing $\mathcal{B}$, we find that

$$\mathcal{B}_{\rm max} \approx 3.29 \leq \kappa_{d=2} = 2\pi. \tag{9.223}$$

This provides evidence that (9.32) holds when the DEC is violated, and that the $\mathcal{O}\left(\ell^d \langle T_{tt}\rangle / c_{\rm eff}\right)$ corrections are not needed, even though we could not prove their absence outside thin shell spacetimes. In fact, given the large gap between $\mathcal{B}_{\rm max}$ and $\kappa_{d=2}$, the numerical results suggest that our proofs might possibly be sharpened.

$d = 3$

Now we consider two potentials:

$$\begin{aligned} V_{\rm I}(\phi) &= \frac{1}{2}\left(0.9 m_{\rm BF}^2\right)\phi^2, \\ V_{\rm II}(\phi) &= 1 - \cosh\sqrt{2}\phi, \end{aligned} \tag{9.224}$$

with ϕ dual to operators with scaling dimensions $\Delta_{\rm I} \approx 1.97$ and $\Delta_{\rm II} = 2$, respectively. The potential $V_{\rm II}$ comes from a consistent truncation and dimensional reduction of eleven-dimensional SUGRA on $\mathrm{AdS}_4 \times S^7$ [324]. We find

$$\begin{aligned} \mathcal{A}_{\rm I,max} &\approx 0.693, \\ \mathcal{A}_{\rm II,max} &\approx 0.702. \end{aligned} \tag{9.225}$$

In both cases $\mathcal{A}_{\rm max} < 1$, and so we have evidence that the conjectured bound (9.28) is true – even without the DEC and outside thin-shell spacetimes.

Now, we have that

$$v_E^{\rm (SAdS)} = \frac{\sqrt{3}}{2^{4/3}} = 0.687\ldots$$

In both cases $\mathcal{A}_{\rm max}$ is close to $v_E^{\rm (SAdS)}$, although it is slightly larger. It seems possible that a stronger bound

$$\mathfrak{R} \leq v_E^{\rm (SAdS)} + \delta v_E \tag{9.226}$$

is true for some small δv_E that potentially depends on the scalar potential.

For $\mathcal{B}$ we find

$$\begin{aligned} \mathcal{B}_{\rm I,max} &\approx 1.71 \leq \kappa_{d=3} \approx 2.62, \\ \mathcal{B}_{\rm II,max} &\approx 1.72. \end{aligned} \tag{9.227}$$

Again, there is a significant gap, with the implications being the same as for $d = 2$.

$d = 4$

We now consider

$$V(\phi) = \frac{1}{2}\left(0.9 m_{\rm BF}^2\right)\phi^2. \tag{9.228}$$

and find

$$\mathcal{A}_{\rm max} \approx 0.643. \tag{9.229}$$

Again we find evidence that (9.8) is true without the DEC or outside thin-shell spacetimes. We have

$$v_E^{\rm (SAdS)} = \frac{\sqrt{2}}{3^{3/4}} = 0.620\ldots, \tag{9.230}$$

and so that the instantaneous growth can be above $v_E^{\rm (SAdS)}$, but possibly only slightly so.

We also find

$$\mathcal{B}_{\rm max} = 1.91 \leq \kappa_{d=4} \approx 2.43. \tag{9.231}$$

Again, there is a significant gap, with the implications being the same as for $d = 2$.

Table 9.1: Proven bounds on entanglement, spatial Wilson loops and equal-time correlators. We suppress $O(1)$ numerical constants in the table. Dots mean corrections scaling as $\mathcal{O}(\ell^d \langle T_{tt}\rangle / c)$ where ℓ is the relevant characteristic length scale, corresponding to strip width of ball radius. We abbreviate the effective central charge and 't Hooft coupling as c and λ, respectively. For proof validity equal to quench+, we mean proofs valid for states dual to spacetimes with thin-shell matter, which includes quenches as a subset.

$\boldsymbol{\partial_t S \leq}$	$\boldsymbol{d}$	**Region** $\boldsymbol{R}$	**Proof validity**	**Eq.**
$\sqrt{\langle T_{tt}\rangle / c}$	2	n intervals	general	(9.25)
$\mathrm{Vol}[R]\,\langle T_{tt}\rangle + \ldots$	≥ 2	small strip or ball	general	(9.30)
$\mathrm{Area}[\partial R][\langle T_{tt}\rangle / c]^{(d-1)/d}$	≥ 2	n strips	quench+	(9.28)
$\mathrm{Area}[\partial R][\langle T_{tt}\rangle / c]^{(d-1)/d}$	≥ 2	ball	quench+	(9.28)
$\mathrm{Vol}[R]\,\langle T_{tt}\rangle$	≥ 2	strip/ball	quench+	(9.32)
$\boldsymbol{\partial_\ell S \geq}$				
$\partial_\ell S_{\text{vacuum}}$	≥ 2	n strips	general	(9.196)
$\boldsymbol{\partial_t \ln \langle \mathcal{W}(C)\rangle \leq}$		$\mathbf{Length}[C]$		
$\sqrt{\lambda}\mathrm{Length}[C]\,[\langle T_{tt}\rangle / c]^{1/2}$	4	any	general	(9.172)
$\sqrt{\lambda}\mathrm{Length}[C]^{d-1}\,\langle T_{tt}\rangle + \ldots$	3, 4	small	general	(9.126)
$\sqrt{\lambda}\mathrm{Length}[C]\,[\langle T_{tt}\rangle / c]^{2/3}$	3	any	quench+	(9.131)
$\boldsymbol{\partial_t \ln \langle O(x)O(0)\rangle \leq}$		$\boldsymbol{\lvert x\rvert}$		
$\Delta\sqrt{\langle T_{tt}\rangle / c}$	2	any	general	(9.170)
$\Delta\lvert x\rvert\,\langle T_{tt}\rangle / c + \ldots$	2	small	general	(9.125)
$\boldsymbol{\partial_x \ln \langle O(x)O(0)\rangle \leq}$				
$\partial_x \ln \langle O(x)O(0)\rangle_{\text{vacuum}}$	2	any	general	(9.199)

9.7 Discussion

In this work we have proven several new upper bounds on the rate of change of entanglement entropy, spacelike Wilson loops, and equal-time two-point functions of heavy operators. The proofs apply for spatially homogeneous and isotropic states in strongly coupled CFTs with a holographic dual. We summarize our bounds in table 9.1. We have also provided numerical evidence that the bounds have broader validity than our proofs. We will now discuss our findings and possible future directions.

A 2d QWEC: The bound (9.5) can also be seen as a quantum weak energy condition (QWEC). Let S be the entropy of be a single interval as a function of one of the endpoints p, so that $\partial_t S$ now refers to the change of S under the perturbation of this single interval endpoint, rather than both. Then we have

$$\langle T_{tt}\rangle \geq \langle T_{tt}\rangle_{\text{vac}} + \frac{3}{2\pi c}\left(\partial_t S\right)^2, \tag{9.232}$$

while the classical weak energy condition implies that $T_{tt} \geq 0$. Equation (9.232) closely

resembles the conformal quantum null energy condition (QNEC) [229, 330–334] in two dimensions.[17] Consider $2d$ Minkowski space, where $\langle T_{tt}\rangle_{\text{vac}} = 0$. Letting $x^{\pm}$ be null coordinates, the conformal QNEC says that [330, 333]

$$\langle T_{++}\rangle\,|_p \geq \frac{1}{2\pi}\partial_+^2 S + \frac{3}{\pi c}\left(\partial_+ S\right)^2 . \tag{9.233}$$

The structural similarity between (9.232) and (9.233) is obvious. While (9.232) does not contain a second derivative, it is in principle possible that (9.232) could be true also for inhomogeneous states, provided we include a term $a\partial_t^2 S$ to the right hand side for some fixed constant a. In fact, the conformal QNEC suggests that $a = (4\pi)^{-1}$, since in the special case of a half-space in a homogeneous state, where $\partial_x S = 0$, the conformal QNEC and $T_\mu{}^\mu = 0$ implies

$$\langle T_{tt}\rangle\,|_p \geq \frac{1}{4\pi}\partial_t^2 S + \frac{3}{2\pi c}\left(\partial_t S\right)^2 . \tag{9.234}$$

Why do things fall? In [252] it was proposed that the process of gravitational attraction is dual to the increase of complexity in the CFT. Assuming the complexity=volume conjecture [274], this was given a precise realization in [253–255] (see also [306]), where it was shown that the rate of change of the volume of a maximal volume slice is given by the momentum integrated on the slice. However, our formula

$$\frac{\mathrm{d}S_R}{\mathrm{d}t} = \int_X G t^a n^b \mathcal{T}_{ab} \tag{9.235}$$

shows that change in entanglement can also be seen as directly responsible for the radial momentum of matter. Thus, at present, "the increase of entanglement" seems like an equally good explanation for why things fall.

Relevant scalars, compact dimensions, and DEC breaking: Our proofs rely critically on the dominant energy condition – almost all steps of the proofs break without it. This rules out having scalars with negative squared mass, which are dual to relevant operators in the CFT. Nevertheless, we found numerical evidence that the bounds hold true without the DEC, as long as the scalar theories we consider allow a positive mass theorem, so that AdS is stable and $\langle T_{tt}\rangle$ is guaranteed to be positive.

However, there are other reasons to believe that our bounds remain true for these theories beyond our numerical findings – at least when working with top-down theories. Consider working with a theory that is a dimensional reduction and consistent truncation of type IIA, IIB, or eleven-dimensional SUGRA, so that any solution can be lifted to solutions on asymptotically $\mathrm{AdS}_{d+1}\times K$ spacetimes for some compact manifold K. These solutions will typically be warped products rather than direct products, but there exists significant evidence [336] that the entropy computed by the HRT formula in the uplifted spacetime agrees with the one computed in the dimensionally reduced spacetime – even when the product is not direct. But in the uplifted spacetime the DEC holds, since it

[17] See [335] for a study on how the QNEC constrains entanglement growth.

holds for type II and eleven-dimensional SUGRA. Thus, if our methods can be generalized to work for warped compactifications over spherically symmetric AAdS_{d+1} bases, this appears to be an avenue to prove our bounds even with relevant scalars turned on. The drawback is that the proofs might have to be carried out separately for each family of compactifications.

Strengthened bounds: Our proof that

$$\left|\frac{\mathrm{d}S_R}{\mathrm{d}t}\right| \leq \frac{1}{4}\mathrm{Area}[\partial R]c_{\mathrm{eff}}\left[\frac{16\pi}{(d-1)c_{\mathrm{eff}}}\langle T_{tt}\rangle\right]^{\frac{d-1}{d}}, \tag{9.236}$$

which implies that $\mathfrak{R} \leq 1$ in neutral states, only applied to thin-shell spacetimes, which are dual to CFT states where all dynamics happen at a single energy scale (that evolves with time). However, we gave numerical evidence that this bound also holds in general planar symmetric spacetimes with extended matter profiles. A natural extension of this work is trying to generalize the proof to include this. This will likely require a better understanding of non-linearities of the Einstein constraint equations.

Next, we found that in our numerical maximization of $\mathfrak{R}$ over a ten-parameter family of initial datasets in $d = 3, 4$, that

$$\mathfrak{R} \leq v_E^{(\mathrm{SAdS})} + \delta v_E, \tag{9.237}$$

where

$$v_E^{(\mathrm{SAdS})} = \sqrt{\frac{d}{d-2}}\left(\frac{d-2}{2(d-1)}\right)^{\frac{d-1}{d}} \tag{9.238}$$

is the entanglement velocity computed in a holographic quench having a neutral final state, and δv_E a small correction that seemed to depend on the scalar potential, but which was always small for the theories we studied (less than 0.03). This hints that it might be possible to strengthen the prefactor in (9.236). Similarly, our numerics suggested that the prefactors of (9.6) could be strengthened, and furthermore that this bound is true without $\mathcal{O}\left(\ell^d \langle T_{tt}\rangle / c_{\mathrm{eff}}\right)$ corrections.

$1/N$ corrections: It seems quite likely that $\mathfrak{R} \leq 1$ remains true with perturbative $1/N$ corrections. In fact, the pure QFT proofs of $\mathfrak{R} \leq 1$ for large subregions [244, 245] made no assumption about large-N, so only intermediate and small subregions could be sources violation. But for small subregions we showed that $\mathfrak{R} \leq \mathcal{O}(\ell/\beta) \ll 1$ for β the effective inverse temperature, which means perturbative $1/N$ corrections are unlikely to pose a of danger.[18] For intermediate sized regions things are less clear, but for $d = 3, 4$ we numerically did not manage to push $\mathfrak{R}$ close to 1, hinting that $1/N$ corrections do not pose a danger in these dimensions.

[18]The discovery of quantum extremal surfaces (QES) [228] far from classical extremal surfaces [14, 15] might make this argument somewhat less convincing, but it seems unlikely that these dominate/exist for small subregions, whose QES reside close to the conformal boundary.

Disentangling the vacuum: Under our assumptions, we have proven for strips that the vacuum-subtracted entanglement is positive. Thus it is impossible to disentangle the vacuum in a spatially uniform way without either breaking the existence of a holographic dual, or turning on operators dual to fields that violate the DEC in the bulk. In the scenario where classical DEC violation is caused by tachyonic scalars only, this implies that all uniform states with less entanglement than the vacuum must have non-zero VEV for some relevant scalar single trace primaries.

Finite coupling: Our bounds were proven at strong coupling, but it seems possible that our bounds survive for arbitrary coupling. In [245] it was found that the entanglement velocity of a free theory (for $d > 2$) is strictly smaller than the holographic strong coupling result, suggesting that dialing up the coupling increases the capability of generating entanglement.

Primaries close to the unitarity bound: In order to turn on bulk fields dual to relevant CFT operators with scaling dimensions Δ in the window

$$\frac{d-2}{2} \leq \Delta < \frac{d}{2}, \tag{9.239}$$

we must consider scalars with masses

$$m^2_{\text{BF}} \leq m^2 < m^2_{\text{BF}} + 1/L^2, \tag{9.240}$$

and turn on the slow falloffs rather than fast falloffs (see for example [337–340]). This leads to violation of the falloff assumptions (9.19), and causes the ordinary definition of the spacetime mass to be divergent. Then neither of the Hawking masses reduce to the CFT energy at conformal infinity. Consequently, significant modifications of our proofs would be required. The same holds if we turn on sources that perturb us away from a CFT. Things can get even more challenging, given that for some falloffs $\partial_t S$ itself might become divergent [247]. In this case we should only try to bound finite quantities, like the mutual information or the renormalized entanglement entropy [299, 300], where these divergences cancel.

Hartman-Maldacena surfaces and half-spaces: Our bounds are restricted to subregions that lie in a single component of the conformal boundary. Our formalism can however readily be modified to deal with HRT surfaces corresponding to a CFT region R with connected components in different CFTs, so that the corresponding HRT surface threads a wormhole, like those studied in [341].[19] It would be interesting to see if the bounds remain unchanged. We also only considered strips of finite width, but it is clear that our formalism can also handle half-spaces, where $\ell = \infty$. Since (9.5) and (9.8) do not depend on ℓ, they almost certainly remain true for half-spaces.

End-of-the-world branes: Our bounds are proven with the assumption that the Cauchy slices are complete manifolds, which rules out spacetimes with end-of-the-world

[19] See [342] for a discussion of speed limits for these surfaces in static black holes.

(EOW) branes. However, for HRT surfaces that do not end on the EOW brane, our proofs survive as long as we assume that the Hawking mass of the brane is positive, which ensures that Lemma 3 remains true. In the case where the surfaces end on the EOW brane, we expect the analysis to look similar to the analysis for HRT surfaces threading a wormhole.

Vaidya has optimal entanglement growth: There is a sense in which Vaidya spacetimes are maximizing the growth of entanglement for some given distribution of bulk energy density $\mathcal{E}(r)$, within the class DEC respecting planar spacetimes. In (9.88), we saw that the DEC imposed that the energy density at a point was lower bounded by the momentum-density the same point (up to a factor). As is clear from our proofs, excess energy density above the lower bound contributes to increasing the CFT energy without increasing $\partial_t S$, and so we see that spacetimes saturating the DEC have the greatest $\partial_t S$ compatible with their distribution of energy density. But a direct computation shows that all Vaidya spacetimes saturate the DEC. This makes sense, since we have shown that infalling matter leads to entanglement growth and outgoing matter gives entanglement decrease, and in Vaidya no matter is wasted on being outgoing. While this is no proof, it suggests that speed limits that hold in all Vaidya spacetimes also hold in other planar-symmetric spacetimes respecting the DEC.

Inhomogeneous states: It would be interesting to prove bounds for inhomogeneous states, but this appears to be a difficult task, given how crucial the bulk planar symmetry was for our proofs. Furthermore, our bounds imply a strengthening of the positive mass theorem (PMT) for planar symmetry, and if generalizations of our results exist without the uniformity assumption, it appears likely that these result will strengthen the general PMT for AAdS spacetimes. Given how challenging it was to prove the PMT [343, 344], and how the Penrose inequality, which is the most famous strengthening of the PMT, still does not have a general proof, this is a daunting task.

Bounds with charge: It is a persistent finding that $U(1)$ gauge fields tend to slow down the growth of extremal surfaces of various dimensions [240, 241, 246, 345]. It thus seems plausible that our bounds can be strengthened by taking into account nonzero charges in the CFT. It is suggestive that, in spherical symmetry, $U(1)$ gauge fields contribute energy density, but they have no pure contribution to the momentum density – that is – they only contribute to $\mathcal{J}$ through gauge covariant derivatives acting on other matter fields.

Approximate bounds for large regions: To derive our bounds scaling with the volume of the region R, we used the inequality

$$\frac{L^2}{r_0} \leq \eta_d \ell, \tag{9.241}$$

where η_d is a numerical constant. Assume now that we consider a state that has volume law scaling for the entropy when ℓ is roughly above some length scale β. For $\ell \gg \beta$, as

we increase ℓ, we expect r_0 to saturate at some radius r_{barrier}, and so (9.241) becomes a very poor bound. It seems likely that we can get stronger approximate bounds in this limit, by relating r_{barrier} to an effective inverse temperature β_{eff}, so that we effectively get a bound like $|\partial_t S| \leq \#\text{Area}[\partial R]\beta_{\text{eff}} \langle T_{tt}\rangle$. This bound might or might not reduce to (9.236).

A numerical laboratory: Our formalism makes it very easy to numerically compute properties HRT surfaces in planar symmetric spacetimes and test various hypothesis about their behavior without constructing full spacetimes and having to deal with the evolution of the Einstein equations. We imagine this can be used as a laboratory to learn more about the properties of HRT surfaces.

Other boundary geometries: Except for $d = 2$, our proofs always assumed Minkowski space on the boundary. However, our bounds survive if we compactify on a torus, so the boundary geometry is $\mathbb{R} \times T^{d-1}$, provided we make a few additional assumptions. For the bounds of the type $|\partial_t S| \leq \kappa \text{Vol}[R] \langle T_{tt}\rangle + \ldots$ (and the similar bounds for Wilson loops), we should always consider regions less than half the system size – otherwise Vol$[R]$ should be replaced with the volume of the complement. For bounds with multiple strips, if we have a torus, we need to make sure that the entangling surfaces are all parallel, which happens automatically in Minkowski due to the parallel postulate.

Next, our proofs for single regions should imply growth bounds for CFTs on the static cylinder $\mathbb{R} \times S^{d-1}$, as long as we take the regions to be very small compared to the curvature radius of the boundary sphere. The results for balls will translate to results for small caps, while the result for strips will translate to results for thin belts around the equator.

Acknowledgments

It is a pleasure to thank Sean Colin-Ellerin, Netta Engelhardt, Gary Gibbons, Matt Headrick, Hong Liu, Dan Roberts, Jon Sorce, and Brian Swingle for discussions. A.D. was supported by the University of Minnesota Doctoral Dissertation Fellowship and by the National Science Foundation Graduate Research Fellowship under Grant No. 00039202. The research of Å.F. is supported in part by the John Templeton Foundation via the Black Hole Initiative, NSF grant no. PHY-2011905, and an Aker Scholarship. The research of Å.F. was also supported in part by the Heising-Simons Foundation, the Simons Foundation, and NSF grant no. PHY-1748958.

Bibliography

[1] J. D. Bekenstein, *Black holes and the second law*, *Lett. Nuovo Cim.* **4** (1972) 737–740.

[2] J. D. Bekenstein, *Black holes and entropy*, *Phys. Rev. D* **7** (1973) 2333–2346.

[3] J. M. Bardeen, B. Carter, and S. W. Hawking, *The Four laws of black hole mechanics*, *Commun. Math. Phys.* **31** (1973) 161–170.

[4] S. W. Hawking, *Black hole explosions*, *Nature* **248** (1974) 30–31.

[5] S. W. Hawking, *Particle Creation by Black Holes*, *Commun. Math. Phys.* **43** (1975) 199–220. [Erratum: Commun.Math.Phys. 46, 206 (1976)].

[6] J. D. Bekenstein, *Generalized second law of thermodynamics in black-hole physics*, *Phys. Rev. D* **9** (Jun, 1974) 3292–3300.

[7] G. W. Gibbons and S. W. Hawking, eds., *Euclidean quantum gravity*. 1994.

[8] S. W. Hawking, *Black Holes and Thermodynamics*, *Phys. Rev. D* **13** (1976) 191–197.

[9] S. W. Hawking, *Quantum Gravity and Path Integrals*, *Phys. Rev. D* **18** (1978) 1747–1753.

[10] A. Einstein, *Die Feldgleichungen der Gravitation*, *Sitzungsberichte der Königlich Preußischen Akademie der Wissenschaften (Berlin), Seite 844-847.* (1915).

[11] A. Einstein, *Die Grundlage der allgemeinen Relativitätstheorie*, *Annalen der Physik* **354** (1916) 769–822.

[12] S. W. Hawking, *Breakdown of Predictability in Gravitational Collapse*, *Phys. Rev. D* **14** (1976) 2460–2473.

[13] J. M. Maldacena, *The Large N limit of superconformal field theories and supergravity*, *Adv. Theor. Math. Phys.* **2** (1998) 231, [hep-th/9711200]. [Adv. Theor. Math. Phys.2,231(1998)].

[14] G. Penington, *Entanglement Wedge Reconstruction and the Information Paradox*, *JHEP* **09** (2020) 002, [arXiv:1905.08255].

[15] A. Almheiri, N. Engelhardt, D. Marolf, and H. Maxfield, *The entropy of bulk quantum fields and the entanglement wedge of an evaporating black hole*, *JHEP* **12** (2019) 063, [arXiv:1905.08762].

[16] M. E. Peskin and D. V. Schroeder, *An Introduction to quantum field theory*. Addison-Wesley, Reading, USA, 1995.

[17] S. M. Carroll, *Spacetime and Geometry*. Cambridge University Press, 7, 2019.

[18] S. W. Hawking and G. F. R. Ellis, *The Large Scale Structure of Space-Time*. Cambridge Monographs on Mathematical Physics. Cambridge University Press, 2, 2011.

[19] N. D. Birrell and P. C. W. Davies, *Quantum Fields in Curved Space*. Cambridge Univ. Press, Cambridge, UK, 1984.

[20] W. G. Unruh, *Notes on black hole evaporation*, *Phys. Rev.* **D14** (1976) 870.

[21] G. E. A. Matsas and D. A. T. Vanzella, *Decay of protons and neutrons induced by acceleration*, *Phys. Rev.* **D59** (1999) 094004, [gr-qc/9901008].

[22] M. H. Lynch and N. Afshordi, *Temperatures of renormalizable quantum field theories in curved spacetime*, arXiv:1611.06619.

[23] A. Dhumuntarao, J. T. Gálvez Ghersi, and N. Afshordi, *Instantaneous Temperatures á la Hadamard: Towards a generalized Stefan-Boltzmann law for curved spacetime*, arXiv:1804.05382.

[24] K. Martel and E. Poisson, *Regular coordinate systems for Schwarzschild and other spherical space-times*, *Am. J. Phys.* **69** (2001) 476–480, [gr-qc/0001069].

[25] M. Visser, *Essential and inessential features of Hawking radiation*, *Int. J. Mod. Phys. D* **12** (2003) 649–661, [hep-th/0106111].

[26] B. Carter, *Axisymmetric Black Hole Has Only Two Degrees of Freedom*, *Phys. Rev. Lett.* **26** (1971) 331–333.

[27] W. Israel, *Event horizons in static vacuum space-times*, *Phys. Rev.* **164** (1967) 1776–1779.

[28] S. W. Hawking, *Gravitational radiation from colliding black holes*, *Phys. Rev. Lett.* **26** (1971) 1344–1346.

[29] G. W. Gibbons and S. W. Hawking, *Action Integrals and Partition Functions in Quantum Gravity*, *Phys. Rev.* **D15** (1977) 2752–2756.

[30] S. Hawking and G. T. Horowitz, *The Gravitational Hamiltonian, action, entropy and surface terms*, *Class. Quant. Grav.* **13** (1996) 1487–1498, [gr-qc/9501014].

[31] R. Emparan, C. V. Johnson, and R. C. Myers, *Surface terms as counterterms in the AdS / CFT correspondence*, *Phys. Rev.* **D60** (1999) 104001, [hep-th/9903238].

[32] A. Chamblin, R. Emparan, C. V. Johnson, and R. C. Myers, *Charged ads black holes and catastrophic holography*, *Phys.Rev.D* **60** (1999) 064018, [hep-th/9902170].

[33] A. Chamblin, R. Emparan, C. V. Johnson, and R. C. Myers, *Holography, thermodynamics and fluctuations of charged ads black holes*, *Phys. Rev. D* **60** (1999) 104026, [hep-th/9904197].

[34] D. Birmingham, *Topological black holes in Anti-de Sitter space*, *Class. Quant. Grav.* **16** (1999) 1197–1205, [hep-th/9808032].

[35] A. Dhumuntarao and R. Mann, *Criticality of lower dimensional AdSd black holes*, *Phys. Rev. D* **104** (2021), no. 6 064006, [arXiv:2106.04087].

[36] J. D. E. Creighton and R. B. Mann, *Quasilocal thermodynamics of dilaton gravity coupled to gauge fields*, *Phys. Rev. D* **52** (1995) 4569–4587, [gr-qc/9505007].

[37] D. Kastor, S. Ray, and J. Traschen, *Enthalpy and the Mechanics of AdS Black Holes*, *Class. Quant. Grav.* **26** (2009) 195011, [arXiv:0904.2765].

[38] B. P. Dolan, *The cosmological constant and the black hole equation of state*, *Class. Quant. Grav.* **28** (2011) 125020, [arXiv:1008.5023].

[39] B. P. Dolan, *Compressibility of rotating black holes*, *Phys. Rev.* **D84** (2011) 127503, [arXiv:1109.0198].

[40] B. P. Dolan, *Pressure and volume in the first law of black hole thermodynamics*, *Class. Quant. Grav.* **28** (2011) 235017, [arXiv:1106.6260].

[41] L. Smarr, *Mass formula for Kerr black holes*, *Phys. Rev. Lett.* **30** (1973) 71–73. [Erratum: Phys. Rev. Lett.30,521(1973)].

[42] M. M. Caldarelli, G. Cognola, and D. Klemm, *Thermodynamics of Kerr-Newman-AdS black holes and conformal field theories*, *Class. Quant. Grav.* **17** (2000) 399–420, [hep-th/9908022].

[43] D. Kubiznak and R. B. Mann, *P-V criticality of charged AdS black holes*, *JHEP* **07** (2012) 033, [arXiv:1205.0559].

[44] S. Gunasekaran, R. B. Mann, and D. Kubiznak, *Extended phase space thermodynamics for charged and rotating black holes and Born-Infeld vacuum polarization*, *JHEP* **11** (2012) 110, [arXiv:1208.6251].

[45] N. Altamirano, D. Kubizňák, and R. B. Mann, *Reentrant phase transitions in rotating anti–de sitter black holes*, *Phys. Rev. D* **88** (Nov, 2013) 101502(R).

[46] N. Altamirano, D. Kubiznak, R. B. Mann, and Z. Sherkatghanad, *Thermodynamics of rotating black holes and black rings: phase transitions and thermodynamic volume*, *Galaxies* **2** (2014) 89–159, [arXiv:1401.2586].

[47] M. Banados, C. Teitelboim, and J. Zanelli, *The Black hole in three-dimensional space-time*, *Phys. Rev. Lett.* **69** (1992) 1849–1851, [hep-th/9204099].

[48] M. Bañados, M. Henneaux, C. Teitelboim, and J. Zanelli, *Geometry of the 2+1 black hole*, *Phys. Rev. D* **48** (Aug, 1993) 1506–1525.

[49] A. M. Frassino, R. B. Mann, and J. R. Mureika, *Lower-Dimensional Black Hole Chemistry*, *Phys. Rev. D* **92** (2015), no. 12 124069, [arXiv:1509.05481].

[50] D. Kubiznak, R. B. Mann, and M. Teo, *Black hole chemistry: thermodynamics with Lambda*, *Class. Quant. Grav.* **34** (2017), no. 6 063001, [arXiv:1608.06147].

[51] R. B. Mann, *Conservation laws and two-dimensional black holes in dilaton gravity*, *Phys. Rev. D* **47** (May, 1993) 4438–4442.

[52] D. Louis-Martinez and G. Kunstatter, *Two-dimensional dilaton gravity coupled to an abelian gauge field*, *Phys. Rev. D* **52** (Sep, 1995) 3494–3505.

[53] R. M. Wald, *Black hole entropy is the Noether charge*, *Phys. Rev. D* **48** (1993), no. 8 3427–3431, [gr-qc/9307038].

[54] R. C. Myers, *Black Hole Entropy in Two-Dimensions*, *Phys. Rev. D* **50** (1994) 6412–6421, [hep-th/9405162].

[55] A. Cisterna, C. Henríquez-Báez, and J. Oliva, *Stabilizing Homogeneous Black Strings in AdS*, *JHEP* **01** (2020) 052, [arXiv:1909.05404].

[56] K. C. K. Chan, J. D. E. Creighton, and R. B. Mann, *Conserved masses in ghs einstein and string black holes and consistent thermodynamics*, *Phys. Rev. D* **54** (Sep, 1996) 3892–3899.

[57] A. Dhumuntarao and R. Mahbub, *Gravitational instabilities of uniform black strings in AdS space*, *Phys. Rev. D* **105** (2022), no. 4 L041501, [arXiv:2110.08334].

[58] R. Gregory and R. Laflamme, *Black strings and p-branes are unstable*, *Physical Review Letters* **70** (May, 1993) 2837–2840.

[59] R. Gregory and R. Laflamme, *The instability of charged black strings and p-branes*, *Nuclear Physics B* **428** (Oct, 1994) 399–434.

[60] G. Gibbons and S. A. Hartnoll, *Gravitational instability in higher dimensions*, *Phys. Rev. D* **66** (Sep, 2002) 064024.

[61] H. Kudoh, *Origin of black string instability*, *Phys. Rev. D* **73** (May, 2006) 104034.

[62] R. Gregory, *Black string instabilities in anti-de sitter space*, *Classical and Quantum Gravity* **17** (Aug, 2000) L125–L131.

[63] L. Liu and B. Wang, *Stability of BTZ black strings*, *Phys. Rev. D* **78** (Sep, 2008) 064001.

[64] G. Kang, *On the stability of black strings / branes*, in *11th Workshop on General Relativity and Gravitation*, 2, 2002. hep-th/0202147.

[65] T. Hirayama and G. Kang, *Stable black strings in anti–de sitter space*, *Phys. Rev. D* **64** (Aug, 2001) 064010.

[66] G. Kang and J. Lee, *Classical stability of black D3 branes*, *JHEP* **03** (2004) 039, [hep-th/0401225].

[67] R. B. Mann, E. Radu, and C. Stelea, *Black string solutions with negative cosmological constant*, *JHEP* **09** (2006) 073, [hep-th/0604205].

[68] Y. Brihaye, T. Delsate, and E. Radu, *On the stability of AdS black strings*, *Phys. Lett. B* **662** (2008) 264–269, [arXiv:0710.4034].

[69] J. J. Friess, S. S. Gubser, and I. Mitra, *Counterexamples to the correlated stability conjecture*, *Phys. Rev. D* **72** (Nov, 2005) 104019.

[70] A. Bernamonti, M. M. Caldarelli, D. Klemm, R. Olea, C. Sieg, and E. Zorzan, *Black strings in AdS(5)*, *JHEP* **01** (2008) 061, [arXiv:0708.2402].

[71] D. Marolf and J. E. Santos, *Phases of Holographic Hawking Radiation on spatially compact spacetimes*, *JHEP* **10** (2019) 250, [arXiv:1906.07681].

[72] Y. Bea, O. J. C. Dias, T. Giannakopoulos, D. Mateos, M. Sanchez-Garitaonandia, J. E. Santos, and M. Zilhao, *Crossing a large-N phase transition at finite volume*, *JHEP* **02** (2021) 061, [arXiv:2007.06467].

[73] V. E. Hubeny, D. Marolf, and M. Rangamani, *Hawking radiation from AdS black holes*, *Class. Quant. Grav.* **27** (2010) 095018, [arXiv:0911.4144].

[74] V. E. Hubeny, D. Marolf, and M. Rangamani, *Black funnels and droplets from the AdS C-metrics*, *Class. Quant. Grav.* **27** (2010) 025001, [arXiv:0909.0005].

[75] H. S. Reall, *Classical and thermodynamic stability of black branes*, *Phys. Rev. D* **64** (Jul, 2001) 044005.

[76] S. S. Gubser and I. Mitra, *The Evolution of Unstable Black Holes in Anti-de Sitter Space*, *Journal of High Energy Physics* **2001** (aug, 2001) 018–018.

[77] S. S. Gubser and I. Mitra, *Instability of charged black holes in Anti-de Sitter space*, *Clay Math. Proc.* **1** (2002) 221, [hep-th/0009126].

[78] S. F. Ross and T. Wiseman, *Smeared D0 charge and the Gubser-Mitra conjecture*, *Class. Quant. Grav.* **22** (2005) 2933–2946, [hep-th/0503152].

[79] L. Lehner and F. Pretorius, *Final state of gregory-laflamme instability*, 2011.

[80] S. S. Gubser and A. Ozakin, *Universality classes for horizon instabilities*, *JHEP* **05** (2003) 010, [hep-th/0301002].

[81] T. Hirayama, G. Kang, and Y. Lee, *Classical stability of charged black branes and the gubser-mitra conjecture*, *Phys. Rev. D* **67** (Jan, 2003) 024007.

[82] A. Buchel, *A Holographic perspective on Gubser-Mitra conjecture*, *Nucl. Phys. B* **731** (2005) 109–124, [hep-th/0507275].

[83] U. Miyamoto, *Analytic evidence for the Gubser-Mitra conjecture*, *Phys. Lett. B* **659** (2008) 380–384, [arXiv:0709.1028].

[84] S. Chen, K. Schleich, and D. M. Witt, *Thermodynamics and stability of flat anti–de sitter black strings*, *Phys. Rev. D* **78** (Dec, 2008) 126001.

[85] S. Hollands and R. M. Wald, *Stability of Black Holes and Black Branes*, *Commun. Math. Phys.* **321** (2013) 629–680, [arXiv:1201.0463].

[86] A. Cisterna and J. Oliva, *Exact black strings and p-branes in general relativity*, *Class. Quant. Grav.* **35** (2018), no. 3 035012, [arXiv:1708.02916].

[87] P. Breitenlohner and D. Z. Freedman, *Stability in Gauged Extended Supergravity*, *Annals Phys.* **144** (1982) 249.

[88] P. Breitenlohner and D. Z. Freedman, *Positive Energy in anti-De Sitter Backgrounds and Gauged Extended Supergravity*, *Phys. Lett. B* **115** (1982) 197–201.

[89] P. Pani, *Advanced methods in black-hole perturbation theory*, *International Journal of Modern Physics A* **28** (Sep, 2013) 1340018, [arXiv:1305.6759].

[90] M. Headrick, "Diffgeo mathematica package."

[91] C. Henríquez-Báez, *On the stability of homogeneous black strings in ads*, 2021.

[92] S. Deser and C. Teitelboim, *Duality Transformations of Abelian and Nonabelian Gauge Fields*, *Phys. Rev. D* **13** (1976) 1592–1597.

[93] C. Vafa, *Geometric physics*, in *International Congress of Mathematicians*, 8, 1998. hep-th/9810149.

[94] M. Ammon and J. Erdmenger, *Gauge/gravity duality*. Cambridge University Press, Cambridge, 2015.

[95] S. S. Gubser, I. R. Klebanov, and A. M. Polyakov, *Gauge theory correlators from noncritical string theory*, *Phys. Lett.* **B428** (1998) 105–114, [hep-th/9802109].

[96] E. Witten, *Anti-de Sitter space and holography*, *Adv. Theor. Math. Phys.* **2** (1998) 253–291, [hep-th/9802150].

[97] S. P. Bartz, A. Dhumuntarao, and J. I. Kapusta, *Dynamical AdS/Yang-Mills model*, *Phys. Rev. D* **98** (2018), no. 2 026019, [arXiv:1801.06118].

[98] J. Erlich, E. Katz, D. T. Son, and M. A. Stephanov, *QCD and a holographic model of hadrons*, *Phys. Rev. Lett.* **95** (2005) 261602, [hep-ph/0501128].

[99] L. Da Rold and A. Pomarol, *Chiral symmetry breaking from five dimensional spaces*, *Nucl. Phys. B* **721** (2005) 79–97, [hep-ph/0501218].

[100] A. Karch, E. Katz, D. T. Son, and M. A. Stephanov, *Linear confinement and AdS/QCD*, *Phys. Rev. D* **74** (2006) 015005, [hep-ph/0602229].

[101] T. Gherghetta, J. I. Kapusta, and T. M. Kelley, *Chiral symmetry breaking in the soft-wall AdS/QCD model*, *Phys. Rev. D* **79** (2009) 076003, [arXiv:0902.1998].

[102] T. M. Kelley, S. P. Bartz, and J. I. Kapusta, *Pseudoscalar Mass Spectrum in a Soft-Wall Model of AdS/QCD*, *Phys. Rev. D* **83** (2011) 016002, [arXiv:1009.3009].

[103] P. Colangelo, F. De Fazio, F. Giannuzzi, F. Jugeau, and S. Nicotri, *Light scalar mesons in the soft-wall model of AdS/QCD*, *Phys. Rev. D* **78** (2008) 055009, [arXiv:0807.1054].

[104] L.-X. Cui, Z. Fang, and Y.-L. Wu, *Infrared-Improved Soft-wall AdS/QCD Model for Mesons*, *Eur. Phys. J. C* **76** (2016), no. 1 22, [arXiv:1310.6487].

[105] B. Batell and T. Gherghetta, *Dynamical Soft-Wall AdS/QCD*, *Phys. Rev. D* **78** (2008) 026002, [arXiv:0801.4383].

[106] J. I. Kapusta and T. Springer, *Potentials for soft wall AdS/QCD*, *Phys. Rev. D* **81** (2010) 086009, [arXiv:1001.4799].

[107] U. Gursoy, E. Kiritsis, and F. Nitti, *Exploring improved holographic theories for QCD: Part II*, *JHEP* **02** (2008) 019, [arXiv:0707.1349].

[108] U. Gursoy, E. Kiritsis, L. Mazzanti, and F. Nitti, *Deconfinement and Gluon Plasma Dynamics in Improved Holographic QCD*, *Phys. Rev. Lett.* **101** (2008) 181601, [arXiv:0804.0899].

[109] C. Csaki and M. Reece, *Toward a systematic holographic QCD: A Braneless approach*, *JHEP* **05** (2007) 062, [hep-ph/0608266].

[110] D. Li and M. Huang, *Dynamical holographic QCD model for glueball and light meson spectra*, *JHEP* **11** (2013) 088, [arXiv:1303.6929].

[111] D. Li, M. Huang, and Q.-S. Yan, *A dynamical soft-wall holographic QCD model for chiral symmetry breaking and linear confinement*, *Eur. Phys. J. C* **73** (2013) 2615, [arXiv:1206.2824].

[112] S. He, S.-Y. Wu, Y. Yang, and P.-H. Yuan, *Phase Structure in a Dynamical Soft-Wall Holographic QCD Model*, *JHEP* **04** (2013) 093, [arXiv:1301.0385].

[113] S. P. Bartz and J. I. Kapusta, *Dynamical three-field AdS/QCD model*, *Phys. Rev. D* **90** (2014), no. 7 074034, [arXiv:1406.3859].

[114] C. P. Herzog, *A Holographic Prediction of the Deconfinement Temperature*, *Phys. Rev. Lett.* **98** (2007) 091601, [hep-th/0608151].

[115] C. A. Ballon Bayona, H. Boschi-Filho, N. R. F. Braga, and L. A. Pando Zayas, *On a Holographic Model for Confinement/Deconfinement*, *Phys. Rev. D* **77** (2008) 046002, [arXiv:0705.1529].

[116] C. Csaki, H. Ooguri, Y. Oz, and J. Terning, *Glueball mass spectrum from supergravity*, *JHEP* **01** (1999) 017, [hep-th/9806021].

[117] A. Ballon-Bayona, H. Boschi-Filho, L. A. H. Mamani, A. S. Miranda, and V. T. Zanchin, *Effective holographic models for QCD: glueball spectrum and trace anomaly*, *Phys. Rev. D* **97** (2018), no. 4 046001, [arXiv:1708.08968].

[118] H. B. Meyer, *Glueball regge trajectories*, other thesis, 2004.

[119] H. B. Meyer and M. J. Teper, *Glueball Regge trajectories and the pomeron: A Lattice study*, *Phys. Lett. B* **605** (2005) 344–354, [hep-ph/0409183].

[120] K. Skenderis and P. K. Townsend, *Gravitational stability and renormalization group flow*, *Phys. Lett. B* **468** (1999) 46–51, [hep-th/9909070].

[121] O. DeWolfe, D. Z. Freedman, S. S. Gubser, and A. Karch, *Modeling the fifth-dimension with scalars and gravity*, *Phys. Rev. D* **62** (2000) 046008, [hep-th/9909134].

[122] L. Randall and R. Sundrum, *A Large mass hierarchy from a small extra dimension*, *Phys. Rev. Lett.* **83** (1999) 3370–3373, [hep-ph/9905221].

[123] L. Randall and R. Sundrum, *An Alternative to compactification*, *Phys. Rev. Lett.* **83** (1999) 4690–4693, [hep-th/9906064].

[124] A. Dhumuntarao, J. I. Kapusta, and C. Plumberg, *Randall-Sundrum Model with a Dilaton Field at Finite Temperature*, *Phys. Rev. D* **101** (2020), no. 6 066023, [arXiv:2001.00038].

[125] E. Witten, *Anti-de Sitter space, thermal phase transition, and confinement in gauge theories*, *Adv. Theor. Math. Phys.* **2** (1998) 505–532, [hep-th/9803131].

[126] A. Karch and E. Katz, *Adding flavor to AdS / CFT*, *JHEP* **06** (2002) 043, [hep-th/0205236].

[127] A. Falkowski and M. Perez-Victoria, *Electroweak Breaking on a Soft Wall*, *JHEP* **12** (2008) 107, [arXiv:0806.1737].

[128] P. Kovtun, D. T. Son, and A. O. Starinets, *Holography and hydrodynamics: Diffusion on stretched horizons*, *JHEP* **10** (2003) 064, [hep-th/0309213].

[129] A. Buchel and J. T. Liu, *Universality of the shear viscosity in supergravity*, *Phys. Rev. Lett.* **93** (2004) 090602, [hep-th/0311175].

[130] A. Buchel, *Bulk viscosity of gauge theory plasma at strong coupling*, *Phys. Lett. B* **663** (2008) 286–289, [arXiv:0708.3459].

[131] J. I. Kapusta and T. Springer, *Shear Transport Coefficients from Gauge/Gravity Correspondence*, *Phys. Rev. D* **78** (2008) 066017, [arXiv:0806.4175].

[132] S. P. Bartz, A. Dhumuntarao, and J. I. Kapusta, *Dynamical AdS/Yang-Mills model*, *Phys. Rev. D* **98** (2018), no. 2 026019, [arXiv:1801.06118].

[133] R. Rattazzi and A. Zaffaroni, *Comments on the holographic picture of the Randall-Sundrum model*, *JHEP* **04** (2001) 021, [hep-th/0012248].

[134] N. Arkani-Hamed, M. Porrati, and L. Randall, *Holography and phenomenology*, *JHEP* **08** (2001) 017, [hep-th/0012148].

[135] U. Gursoy, E. Kiritsis, L. Mazzanti, and F. Nitti, *Holography and Thermodynamics of 5D Dilaton-gravity*, *JHEP* **05** (2009) 033, [arXiv:0812.0792].

[136] A. S. Miranda, C. A. Ballon Bayona, H. Boschi-Filho, and N. R. F. Braga, *Black-hole quasinormal modes and scalar glueballs in a finite-temperature AdS/QCD model*, *JHEP* **11** (2009) 119, [arXiv:0909.1790].

[137] A. S. Miranda, C. A. Ballon Bayona, H. Boschi-Filho, and N. R. F. Braga, *Glueballs at finite temperature from AdS/QCD*, *Nucl. Phys. Proc. Suppl.* **199** (2010) 107–112, [arXiv:0910.4319].

[138] R. Yaresko, J. Knaute, and B. Kämpfer, *Cross-over versus first-order phase transition in holographic gravity–single-dilaton models of QCD thermodynamics*, *Eur. Phys. J. C* **75** (2015), no. 6 295, [arXiv:1503.09065].

[139] R. Zóllner and B. Kämpfer, *Phase structures emerging from holography with Einstein gravity – dilaton models at finite temperature*, 1807.04260.

[140] D. Bunk, J. Hubisz, and B. Jain, *A Perturbative RS I Cosmological Phase Transition*, *Eur. Phys. J. C* **78** (2018), no. 1 78, [arXiv:1705.00001].

[141] D. K. Park, H. Kim, Y.-G. Miao, and H. J. W. Muller-Kirsten, *Randall-Sundrum scenario at nonzero temperature*, *Phys. Lett. B* **519** (2001) 159–163, [hep-th/0107156].

[142] E. Kiritsis, F. Nitti, and L. Silva Pimenta, *Exotic RG Flows from Holography*, *Fortsch. Phys.* **65** (2017), no. 2 1600120, [arXiv:1611.05493].

[143] G. W. Gibbons and M. J. Perry, *Black Holes and Thermal Green's Functions*, *Proc. Roy. Soc. Lond. A* **358** (1978) 467–494.

[144] J. I. Kapusta and K. A. Olive, *Thermodynamics of Hadrons: Delimiting the Temperature*, *Nucl. Phys. A* **408** (1983) 478–494.

[145] J. I. Kapusta, *Finite Temperature Field Theory*. Cambridge Monographs on Mathematical Physics. Cambridge University Press, Cambridge, 1989.

[146] A. Cherman and A. Dhumuntarao, *Confinement and graded partition functions for $\mathcal{N} = 4$ sym*, *Phys. Rev. D* **103** (Mar, 2021) 066013, [arXiv:2012.12341].

[147] D. J. Gross, R. D. Pisarski, and L. G. Yaffe, *QCD and instantons at finite temperature*, *Rev. Mod. Phys.* **53** (1981) 43.

[148] D. Gaiotto, A. Kapustin, N. Seiberg, and B. Willett, *Generalized global symmetries*, *JHEP* **02** (2015) 172, [arXiv:1412.5148].

[149] J. Greensite, *The Confinement problem in lattice gauge theory*, *Prog. Part. Nucl. Phys.* **51** (2003) 1, [hep-lat/0301023].

[150] B. Sundborg, *The Hagedorn transition, deconfinement and N=4 SYM theory*, *Nucl. Phys.* **B573** (2000) 349–363, [hep-th/9908001].

[151] O. Aharony, J. Marsano, S. Minwalla, K. Papadodimas, and M. Van Raamsdonk, *The Hagedorn - deconfinement phase transition in weakly coupled large N gauge theories*, *Adv. Theor. Math. Phys.* **8** (2004) 603–696, [hep-th/0310285].

[152] O. Aharony, J. Marsano, S. Minwalla, K. Papadodimas, and M. Van Raamsdonk, *A First order deconfinement transition in large N Yang-Mills theory on a small S**3*, *Phys. Rev.* **D71** (2005) 125018, [hep-th/0502149].

[153] P. Kovtun, M. Unsal, and L. G. Yaffe, *Volume independence in large N_c QCD-like gauge theories*, *JHEP* **06** (2007) 019, [hep-th/0702021].

[154] G. Basar, A. Cherman, D. Dorigoni, and M. Ünsal, *Volume independence in the large n limit and an emergent fermionic symmetry*, *Phys. Rev. Lett.* **111** (Sep, 2013) 121601.

[155] G. Basar, A. Cherman, and D. A. McGady, *Bose-Fermi degeneracies in large N adjoint QCD*, *JHEP* **07** (2015) 016, [arXiv:1409.1617].

[156] A. Cherman, M. Shifman, and M. Ünsal, *Bose-Fermi cancellations without supersymmetry*, *Phys. Rev.* **D99** (2019), no. 10 105001, [arXiv:1812.04642].

[157] A. Cherman, S. Kamata, T. Schäfer, and M. Ünsal, *Flow of Hagedorn singularities and phase transitions in large N gauge theories*, *Phys. Rev. D* **101** (2020), no. 1 014012, [arXiv:1910.12312].

[158] T. Kanazawa and M. Ünsal, *Quantum distillation in QCD*, *Phys. Rev. D* **102** (2020), no. 3 034013, [arXiv:1909.05222].

[159] T. Harmark and M. Wilhelm, *Hagedorn Temperature of AdS_5/CFT_4 via Integrability*, *Phys. Rev. Lett.* **120** (2018), no. 7 071605, [arXiv:1706.03074].

[160] T. Harmark and M. Wilhelm, *The Hagedorn temperature of AdS_5/CFT_4 at finite coupling via the Quantum Spectral Curve*, *Phys. Lett.* **B786** (2018) 53–58, [arXiv:1803.04416].

[161] D. Yamada and L. G. Yaffe, *Phase diagram of N=4 super-Yang-Mills theory with R-symmetry chemical potentials*, *JHEP* **09** (2006) 027, [hep-th/0602074].

[162] F. Benini and P. Milan, *Black Holes in 4D $\mathcal{N}$=4 Super-Yang-Mills Field Theory*, *Phys. Rev. X* **10** (2020), no. 2 021037, [arXiv:1812.09613].

[163] C. Copetti, A. Grassi, Z. Komargodski, and L. Tizzano, *Delayed Deconfinement and the Hawking-Page Transition*, arXiv:2008.04950.

[164] J. C. Myers and M. C. Ogilvie, *New phases of SU(3) and SU(4) at finite temperature*, *Phys. Rev.* **D77** (2008) 125030, [arXiv:0707.1869].

[165] M. Mussel and R. Yacoby, *The 2-loop partition function of large N gauge theories with adjoint matter on S**3*, *JHEP* **12** (2009) 005, [arXiv:0909.0407].

[166] Z.-W. Chong, M. Cvetič, H. Lü, and C. N. Pope, *Five-dimensional gauged supergravity black holes with independent rotation parameters*, *Phys. Rev. D* **72** (Aug, 2005) 041901.

[167] Z. Chong, M. Cvetic, H. Lu, and C. Pope, *Non-extremal rotating black holes in five-dimensional gauged supergravity*, *Phys. Lett. B* **644** (2007) 192–197, [hep-th/0606213].

[168] Z.-W. Chong, M. Cvetič, H. Lü, and C. N. Pope, *General nonextremal rotating black holes in minimal five-dimensional gauged supergravity*, *Phys. Rev. Lett.* **95** (Oct, 2005) 161301.

[169] M. Cvetic and S. S. Gubser, *Phases of R charged black holes, spinning branes and strongly coupled gauge theories*, *JHEP* **04** (1999) 024, [hep-th/9902195].

[170] M. Cvetič, H. Lü, and C. N. Pope, *Charged rotating black holes in five dimensional $U(1)^3$ gauged$\mathcal{N} = 2$ supergravity*, *Phys. Rev. D* **70** (Oct, 2004) 081502.

[171] S. W. Hawking and D. N. Page, *Thermodynamics of Black Holes in anti-De Sitter Space*, *Commun. Math. Phys.* **87** (1983) 577.

[172] O. Aharony and E. Witten, *Anti-de Sitter space and the center of the gauge group*, *JHEP* **11** (1998) 018, [hep-th/9807205].

[173] G. Aarts, S. Kumar, and J. Rafferty, *Holographic Roberge-Weiss Transitions*, *JHEP* **07** (2010) 056, [arXiv:1005.2947].

[174] M. Hanada, G. Ishiki, and H. Watanabe, *Partial Deconfinement*, *JHEP* **03** (2019) 145, [arXiv:1812.05494]. [Erratum: JHEP 10, 029 (2019)].

[175] D. Berenstein, *Submatrix deconfinement and small black holes in AdS*, *JHEP* **09** (2018) 054, [arXiv:1806.05729].

[176] M. Hanada, A. Jevicki, C. Peng, and N. Wintergerst, *Anatomy of Deconfinement*, *JHEP* **12** (2019) 167, [arXiv:1909.09118].

[177] M. Hanada and B. Robinson, *Partial-Symmetry-Breaking Phase Transitions*, *Phys. Rev. D* **102** (2020), no. 9 096013, [arXiv:1911.06223].

[178] M. Hanada, G. Ishiki, and H. Watanabe, *Partial deconfinement in gauge theories*, *PoS* **LATTICE2019** (2019) 055, [arXiv:1911.11465].

[179] M. Hanada, H. Shimada, and N. Wintergerst, *Color Confinement and Bose-Einstein Condensation*, arXiv:2001.10459.

[180] H. Watanabe, G. Bergner, N. Bodendorfer, S. Shiba Funai, M. Hanada, E. Rinaldi, A. Schäfer, and P. Vranas, *Partial Deconfinement at Strong Coupling on the Lattice*, arXiv:2005.04103.

[181] A. Arabi Ardehali, J. Hong, and J. T. Liu, *Asymptotic growth of the 4d $\mathcal{N} = 4$ index and partially deconfined phases*, *JHEP* **07** (2020) 073, [arXiv:1912.04169].

[182] J. Kinney, J. M. Maldacena, S. Minwalla, and S. Raju, *An Index for 4 dimensional super conformal theories*, *Commun. Math. Phys.* **275** (2007) 209–254, [hep-th/0510251].

[183] L. Rastelli and S. S. Razamat, *The supersymmetric index in four dimensions*, *J. Phys. A* **50** (2017), no. 44 443013, [arXiv:1608.02965].

[184] A. Gadde, *Lectures on the Superconformal Index*, arXiv:2006.13630.

[185] S. M. Hosseini, K. Hristov, and A. Zaffaroni, *An extremization principle for the entropy of rotating BPS black holes in AdS_5*, *JHEP* **07** (2017) 106, [arXiv:1705.05383].

[186] A. Cabo-Bizet, D. Cassani, D. Martelli, and S. Murthy, *Microscopic origin of the Bekenstein-Hawking entropy of supersymmetric AdS_5 black holes*, *JHEP* **10** (2019) 062, [arXiv:1810.11442].

[187] S. Choi, J. Kim, S. Kim, and J. Nahmgoong, *Large AdS black holes from QFT*, arXiv:1810.12067.

[188] S. Choi, J. Kim, S. Kim, and J. Nahmgoong, *Comments on deconfinement in AdS/CFT*, arXiv:1811.08646.

[189] C. Closset, H. Kim, and B. Willett, *Supersymmetric partition functions and the three-dimensional A-twist*, *JHEP* **03** (2017) 074, [arXiv:1701.03171].

[190] F. Benini and P. Milan, *A Bethe Ansatz type formula for the superconformal index*, *Commun. Math. Phys.* **376** (2020), no. 2 1413–1440, [arXiv:1811.04107].

[191] A. González Lezcano and L. A. Pando Zayas, *Microstate counting via Bethe Ansätze in the 4d $\mathcal{N} = 1$ superconformal index*, *JHEP* **03** (2020) 088, [arXiv:1907.12841].

[192] A. Lanir, A. Nedelin, and O. Sela, *Black hole entropy function for toric theories via Bethe Ansatz*, *JHEP* **04** (2020) 091, [arXiv:1908.01737].

[193] M. Honda, *Quantum Black Hole Entropy from 4d Supersymmetric Cardy formula*, *Phys. Rev. D* **100** (2019), no. 2 026008, [arXiv:1901.08091].

[194] A. Arabi Ardehali, *Cardy-like asymptotics of the 4d $\mathcal{N} = 4$ index and AdS_5 blackholes*, *JHEP* **06** (2019) 134, [arXiv:1902.06619].

[195] A. Cabo-Bizet, D. Cassani, D. Martelli, and S. Murthy, *The asymptotic growth of states of the 4d $\mathcal{N} = 1$ superconformal index*, *JHEP* **08** (2019) 120, [arXiv:1904.05865].

[196] A. Amariti, I. Garozzo, and G. Lo Monaco, *Entropy function from toric geometry*, arXiv:1904.10009.

[197] A. Cabo-Bizet and S. Murthy, *Supersymmetric phases of 4d $\mathcal{N} = 4$ SYM at large N*, *JHEP* **09** (2020) 184, [arXiv:1909.09597].

[198] A. Cabo-Bizet, D. Cassani, D. Martelli, and S. Murthy, *The large-N limit of the 4d $\mathcal{N} = 1$ superconformal index*, *JHEP* **11** (2020) 150, [arXiv:2005.10654].

[199] P. Agarwal, S. Choi, J. Kim, S. Kim, and J. Nahmgoong, *AdS black holes and finite N indices*, arXiv:2005.11240.

[200] F. Benini, E. Colombo, S. Soltani, A. Zaffaroni, and Z. Zhang, *Superconformal indices at large N and the entropy of $AdS_5 \times SE_5$ black holes*, *Class. Quant. Grav.* **37** (2020), no. 21 215021, [arXiv:2005.12308].

[201] A. González Lezcano, J. Hong, J. T. Liu, and L. A. Pando Zayas, *Sub-leading Structures in Superconformal Indices: Subdominant Saddles and Logarithmic Contributions*, arXiv:2007.12604.

[202] A. Zaffaroni, *Lectures on AdS Black Holes, Holography and Localization*, 2, 2019. arXiv:1902.07176.

[203] K. Goldstein, V. Jejjala, Y. Lei, S. van Leuven, and W. Li, *Residues, modularity, and the Cardy limit of the 4d $\mathcal{N} = 4$ superconformal index*, arXiv:2011.06605.

[204] A. Cabo-Bizet, *From multi-gravitons to Black holes: The role of complex saddles*, arXiv:2012.04815.

[205] A. Strominger and C. Vafa, *Microscopic origin of the Bekenstein-Hawking entropy*, *Phys. Lett. B* **379** (1996) 99–104, [hep-th/9601029].

[206] P. Calabrese and J. L. Cardy, *Entanglement entropy and quantum field theory*, *J. Stat. Mech.* **0406** (2004) P06002, [hep-th/0405152].

[207] S. Ryu and T. Takayanagi, *Holographic derivation of entanglement entropy from AdS/CFT*, *Phys. Rev. Lett.* **96** (2006) 181602, [hep-th/0603001].

[208] S. Ryu and T. Takayanagi, *Aspects of Holographic Entanglement Entropy*, *JHEP* **08** (2006) 045, [hep-th/0605073].

[209] V. E. Hubeny, M. Rangamani, and T. Takayanagi, *A Covariant holographic entanglement entropy proposal*, *JHEP* **07** (2007) 062, [arXiv:0705.0016].

[210] T. Nishioka, *Entanglement entropy: holography and renormalization group*, *Rev. Mod. Phys.* **90** (2018), no. 3 035007, [arXiv:1801.10352].

[211] C. Holzhey, F. Larsen, and F. Wilczek, *Geometric and renormalized entropy in conformal field theory*, *Nucl. Phys. B* **424** (1994) 443–467, [hep-th/9403108].

[212] P. Calabrese and J. L. Cardy, *Evolution of entanglement entropy in one-dimensional systems*, *J. Stat. Mech.* **0504** (2005) P04010, [cond-mat/0503393].

[213] M. Van Raamsdonk, *Building up spacetime with quantum entanglement*, *Gen. Rel. Grav.* **42** (2010) 2323–2329, [arXiv:1005.3035].

[214] Å. Folkestad and A. Dhumuntarao, *Maximal Entangling Rates from Holography*, arXiv:2211.07654.

[215] A. Kitaev and J. Preskill, *Topological entanglement entropy*, *Phys. Rev. Lett.* **96** (2006) 110404, [hep-th/0510092].

[216] M. Levin and X.-G. Wen, *Detecting Topological Order in a Ground State Wave Function*, *prl* **96** (Mar., 2006) 110405, [cond-mat/0510613].

[217] A. Hamma, R. Ionicioiu, and P. Zanardi, *Ground state entanglement and geometric entropy in the kitaev model*, *Physics Letters A* **337** (mar, 2005) 22–28.

[218] C. H. Bennett and S. J. Wiesner, *Communication via one- and two-particle operators on einstein-podolsky-rosen states*, *Phys. Rev. Lett.* **69** (Nov, 1992) 2881–2884.

[219] C. H. Bennett, G. Brassard, C. Crépeau, R. Jozsa, A. Peres, and W. K. Wootters, *Teleporting an unknown quantum state via dual classical and einstein-podolsky-rosen channels*, *Phys. Rev. Lett.* **70** (Mar, 1993) 1895–1899.

[220] C. H. Bennett and G. Brassard, *Quantum cryptography: Public key distribution and coin tossing*, *Theoretical Computer Science* **560** (dec, 2014) 7–11.

[221] L. Bombelli, R. K. Koul, J. Lee, and R. D. Sorkin, *Quantum source of entropy for black holes*, *Phys. Rev. D* **34** (Jul, 1986) 373–383.

[222] D. N. Page, *Information in black hole radiation*, *Phys. Rev. Lett.* **71** (1993) 3743–3746, [hep-th/9306083].

[223] A. C. Wall, *A proof of the generalized second law for rapidly changing fields and arbitrary horizon slices*, *Phys. Rev. D* **85** (2012) 104049, [arXiv:1105.3445]. [Erratum: Phys.Rev.D 87, 069904 (2013)].

[224] A. C. Wall, *Maximin Surfaces, and the Strong Subadditivity of the Covariant Holographic Entanglement Entropy*, *Class. Quant. Grav.* **31** (2014), no. 22 225007, [arXiv:1211.3494].

[225] A. Almheiri, D. Marolf, J. Polchinski, and J. Sully, *Black Holes: Complementarity or Firewalls?*, *JHEP* **02** (2013) 062, [arXiv:1207.3123].

[226] J. Maldacena and L. Susskind, *Cool horizons for entangled black holes*, *Fortsch. Phys.* **61** (2013) 781–811, [arXiv:1306.0533].

[227] T. Faulkner, A. Lewkowycz, and J. Maldacena, *Quantum corrections to holographic entanglement entropy*, *JHEP* **11** (2013) 074, [arXiv:1307.2892].

[228] N. Engelhardt and A. C. Wall, *Quantum Extremal Surfaces: Holographic Entanglement Entropy beyond the Classical Regime*, *JHEP* **01** (2015) 073, [arXiv:1408.3203].

[229] R. Bousso, Z. Fisher, S. Leichenauer, and A. C. Wall, *Quantum focusing conjecture*, *Phys. Rev. D* **93** (2016), no. 6 064044, [arXiv:1506.02669].

[230] H. Casini and M. Huerta, *A Finite entanglement entropy and the c-theorem*, *Phys. Lett. B* **600** (2004) 142–150, [hep-th/0405111].

[231] H. Casini and M. Huerta, *A c-theorem for the entanglement entropy*, *J. Phys. A* **40** (2007) 7031–7036, [cond-mat/0610375].

[232] I. R. Klebanov, D. Kutasov, and A. Murugan, *Entanglement as a probe of confinement*, *Nucl. Phys. B* **796** (2008) 274–293, [arXiv:0709.2140].

[233] P. V. Buividovich and M. I. Polikarpov, *Numerical study of entanglement entropy in SU(2) lattice gauge theory*, *Nucl. Phys. B* **802** (2008) 458–474, [arXiv:0802.4247].

[234] R. C. Myers and A. Sinha, *Seeing a c-theorem with holography*, *Phys. Rev. D* **82** (2010) 046006, [arXiv:1006.1263].

[235] R. C. Myers and A. Sinha, *Holographic c-theorems in arbitrary dimensions*, *JHEP* **01** (2011) 125, [arXiv:1011.5819].

[236] H. Casini and M. Huerta, *On the RG running of the entanglement entropy of a circle*, *Phys. Rev. D* **85** (2012) 125016, [arXiv:1202.5650].

[237] S. N. Solodukhin, *The a-theorem and entanglement entropy*, arXiv:1304.4411.

[238] V. Balasubramanian, A. Bernamonti, J. de Boer, N. Copland, B. Craps, E. Keski-Vakkuri, B. Muller, A. Schafer, M. Shigemori, and W. Staessens, *Thermalization of Strongly Coupled Field Theories*, *Phys. Rev. Lett.* **106** (2011) 191601, [arXiv:1012.4753].

[239] V. Balasubramanian, A. Bernamonti, J. de Boer, N. Copland, B. Craps, E. Keski-Vakkuri, B. Muller, A. Schafer, M. Shigemori, and W. Staessens, *Holographic Thermalization*, *Phys. Rev. D* **84** (2011) 026010, [arXiv:1103.2683].

[240] H. Liu and S. J. Suh, *Entanglement Tsunami: Universal Scaling in Holographic Thermalization*, *Phys. Rev. Lett.* **112** (2014) 011601, [arXiv:1305.7244].

[241] H. Liu and S. J. Suh, *Entanglement growth during thermalization in holographic systems*, *Phys. Rev. D* **89** (2014), no. 6 066012, [arXiv:1311.1200].

[242] K. Van Acoleyen, M. Mariën, and F. Verstraete, *Entanglement rates and area laws*, *Phys. Rev. Lett.* **111** (Oct, 2013) 170501.

[243] S. Bravyi, *Upper bounds on entangling rates of bipartite hamiltonians*, *Phys. Rev. A* **76** (Nov, 2007) 052319.

[244] T. Hartman and N. Afkhami-Jeddi, *Speed Limits for Entanglement*, arXiv:1512.02695.

[245] H. Casini, H. Liu, and M. Mezei, *Spread of entanglement and causality*, *JHEP* **07** (2016) 077, [arXiv:1509.05044].

[246] M. Mezei, *On entanglement spreading from holography*, *JHEP* **05** (2017) 064, [arXiv:1612.00082].

[247] D. Marolf and A. C. Wall, *State-Dependent Divergences in the Entanglement Entropy*, *JHEP* **10** (2016) 109, [arXiv:1607.01246].

[248] S. Kundu and J. F. Pedraza, *Spread of entanglement for small subsystems in holographic CFTs*, *Phys. Rev. D* **95** (2017), no. 8 086008, [arXiv:1602.05934].

[249] V. Balasubramanian and S. F. Ross, *Holographic particle detection*, *Phys. Rev. D* **61** (2000) 044007, [hep-th/9906226].

[250] P. Calabrese and J. L. Cardy, *Time-dependence of correlation functions following a quantum quench*, *Phys. Rev. Lett.* **96** (2006) 136801, [cond-mat/0601225].

[251] P. Calabrese and J. Cardy, *Quantum Quenches in Extended Systems*, *J. Stat. Mech.* **0706** (2007) P06008, [arXiv:0704.1880].

[252] L. Susskind, *Why do Things Fall?*, arXiv:1802.01198.

[253] J. L. F. Barbón, J. Martín-García, and M. Sasieta, *Momentum/Complexity Duality and the Black Hole Interior*, *JHEP* **07** (2020) 169, [arXiv:1912.05996].

[254] J. L. F. Barbon, J. Martin-Garcia, and M. Sasieta, *Proof of a Momentum/Complexity Correspondence*, *Phys. Rev. D* **102** (2020), no. 10 101901, [arXiv:2006.06607].

[255] J. L. F. Barbon, J. Martin-Garcia, and M. Sasieta, *A Generalized Momentum/Complexity Correspondence*, *JHEP* **04** (2021) 250, [arXiv:2012.02603].

[256] N. Engelhardt and A. C. Wall, *Coarse Graining Holographic Black Holes*, *JHEP* **05** (2019) 160, [arXiv:1806.01281].

[257] V. Balasubramanian and P. Kraus, *A Stress tensor for Anti-de Sitter gravity*, *Commun. Math. Phys.* **208** (1999) 413–428, [hep-th/9902121].

[258] J. Abajo-Arrastia, J. Aparicio, and E. Lopez, *Holographic Evolution of Entanglement Entropy*, *JHEP* **11** (2010) 149, [arXiv:1006.4090].

[259] W. Baron, D. Galante, and M. Schvellinger, *Dynamics of holographic thermalization*, *JHEP* **03** (2013) 070, [arXiv:1212.5234].

[260] E. Caceres and A. Kundu, *Holographic Thermalization with Chemical Potential*, *JHEP* **09** (2012) 055, [arXiv:1205.2354].

[261] D. Galante and M. Schvellinger, *Thermalization with a chemical potential from AdS spaces*, *JHEP* **07** (2012) 096, [arXiv:1205.1548].

[262] S. H. Shenker and D. Stanford, *Black holes and the butterfly effect*, *JHEP* **03** (2014) 067, [arXiv:1306.0622].

[263] S. H. Shenker and D. Stanford, *Multiple Shocks*, *JHEP* **12** (2014) 046, [arXiv:1312.3296].

[264] Y.-Z. Li, S.-F. Wu, Y.-Q. Wang, and G.-H. Yang, *Linear growth of entanglement entropy in holographic thermalization captured by horizon interiors and mutual information*, *JHEP* **09** (2013) 057, [arXiv:1306.0210].

[265] I. Aref'eva, A. Bagrov, and A. S. Koshelev, *Holographic Thermalization from Kerr-AdS*, *JHEP* **07** (2013) 170, [arXiv:1305.3267].

[266] P. Caputa, G. Mandal, and R. Sinha, *Dynamical entanglement entropy with angular momentum and U(1) charge*, *JHEP* **11** (2013) 052, [arXiv:1306.4974].

[267] T. Ugajin, *Two dimensional quantum quenches and holography*, arXiv:1311.2562.

[268] M. Alishahiha, M. R. Mohammadi Mozaffar, and M. R. Tanhayi, *On the Time Evolution of Holographic n-partite Information*, *JHEP* **09** (2015) 165, [arXiv:1406.7677].

[269] P. Fonda, L. Franti, V. Keränen, E. Keski-Vakkuri, L. Thorlacius, and E. Tonni, *Holographic thermalization with Lifshitz scaling and hyperscaling violation*, *JHEP* **08** (2014) 051, [arXiv:1401.6088].

[270] V. Keranen, H. Nishimura, S. Stricker, O. Taanila, and A. Vuorinen, *Dynamics of gravitational collapse and holographic entropy production*, *Phys. Rev. D* **90** (2014), no. 6 064033, [arXiv:1405.7015].

[271] M. Alishahiha, A. Faraji Astaneh, and M. R. Mohammadi Mozaffar, *Thermalization in backgrounds with hyperscaling violating factor*, *Phys. Rev. D* **90** (2014), no. 4 046004, [arXiv:1401.2807].

[272] E. Caceres, A. Kundu, J. F. Pedraza, and D.-L. Yang, *Weak Field Collapse in AdS: Introducing a Charge Density*, *JHEP* **06** (2015) 111, [arXiv:1411.1744].

[273] A. Buchel, R. C. Myers, and A. van Niekerk, *Nonlocal probes of thermalization in holographic quenches with spectral methods*, *JHEP* **02** (2015) 017, [arXiv:1410.6201]. [Erratum: JHEP 07, 137 (2015)].

[274] D. Stanford and L. Susskind, *Complexity and Shock Wave Geometries*, *Phys. Rev. D* **90** (2014), no. 12 126007, [arXiv:1406.2678].

[275] K. Babaei Velni, M. R. Mohammadi Mozaffar, and M. H. Vahidinia, *Evolution of entanglement wedge cross section following a global quench*, *JHEP* **08** (2020) 129, [arXiv:2005.05673].

[276] S. Leichenauer and M. Moosa, *Entanglement Tsunami in (1+1)-Dimensions*, *Phys. Rev. D* **92** (2015) 126004, [arXiv:1505.04225].

[277] C. Ecker, D. Grumiller, and S. A. Stricker, *Evolution of holographic entanglement entropy in an anisotropic system*, *JHEP* **07** (2015) 146, [arXiv:1506.02658].

[278] V. Ziogas, *Holographic mutual information in global Vaidya-BTZ spacetime*, *JHEP* **09** (2015) 114, [arXiv:1507.00306].

[279] K. A. Sohrabi, *Inhomogeneous Thermal Quenches*, *Phys. Rev. D* **96** (2017), no. 2 026012, [arXiv:1509.00245].

[280] E. Caceres, M. Sanchez, and J. Virrueta, *Holographic Entanglement Entropy in Time Dependent Gauss-Bonnet Gravity*, *JHEP* **09** (2017) 127, [arXiv:1512.05666].

[281] M. Rangamani, M. Rozali, and A. Vincart-Emard, *Dynamics of Holographic Entanglement Entropy Following a Local Quench*, *JHEP* **04** (2016) 069, [arXiv:1512.03478].

[282] D. Roychowdhury, *Holographic thermalization from nonrelativistic branes*, *Phys. Rev. D* **93** (2016), no. 10 106008, [arXiv:1601.00136].

[283] C. Ecker, D. Grumiller, P. Stanzer, S. A. Stricker, and W. van der Schee, *Exploring nonlocal observables in shock wave collisions*, *JHEP* **11** (2016) 054, [arXiv:1609.03676].

[284] A. O'Bannon, J. Probst, R. Rodgers, and C. F. Uhlemann, *First law of entanglement rates from holography*, *Phys. Rev. D* **96** (2017), no. 6 066028, [arXiv:1612.07769].

[285] S. F. Lokhande, G. W. J. Oling, and J. F. Pedraza, *Linear response of entanglement entropy from holography*, *JHEP* **10** (2017) 104, [arXiv:1705.10324].

[286] R. C. Myers, M. Rozali, and B. Way, *Holographic Quenches in a Confined Phase*, *J. Phys. A* **50** (2017), no. 49 494002, [arXiv:1706.02438].

[287] I. Y. Aref'eva, M. A. Khramtsov, and M. D. Tikhanovskaya, *Thermalization after holographic bilocal quench*, *JHEP* **09** (2017) 115, [arXiv:1706.07390].

[288] V. Jahnke, *Delocalizing entanglement of anisotropic black branes*, *JHEP* **01** (2018) 102, [arXiv:1708.07243].

[289] M. Flory, J. Erdmenger, D. Fernandez, E. Megias, A.-K. Straub, and P. Witkowski, *Time dependence of entanglement for steady state formation in AdS_3/CFT_2*, *J. Phys. Conf. Ser.* **942** (2017), no. 1 012010, [arXiv:1709.08614].

[290] D. Ávila, V. Jahnke, and L. Patiño, *Chaos, Diffusivity, and Spreading of Entanglement in Magnetic Branes, and the Strengthening of the Internal Interaction*, *JHEP* **09** (2018) 131, [arXiv:1805.05351].

[291] H. Ghaffarnejad, E. Yaraie, and M. Farsam, *Holographic thermalization in AdS-Gauss-Bonnet gravity for small entangled regions*, *Gen. Rel. Grav.* **51** (2019), no. 1 10, [arXiv:1806.05976].

[292] W. Fischler, V. Jahnke, and J. F. Pedraza, *Chaos and entanglement spreading in a non-commutative gauge theory*, *JHEP* **11** (2018) 072, [arXiv:1808.10050]. [Erratum: JHEP 02, 149 (2021)].

[293] M. Mezei, *Membrane theory of entanglement dynamics from holography*, *Phys. Rev. D* **98** (2018), no. 10 106025, [arXiv:1803.10244].

[294] J. Kudler-Flam, I. MacCormack, and S. Ryu, *Holographic entanglement contour, bit threads, and the entanglement tsunami*, *J. Phys. A* **52** (2019), no. 32 325401, [arXiv:1902.04654].

[295] J. Couch, S. Eccles, P. Nguyen, B. Swingle, and S. Xu, *Speed of quantum information spreading in chaotic systems*, *Phys. Rev. B* **102** (2020), no. 4 045114, [arXiv:1908.06993].

[296] Y. Ling, Y. Liu, and Z.-Y. Xian, *Entanglement entropy of an annulus in holographic thermalization*, *Chin. Phys. C* **44** (2020), no. 2 023101, [arXiv:1911.03716].

[297] M. Mezei and W. van der Schee, *Black holes often saturate entanglement entropy the fastest*, *Phys. Rev. Lett.* **124** (2020), no. 20 201601, [arXiv:2001.03172].

[298] K. Goto, M. Nozaki, K. Tamaoka, M. T. Tan, and S. Ryu, *Non-Equilibrating a Black Hole with Inhomogeneous Quantum Quench*, arXiv:2112.14388.

[299] H. Liu and M. Mezei, *A Refinement of entanglement entropy and the number of degrees of freedom*, *JHEP* **04** (2013) 162, [arXiv:1202.2070].

[300] H. Liu and M. Mezei, *Probing renormalization group flows using entanglement entropy*, *JHEP* **01** (2014) 098, [arXiv:1309.6935].

[301] N. Bao, C. Cao, S. Fischetti, and C. Keeler, *Towards Bulk Metric Reconstruction from Extremal Area Variations*, *Class. Quant. Grav.* **36** (2019), no. 18 185002, [arXiv:1904.04834].

[302] S. Fischetti and T. Wiseman, *A Bound on Holographic Entanglement Entropy from Inverse Mean Curvature Flow*, *Class. Quant. Grav.* **34** (2017), no. 12 125005, [arXiv:1612.04373].

[303] C. Fefferman and C. R. Graham, *Conformal invariants*, *Elie Cartan et les Mathématiques d'aujourdhui* (Astérisque) p. 95. 1985.

[304] C. Graham and J. M. Lee, *Einstein metrics with prescribed conformal infinity on the ball*, *Advances in Mathematics* **87** (1991), no. 2 186–225.

[305] C. R. Graham and E. Witten, *Conformal anomaly of submanifold observables in AdS / CFT correspondence*, *Nucl. Phys. B* **546** (1999) 52–64, [hep-th/9901021].

[306] N. Engelhardt and Å. Folkestad, *General bounds on holographic complexity*, *JHEP* **01** (2022) 040, [arXiv:2109.06883].

[307] R. Geroch, *Energy extraction**, *Annals of the New York Academy of Sciences* **224** (1973), no. 1 108–117.

[308] P. Jang and R. Wald *J. Math. Phys.* **18** (1977) 41.

[309] X. Wang, *The Mass of Asymptotically Hyperbolic Manifolds*, *Journal of Differential Geometry* **57** (2001), no. 2 273 – 299.

[310] G. Huisken and T. Ilmanen, *The Inverse Mean Curvature Flow and the Riemannian Penrose Inequality*, *Journal of Differential Geometry* **59** (2001), no. 3 353 – 437.

[311] S. W. Hawking, *Gravitational radiation in an expanding universe*, *Journal of Mathematical Physics* **9** (1968), no. 4 598–604, [https://doi.org/10.1063/1.1664615].

[312] Å. Folkestad, *The Penrose Inequality as a Constraint on the Low Energy Limit of Quantum Gravity*, arXiv:2209.00013.

[313] S. A. Hayward, *Gravitational energy in spherical symmetry*, *Phys. Rev. D* **53** (1996) 1938–1949, [gr-qc/9408002].

[314] H. Bray, S. Hayward, M. Mars, and W. Simon, *Generalized inverse mean curvature flows in spacetime*, *Commun. Math. Phys.* **272** (2007) 119–138, [gr-qc/0603014].

[315] N. Engelhardt and S. Fischetti, *Covariant Constraints on Hole-ography*, *Class. Quant. Grav.* **32** (2015), no. 19 195021, [arXiv:1507.00354].

[316] R. Bousso, *Holography in general space-times*, *JHEP* **06** (1999) 028, [hep-th/9906022].

[317] J. D. Brown and M. Henneaux, *Central Charges in the Canonical Realization of Asymptotic Symmetries: An Example from Three-Dimensional Gravity*, *Commun. Math. Phys.* **104** (1986) 207–226.

[318] J. M. Maldacena, *Wilson loops in large N field theories*, *Phys. Rev. Lett.* **80** (1998) 4859–4862, [hep-th/9803002].

[319] S.-J. Rey and J.-T. Yee, *Macroscopic strings as heavy quarks in large N gauge theory and anti-de Sitter supergravity*, *Eur. Phys. J. C* **22** (2001) 379–394, [hep-th/9803001].

[320] N. Engelhardt and Å. Folkestad, *Negative complexity of formation: the compact dimensions strike back*, *JHEP* **07** (2022) 031, [arXiv:2111.14897].

[321] T. Hertog, G. T. Horowitz, and K. Maeda, *Negative energy density in Calabi-Yau compactifications*, *JHEP* **05** (2003) 060, [hep-th/0304199].

[322] W. Boucher, *Positive energy without supersymmetry*, *Nuclear Physics B* **242** (1984), no. 2 282–296.

[323] P. Townsend, *Positive energy and the scalar potential in higher dimensional (super) gravity theories*, *Physics Letters B* **148** (1984), no. 1 55–59.

[324] M. Cvetic, M. J. Duff, P. Hoxha, J. T. Liu, H. Lu, J. X. Lu, R. Martinez-Acosta, C. N. Pope, H. Sati, and T. A. Tran, *Embedding AdS black holes in ten-dimensions and eleven-dimensions*, *Nucl. Phys. B* **558** (1999) 96–126, [hep-th/9903214].

[325] H. Lu and C. N. Pope, *Exact embedding of N=1, D = 7 gauged supergravity in D = 11*, *Phys. Lett. B* **467** (1999) 67–72, [hep-th/9906168].

[326] H. Lu, C. N. Pope, and T. A. Tran, *Five-dimensional N=4, SU(2) x U(1) gauged supergravity from type IIB*, *Phys. Lett. B* **475** (2000) 261–268, [hep-th/9909203].

[327] M. Cvetic, H. Lu, and C. N. Pope, *Gauged six-dimensional supergravity from massive type IIA*, *Phys. Rev. Lett.* **83** (1999) 5226–5229, [hep-th/9906221].

[328] P. Breitenlohner and D. Z. Freedman, *Positive energy in anti-de Sitter backgrounds AND gauged extended supergravity*, *Phys. Lett.* **B115** (1982) 197.

[329] P. Breitenlohner and D. Z. Freedman, *Stability in Gauged Extended Supergravity*, *Annals Phys.* **144** (1982) 249.

[330] A. C. Wall, *Testing the Generalized Second Law in 1+1 dimensional Conformal Vacua: An Argument for the Causal Horizon*, *Phys. Rev. D* **85** (2012) 024015, [arXiv:1105.3520].

[331] R. Bousso, Z. Fisher, J. Koeller, S. Leichenauer, and A. C. Wall, *Proof of the Quantum Null Energy Condition*, *Phys. Rev. D* **93** (2016), no. 2 024017, [arXiv:1509.02542].

[332] C. Akers, J. Koeller, S. Leichenauer, and A. Levine, *Geometric Constraints from Subregion Duality Beyond the Classical Regime*, arXiv:1610.08968.

[333] J. Koeller and S. Leichenauer, *Holographic Proof of the Quantum Null Energy Condition*, *Phys. Rev. D* **94** (2016), no. 2 024026, [arXiv:1512.06109].

[334] S. Balakrishnan, T. Faulkner, Z. U. Khandker, and H. Wang, *A General Proof of the Quantum Null Energy Condition*, *JHEP* **09** (2019) 020, [arXiv:1706.09432].

[335] M. Mezei and J. Virrueta, *The Quantum Null Energy Condition and Entanglement Entropy in Quenches*, arXiv:1909.00919.

[336] P. A. R. Jones and M. Taylor, *Entanglement entropy in top-down models*, *JHEP* **08** (2016) 158, [arXiv:1602.04825].

[337] T. Hertog and G. T. Horowitz, *Towards a big crunch dual*, *JHEP* **07** (2004) 073, [hep-th/0406134].

[338] M. Henneaux, C. Martinez, R. Troncoso, and J. Zanelli, *Asymptotically anti-de Sitter spacetimes and scalar fields with a logarithmic branch*, *Phys. Rev. D* **70** (2004) 044034, [hep-th/0404236].

[339] M. Henneaux, C. Martinez, R. Troncoso, and J. Zanelli, *Asymptotic behavior and Hamiltonian analysis of anti-de Sitter gravity coupled to scalar fields*, *Annals Phys.* **322** (2007) 824–848, [hep-th/0603185].

[340] T. Hertog and K. Maeda, *Black holes with scalar hair and asymptotics in $N = 8$ supergravity*, *JHEP* **07** (2004) 051, [hep-th/0404261].

[341] T. Hartman and J. Maldacena, *Time Evolution of Entanglement Entropy from Black Hole Interiors*, *JHEP* **05** (2013) 014, [arXiv:1303.1080].

[342] Z. Li and R.-Q. Yang, *Upper bounds of holographic entanglement entropy growth rate for thermofield double states*, *JHEP* **10** (2022) 072, [arXiv:2205.15154].

[343] R. Schoen and S. T. Yau, *Proof of the positive mass theorem. ii*, *Comm. Math. Phys.* **79** (1981), no. 2 231–260.

[344] E. Witten, *A Simple Proof of the Positive Energy Theorem*, *Commun. Math. Phys.* **80** (1981) 381.

[345] D. Carmi, S. Chapman, H. Marrochio, R. C. Myers, and S. Sugishita, *On the Time Dependence of Holographic Complexity*, *JHEP* **11** (2017) 188, [arXiv:1709.10184].

[346] R. S. Hamilton, *Three-manifolds with positive Ricci curvature*, *J. Differential Geom.* **17** (1982), no. 2 255–306.

[347] G. Perelman, *The entropy formula for the Ricci flow and its geometric applications*, *ArXiv Mathematics e-prints* (Nov, 2002) [math/0211159].

[348] G. Perelman, *Ricci flow with surgery on three-manifolds*, *arXiv Mathematics e-prints* (Mar., 2003) math/0303109, [math/0303109].

[349] P. Topping, *Lectures on the Ricci Flow*. London Mathematical Society Lecture Note Series. Cambridge University Press, 2006.

[350] M. Headrick and T. Wiseman, *Ricci flow and black holes*, *Class. Quant. Grav.* **23** (2006) 6683–6708, [hep-th/0606086].

[351] D. Friedan, *Nonlinear models in $2 + \epsilon$ dimensions*, *Phys. Rev. Lett.* **45** (Sep, 1980) 1057–1060.

[352] E. Woolgar, *Some Applications of Ricci Flow in Physics*, *Can. J. Phys.* **86** (2008) 645–651, [arXiv:0708.2144].

[353] S. Jackson, R. Pourhasan, and H. Verlinde, *Geometric RG Flow*, arXiv:1312.6914.

[354] P. Figueras, J. Lucietti, and T. Wiseman, *Ricci solitons, Ricci flow, and strongly coupled CFT in the Schwarzschild Unruh or Boulware vacua*, *Class. Quant. Grav.* **28** (2011) 215018, [arXiv:1104.4489].

[355] V. Shyam, *Finite Cutoff AdS_5 Holography and the Generalized Gradient Flow*, *JHEP* **12** (2018) 086, [arXiv:1808.07760].

[356] E. P. Verlinde and H. L. Verlinde, *RG flow, gravity and the cosmological constant*, *JHEP* **05** (2000) 034, [hep-th/9912018].

[357] M. Visser, *How to Wick rotate generic curved spacetime*, arXiv:1702.05572.

[358] S. W. Hawking, *EUCLIDEAN QUANTUM GRAVITY*, *NATO Sci. Ser. B* **44** (1979) 145.

[359] S. W. Hawking, *THE PATH INTEGRAL APPROACH TO QUANTUM GRAVITY*, pp. 746–789. 1980.

[360] P. O. Mazur and E. Mottola, *The Gravitational Measure, Solution of the Conformal Factor Problem and Stability of the Ground State of Quantum Gravity*, *Nucl. Phys. B* **341** (1990) 187–212.

Appendix A

Appendix

A.1 Spherical Reduction

We review the dimensional reduction procedure we employ to obtain Eqn. (2.40) in detail. Consider Einstein gravity coupled to a cosmological constant with additional matter degrees of freedom. The bulk action is

$$\mathcal{I}_{\text{bulk}} = -\frac{1}{16\pi}\int \left[\tilde{R} - 2\Lambda - \mathcal{L}\right]\sqrt{-\tilde{g}}\mathrm{d}^{d+2}x \tag{A.1}$$

where $\mathcal{L}$ is the matter Lagrangian, $\Lambda = -d(d+1)/2\ell^2$ is the cosmological constant, and $\tilde{g}$ is the metric in $(d+2)$-dimensions with Ricci curvature $\tilde{R}$. Evaluating the action on-shell leads to well known infinite volume divergences [31, 32, 43] and hence the theory must be regulated with additional surface terms given by

$$\mathcal{I} = \mathcal{I}_{\text{bulk}}[\tilde{g}] + \mathcal{I}_{\text{surf}}[\tilde{h}] - \mathcal{I}_{\text{ct}}[\tilde{h}] \tag{A.2}$$

where the induced metric on the boundary is defined by $\tilde{h}_{MN} = \tilde{g}_{MN} - \tilde{n}_M\tilde{n}_N$ with $\tilde{n}_M$ being the outward pointing unit normal. The remaining surface and counterterm actions (up to $d = 6$) are defined on a spacelike hypersurface via

$$\mathcal{I}_{\text{surf}} = -\frac{1}{8\pi}\int \left[\tilde{\mathcal{K}} + 2\tilde{n}_M F^{MN}A_N\right]\sqrt{-\tilde{h}}\mathrm{d}^{d+1}x \tag{A.3}$$

$$\mathcal{I}_{\text{ct}} = -\frac{1}{8\pi}\int \left[\frac{d}{\ell} + \frac{\ell c_1(d)}{2(d-1)}\tilde{\mathcal{R}} + \frac{\ell^3 c_2(d)}{2(d-1)^2}\times \left(\tilde{\mathcal{R}}^{MN}\tilde{\mathcal{R}}_{MN} - \frac{d+1}{4d}\tilde{\mathcal{R}}^2\right)\right]\sqrt{-\tilde{h}}\mathrm{d}^{d+1}x \tag{A.4}$$

where $\tilde{\mathcal{K}}_{MN} = (1/2)\tilde{n}_{(M;N)}$ and $\tilde{\mathcal{R}}_{MN}$ are the extrinsic and Ricci curvatures of the boundary. The coefficients $c_i(d)$ are present to regulate Casimir contributions when computing the on-shell action for black string geometries.

We will consider metrics of the form

$$\mathrm{d}s^2_{d+2} = \tilde{g}_{MN}\mathrm{d}x^M\mathrm{d}x^N = g_{ab}\mathrm{d}x^a\mathrm{d}x^b + \psi(x^a)^2\mathrm{d}\Omega_2^2 \tag{A.5}$$

and study compactifications of the round S^2. Note that these metrics are solutions to Eqn. (A.1). To see this, consider first $d = 2$ and $\mathcal{L} = F^2$. Then the static, spherically symmetric, charged black hole solution is the RN-AdS$_4$ with $\psi = r$. Note that when $d = 3$, the horizon has the topology $S^2 \times S^1$ or $S^2 \times \mathbb{R}$ corresponding to a closed or extended black string. Recently, homogeneous asymptotically AdS$_n \times \mathbb{R}^p$ black strings have been stabilized using p minimally coupled scalar fields that depend on the extended p-directions [55]. We consider here $p = 1$ in order to support inhomogeneous, asymptotically AdS, charged black strings in $d = 3$ which admit horizon topologies $S^2 \times \mathbb{R}$ (or S^1).

We are now in a position to perform a consistent truncation of the theory along the S^2 of the horizon to d-dimensions. To do so, one further requires the data

$$\sqrt{-\tilde{g}} = \psi^2 \det(\Omega_2)\sqrt{-g}, \tag{A.6}$$

$$\tilde{R} = R + \frac{2}{\psi^2} - \frac{4\Box\psi}{\psi} - \frac{2(\nabla\psi)^2}{\psi^2}, \tag{A.7}$$

$$\sqrt{-\tilde{h}} = \psi^2 \det(\Omega_2)\sqrt{-h}, \tag{A.8}$$

$$\tilde{\mathcal{K}} = \mathcal{K} + \frac{2}{\psi}\sqrt{-g}\,\tilde{n}^a\nabla_a\psi, \tag{A.9}$$

$$\tilde{\mathcal{R}}^{MN}\tilde{\mathcal{R}}_{MN} = \frac{1}{2}\tilde{\mathcal{R}}^2 = \frac{2}{\psi^4}. \tag{A.10}$$

where the derivative operators are computed on the base g_{ab}, $\mathcal{K} = n^a_{;a}$, and $\tilde{n}_a = n_a$. Using this data, the spherical directions and the surface term in $\tilde{R}$ can be integrated away. The effective bulk theory is

$$\mathcal{I}_{\text{bulk}} = -\int \left[\frac{1}{2}(\nabla\psi)^2 + \frac{\psi^2}{4}(R - 2\Lambda - \mathcal{L}) + \frac{\lambda}{2}\right]\sqrt{-g}\mathrm{d}^d x. \tag{A.11}$$

where $\lambda = 1$ is related to the curvature of the round unit S^2. The remaining surface and counterterm actions

$$\mathcal{I}_{\text{surf}} = -\frac{1}{2}\int \psi^2\Big[\mathcal{K} + 2n_a F^{ab}A_b\Big]\sqrt{-h}\mathrm{d}^{d-1}x, \tag{A.12}$$

$$\mathcal{I}_{\text{ct}} = -\frac{1}{2}\int \psi^2\left[\frac{d}{\ell} + \frac{\ell}{(d-1)}\frac{c_1(d)}{\psi^2}\right. \\ \left. + \frac{\ell^3}{2d(d-1)^2}\frac{c_2(d)}{\psi^4}\right]\sqrt{-h}\mathrm{d}^{d-1}x. \tag{A.13}$$

guarantee that the total action is finite when computing the value on-shell. For $d = 2, 3$, the coefficients take the form

$$c_1(d) = \frac{d}{2}, \qquad c_2(d) = -\left(\frac{d-2}{2}\right)\left(\frac{d}{d-1}\right)^2. \tag{A.14}$$

This choice naturally eliminates any additional Casimir contributions along the non-compact directions for $d \leq 6$.

A.2 Metric Perturbations

After the scalar perturbations decouple, the metric perturbation become trace free $\bar{g}^{ab}H_{ab} = 0$ which we may use to set the function $K(r)$. Performing the KK compactification allows us to decompose the metric perturbations into a scalar part h_{zz}, a vector part $h_{\mu z}$, and a tensor part $h_{\mu\nu}$. It is straightforward to show that no unstable modes exist within the scalar and vector sectors [59, 62] which meet the criteria of being well behaved at the radial boundary and the future event horizon (see [60] for an indepth discussion). The metric perturbations in Eqn. (8) then consists of linear, coupled, second order ODEs for (h_{tt}, h_{rr}, h_{tr}). By taking the combination $h_{\pm} = \frac{h_{tt}}{V} \pm V h_{rr}$, we find an algebraic relation for h_+ and two first order linear ODEs for the perturbations (h_-, h_{tr})

$$\begin{aligned} h_+ \frac{V}{2}\left[m_n^2 + \frac{(d-4)(d-3)(1-V)}{2r^2} - \frac{(d+1)\Lambda_{\rm bdy}}{d-3}\right] = \\ h_-\Bigg[\Omega^2 + \frac{m_n^2 V}{2} + \frac{(d-4)}{4r^2}\left(V^2 + (d-5)V - (d-4)\right) \\ + \frac{\Lambda_{\rm bdy}}{(d-3)}\left((d-4) - \frac{\Lambda_{\rm bdy} r^2}{(d-3)} - \frac{(d+3)V}{2}\right)\Bigg] \\ + h_{tr}\frac{V}{r}\Bigg[\frac{2(d-4)\Lambda_{\rm bdy}}{(d-3)\Omega} - \frac{4\Lambda_{\rm bdy}^2 r^2}{(d-3)^2\Omega} + \frac{\Lambda_{\rm bdy} m_n^2 r^2}{(d-3)\Omega} - \frac{2(d-2)\Lambda_{\rm bdy} V}{(d-3)\Omega} \\ - \frac{m_n^2(-(d-2)V + d - 4)}{2\Omega} - (d-3)\Omega\Bigg]. \end{aligned} \tag{A.15}$$

$$h_-'(r) = \frac{h_{tr}}{\Omega}\left(m_n^2 - \frac{4\Lambda_{\rm bdy}}{d-3}\right) + \frac{h_-}{2rV}\left((d-4) + (5-2d)V - \frac{2\Lambda_{\rm bdy} r^2}{d-3}\right) + \frac{(d-3)h_+}{2r} \tag{A.16}$$

$$h_{tr}' = (h_- + h_+)\frac{\Omega}{2V} - \frac{h_{tr}}{rV}\left((d-4) + V - \frac{2\Lambda_{\rm bdy} r^2}{d-3}\right) \tag{A.17}$$

As a consistency check, the limit where $(\Lambda_{\rm bulk}, \Lambda_{\rm bdy}) \to 0$ reduces the system (h_+, h_-, h_{tr}) to [59] and we are able to reproduce the classical instability of Schwarzschild black strings. Via the scaling $r \to \ell_{d-1} u$, $\Omega \to \ell_{d-1}^{-1}\omega$, $m_n \to \ell_{d-1}^{-1} k_n$, and after some algebraic manipulations, we find a single second order ODE for h_{tr} of the form

$$\mathfrak{A}(u)H''(u) + \mathfrak{B}(u)\frac{H''(u)}{u} + \mathfrak{C}(u)\frac{H(u)}{u^2 V(u)^2} = 0 \tag{A.18}$$

where $V(u) = 1 - (1+u_+^2)(u_+/u)^{d-4} + u^2$, $u_+ \ll 1$ is used in the numerical simulation, and the coefficient functions are

$$\begin{aligned} \mathfrak{A}(u) = (d-4)^2 V(u)^2 - 2V(u)\left(u^2\left(d^2 + 2k_n^2 - 4\right) + (d-4)^2\right) \\ + \left((d-2)u^2 + d - 4\right)^2 - 4u^2\omega^2 \end{aligned}$$

$$
\begin{aligned}
\mathfrak{B}(u) =& V(u)\left(u^2\left(4(d-5)k_n^2+(d-2)(d(3d-14)-4)\right)+3(d-4)^2V(u)+3(d-6)(d-4)^2\right)\\
&+4(2d-9)u^2\omega^2-\left((d-2)u^2+d-4\right)\left(u^2\left((d-2)(6d+1)+8k_n^2\right)+3(d-4)(2d-9)\right)\\
&+\frac{3}{V(u)}\left((d-2)u^2+d-4\right)\left(\left((d-2)u^2+d-4\right)^2-4u^2\omega^2\right)
\end{aligned}
$$

$$
\begin{aligned}
\mathfrak{C}(u) =& V(u)\Bigg\{V(u)\Bigg(V(u)\Big[u^2\left(\left(d^2-12\right)k_n^2+(d-2)(d((d-5)d+14)-28)\right)\\
&\qquad+(d-4)^2V(u)+((d-5)d+2)(d-4)^2\Big]\\
&\qquad+u^2\left[((44-5d)d-92)\omega^2-2(d-4)(d-2)\left(d^2+k_n^2-11\right)\right]\\
&\qquad+u^4\left(-2(d-8)(d-2)k_n^2-(d-2)^2(d(d+2)-13)+4k_n^4\right)\\
&\qquad-(d-4)^2((d-2)d-9)\Bigg)\\
&\quad+2u^2\omega^2\left(u^2\left((d-2)(5d-14)+4k_n^2\right)+5(d-4)^2\right)\\
&\quad+\left((d-2)u^2+d-4\right)^2\left(u^2k_n^2-(d-7)\left((d-2)u^2+d-4\right)\right)\Bigg\}\\
&-5u^2\omega^2\left((d-2)u^2+d-4\right)^2+\left((d-2)u^2+d-4\right)^4+4u^4\omega^4
\end{aligned}
$$

A.3 Extremal Surfaces and Global Theorems

A.3.1 The mean curvature of X in Σ

Let now $A, B, \ldots$ be indices for tensors on X, and $\alpha, \beta, \ldots$ be indices for tensors on Σ, and consider intrinsic coordinates on Σ and X from Sec. 9.2.2. The induced metrics are

$$
\begin{aligned}
\mathrm{d}s^2|_\Sigma &= H_{\mu\nu}\mathrm{d}x^\mu\mathrm{d}x^\nu = B(r)\mathrm{d}r^2+r^2\left[\mathrm{d}\phi^2+\delta_{ij}\mathrm{d}x^i\mathrm{d}x^j\right]\\
\mathrm{d}s^2|_X &= \gamma_{AB}\mathrm{d}y^A\mathrm{d}y^B = \left[B(r)+r^2\Phi'(r)^2\right]\mathrm{d}r^2+r^2\delta_{ij}\mathrm{d}x^i\mathrm{d}x^j.
\end{aligned}
\tag{A.19}
$$

A basis of tangent vectors to X in Σ is $\{e_A^\alpha\}$, with coordinate expressions

$$
\begin{aligned}
e_r^\mu &= (1,\Phi(r),0),\\
e_i^\mu &= (0,0,\delta_i^\alpha).
\end{aligned}
\tag{A.20}
$$

The normal to X inside Σ reads

$$
n_\mu = \sqrt{\frac{Br^2}{B+r^2(\Phi')^2}}\,(\Phi'(r),-1,0) \tag{A.21}
$$

With this in hand, we can compute the mean curvature of X in Σ:

$$
\begin{aligned}
\mathcal{K} &= \gamma^{AB}e_A^\mu e_B^\nu\nabla_\mu n_\nu\\
&= \frac{1}{r\sqrt{B}\left[B+r^2(\Phi')^2\right]^{3/2}}\left[(d-1)r^3\Phi'(r)^3+\left(dB-\frac{1}{2}rB'\right)r\Phi'+r^2B\Phi''\right].
\end{aligned}
\tag{A.22}
$$

A.3.2 Explicit form of $K - n^\alpha n^\beta K_{\alpha\beta}$

Noting that

$$n^\mu = \sqrt{\frac{Br^2}{B + r^2(\Phi')^2}} \left(\frac{\Phi'(r)}{B(r)}, -\frac{1}{r^2}, 0 \right) \tag{A.23}$$

we get

$$\begin{aligned} K = H^{\alpha\beta} K_{\alpha\beta} &= \frac{1}{B} K_{rr} + \frac{d-1}{r^2} K_{\phi\phi}, \\ K_{\alpha\beta} n^\alpha n^\beta &= \frac{Br^2}{B + r^2 \Phi'(r)^2} \left[\frac{\Phi'(r)^2}{B^2} K_{rr} + \frac{1}{r^4} K_{\phi\phi} \right]. \end{aligned} \tag{A.24}$$

Inserting $K_{rr}(r) = B(r)F(r)$ and doing some algebra, $K - n^\alpha n^\beta K_{\alpha\beta} = 0$ becomes (9.53).

A.3.3 Deriving formulas for $\partial_t S$ and $\partial_\ell S$

A formula for $\partial_t S$

In this section, we show that the entropy growth is proportional to the infalling matter flux. We will first need to prove that

$$\left. \frac{\mathrm{dArea}[X_t]}{\mathrm{d}t} \right|_{t=0} = \int_{\partial X} N^a \eta_a = -\frac{\mathrm{Area}[\partial R]}{L^{d-2}} \lim_{r\to\infty} r^{d-3} K_{\phi\phi} \tag{A.25}$$

For the calculation, we will construct the vector η^a, which is tangent to the boundary $\partial\mathcal{M}$, and N^a, the outwards unit normal to $\partial\Sigma = \partial\mathcal{M} \cap \Sigma$ in Σ, in a coordinate system. To do so, introduce the ADM coordinates adapted to the extended homology hypersurface

$$\mathrm{d}s^2|_{\mathcal{M}} = -r^2 \mathrm{d}\tau^2 + H_{\mu\nu}(\tau, x) \mathrm{d}x^\nu \mathrm{d}x^\nu, \tag{A.26}$$

where we took the shift to be vanishing, and the lapse to be r. $x^\mu = (r, \boldsymbol{x})$ are the coordinates on Σ, and $H_{\mu\nu}(\tau = 0, x)$ its induced metric, given by (9.35). The extrinsic curvature of Σ reads

$$K_{\alpha\beta} = \frac{1}{2r} \partial_\tau H_{\alpha\beta}|_{\tau=0}. \tag{A.27}$$

Imagine now we have the coordinates $z^i = (t, \boldsymbol{x})$ on $\partial\mathcal{M}$ and take $\partial\Sigma$ to be located at $(r = r_c, t = \tau = 0)$ with a temporary cutoff $r = r_c$. We want to find embedding coordinates $(r(t), \tau(t))$ for $\partial\mathcal{M}$ such that the induced metric reads

$$\mathrm{d}s^2|_{\partial\mathcal{M}} = h_{ij} \mathrm{d}z^i \mathrm{d}z^j = \frac{r_c^2}{L^2} \left[-\mathrm{d}t^2 + L^2 \mathrm{d}\phi^2 + L^2 \, \mathrm{d}\boldsymbol{x}^2 \right] \tag{A.28}$$

The components of the induced metric then satisfy

$$h_{tt} = g_{rr} \dot{r}^2 - r^2 \dot{\tau}^2 = -\frac{r_c^2}{L^2}, \tag{A.29}$$

$$h_{\phi\phi} = g_{\phi\phi} = r_c^2. \tag{A.30}$$

Taking the derivative of the second equation, and then setting $t = 0$ gives a system of equations that is easily solved to give (see the appendix of [306])

$$\dot{\tau}(0) = \frac{1}{L\sqrt{1 - BK_{\phi\phi}^2 r^{-2}}}\bigg|_{r=r_c}, \tag{A.31}$$

$$\dot{r}(0) = -\frac{K_{\phi\phi}}{L\sqrt{1 - BK_{\phi\phi}^2 r^{-2}}}\bigg|_{r=r_c}, \tag{A.32}$$

where we have chosen the branch $\dot{\tau} > 0$. Thus, η^a in our ADM coordinate system reads

$$\eta^a = (\partial_t)^a = \dot{\tau}(0)(\partial_t)^a + \dot{r}(0)(\partial_r)^a. \tag{A.33}$$

Now, the tangents to ∂X are tangent to ∂R, and the sole remaining tangent vector e_r^α in (A.20) is then the normal to $\partial\Sigma$. Hence, up to a normalization C,

$$N^\mu = Ce_r^\mu = C(1, \Phi', 0), \tag{A.34}$$

which can be unit normalized and pushed forward to a spacetime vector yielding (in the coordinates (A.26)),

$$N^a = \frac{1}{\sqrt{B(r) + r_c^2\Phi'(r)^2}}(0, 1, \Phi'(r), 0)|_{r=r_c}. \tag{A.35}$$

We can now compute the integral on the cutoff regulated ∂X:

$$\begin{aligned}\int_{\partial X} \eta^a N_a &= -\frac{K_{\phi\phi}}{L\sqrt{1 - B(r_c)K_{\phi\phi}^2/r_c^2}} \times \frac{B(r_c)}{\sqrt{B(r_c) + r_c^2(\partial_r\Phi)^2}} \times r_c^{d-2}\int \mathrm{d}^{d-2}\boldsymbol{x} \\ &= -\frac{K_{\phi\phi}\sqrt{B(r_c)}}{L\sqrt{1 - B(r_c)K_{\phi\phi}^2/r_c^2}} \times \sqrt{1 - (r_0/r_c)^2} \times r_c^{d-2}\frac{\mathrm{Area}[\partial R]}{L^{d-2}},\end{aligned} \tag{A.36}$$

where we have used the differential equation for the embedding function $\Phi(r)$. In the large r limit, the asymptotic behaviors are

$$B(r) \sim \mathcal{O}(r^{-2}), \qquad K_{\phi\phi} \sim \mathcal{O}(r^{-(d-3)}). \tag{A.37}$$

Taking the cutoff to the boundary, one finds the area growth to be given by (9.42).

A covariant formula for $\partial_t S$

Now let us write the integral formula for $\partial_t S$ in a covariant way. Letting t^a be the future unit normal to Σ and n^a the outwards normal to X tangent to Σ, we have for some

function G on X that only depends on r:

$$\begin{aligned} 8\pi G_N \int_X G(r) t^a n^b \mathcal{T}_{ab} &= \int \mathrm{d}^{d-2}\boldsymbol{x} \int_{r_0}^{\infty} \mathrm{d}r r^{d-2} \sqrt{B + r^2(\Phi')^2} G(r) n^r \mathcal{J} \\ &= \frac{\mathrm{Area}[\partial R]}{L^{d-2}} \int \mathrm{d}r r^{d-2} \frac{\sqrt{B} r}{B + r^2(\Phi')^2} \Phi' G(r) \mathcal{J} \\ &= \frac{\mathrm{Area}[\partial R]}{L^{d-2}} \int \mathrm{d}r r^{d-2} \left(\frac{r_0}{r}\right)^{2d-2} G(r) \mathcal{J} \sqrt{(r/r_0)^{2d-2} - 1} \\ &= \frac{\mathrm{Area}[\partial R]}{L^{d-2}} \int \mathrm{d}r \frac{r_0^{d-1}}{r^d} G(r) \mathcal{J} \sqrt{r^{2d-2} - r_0^{2d-2}}, \end{aligned} \tag{A.38}$$

where we used (A.21) and (9.39). Letting

$$G(r) = \frac{2\pi r^d}{(d-1) r_0^{d-1}}, \tag{A.39}$$

we get a covariant formula for the entropy growth

$$\frac{\mathrm{d}S_R}{\mathrm{d}t} = \int_X G t^a n^b \mathcal{T}_{ab} \tag{A.40}$$

A formula for $\partial_\ell S$

Consider a one-parameter family of HRT surfaces X_ℓ anchored at the strip region R_ℓ, given by (9.21), but letting now ℓ vary, holding t fixed. Taking the vector field η^a generating the flow of ∂X_ℓ to be $\eta^a|_{\partial\mathcal{M}} = \frac{1}{L}(\partial_\phi)^a$, (9.40) becomes

$$\frac{\mathrm{d}}{\mathrm{d}\ell} \mathrm{Area}[X_\ell] = \frac{\mathrm{Area}[\partial R]}{L^{d-1}} \lim_{r\to\infty} r^{d-2} g_{\phi\phi} N^\phi. \tag{A.41}$$

Using (A.35), (A.26), and (9.39), this evaluates to

$$\frac{\mathrm{d}}{\mathrm{d}\ell} \mathrm{Area}[X_\ell] = \frac{\mathrm{Area}[\partial R]}{L^{d-1}} \lim_{r\to\infty} r^d \frac{\Phi'}{\sqrt{B + r^2(\Phi')^2}} = \frac{\mathrm{Area}[\partial R]}{L^{d-1}} r_0^{d-1}. \tag{A.42}$$

A.3.4 Expression for $\partial_t \|X_t\|$

The derivation of (9.147) is almost identical to the derivation in Sec. A.3.3. Let us just highlight what must be changed. First, we do not have an explicit formula for $\Phi'(r)$, but this does not matter, since everything we need is its rate of falloff, which we can read off to be $\Phi'(r) \sim \mathcal{O}\left(1/r^{q+2}\right)$ from (9.142). Next, in (A.36), it is sufficient to replace $r_c^{d-2} \to r_c^q$. After doing that, and taking into account that $K_{\phi\phi}$ now has falloff $\mathcal{O}(1/r^{q-1})$, the $r_c \to \infty$ limit of (A.36) with these modifications gives (9.147).

A.3.5 Geometric properties of X and Σ

Let us now prove various properties of extended homology hypersurfaces. We give the proof for HRT surfaces of strips and comment how the proofs are modified for $(q+1)$-dimension extremal surfaces anchored at spheres.

Lemma 7. *The extended homology hypersurface Σ of a strip region in a spacetime with planar symmetry cannot have a throat in its interior, i.e., a radius where $B(r)$ diverges.*

Proof. Assume for contradiction that Σ has a throat T in its interior – if there are multiple, take T to be the outermost one. Since Σ by definition terminates at the plane tangent to the tip of X, this means that X must pass beyond the throat. But if X crosses the throat, there must be a point on $X \cap T$ where X is not tangent to T. Let now $U \subset \Sigma$ be the region outside T, which we can always cover with a coordinate system

$$\mathrm{d}s^2|_U = B(r)\mathrm{d}r^2 + r^2\mathrm{d}\boldsymbol{x}^2, \quad r \in [r_T, \infty), \quad B(r_T) = \infty, \quad B(r > r_T) < \infty. \tag{A.43}$$

where the throat is at $r = r_T$. The fact that X is not tangent to T means that $|\Phi'(r_T)| < \infty$. But the solution for the extremal surface reads

$$\Phi'(r)^2 = \frac{B(r)}{r^2(r^{2d-2}c - 1)} \tag{A.44}$$

for some constant c, and so $|\Phi'(r_T)| = \infty$, which is a contradiction. Hence T cannot exist in the interior of Σ. □

This proof goes through the case of X anchored at a dimension q sphere, as discussed in Sec. 9.3, simply taking Φ' to be computed from (9.142).

Next, we have the following:

Lemma 8. *The HRT surface X of a strip region R can only have one turning point.*

Proof. Assume for contradiction that X has multiple turning points. Then there must be at least one turning point of X in the interior of Σ that is a local maximum of the embedding function $r(\phi)$. Let $\phi = \phi_t$ where this turning point occurs, and let us restrict our attention to a neighbourhood $\phi \in \mathcal{O}_\epsilon = (\phi_t, \phi_t + \epsilon)$, where we can invert $r(\phi)$ to get $\Phi(r)$, describing the embedding in $\mathcal{O}_\epsilon$. We see that $\Phi'(r) < 0$ and $\Phi''(r) < 0$ in this neighbourhood. Now, the equation for the HRT surface in the neighbourhood $\mathcal{O}_\epsilon$ is

$$(d-1)r^3\Phi'^3 + r^2B\Phi'' + r\Phi'\left(dB - \frac{r}{2}B'\right) = 0. \tag{A.45}$$

Since we are in the interior of Σ, B is bounded on $\mathcal{O}_\epsilon$ by Lemma 7. Since Φ' diverges at the turning point, the equation for Φ' near the turning point reads

$$r^2B\Phi'' = -(d-1)r^3\Phi'^3\left[1 + \mathcal{O}\left(\frac{1}{(\Phi')^2}\right)\right], \tag{A.46}$$

where the correction can be neglected to arbitrarily good precision since B is bounded. But this implies that Φ'' and Φ' must have opposite signs in $\mathcal{O}_\epsilon$ for sufficiently small ϵ, which is a contradiction. Hence X can only have one turning point. □

We did not consider the case where $r'(\phi_t) = r''(\phi_t) = 0$, but this was shown to be ruled out by [315]. Also, note that this proof survives the case of spherical boundary anchoring and a $(q+1)$-dimensional extremal surface, since the new term $(\Phi')^3\chi(r)$ in the extremality equation (9.138) is subleading at the prospective turning point, since it scales like $\chi \sim 1/\Phi'$. Thus, (A.46) remains true (up to a numerical factor and an $\mathcal{O}(1/\Phi')$ correction).

A.3.6 General extremality conditions

Let

$$H_{ab} = g_{ab} + t_a t_b \tag{A.47}$$

be the induced metric on Σ. Then we have $h^{ab} = H^{ab} - \delta^{IJ} n_I^a n_J^b$, and so

$$\begin{aligned} \mathcal{K}^0 &= (H^{ab} - \delta^{IJ} n_I^a n_J^b)\nabla_a t_b \\ &= K - \delta^{IJ} n_I^a n_J^b \nabla_{(a} t_{b)} \\ &= K - \delta^{IJ} n_I^a n_J^b K_{ab} \end{aligned} \tag{A.48}$$

where we in the last line used that $n_I^a n_J^b$ is tangent to Σ, which projects out the difference $\nabla_{(a}t_{b)} - K_{ab}$. Now, a collection of tangents e_I^μ to X are

$$\begin{aligned} e^\mu{}_r &= (1, \Phi'(r), 0, 0), \\ e^\mu{}_i &= (0, 0, \delta_i^\mu, 0), \end{aligned} \tag{A.49}$$

where i runs over sphere directions. The second to last slot here runs over the sphere directions, with the last slot runs over the $\boldsymbol{z}$-directions. The unit normals to X (in Σ) are

$$\begin{aligned} n^r{}_\mu &= (\alpha, \beta, 0, 0), \\ n^i{}_\mu &= (0, 0, 0, r\delta^{y^i}_\mu), \end{aligned} \tag{A.50}$$

for some α, β we now work out, and where the coordinates are with respect to the index μ on Σ. r, i should be view as indices in the orthonormal tangent basis labeled by I on X. Now

$$\begin{aligned} 0 &= n^r{}_\mu e^\mu{}_r = \alpha + \beta\Phi'(r), \\ 1 &= H^{\mu\nu} n^r{}_\mu n^r{}_\nu = \frac{\alpha^2}{B} + \frac{\beta^2}{r^2}. \end{aligned} \tag{A.51}$$

Solving for α, β, we get

$$n^r{}_\mu = \sqrt{\frac{Br^2}{B + r^2(\Phi')^2}}\,(\Phi', -1, 0, 0)\,, \quad n^{r\mu} = \sqrt{\frac{Br^2}{B + r^2(\Phi')^2}}\left(\frac{1}{B}\Phi', -\frac{1}{r^2}, 0, 0\right). \tag{A.52}$$

Now we want to impose

$$\mathcal{K}^0 = K - \delta^{IJ} n_I^a n_J^b K_{ab} = 0. \tag{A.53}$$

Explicitly we have

$$K = H^{\mu\nu}K_{\mu\nu} = \frac{1}{B}K_{rr} + \frac{1}{r^2}K_{\phi\phi} + \frac{w^{ij}}{r^2\phi^2} \times \underbrace{\phi^2 w_{ij}K_{\phi\phi}}_{K_{ij}} + \frac{d-2-q}{r^2}\underbrace{K_{\phi\phi}}_{K_{zz}}, \\ = \frac{1}{B}K_{rr} + \frac{d-1}{r^2}K_{\phi\phi}, \tag{A.54}$$

and

$$\delta^{IJ}n^a_I n^b_J K_{ab} = (n^{rr})^2 K_{rr} + (n^{r\phi})^2 K_{\phi\phi} + (d-2-q)\frac{1}{r^2}K_{\phi\phi}. \tag{A.55}$$

Thus, with $K_{rr} = BF$, condition (A.53) reads

$$\left[1 - B(n^r_r)^2\right] F + \left[\frac{q+1}{r^2} - (n^\phi_r)^2\right] K_{\phi\phi} = 0 \tag{A.56}$$

Using the explicit formula for n^r_r, n^ϕ_r in (A.52), inserting the explicit formula for $\Phi(r)$ from (9.142), and solving for $F(r)$, we find (9.150).

Note also that thanks to (A.54), (9.77) is unchanged, and so the proof that $\pm\theta_\pm[\partial\Sigma] \geq 0$ for strips survive for dimension–$q+1$ surfaces anchored at q-spheres.

A.4 Lorentzian Einstein Ricci Flows

The purpose of this note is to study the Ricci flow [346–349] for the Lorentzian Einstein-Hilbert action

$$\mathcal{A}_L = \frac{1}{2\kappa}\int_{\mathcal{M}} R\sqrt{-g}\mathrm{d}^d x \tag{A.57}$$

where R is the scalar curvature for a $d-$dimensional manifold $(\mathcal{M}, g)$ without boundary ($d \geq 3$) and $\kappa = 8\pi G_d$. Such geometric flows are interesting to consider as they connect on-shell saddle points of the action via deformations off-shell. The simplest example connects the four-dimensional Schwarzschild black hole to Minkowski spacetime in Euclidean signature [350]. The transition between these geometries was shown to pass through a singularity in finite time. The Ricci flow has been studied several times – originally in the context of non-linear sigma models [351], and later as a geometrization of RG flows in AdS/CFT [352–356].

A.4.1 The Ricci Flow

For a d-dimensional manifold equipped with a Riemannian metric $(\mathcal{M}, g)$, the Ricci flow is a first order PDE in the space of Riemannian metrics $\mathfrak{G}$ canonically given by

$$\dot{g}_{ab}(t) = -2R_{ab}(t), \qquad g_{ab}(0) = g^i_{ab}. \tag{A.58}$$

The parameter t appearing equation is an auxiliary time which characterizes the deformations of the metric along the flow. The Ricci flow is well-defined in Euclidean signature

where the PDE is parabolic (up to diffeomorphism invariance). The flow deforms the initial metric g^i in the direction of its curvature and eventually terminates at $t^\star$ when the metric $g_{ab}(t^\star)$ is Ricci flat, $R_{ab}(t^\star) = 0$. As a simple example, we can study the homothetic evolution of Einstein spaces $R_{ab}(t) = \frac{2\Lambda}{d-2} g^i_{ab}$ discussed earlier by Topping [349]. In Lorentzian signature, this includes maximally symmetric spacetimes, Schwarzschild black holes ($\Lambda = 0$), and (A)dS black hole solutions ($\Lambda \neq 0$). A straightforward computation shows

$$g_{ab}(t) = \left(1 - \frac{4\Lambda}{d-2} t\right) g^i_{ab}. \tag{A.59}$$

Hence, spaces which are Ricci flat are fixed points whereas positively curved Einstein spaces ($\Lambda > 0$) become singular in finite time $t_c = \frac{(d-2)}{4\Lambda}$ and negatively curved Einstein spaces ($\Lambda < 0$) diverge homogeneously.

In general, the Ricci flow describes a modified heat equation for Riemannian metrics. This is most easily seen for the flat space fixed point. First, consider a linearization of the flow around Ricci-flat space, i.e., $g_{ab}(t) = \bar{g}_{ab} + \epsilon h_{ab}(t)$. Then, up to linear order in ϵ, the flow reduces to

$$\dot{h}_{ab} = -\bar{\Delta}_{\mathrm{L}} h_{ab} + 2\bar{\nabla}_{(a}\xi_{b)} + \mathcal{O}(\epsilon^2) \tag{A.60}$$

where $\xi_b = \frac{1}{2}\bar{\nabla}_b h^c{}_c - \bar{\nabla}_c h^c{}_b$ and $\bar{\Delta}_L$ is the Lichnerowicz operator $\bar{\Delta}_L h_{ab} = -\bar{\nabla}^2 h_{ab} - 2\bar{R}_a{}^c{}_b{}^d h_{cd}$ computed using $\bar{g}_{ab} = g_{ab}(t^\star)$. When the background is Euclidean space, $\bar{g}_{ab} = \delta_{ab}$, one recovers a heat equation with an additional contribution in the form of a diffeomorphism which vanishes for pure gauge perturbations, i.e., $h_{ab} = \partial_{(a} u_{b)}$. For a non-trivial Ricci-flat fixed point, the flow may develop curvature singularities in finite time as evidenced by a squashed sphere [349]. Perelman developed a rich set of methods to surgically remove these singularities which eventually lead to the proof of the Poincaré conjecture [347]. Further results establish the short-time existence of the flow which then allows the geometry to be analytically or numerically evolved (see [349, 350, 354]).

A.4.2 Einstein-Ricci Flows

Just as the heat equation can be interpreted as a gradient flow problem for the Dirichlet energy functional $E[f] = \frac{1}{2}\int_{\mathcal{M}} |\nabla f|^2 \sqrt{g} \mathrm{d}^d x$ with respect to the inner product $\langle f_i, f_j \rangle = \int_{\mathcal{M}} f_i f_j \sqrt{g} \mathrm{d}^d x$ in Euclidean space, the Ricci flow, Eqn. (A.58), also admits a similar formulation. In this work, we first review the Ricci flow for the Euclidean Einstein-Hilbert functional. As discussed earlier in [347–350], the flow is ill-behaved for Riemannian metrics. However, the main observation of this paper is to show that under a Wick rotation of the Lorentzian Einstein-Hilbert action, Eqn. (A.57), the flow is well-behaved. We will also generalize our discussion to include minimally-coupled[1] matter contributions.

[1] In fact, the $\mathcal{W}$ and $\mathcal{F}$ entropy functionals considered by Perelman [347, 349] are examples of non-minimally coupled matter configurations which reproduce the Ricci flow problem up to diffeomorphisms.

Riemannian Einstein-Ricci Flows

To motivate the Ricci flow for Eqn. (A.57), consider the variation of the Einstein-Hilbert action $\mathcal{A}[g_{ab}(t)]$ for *Riemannian* manifolds without boundary. Upon integrating a total divergence, one finds

$$\frac{\mathrm{d}}{\mathrm{d}t}\mathcal{A}[g(t)] = \frac{1}{2\kappa}\int_{\mathcal{M}} (R_{ab} - (1/2)Rg_{ab})\dot{g}^{ab}\sqrt{g}\,\mathrm{d}^d x. \tag{A.61}$$

In order to understand this as a gradient flow, we consider $\mathcal{A}$ to be a Dirichlet energy functional on the space of metrics with an inner product $\langle \dot{g}_i, \dot{g}_j\rangle = \int_{\mathcal{M}} \dot{g}_{ab}\dot{g}^{ab}$. We wish to find a flow such that the Dirichlet energy converges onto its stationary points. This can be achieved for the Einstein-Ricci flow

$$\dot{g}_{ab}(t) = -2R_{ab}(t) + R(t)g_{ab}(t), \qquad g_{ab}(0) = g^i_{ab}. \tag{A.62}$$

Evaluating the action along this flow, one finds that the Dirichlet functional decreases

$$\dot{\mathcal{A}}[g(t)] = -\int_{\mathcal{M}} \dot{g}_{ab}\dot{g}^{ab}\sqrt{g}\mathrm{d}^d x \leq 0 \tag{A.63}$$

where we have set $\kappa = 1$. At the stationary points $t^\star$ of the Einstein-Ricci flow, Eqn. (A.67), one recovers the Riemannian Einstein field equations $R_{ab} - (1/2)Rg_{ab}|_{t^\star} = 0$. Although the stationary points of the Ricci flow and the Einstein-Ricci flow are identical, i.e., Ricci flat spaces, the Einstein-Ricci flow behaves badly from the perspective of PDE theory. If we consider an analogous linearization around the Ricci flat fixed point, we would find linear corrections of the form

$$\dot{h}_{ab} = -\bar{\Delta}_{\mathrm{L}} h_{ab} + \bar{g}_{ab}\Big(\bar{\nabla}_c\bar{\nabla}_d h^{cd} - \bar{\nabla}^2 h_c{}^c\Big) + 2\bar{\nabla}_{(a}\xi_{b)}. \tag{A.64}$$

For Euclidean spaces $\bar{g}_{ab} = \delta_{ab}$, the perturbations can be decomposed to parts where the corrections from the scalar curvature vanish and a part with Weyl scalings $h_{ab}(t) = f(t)\delta_{ab}$ which can be shown to evolve with a diffusion constant $(2-d)$ [349, 350]. Hence, the flow may then be expressed as $\dot{f} = (2-d)\nabla^2 f + \cdots$ which is a backwards heat equation. For the Einstein-Ricci flow to be well posed, one either must consider $t \to -t$ or change the inner product in Riemannian signature to counteract the overall signature. Either prescription causes the Riemannian Dirichlet functional to increase along the flow.

Lorentzian Einstein-Ricci Flows

As we have shown, the Einstein-Hilbert action for Riemannian manifolds[2] has an ill-posed Einstein-Ricci flow problem. We show the same is not true for Lorentzian spacetimes which are brought over into the Euclidean section via Wick rotation. One may worry

[2]This statement holds even if the manifold has a boundary.

that Lorentzian spacetimes must be static in order to have a well defined Euclidean section. However, the procedure of performing complex deformations on Lorentzian metrics, rather than on Lorentzian time, is now well understood (see [357] and references therein). One starts with the path integral for the Lorentzian Einstein-Hilbert action

$$\mathcal{Z}_L = \int e^{\mathrm{i}\mathcal{A}_L}\mathcal{D}g = \int \exp\left(\frac{\mathrm{i}}{2}\int_{\mathcal{M}} R_L\sqrt{-g_L}\mathrm{d}^d x\right)\mathcal{D}g_L \tag{A.65}$$

where $\mathcal{D}g_L$ is the measure on the space of Lorentzian metrics $\mathfrak{G}_L$ and $\mathcal{M}$ is time-orientable with the Lorentzian volume form being $\sqrt{-g_L}\mathrm{d}^d x$. In general, the path integral is not positive definite and oscillates rapidly due to the phase $e^{\mathrm{i}\mathcal{A}_L}$. However, that $\mathcal{M}$ is time-orientable is equivalent to the existence of a non-vanishing timelike vector field V [18, 357]. Hence, the Lorentzian path integral can be analytically continued into the Euclidean section via deformations $g_\varepsilon = g + \mathrm{i}\varepsilon(V\otimes V/g(V,V))$ as noted by Visser [357]. Choosing a contour which avoids the degenerate pole at $\varepsilon = \mathrm{i}$, one recovers the Euclidean path integral (partition function)

$$\mathcal{Z} = \int e^{\mathcal{A}_D}\mathcal{D}g = \int \exp\left(-\frac{1}{2}\int_{\mathcal{M}} R\sqrt{g}\mathrm{d}^d x\right)\mathcal{D}g. \tag{A.66}$$

where we are once again in the space of Riemannian metrics $\mathfrak{G}$ with measure $\mathcal{D}g$.

It is worth noting that the partition function is not bounded either above or below as conformal fluctuations can be made arbitrarily large [7, 358–360]. However as the semiclassical approximation, near the most dominant saddle point, does reproduce the thermodynamics of black holes, the Euclidean path integral approach does have enough merit to warrant consideration of the deformed Einstein-Hilbert action $\mathcal{A}_D$ as a Dirichlet functional. One may object that the Dirichlet functional should be positive definite for a well defined variational problem, so we restrict our considerations to spaces with non-positive scalar curvature $R \leq 0$. This is quite natural to do from the perspective of black hole thermodynamics in AdS and Minkowski spacetimes.

For our purposes, we consider $\mathcal{A}_D$ as the Dirichlet functional for the Ricci flow problem. Upon first variation, we find

$$\dot{\mathcal{A}}_D[g(t)] = -\frac{1}{2}\int_{\mathcal{M}} (R_{ab} - (1/2)Rg_{ab})\dot{g}^{ab}\sqrt{g}\,\mathrm{d}^d x. \tag{A.67}$$

Then using standard inner product norm $\langle \dot{g}_i, \dot{g}_j\rangle = \int_{\mathcal{M}} \dot{g}_{ab}\dot{g}^{ab}\sqrt{g}\mathrm{d}^d x$, the Dirichlet functional decreases $\dot{\mathcal{A}}_D \leq 0$ along the flow

$$\dot{g}_{ab}(t) = 2R_{ab}(t) - R(t)g_{ab}(t), \qquad g_{ab}(0) = g^i_{ab}. \tag{A.68}$$

Henceforth, we refer to the PDE, Eqn. (A.68), as the Lorentzian Einstein-Ricci flow. We observe (i) one recovers Einstein gravity at the fixed points of the flow, and (ii) linearizations around the stationary point lead to

$$\dot{h}_{ab} = \bar{\Delta}_{\mathrm{L}} h_{ab} - \bar{g}_{ab}\left(\bar{\nabla}_c\bar{\nabla}_d h^{cd} - \bar{\nabla}^2 h_c{}^c\right) - 2\bar{\nabla}_{(a}\xi_{b)} \tag{A.69}$$

yielding a positive diffusion constant $\dot{f} = (d-2)\nabla^2 f + \cdots$ and a well-posed heat equation for Weyl scalings. To our knowledge, the Lorentzian Einstein-Ricci flow is the first to simultaneously minimize the Euclidean gravity functional and remain well-posed in forward flow time for Ricci-flat spaces.

As an example, consider the homothetic evolution of Einstein spaces $R_{ab}(t) = \frac{2\Lambda}{d-2}\bar{g}_{ab}$. One can check that the exact solution to the Lorentzian Einstein-Ricci flow is

$$g_{ab}(t) = \left[(2/d) + (1-(2/d))e^{-\frac{2d\Lambda}{d-2}t}\right]\bar{g}_{ab}. \tag{A.70}$$

Again, Ricci flat spaces are fixed points which are unchanged along the evolution whereas now negatively curved spaces ($\Lambda < 0$) expand exponentially. Although we consider only non-positive scalar curvature, it is worth noting the finite time singularity of the Ricci flow mentioned earlier is not observed for positively curved spaces ($\Lambda > 0$).

A.4.3 Generalizations

The Lorentzian Einstein-Ricci flow presented thus far is not unique. Indeed, we could add terms which respect the contracted Bianchi identity $\nabla_a(R^{ab} - (1/2)Rg^{ab}) = 0$ which would only shift the fixed points structure of the flow [350]. Concretely, consider the Lorentzian action

$$\mathcal{I}_L = \frac{1}{2}\int_{\mathcal{M}} (R - 2\Lambda - \mathcal{L}_{\mathrm{M}})\sqrt{-g}\mathrm{d}^d x \tag{A.71}$$

where we restrict the matter content $\mathcal{L}_{\mathrm{M}} \equiv \mathcal{L}_{\mathrm{M}}(\Phi^I, \nabla\Phi^I)$ to be well defined in the Euclidean section and fixed along the flow $\dot{\Phi}^I = 0$. We can construct a deformed Einstein-Hilbert action $\mathcal{I}_D$ via a Wick rotation. The Lorentzian Einstein-Ricci flow problem for the Dirichlet functional $\mathcal{I}_D$ may be formulated as follows; $\dot{\mathcal{I}}_D[g(t)] \leq 0$ on the standard inner product norm $\langle \dot{g}_i, \dot{g}_j \rangle = \int_{\mathcal{M}} \dot{g}_{ab}\dot{g}^{ab}\sqrt{g}\mathrm{d}^d x$ for the flow

$$\begin{aligned} \dot{g}_{ab}(t) &= 2R_{ab}(t) - R(t)g_{ab}(t) + 2\Lambda g_{ab}(t) - 2T_{ab}(g(t)), \\ g_{ab}(0) &= \bar{g}_{ab}, \end{aligned} \tag{A.72}$$

where the stress energy is $T_{ab} = (2/\sqrt{g})\partial(\sqrt{g}\mathcal{L}_{\mathrm{M}})/\partial g^{ab}$. A few comments are in order. In the absence of matter, the fixed points are now Einstein spaces rather than Ricci-flat spaces. Furthermore, the additional contribution from the cosmological constant respects the diffusive nature of the flow under a linearization as no kinetic terms are added by Weyl scalings, and the Bianchi identity is manifestly obeyed $\nabla_a(R^{ab} - (1/2)Rg^{ab} + \Lambda g^{ab}) = 0$. In the presence of matter, the flow reduces to $R_{ab} - (1/2)Rg_{ab} + \Lambda g_{ab}|_{t^\star} = T_{ab}|_{t^\star}$, and thus imposes $\nabla_a T^{ab}|_{t^\star} = 0$. The conservation of stress-energy is equivalent to the statement $\delta\mathcal{I}_D[g(t^\star), \Phi_i]/\delta\Phi_i|_{\text{on-shell}} = 0$. To understand the corrections from the stress-energy, consider a linearization of the stress-energy and the flow around $\Lambda = 0, \bar{g}_{ab} = \delta_{ab}$.

This yields

$$T_{ab}(g(t)) = T_{ab}(\bar{g}) + \epsilon \frac{\partial T_{ab}}{\partial g_{cd}}\Big|_{t^\star} h_{cd} + \mathcal{O}(\epsilon^2), \tag{A.73}$$

$$\begin{aligned}\dot{h}_{ab} =& \bar{\Delta}_{\rm L} h_{ab} - \bar{g}_{ab}\Big(\bar{\nabla}_c \bar{\nabla}_d h^{cd} - \bar{\nabla}^2 h_c{}^c\Big) - 2\bar{\nabla}_{(a}\xi_{b)} \\ &+ 2\Lambda h_{ab} - 2\frac{\partial T_{ab}}{\partial g_{cd}}\Big|_{t^\star} h_{cd}.\end{aligned} \tag{A.74}$$

Hence a Weyl fluctuation, $h_{ab} = f(t)\delta_{ab}$, would satisfy $\dot{f} = (d-2)\nabla^2 f - \mu f + \cdots$ where $\mu = 2(\partial T_{ab}/\partial g_{cd})|_{t^\star}\delta_{cd}\delta^{ab}$. We can understand these fluctuations $\Delta T_{ab}(t) = T_{ab}(g(t)) - T_{ab}(\bar{g})$ as sources $Q_{ab}(t) = \Delta T_{ab}(t)$ in the heat equation. In Euclidean space, matter contributions will source exponential factors of the form $e^{-\mu t}$ which competes with diffusion if $\mu < 0$ at $t \gg 1$. In general, the details depend on the stress-energy of $\mathcal{L}_{\rm M}$ in Lorentzian spacetime and we expect the flow to converge only if μ is non-negative in Euclidean signature.

A.4.4 Einstein-Ricci Flows as RG Flows

The Ricci flow was originally motivated as an RG flow on the worldsheet for 2d non-linear sigma models [350, 351]. In the context of entanglement entropy and AdS/CFT, shape deformations of entanglement surfaces and geometric flows of Randall-Sundrum surfaces have been shown to reproduce the Ricci flow up to corrections [353, 356].

In light of this, it is suggestive to consider the Lorentzian Einstein-Ricci flow as an RG flow. We can understand the gradient flow as an RG process by identifying t as a renormalization scale with cutoffs at $t_0 \leq t \leq t^\star$. Then we may write the generalized Lorentzian Einstein-Ricci flow somewhat suggestively as

$$\dot{\Phi}^I = \beta^I, \tag{A.75}$$

$$\dot{g}_{ab} = \beta_{ab} + 2\Lambda g_{ab} - 2T_{ab}. \tag{A.76}$$

where $\beta_{ab} = 2R_{ab} - Rg_{ab}$ and β^I are the beta functions for the matter. As the flow connects configurations $[g(t_0), \Phi^I(t_0)]$ to $[g(t^\star), \Phi^I(t^\star)]$, we construct an off-shell partition function $Z_t[g, \Phi]$ along the flow

$$Z_t[g,\Phi] = \int \exp\Big(\mathcal{A}_t^{\rm eff}[g,\Phi]\Big)\mathcal{D}g\mathcal{D}\Phi\Big|_{t_0\leq t\leq t^\star} \tag{A.77}$$

where we have integrated out modes with Dirichlet energies outside of the domain of t. As the first variation of the action may be written as

$$\frac{{\rm d}\mathcal{A}_t^{\rm eff}}{{\rm d}t} = \left(\dot{\Phi}^I \frac{\delta}{\delta\Phi^I} + \dot{g}_{ab}\frac{\delta}{\delta g_{ab}}\right)\mathcal{A}_t^{\rm eff}. \tag{A.78}$$

One finds the relation, upon using Eqn. (A.75)–(A.76),

$$\frac{{\rm d}Z_t}{{\rm d}t} = \left(\beta^I \frac{\delta}{\delta\Phi^I} + (\beta_{ab} + 2\Lambda g_{ab} - 2T_{ab})\frac{\delta}{\delta g_{ab}}\right)Z_t = 0 \tag{A.79}$$

which takes the conventional Callan-Symanzik form. In a usual RG flow, one consider the couplings of the theory to run with the scale. The situation here is qualitatively different as we are considering the deformations of the metric and the matter content along the flow. Essentially, this geometric RG flow deforms an initial metric g^i from the UV stating point to a smoother final configuration at the IR fixed point by virtue of "coarse graining" inhomogeneities. This perspective has been espoused thoroughly in the context of AdS/CFT subject to further geometric restrictions [353]. We suspect their analysis can be extended to the generalized Lorentzian Einstein-Ricci flows considered here.

A.4.5 Conclusions

We have presented an analysis of the Ricci flow problem for the Lorentzian Einstein-Hilbert action and its generalization in Eqn. (A.72). This was done by an analytic continuation into the Euclidean section and constructing a gradient flow problem for the Dirichlet functional $\mathcal{I}_D$. For linearizations around Euclidean space and in the absence of matter, the flow is well-posed converging onto Einstein spaces at the fixed points.

Several extensions of our analysis are available. One could include non-minimally coupled, dynamical matter configurations to the Lorentzian action with higher order curvature interaction and study the resulting flow equations. Furthermore, it may be useful to study flows of Euclidean black hole spacetimes with conserved charges in the Wald-Iyer formalism. In the context of AdS/CFT, the geometric flows considered here should be dual to RG flows in the boundary CFT [355]. As such, it should be possible to study the geometric flow of Euclidean AdS black holes with conserved R-charge as a corresponding RG flow for $\mathcal{N} = 4$ SYM at finite temperature on S^3 with a $U(1)$ chemical potential. Two questions, which are related, pertain to the Hawking-Page phase transition and the interpretation of the flow time as a spacetime dimension. In [355, 356], the radial direction of AdS_5 was argued as a flow time and identified with the RG scale. The corresponding RG equations had a similar form to Eqn. (A.75)–(A.76) in the absence of stress-energy. We know that the confinement/deconfinement phase transition in $\mathcal{N} = 4$ is dual to a Hawking-Page phase transition in the bulk [125]. Hence placing strong RG cutoffs in AdS will screen the black hole spectrum and thus keep the CFT confining. It is natural to wonder how the confinement/deconfinement phase transition may be evaded based on RG scalings and if the flow parameter may be related to thermodynamic parameters. Recently, we have shown that evading the deconfinement/confinement phase transition relied on deforming the R-charge to imaginary values [146]. In the context of this paper, we suspect the flow parameter t may be related to the imaginary R-charge.

Acknowledgments

I would like to thank Niayesh Afshordi, José Tomás Gálvez Ghersi, Soham Mukherjee,

Thanu Padmanabhan, Matthew Robbins, Vasudev Shyam, Rafael Sorkin, and Apoorv Tiwari for their valuable comments during the inception of this paper. I appreciate conversations with Jiaping Wang for the present version of this paper. Research at the Perimeter Institute is supported by the Government of Canada through the Department of Innovation, Science and Economic Development Canada. AD is supported by the National Science Foundation Graduate Research Fellowship Program under Grant No. 00039202 and by the University of Minnesota.